Technical Report Documentation Page

1. Report No.	2. Government Accession No.	3. Recipient's Catalog No.
4. Title and Subtitle **MBTC - 2032** **Development of Testing Protocol and Correlations for Resilient Modulus of Subgrade Soils** **Final Report**		5. Report Date **Jan 2005** 6. Performing Organization Code
7. Author(s) **Norman D. Dennis, Jr. Kyle Bennett**		8. Performing Organization Report No.
9. Performing Organization Name and Address **University of Arkansas, Department of Civil Engineering** **4190 Bell Engineering Center** **Fayetteville, AR 72701**		10. Work Unit No. (TRAIS) 11. Contract or Grant No. **MBTC - 2032**
12. Sponsoring Agency Name and Address **Arkansas State Highway and Transportation Department** **P.O. Box 2261** **Little Rock, AR 72203-2261**		13. Type of Report and Period covered **Final Report** **1 July 2002 thru 30 June 2005** 14. Sponsoring Agency Code
15. Supplementary Notes		

16. Abstract

This study provides both a description of the theoretical aspects of Spectral Analysis of Surface Waves (SASW) method for determining the thickness and resilient moduli of pavement systems, and presents the results of testing performed using an SASW system assembled as part of this research. The SASW method is based on the dispersive behavior of surface waves in a layered medium. Dispersion is the term used to describe the fact that the rate at which seismic surface waves (Rayleigh waves) travel through a medium depends upon the frequency of the waves, and this dependency can be used to determine mechanical properties of the medium through which the waves travel. Plotting Rayleigh wave velocity versus frequency (or wavelength) produces a graph called a dispersion curve. This dispersion curve can be used to develop a modulus versus depth profile through the use of a backcalculation procedure. Once the modulus versus depth profile is known, the resilient modulus and thickness of individual layers can be directly obtained.

The results obtained from SASW testing at ten flexible pavement sites throughout the state of Arkansas are presented as part of this report. The thickness and resilient modulus of each layer of each pavement section are estimated from the SASW data using two methods of analysis; simple inversion, and software provided by the University of Texas at El Paso. The thickness results obtained from SASW analyses are compared to known thicknesses measured from cores taken at each of the test sites. The resilient moduli predicted by SASW analysis are compared to the resilient moduli predicted by laboratory resilient modulus testing, the resilient moduli predicted by FWD analysis, and to Standard Penetration test N-values. The simple inversion procedure provided the most consistent results for SASW testing. SASW methods proved to be very accurate in predicting the thickness of various layers in a pavement system and correlated well with the results from laboratory resilient modulus testing.

17. Key Words	18. Distribution Statement
SASW, Pavement Thickness, Resilient Modulus, Signal Processing	**No Restrictions**

19. Security Classif. (Of this report)	20. Security Classif. (Of this page)	21. No. of Pages	22. Price
(none)	**(none)**	**247**	

Form DOT F 1700.7 (8-72) Reproduction of completed page authorized

Development of Testing Protocol and Correlations for Resilient Modulus of Subgrade Soils

By

Norman D. Dennis, Jr., Ph.D., P.E.
Kyle A. Bennett, MSCE, E.I.

Report prepared by
University Arkansas Department of Civil Engineering

for
Arkansas State Highway and Transportation Department, Little Rock, Arkansas

Contract Number MBTC-2032

January 2006

Disclaimer

This report reflects the views of the authors only, not the Arkansas State Highway and Transportation Department. The content of this report do not constitute a standard, regulation, or specification.

TABLE OF CONTENTS

A CD-ROM containing the raw SASW and FWD data files acquired from each site, data reduction tables used for analysis, and laboratory test results for the soils present at each site is enclosed with this document.

LIST OF FIGURES

LIST OF TABLES

CHAPTER 1

INTRODUCTION

1.1 Problem Statement

Mechanistic pavement design procedures to be presented in the upcoming American Association of State Highway and Transportation Officials (AASHTO) 200X Mechanistic-Empirical Design Guide defines resilient modulus as the primary material property of interest when determining the support characteristics of subgrade soils and untreated base and subbase material. The design transfer functions developed for the 200X design guide are based on resilient moduli measured using laboratory testing procedures. AASHTO currently recommends that the resilient modulus of subgrade soils be determined in accordance with AASHTO T-307. Unfortunately, AASHTO T-307 requires the use of expensive laboratory equipment, is time consuming, and must be run by highly skilled technicians. Thus, it is desirable to develop a method of determining resilient modulus which yields results similar to those found by AASHTO T-307, but does not have the aforementioned drawbacks.

Non-destructive testing (NDT) techniques are commonly used to estimate the resilient moduli of materials used in pavement systems. Non-destructive testing offers several advantages over laboratory testing of resilient moduli. NDT tests can typically be carried out much faster, and at much less expense than can laboratory tests. NDT testing also offers the advantage of testing the materials in-situ, which gives a better representation of the material properties under field conditions. A larger volume of

material is evaluated during NDT testing than during laboratory testing, which increases the accuracy of the obtained modulus values. Testing resilient modulus in-situ is especially beneficial as resilient modulus is heavily dependent upon both environmental conditions and state of stress. Considering all of these benefits, NDT testing may be considered a good tool to rapidly determine resilient modulus and to insure laboratory values are appropriate.

One of the most popular NDT methods currently used to estimate resilient modulus is the Falling Weight Deflectometer (FWD). FWD testing allows for the resilient modulus of each layer of a pavement system to be estimated using a backcalculation procedure. However, results obtained from laboratory testing and FWD testing generally do not agree (Mikhail, 1999). Additionally, FWD testing suffers from several limitations including the attempt to model a dynamic load with an ill-conditioned static analysis procedure, which does not produce unique results.

An NDT that is gaining popularity for use in determining moduli of layered systems is spectral analysis of surface waves (SASW). SASW allows the resilient modulus and thickness of each layer of a pavement system to be estimated using a combination of elastic wave propagation theory and signal processing techniques. SASW testing offers a fast, economical and theoretically sound alternative to both laboratory resilient modulus and FWD testing. Additionally, if meaningful correlations can be established between the resilient modulus found using SASW and the resilient modulus found by laboratory triaxial testing, then the SASW method could potentially replace the laboratory triaxial method as the preferred technique for determining resilient modulus for roadway design procedures.

One of the primary difficulties in estimating appropriate values of resilient moduli for pavement design purposes is that the resilient modulus of a material is not a constant property. Resilient modulus changes as a function of both environmental and stress conditions. As such, resilient modulus is considered to be a seasonally variable material property, and this variability must be accounted for to appropriately design pavement systems. Currently the AHTD uses FWD testing to attempt to account for the seasonal variation in resilient modulus. SASW testing may prove to be a more useful field evaluation technique because of its ability to simultaneously estimate layer thicknesses and resilient moduli.

1.2 Background

The concept of using surface waves to evaluate properties of subsurface materials was first proposed in the 1950's in the form of the steady state Rayleigh wave technique (Rossett, 1990). This method was proposed for evaluation of the elastic properties of pavement systems, but never gained wide acceptance due to the amount of time required to perform the field testing and the non-portable nature of the equipment involved (Rossett, 1990). In the 1980's, a modification to the steady state Rayleigh wave technique was made which took advantage of the concepts of signal analysis and the properties of transient impacts (Foti, 2000). Utilization of these concepts as well as the availability of more sophisticated electronic equipment allowed for rapid testing using portable equipment. The method of using signal analysis techniques to analyze surface waves became known as spectral analysis of surface waves (SASW).

The SASW method is based on the dispersive behavior of surface waves in a layered medium (Nazarian, 1995). Dispersion is the term used to describe the fact that the rate at which a Rayleigh wave travels through a medium depends upon the frequency of the wave, and this dependency can be used to determine mechanical properties of the medium through which the wave travels (Foti, 2000). Plotting Rayleigh wave velocity versus frequency (or wavelength) produces a graph called a dispersion curve. This dispersion curve can be used to develop a modulus versus depth profile through the use of a backcalculation procedure. Once the modulus versus depth profile is known, the resilient modulus and thickness of individual layers can be directly obtained.

To conduct SASW testing two receivers are placed on the pavement (or ground) surface. The receivers are connected to a digital signal analyzer (DSA). A transient impact is applied to the pavement surface which generates seismic surface waves. The particle motion associated with the passage of the surface waves is sensed by the receivers, and transformed into electrical signals. The DSA uses Fourier and spectral analysis procedures to determine the cross power and coherence values of the electrical signals as a function of frequency (Nazarian, 1995). From this information, Rayleigh wave velocity and wavelength can be calculated as a function of frequency. These two pieces of information allow for the dispersion curve previously mentioned to be constructed.

1.3 Objectives

The purpose of this research is to investigate the suitability of the spectral analysis of surface waves technique for determination of in-situ properties of flexible pavement

sections in the state of Arkansas. This will be accomplished by assembling a portable SASW system that is capable of measuring and analyzing seismic surface waves. The SASW system will then be used to collect data from flexible pavement sections at ten sites within the state of Arkansas. The collected data will then be analyzed using both manual and automated data reduction procedures to obtain a resilient modulus and thickness for each layer of the pavement system. The sites tested will be chosen such that they represent a wide variety of soil types typically found in Arkansas.

FWD testing will be performed by the Arkansas Highway and Transportation Department (AHTD) at each of the ten sites. Additionally, laboratory resilient modulus testing will be conducted on undisturbed Shelby tube samples obtained from each of the ten sites. The results obtained from SASW testing will be compared to the results from FWD and laboratory testing. Any trends or correlations that appear to exist between methods of determining resilient modulus will be discussed.

CHAPTER 2

LITERATURE REVIEW

The purpose of this chapter is to present the fundamental concepts that form the foundation of the spectral analysis of surface waves technique. This chapter is divided into four major sections. The properties and behavior of elastic waves is discussed in Part I. Part II presents the fundamental aspects of signal processing necessary to perform SASW testing. Part III shows how the spectral analysis of surface waves technique combines elastic wave theory and signal processing techniques to predict properties of layered pavement systems. Part IV then presents three case histories to demonstrate how others have used the SASW technique to evaluate pavement sections.

2.1 Literature Review Part I: Elastic Waves

The spectral analysis of surface waves technique relies upon wave propagation theory. This chapter presents a review of basic concepts of wave theory that provide the basis for SASW testing. When applying wave theory to geo-materials it is common to apply simplifying assumptions that allow for the creation of a manageable model. The assumptions that were made for this study are covered in the first section. An overview of some of the terminology commonly used when discussing waves is presented next. A description of the types of seismic waves and their defining characteristics is then given. Lastly, the behavior and properties of seismic waves in an elastic medium is covered.

2.1.1 Model Assumptions

One of the most important factors governing the behavior of soils is the magnitude of strains which are encountered. A variety of testing methods exist that can evaluate soil behavior over a wide range of strain levels. Using results from these tests, several models for soil behavior have been developed which attempt to account for the effects of varying strain magnitudes, including: linear elastic, visco-elastic, non-linear elastic, non-linear elasto-plastic and perfectly plastic models (Foti, 2000). To choose an appropriate model the effect of strain magnitude on soil behavior needs to be understood.

The shear stress vs. shear strain relationship in soil is curvilinear in nature (Das, 1992). Figure 2.1 shows a shear stress vs. shear strain diagram for a typical soil. Each hysteresis loop represents the behavior of the soil under cyclic loading conditions. The shear modulus of the soil is found by connecting the tips of a single hysteresis loop, and

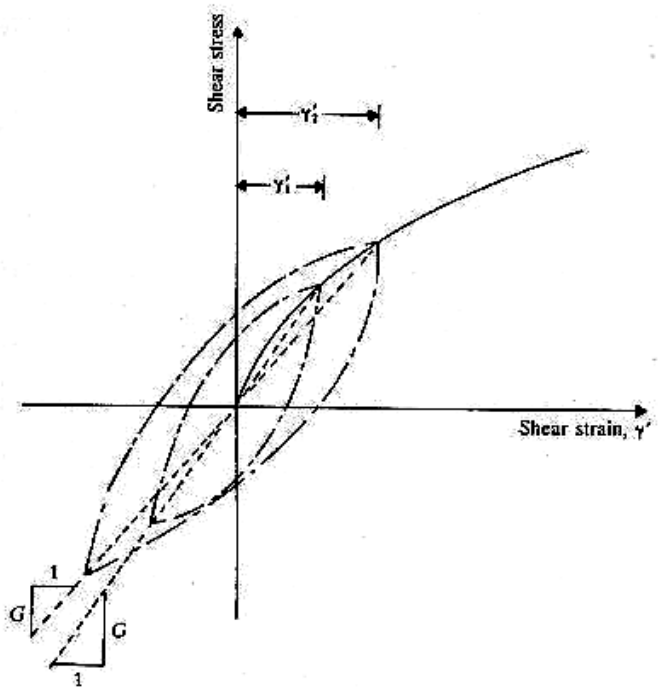

Figure 2.1 Hysteresis loops for a typical soil demonstrating the curvilinear shear stress vs. shear strain relationship (from Das, 1992)

is called the secant shear modulus (Luna et al. 2000). Looking at Figure 2.1 it is apparent that the shear modulus decreases as the shear strain increases. At very low levels of strain the value of the shear modulus reaches a maximum value called G_{max}.

Another way of looking at the effects of shear strain on shear modulus is to construct a modulus reduction curve. The modulus reduction curve plots values of shear modulus normalized with respect to the maximum shear modulus (G_{max}) as a function of shear strain. Figure 2.2 shows a typical modulus reduction curve. Note that the initial portion of the modulus reduction curve is flat indicating that for strains below 10^{-3} the shear modulus remains nearly constant. Because the shear modulus remains nearly constant in this range it may be considered an elastic parameter without introducing a substantial amount of error into the soil model (Luna et al, 2000).

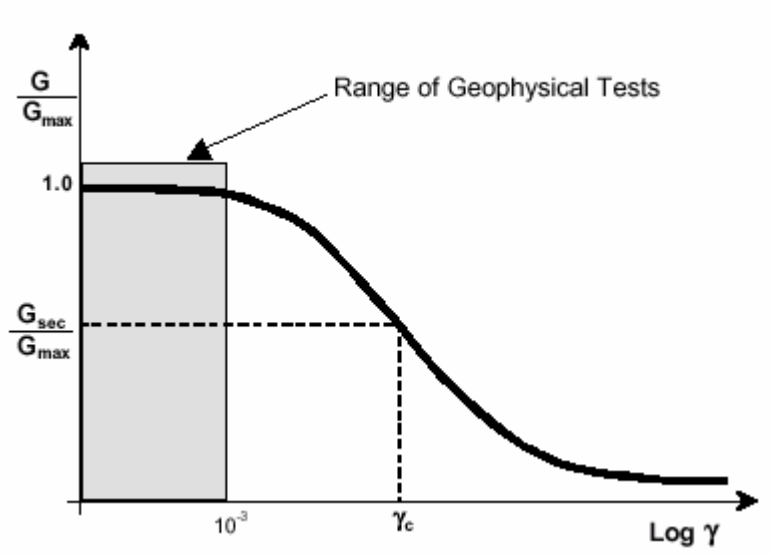

Figure 2.2 Typical modulus reduction curve (from Luna et al, 2003)

Seismic geophysical methods, including spectral analysis of surface wave testing, are conducted at very low strain levels, typically less than 10^{-4} (Luna et al, 2000) in magnitude. Therefore, the shear modulus for these values of strains is almost constant

which allows the soil to be modeled using an equivalent linear elastic soil model. The linear elastic soil model specifies that stress and strain are linearly related (Hooke's law). This model is the most commonly used under dynamic conditions, but it should be noted that this model cannot model some aspects of soil behavior that occurs due to cyclic loading (Luna et al, 2000). The assumption of linear elastic soil behavior will be used throughout this study.

Geo-material properties are inherently variable in nature from one location to the next. Properties of these materials can vary widely and sporadically in both the vertical and horizontal directions. Perhaps one of the most commonly made assumptions when dealing with variable materials is to consider the properties of a given material to be constant. Assuming constant material properties serves two important purposes. First, by assuming constant properties the amount of field exploration necessary to create a soil model is kept to a reasonable level. Second, the mathematical models used to predict the behavior of the soil are kept to a reasonable level of complexity.

In this study the properties of a given material will be considered to be constant in the horizontal direction (isotropic). The vertical direction will be modeled through the use of layers. Material properties may be different between layers, but will always be considered homogenous throughout a single layer.

2.1.2 Wave Terminology

In order for a wave to exist it must have a medium through which to travel. Typical examples of waves and a medium through which they may travel are: ocean waves traveling through water, sounds waves traveling through air, and electromagnetic waves traveling through a vacuum. This study will be concerned with seismic waves and

their properties when traveling through solid media such as asphalt, concrete, soil, and rock. Two definitions relating to the medium through which seismic waves travel are important for developing the concepts of seismic wave propagation. The two definitions are relatively simple; however they are important in that they dictate the types of seismic waves that can be generated. Whole space is defined as a medium that has constant properties and extends infinitely in all directions. Half space is defined as a whole space that extends infinitely in only two directions and intersects a free surface in the third direction. A whole or half space can be called ideal if its material properties obey the theory of elasticity. The term layered ideal whole space or layered ideal half space will be used to describe a medium which is isotropic, consists of multiple layers each of which is homogenous, and the material contained in each layer is elastic in nature. A simple illustration of whole space, half space and layered half space is shown below.

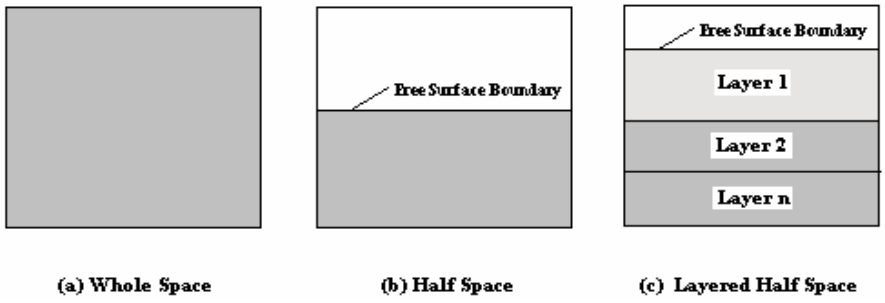

Figure 2.3 Illustration of whole space, half space and layered half space concepts

Imagine that a seismic disturbance occurs within a whole space. The disturbance will move away from the location of its origin in a spherical manner due to the fact that the material properties are uniform in all directions. The collection of points that define

the disturbance at any given time is called the wavefront. A vector drawn normal to the wavefront is known as a ray or raypath. The raypath indicates the direction in which the wavefront is expanding (Burger, 1992).

This study will frequently discuss waves that are periodic and sinusoidal in shape. Various terms are used to describe the properties of waveforms of this variety. Figure 2.4 shows a periodic, sinusoidal waveform. Two variables can be used to define the shape of a sinusoidal waveform, λ and A. The wavelength (λ) is defined as the distance between two successive points on a wave that have similar displacements. Typically either the distance between successive crests (high points) or troughs (low points) is chosen to measure the wavelength. The amplitude (A) is the maximum displacement a particle will undergo as a result of the wave passing through a material (Burger, 1992).

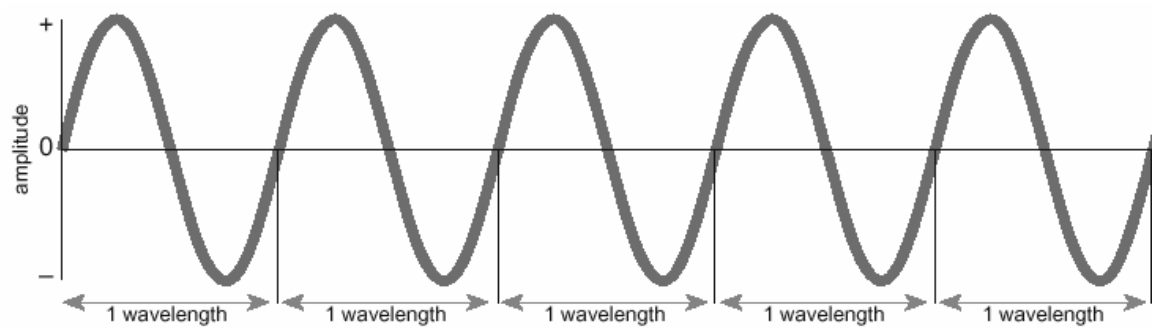

Figure 2.4 Illustration of a sinusoidal waveform

Two additional parameters are often used to describe the rate of propagation of sinusoidal waveforms. The period of a wave, T, is the amount of time it takes a wave to travel a distance of one wavelength (or cycle). Frequency, *f*, is used to describe the information provided by the period in a slightly different fashion. Frequency is the

number of periods (cycles) that occur in a given amount of time. Therefore, the frequency is simply the reciprocal of the period, and can be shown in equation form as

$$f = \frac{1}{T} \tag{2.1}$$

Hertz, or cycles per second, is the unit typically assigned to frequency.

Using the definitions above an important equation vital to SASW testing can be developed. Knowing both the frequency and the wavelength of a sinusoidal wave allows for the velocity of a wave in an elastic medium to be calculated using the equation

$$V = f * \lambda \tag{2.2}$$

2.1.3 Seismic Waves

2.1.3.1 Body Waves

An exact mathematical analysis based on the theory of elasticity can be used to derive equations of motion which show that two types of waves can exist in an ideal whole space due to a disturbance within the whole space. The derivation of the two equations is beyond the scope of this work, but the reader is referred to Graff (1975) for further information on the subject. The results obtained from the derivation show that each type of wave has a characteristic particle motion and propagation velocity with which it is associated.

The first type of waveform is transmitted by particles that oscillate in a back and forth motion around their equilibrium position. This oscillation occurs in the same direction as the propagation direction of the wave. This type of wave is generally called a primary wave or P-wave because it travels the fastest of all the seismic waves, and thus appears first in seismic records (Bath, 1979). P-waves are also called volumetric waves because the push-pull motion of the P-wave causes the medium to undergo volumetric

changes as the wave passes. The P-wave is also sometimes called an irrotational wave due to the fact that all of the particle motion occurs in the same direction as the wave is traveling (Graff, 1975). Other names such as compression wave, dilation wave, or longitudinal wave may also be used to describe a P-wave.

The movement of a P-wave can be visualized by picturing how a slinky would react if it were stretched out between two people, and then hit on one end. The disturbance will propagate from the end at which the disturbance occurred to the opposite end of the slinky. Also, the motion of each coil will be either compressive or dilative and in the same direction as the wave motion (Braile, 2003). P-waves are capable of traveling through all media which permit the passage of seismic waves including gasses, liquids, and solids. P-waves that travel in either gas or liquid are called acoustic waves (EM 1110-1-1802, 1995).

The second type of waveform that can propagate in an elastic whole space is transmitted when particle motion occurs in a plane perpendicular to the direction in which the wave travels. This type of wave travels slower than a P-wave and is the reason it is termed the secondary, or S-wave (Bath, 1992). During the propagation of an S-wave no volume change occurs, and all of the particle motion occurs in the transverse direction which causes the S-wave to be called either an equivolumetric wave or a shear wave. S-waves are also occasionally referred to as rotational waves and transverse waves.

S-wave motion always occurs in the plane perpendicular to the direction the wave is traveling, however that plane may not be convenient for analysis purposes. For this reason, S-waves are often decomposed into horizontal and vertical components (relative to the ground surface) called SH-waves and SV-waves respectively (Bath, 1992).

The motion of an S-wave can also be envisioned using the slinky as an example. The slinky is once again stretched out between two people, however this time one person flicks an end of the slinky causing an up and down motion. The wave will travel to the other end of the slinky, but now the motion of the individual coils will be in the vertical direction (Braile, 2003). This S-wave motion can only be transmitted in material that has shear strength. Thus, shear waves cannot be transmitted through gasses or liquids under normal circumstances.

2.1.3.2 Surface Waves

Seismologists in the 1800's discovered that records obtained from seismographs could not be completely explained using the types of waves known to them at the time (P and S waves). It was observed that the tremors experienced during an earthquake consisted of two minor tremors followed by a single significant tremor. The first minor tremor was known to correspond to the arrival of the P-wave, and the second minor tremor was attributed to the arrival of an S-wave. The third tremor, however, remained a mystery until 1887 when it was explained by Lord Rayleigh (Graff, 1975).

Lord Rayleigh demonstrated mathematically that the third tremor was due to the arrival of a wave that propagated along the surface of the earth. This type of wave is now known as a Rayleigh wave. Elastic wave theory up to this time could not predict such a wave because wave theory had only been applied to the conditions of an ideal elastic whole space. Lord Rayleigh was able to prove the existence of this new type of wave by applying wave theory to an ideal elastic half space, meaning he imposed a free surface boundary condition onto a whole space. Refer to work by Graff (1975) for a full mathematical derivation of the existence of the Rayleigh wave in an ideal half space.

Like P and S waves, the Rayleigh wave can be characterized by both the particle motion it creates and the velocity at which it travels. The Rayleigh wave travels the slowest of all seismic waves, typically arriving slightly after the shear wave in a time history recording of a seismic event (Bath, 1979). The relationship between the Rayleigh wave velocity and the shear wave velocity is a very important relationship when performing spectral analysis of surface wave testing. This relationship will be discussed in further detail in the section 2.1.4.2.

The propagation of the wavefront of a Rayleigh wave is unlike that of the body waves. Rayleigh waves are created by complex interactions of P and S-waves that occur at the free surface boundary of a half space when a disturbance occurs (Graff 1975). As the surface wave name implies, a Rayleigh wave will travel only near the surface of the boundary at which it was created. The particle motion associated with the passage of a Rayleigh wave is a bit more complicated than it is for body waves. Rayleigh wave motion occurs in the vertical plane only. The planar particle motion that occurs when a Rayleigh wave passes consists of two separate displacement components, vertical and horizontal, which are exactly 90˚ out of phase with one another. The two components travel at the same velocity, however they attenuate according to different exponential functions with depth. The vertical component of displacement is larger than the horizontal component of displacement at the free surface boundary which causes the particle motion to be a retrograde ellipse. However, the direction of particle motion changes to that of a prograde ellipse at a depth of approximately $1/2\pi$ of the wavelength because of the differing attenuation properties of the displacement components (Foti,

2000). Figure 2.5 shows both of the displacement components of a Rayleigh wave as a function of depth.

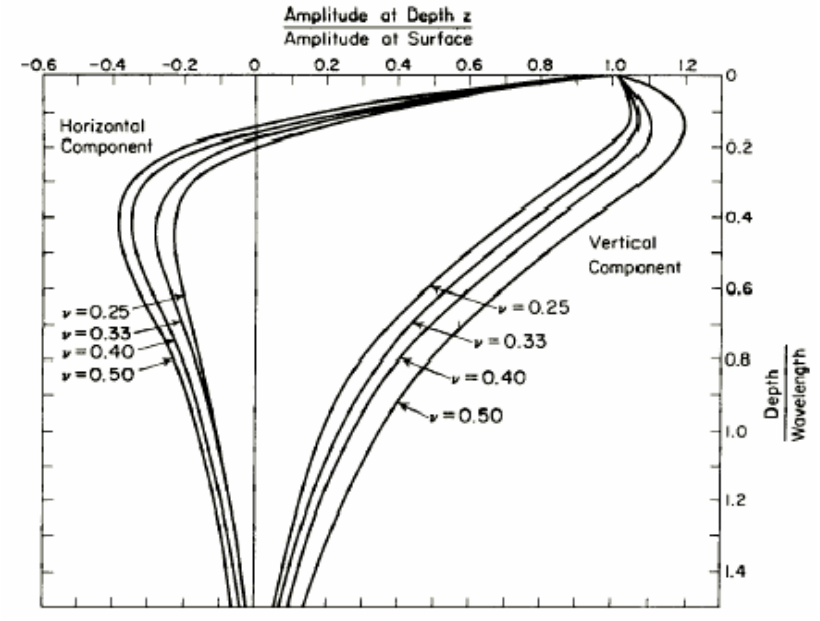

Figure 2.5 Rayleigh wave amplitude as a function of depth for various values of Poisson's ratios (from Richart et al, 1970)

The fact that the amplitude of the displacement components attenuates exponentially with depth is another very important property of Rayleigh waves when applying their usage to SASW analysis. Using Figure 2.5 one can see that nearly all of the particle motion associated with the Rayleigh wave occurs at depths shallower than one and a half wavelengths. Practically speaking, this means that the properties of the medium below the zone in which the Rayleigh wave travels has no impact on the behavior of the wave (Nazarian, 1984).

The discovery of the Rayleigh wave went a long way toward explaining certain anomalies commonly found in seismograph records, however it did not explain them all. A long standing observation in seismology was that earthquakes often contained large

transverse components of motion as part of the major tremor. These large transverse motions could not be explained by either P or S waves because of the large magnitudes, and could not be explained using Rayleigh waves because Rayleigh waves occur only within a vertical plane (Graff, 1975).

To explain the large transverse motion another extension of elastic wave theory was necessary. In 1911 A. E. H. Love used elastic wave theory in a layered medium to derive the mathematical equation for another form of a surface wave called the Love wave. This type of surface wave was found to only exist when a soft layer (called a waveguide) lies on top of a stiffer lower layer. The Love wave is the result of a horizontal shear wave that gets trapped in the soft upper layer and propagated through the medium by a series of multiple reflections that occur at the top and bottom of the layer (Burger, 1992).

Figure 2.6 shows the particle motion associated with the Love waves, Rayleigh waves, P-waves, and S-waves. The motion of the Love wave is identical to that of a horizontal shear wave. The velocity of Love waves tends to be slightly lower than that of a true shear wave, but slightly higher than that of a Rayleigh wave.

2.1.4 Properties of Seismic Waves in an Elastic Medium

2.1.4.1 Elastic Constants

In classic elastic wave theory, wave velocities are typically derived using Lame's elastic constants, μ and λ. These two parameters are not commonly used in geotechnical engineering applications; therefore the first portion of this section will define the common elastic constants used in geotechnical engineering. Once these elastic constants and the relationships between them have been defined, it becomes possible to express

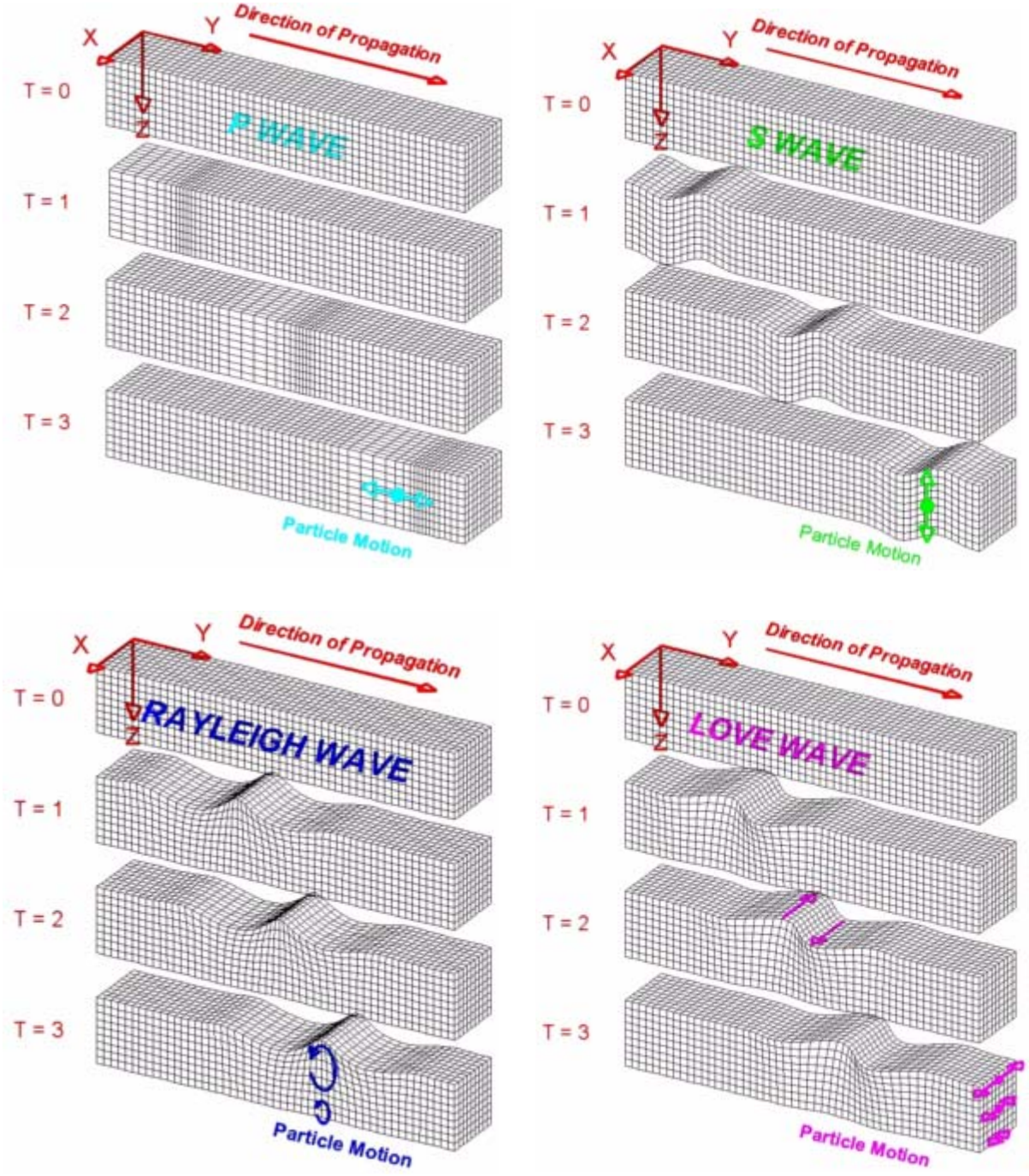

Figure 2.6 Major types of seismic waves and their respective motions (from Braile, 2003)

wave velocity in terms of these commonly used engineering parameters.

According to Hooke's law a linear relationship exists between applied stress (σ) and the resultant strain (ε). For an axially applied stress Hooke's law is defined by

$$\sigma = E\varepsilon \tag{2.3}$$

E is given the name Young's modulus, and is very commonly used to describe material behavior. Another descriptor of material behavior is Poisson's ratio (ν). Poisson's ratio is used to quantify the phenomena that if a material is subjected to a compressive stress along a single axis it will shorten in the same direction in which the stress is applied, but will expand along axes perpendicular to the applied stress. In equation form

$$\nu = \frac{\varepsilon_{(transverse)}}{\varepsilon_{(longitudinal)}} \tag{2.4}$$

Young's modulus predicts the relationship between stress and strain for a material that is subjected to axial compression or extension. If a material is deformed by simple shear a different modulus, called the shear modulus, is used to define the relationship between stress and strain behavior. The equation that shows the linear relationship between shear stress (τ) and shear strain (γ) is

$$\tau = G\gamma \tag{2.5}$$

where G is called the shear or rigidity modulus. The shear modulus and Young's modulus are related to one another through Poisson's ratio by the equation shown below

$$G = \frac{E}{2(1+\nu)} \tag{2.6}$$

Lame's elastic constants can be expressed using combinations of Young's modulus, shear modulus, and Poisson's ratio. Table 2.1 shows the relationships that can be developed.

Table 2.1 Relationships between elastic constants

	G, ν	E, ν
λ	$\frac{2G\nu}{1-2\nu}$	$\frac{\nu E}{(1+\nu)(1-2\nu)}$
μ	G	$\frac{E}{2(1+\nu)}$

2.1.4.2 Seismic Wave Velocity

Elastic wave theory predicts that the rate at which seismic waves move through a material is directly related to the elastic material properties (stiffness) of the material. The significance of the previous statement is that if the propagation velocity of a seismic wave is known the elastic properties of the material can be calculated. One of the most commonly used relationships is the relationship between shear wave velocity and shear modulus. The relationship is a powerful link between seismic wave properties and elastic soil properties. The significance of the relationship goes even further if Poisson's ratio is known, allowing Young's modulus to be obtained through the use of Equation 2.6. The mathematical equations that predict the wave velocities of the various types of seismic waves will be discussed below, along with some important relationships that can be developed between the velocities of the various seismic wave types.

The two equations given below show the velocities of the P wave and S waves as predicted by elastic wave theory, using Lame's constants.

$$V_p = \sqrt{\frac{\lambda + 2\mu}{\rho}} \tag{2.7}$$

$$V_s = \sqrt{\frac{\mu}{\rho}} \tag{2.8}$$

where: V_p = P-wave velocity
V_s = S-wave velocity
λ and μ = Lame's constants
ρ = mass density of the medium

These equations can be written in terms more applicable to engineering work using the relationships in Table 2.1 to rewrite the equations for P and S-wave velocities as

$$V_p = \sqrt{\frac{E}{\rho}\frac{(1-\mu)}{(1-2\mu)(1+\mu)}} \tag{2.9}$$

and

$$V_s = \sqrt{\frac{G}{\rho}} \tag{2.10}$$

If the ratio of the S-wave to P-wave velocity is taken, the resulting equation is a function depending solely on Poisson's ratio. Recalling that Poisson's ratio for all real material lies between 0 and 0.5, it is apparent that the P-wave will always travel faster than the S-wave (Nazarian, 1984).

$$\frac{V_s}{V_p} = \sqrt{\frac{1-2\nu}{2(1-\nu)}} \tag{2.11}$$

The surface waves discussed in section 2.1.3.2 can also be shown to have wave propagation velocities that are directly related to the elastic properties of the medium in which travel occurs. Because the special circumstances necessary for a Love wave to form will not be encountered during this study, its relatively complicated equations of motion will not be presented. The characteristic equation that is used to solve for the velocity of a Rayleigh wave is

$$K^6 - 8K^4 + (24 - 16\gamma^2)K^2 + 16(\gamma^2 - 1) = 0 \tag{2.12}$$

where: $K = \frac{V_R}{V_S}$

$\gamma = \frac{V_s}{V_p}$

V_R= Rayleigh wave velocity

Solution of the above equation in terms of K yields

$$K = \frac{0.87 + 1.12\nu}{1 + \nu} \tag{2.13}$$

If the range of values for Poisson's ratios of real materials is substituted into the above equation it can be seen that the Rayleigh wave velocity is nearly the same as that of the S-wave. The ratio below shows that the Rayleigh wave always travels just a bit slower than does the shear wave.

$$0.87 < \frac{V_R}{V_S} < 0.96$$

Figure 2.7 shows the velocity of the P, S, and Rayleigh waves, normalized by S wave velocity, plotted vs. Poisson's ratio. Three important points illustrated by Figure 2.7 are that the P-wave has the highest velocity followed by the S-wave and then the Rayleigh wave, the S-wave and Rayleigh wave velocities are nearly identical, and Poisson's ratio has very little effect on the relationship between S and Rayleigh wave velocity.

2.1.4.3 Seismic Wave Energy

As a wave travels outward from the source which caused the disturbance, energy is dissipated. Energy dissipated as a function of the distance the wave travels is called geometrical attenuation (Burger, 1992). Spectral analysis of surface waves analysis is

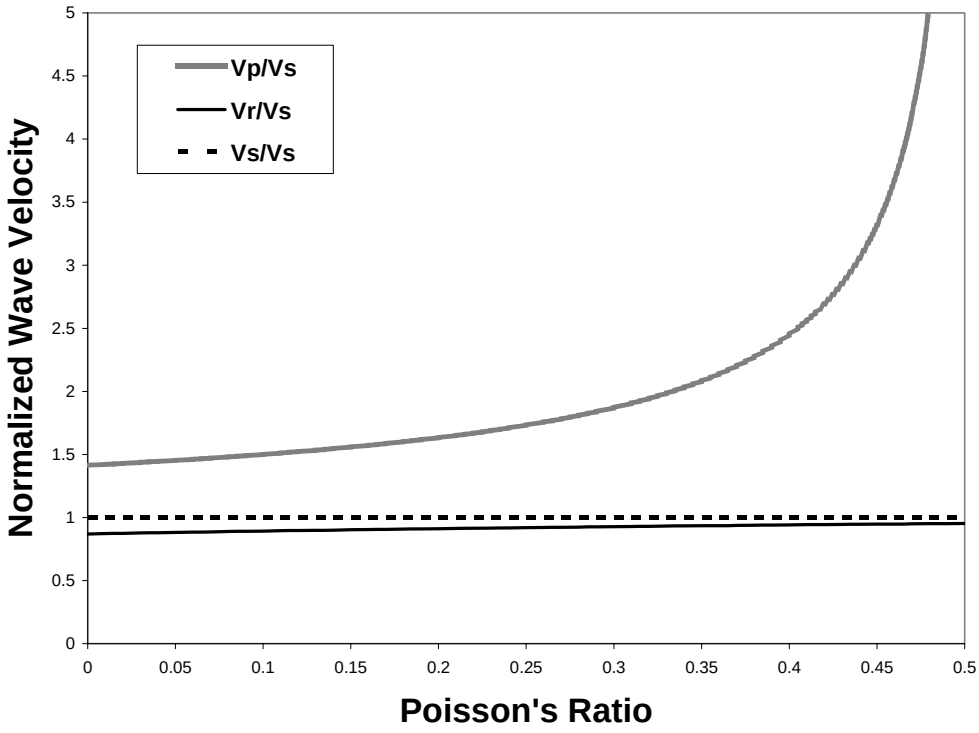

Figure 2.7 Effect of Poisson's ratio on normalized wave velocity

based on the case of a point source acting on the ground surface. The P and S-waves generated due to the point source will attenuate differently than will the resulting Rayleigh wave due to their differing wave fronts. The body waves expand radially outward from the source, while the Rayleigh wave expands along a cylindrical wave front. The Rayleigh wave front is cylindrical due to the fact that it travels solely near the ground surface. A geometrical spreading factor can be used to describe the rate at which the waves attenuate with distance from the source. Body wave attenuation along the ground surface has been found to be proportional to $1/r^2$, where r is the radial distance from the source. Rayleigh waves traveling along the ground surface attenuate much more slowly, proportional to $1/\sqrt{r}$ (Foti, 2000).

Energy partitioning is the term used to describe how wave energy is transformed from one form to another. Miller and Pursey (1955) analyzed the case of a vertical harmonic point source acting on an ideal half space. They found that 67% of the input energy was transformed into the form of a Rayleigh wave, 26% transformed into shear waves, and the remaining 7% into primary waves. Figure 2.8 shows the important properties associated with wave propagation away from a vertical harmonic point source.

When the fact that 67% of the input energy is converted into a Rayleigh wave is considered along with the fact that Rayleigh waves attenuate at a much slower rate than

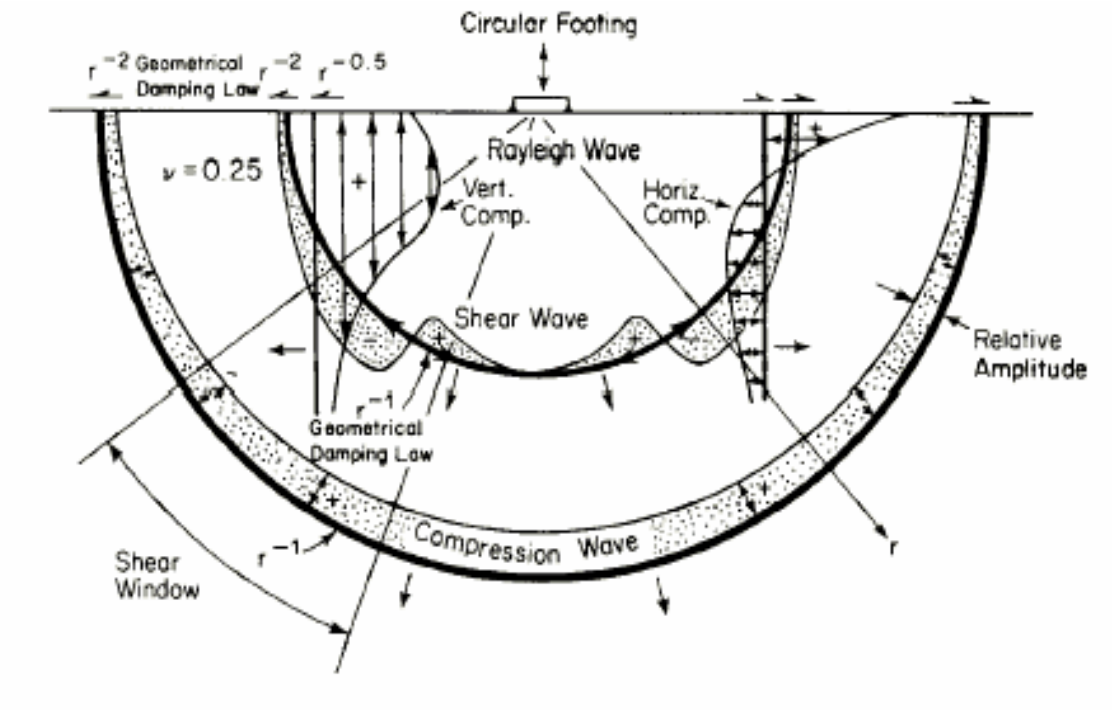

Figure 2.8 Wave field generated due to a harmonic vertical point source acting on a homogenous, isotropic, elastic half-space (from Richart et al, 1970)

body waves, it becomes apparent that Rayleigh waves are the dominant waveform resulting from a vertical source. This fact is well illustrated by looking at work performed by Lamb in 1904. Lamb mathematically predicted the displacements that

occur on the surface of an ideal half space due to a vertical point source acting on the surface at a distance r away. Figure 2.9 shows a graphical depiction of the mathematical solution of the predicted particle motion. The dominance of the Rayleigh wave can clearly be seen in this example.

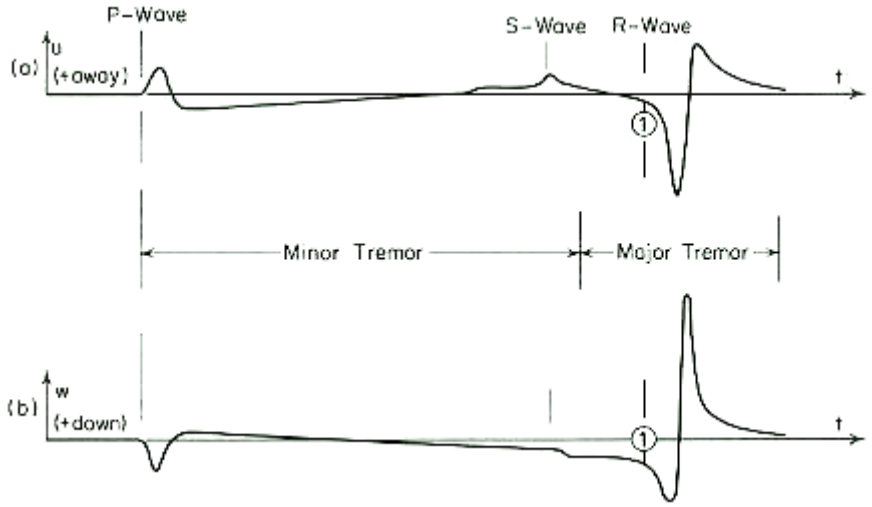

Figure 2.9 Lamb's solution for a vertical point or line source acting on a homogenous, isotropic, elastic half space. Both radial motion (top) and vertical motion (bottom) are shown (from Richart et al, 1970, after Lamb 1904)

2.2 Literature Review Part II: Signal Processing

Signal processing is a broad area of engineering that involves the analysis of electric signals. A signal can be defined as an electrical quantity that is directly related to

the presence or change of a physical phenomenon such as temperature or pressure (Beauchamp, 1979). In SASW testing the signal of interest is generated by the particle motion that occurs due to the passage of seismic waves. This particle motion is transformed into an electrical signal by means of transducers, specifically velocity and acceleration transducers. Properties of the passing seismic waves can then be determined by properly analyzing the acquired signal. This part of the literature review will discuss the aspects of signal processing that are necessary to properly acquire and analyze the signals that represent the passage of the seismic waves used during SASW testing.

2.2.1 Fourier Analysis

One of the principle tools of signal processing is based on work published by Baron Jean Baptiste Fourier in 1822 (Marven, 1996). Fourier analysis allows any signal (waveform) to be decomposed into a series of harmonic waves that have different frequencies. This concept is demonstrated by Figure 2.10. Figure 2.10a shows a complex waveform (upper trace) decomposed into two sine waves (lower trace) as viewed from the time domain. A better representation of this waveform can be obtained by adding a third axis, frequency. Figure 2.10b is a three dimensional view of the waveform once the frequency axis has been added. The individual components of the complex waveform can now be seen much more clearly. Another perspective that can be taken is to view the waveform by looking down the time axis as shown in Figure 2.10c. This view represents the frequency domain, also called the spectrum of the waveform. Each line on the frequency axis represents one sine wave of a given frequency and amplitude, and is referred to as a component (Agilent Technologies, 2000).

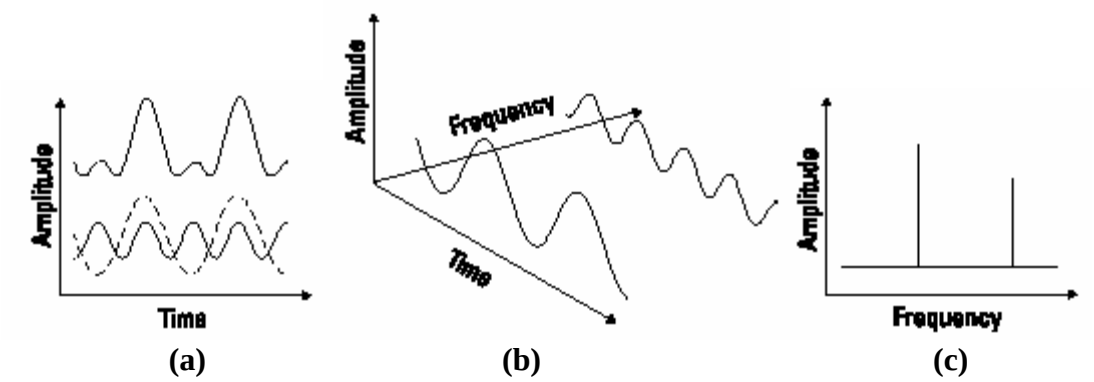

Figure 2.10 Representation of a waveform in (a) time domain view, (b) 3-D view, and (c) frequency domain view (From Agilent Technologies, 2000)

Becoming accustomed to thinking of signals in the frequency domain can be difficult, as the time domain is the more natural way of picturing a signal. Figure 2.11 shows some common signals in both the time and frequency domains to illustrate how the two domains are related. The sine wave in Figure 2.11a is represented as a single line in the frequency domain. A square wave like the one shown in Figure 2.11b is composed of an infinite number of harmonically related sine waves. The frequency spectrum for this type of wave consists of an infinite number of lines spaced as a function of the period of the wave. Of particular interest to this study is the transient signal shown in Figure 2.11c. A transient signal is defined as one which reduces to zero amplitude over a finite time interval. The frequency spectrum of a transient signal is continuous, meaning that an infinite number of frequency components (sine waves) are present in the signal.

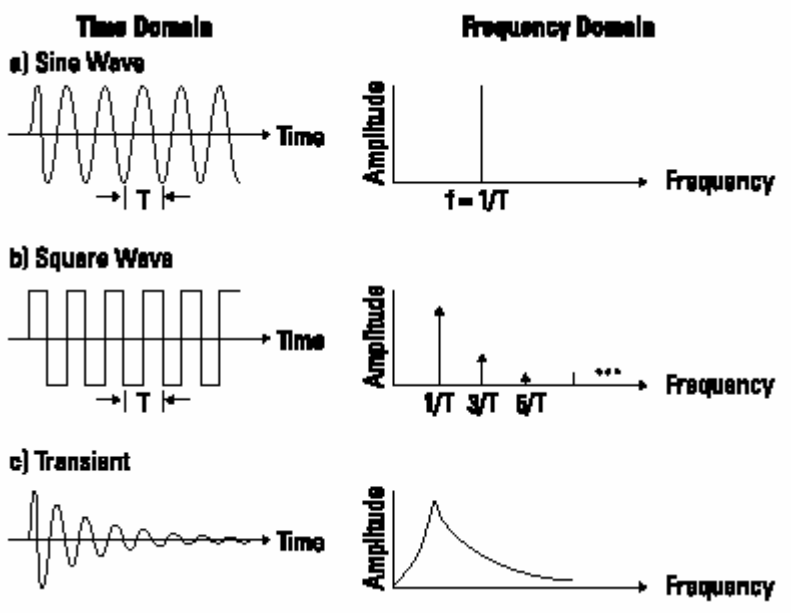

Figure 2.11 Common signals shown in the time and frequency domains (From Agilent Technologies Applicatoin Note 243, 2000)

2.2.1.1 The Phasor Model

The first step in describing the mathematical forms of the Fourier transform is to present the idea of modeling a signal as a phasor. A phasor is defined as a vector which rotates in the complex plane at a rotational speed of ω (radians/sec). Figure 2.12 shows a phasor of magnitude A that has coordinates of *a* on the real axis and *b* on the imaginary axis. The angle θ represents the phase and can be expressed as the rotational speed multiplied by time. Using this model a signal at any given time t can be defined by

$$x(t) = a + jb \tag{2.14}$$

where $j = \sqrt{-1}$

The magnitude A and phase θ can now be expressed as

$$A = \sqrt{(a^2 + b^2} \tag{2.15}$$

$$\theta = \tan^{-1}\frac{b}{a} \tag{2.16}$$

The equations given above are the rectangular form for expressing a complex number.

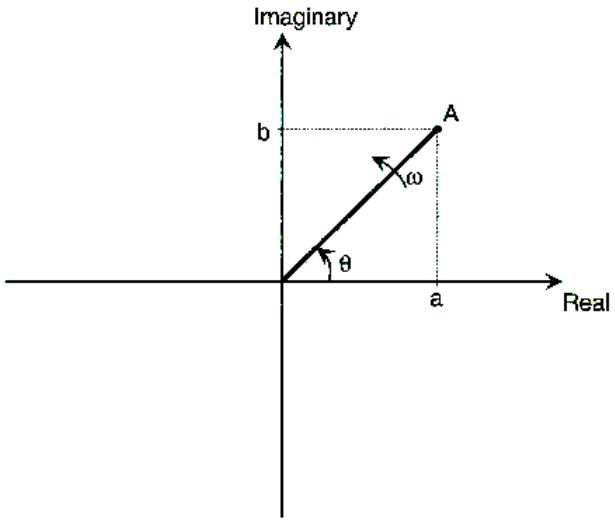

Figure 2.12 Phasor model of a signal (From Marven, 1996)

These equations can also be expressed in polar coordinates by

$$x(t) = Ae^{j\theta} \tag{2.17}$$

$$\text{where } e^{j\theta} = \cos\theta + j\sin\theta \tag{2.18}$$

$$e^{-j\theta} = \cos\theta - j\sin\theta \tag{2.19}$$

Equation 2.17 is also referred to as the magnitude/phase phasor form because A and θ are used to define the phasor directly. To express the most general form of equation 2.17 an initial condition is applied that gives the phase an initial value of α at t = 0. The phase can now be written as

$$\theta = \omega t + \alpha \tag{2.20}$$

Equations 2.18 and 2.19 are known as Eulers formulae. These two formulae allow harmonic waves to be defined using magnitude/phase form phasors. This is

important in signal processing because any signal can be represented by a series of these harmonic waves. Using Eulers formulae the sine and cosine functions are expressed as

$$\sin\theta = \frac{e^{j\theta} - e^{-j\theta}}{2j} \tag{2.21}$$

$$\cos\theta = \frac{e^{j\theta} + e^{-j\theta}}{2} \tag{2.22}$$

A general cosine wave of the form $x(t) = R\cos\theta$ can now be represented in phasor form by applying Equation 2.22 which gives

$$x(t) = \frac{1}{2}R(e^{j(\omega t+\alpha)} + e^{-j(\omega t+\alpha)}) \tag{2.23}$$

Equation 2.23 shows that a cosine wave consists of two phasors. If looked at in rectangular coordinates the two phasors' *a* coordinates are always equal in both magnitude and sign, and their *b* coordinates are always equal in magnitude but opposite in sign. This relationship is known as a conjugate pair. It can be shown that all real signals will be composed of conjugate pairs of phasors which, when summed, lie along the real axis (Marven, 1996). Figure 2.13 shows a cosine wave using the phasor model.

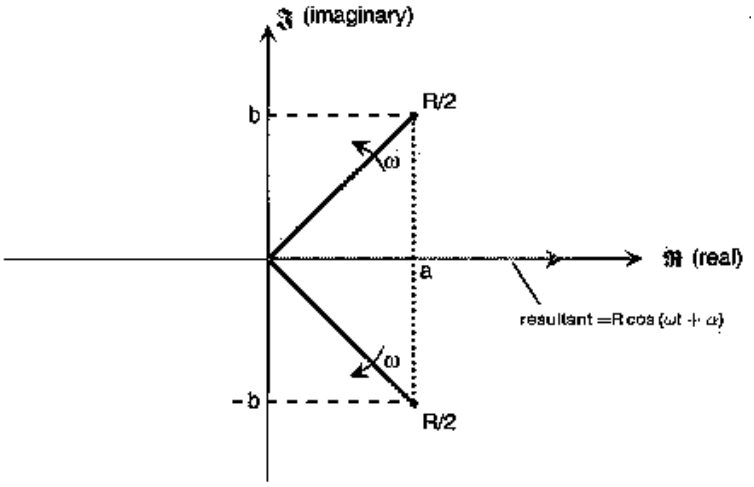

Figure 2.13 Cosine wave modeled using a set of complex phasors (From Marven, 1996)

2.2.1.2 Fourier Series

Fourier's original theorem allows for a function x(t) to be decomposed into a group of sine waves by expanding into series form according to the equation

$$x(t) = A_0 + A_1 \sin(\omega_0 t + \theta_1) + A_2 \sin(2\omega_0 t + \theta_2) + ...A_3 \sin(n\omega_0 t + \theta_n) \quad (2.24)$$

$$\text{and } \omega_0 = \frac{2\pi}{T} \quad (2.25)$$

where T = period

The equations above basically state that a time dependent function can be rewritten as a series of terms that are dependent on frequency. A and θ still represent magnitude and phase respectively. An important characteristic of a series of this type is that x(t) must be a periodic function because each term contains a frequency component that is a multiple of the fundamental frequency f_0 which is related to ω_0 by

$$f_0 = \frac{\omega_0}{2\pi} \quad (2.26)$$

Applying the following relationship to Equation 2.24

$$\sin(a+b) = (\sin a * \cos b) + (\cos a * \sin b) \quad (2.27)$$

and defining that

$$a_k = C_n \sin\theta_n \quad (2.28)$$

$$b_k = C_n \cos\theta_n \quad (2.29)$$

$$C_0 = \frac{a_0}{2} \quad (2.30)$$

allows Fourier's series to be found (Equation 2.31)

$$x(t) = \frac{a_0}{2} + \sum_{k=1}^{n} a_k \cos k\omega_0 t + \sum_{k=1}^{n} b_k \sin k\omega_0 t \quad (2.31)$$

a_k and b_k are called the Fourier coefficients and can be evaluated by taking advantage of a property of sinusoids called orthogonality which states that "a finite value is obtained for the weighted average of the product of sine and sine or cosine and cosine if their frequencies and phase shifts are identical, and a zero result if they are not. Also, the weighted average of the product of sine and cosine will be zero irrespective of frequencies (Beauchamp, 1979)." Applying this principle the equations that represent the Fourier coefficients are

$$a_k = \frac{2}{T}\int_0^T x(t)\sin k\omega_0 t \cdot dt \tag{2.32}$$

$$b_k = \frac{2}{T}\int_0^T x(t)\cos k\omega_0 t \cdot dt \tag{2.33}$$

The equations for the Fourier series and the Fourier coefficients developed above can be written in an equivalent form using the concept that a phasor can be represented in both rectangular and polar coordinates. Deriving the Fourier series using polar coordinates yields a complex representation of the series

$$x(t) = \sum_{k=-n}^{n} A_k e^{jk\omega_0 t} \tag{2.34}$$

$$\text{where } A_k = \frac{a_k - jb_k}{2} \tag{2.35}$$

Further evaluation of A_k yields

$$A_k = \frac{1}{T}\int_0^T x(t)e^{-jkw_0 t} \cdot dt \tag{2.36}$$

Two primary benefits arise from expressing the Fourier series in this form. The first benefit is that the notation is simper. The second benefit is that using this notation it becomes possible to develop the series further, into an even more useful form (Beauchamp, 1979).

Thus far Equation 2.34 has been developed that allows any *periodic* function to be decomposed into a series of harmonic terms that are frequency dependent. The next step in developing Fourier analysis into a form suitable for SASW testing is to eliminate this limitation of periodicity.

2.2.1.3 Fourier Integral Transform

To extend Equation 2.34 such that it is applicable to non-periodic time functions (i.e. transient signals) the assumption that the frequencies that compose the series are harmonically related must be discarded. This is accomplished by taking the limit of Equation 2.34 as the fundamental frequency f_0 approaches 0. The relationship that exists between frequency and period causes the period of analysis to approach infinity as the fundamental frequency approaches 0. Also, the relationship between rotational speed and fundamental frequency necessitates that as the fundamental frequency approaches 0 the rotational speed approaches 0. Applying these relationships to Equation 2.34 results in the Fourier integral transform (Beauchamp, 1979)

$$X(f) = \int_{-\infty}^{\infty} x(t) e^{-j\omega t} \cdot dt \qquad (2.37)$$

The Fourier integral transform is a powerful tool that allows a function to be "transformed" from a time function to a frequency function. The complex spectrum of a signal, consisting of the magnitude and phase for each frequency, can be found using this

transform. The magnitude is the absolute value of the transform while the phase is the argument of the transform.

2.2.1.4 Discrete Fourier Transform and Fast Fourier Transform

Equation 2.37 now allows for non-periodic signals to be evaluated. However, because an integral taken over an infinite amount of time has been introduced, an infinite number of points are needed to define the signal as a function of time. In reality digital computers are necessary to perform signal analysis because of the many calculations involved when transforming between domains. A problem is now apparent because it is obvious that a digital computer cannot continuously sample a signal. A finite version of the Fourier transform must be used if a computer is to record and process a signal.

The discrete Fourier transform, or DFT, is the solution to the problem of not being able to continuously sample a signal. The DFT approximates a true Fourier transform by performing numerical integration on a discrete number of samples. To represent that the value of a signal can only be known (sampled) at a discrete number of points the following equation can be used

$$X(m\Delta f) = \int_{-\infty}^{\infty} x(t)e^{-j2\pi m\Delta ft} \cdot dt \tag{2.38}$$

where m = 0,1,2,…

The integral can now be approximated numerically by calculating the area of rectangles of finite width Δt which can be represented by the equation

$$X(m\Delta f) \approx \Delta t \sum_{n=-\infty}^{n=\infty} x(n\Delta t)e^{-j2\pi m\Delta fn\Delta t} \tag{2.39}$$

Now, to represent that the summed discrete samples cannot be obtained over an infinite amount of time, the final form of the DFT can be expressed as

$$X(m\Delta f) \approx \Delta t \sum_{n}^{n-1} x(n\Delta t) e^{-j2\pi m\Delta f n\Delta t} \tag{2.40}$$

The DFT now allows the frequency spectrum of any signal composed of N samples to be calculated. The DFT performs all of the functions necessary to properly analyze the signals needed for SASW analysis, however, the amount of time necessary for the DFT to be calculated is excessive. The excessive amount of time is due to the fact that N^2 complex operations must be performed for a single DFT. To solve this problem an algorithm that takes advantage of certain symmetries that occur when N is a multiple of 2 is employed. This algorithm that is used to speed up the DFT is called the fast Fourier transform, or FFT. The FFT can be computed in approximately $N\log_2(N)$ operations. This makes the FFT much more memory efficient than the DFT (Agilent Technologies, 2000).

2.2.2 Analog to Digital Conversion

It was stated in section 2.2 that the input signal used in SASW analysis is obtained through the use of transducers that measure the passage of seismic waves. The input signal generated by these transducers is in the form of a continuous, or analog, voltage. It was also stated that the digital computers used to perform signal analysis cannot continuously measure an analog input signal, and therefore a discrete number of data points must be used. To reconcile the difference between the input signal and the capabilities of the computers used for analysis, a process called analog to digital conversion is performed. Analog to digital conversion is the process by which a continuous input signal is transformed into a discrete number of digitized points such that a digital computer can be used for analysis.

To obtain the digitized points necessary for analysis a continuous signal is sampled. Sampling of an analog signal is performed by taking instantaneous measurements of the signal at equal time intervals. This set of measurements forms a digital representation of the original signal. Several problems can develop when a discrete number of measurements is used to represent a continuous signal. Four of the major problems that can develop are due to aliasing, quantization, leakage, and resolution. These four issues will be discussed below.

2.2.2.1 Aliasing

The most severe issue that arises when a continuous signal is sampled is called aliasing. Aliasing occurs when the number of points sampled is insufficient to uniquely define the original signal to a digital computer (Beuachamp, 1979). The rate at which a signal is sampled determines whether or not aliasing will occur. The concept of aliasing will be illustrated using a simple example.

If the temperature of a pond was continuously recorded over a period of five days the graph of temperature vs. time may look something like Figure 2.14. The pond would tend to warm up during the day and then cool off at night in a cyclical manner that is estimated as a sine function here for simplicity. Now imagine that a temperature vs. time plot is created over the same period of time, but now temperatures are recorded only once a day at 4:00pm. Figure 2.15 is the plot that results from this situation.

The sampled, or digitized, points shown in Figure 2.15 are supposed to represent the curve shown in Figure 2.14, however when the points are connected they form a straight line, indicating 0 frequency. This straight line indicates that no temperature change occurred over the five day analysis period which is not the case at all. This

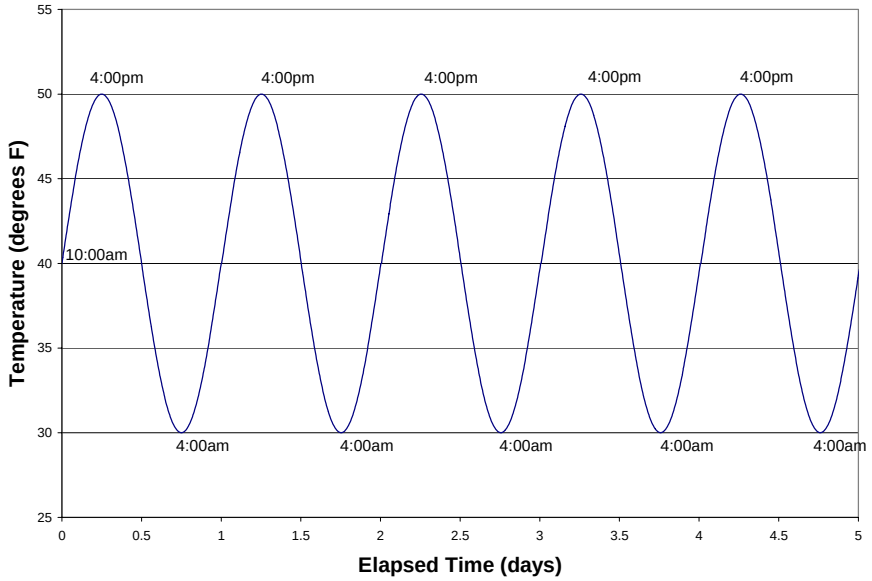

Figure 2.14 Plot of continuous temperature variation of a pond over a five day period

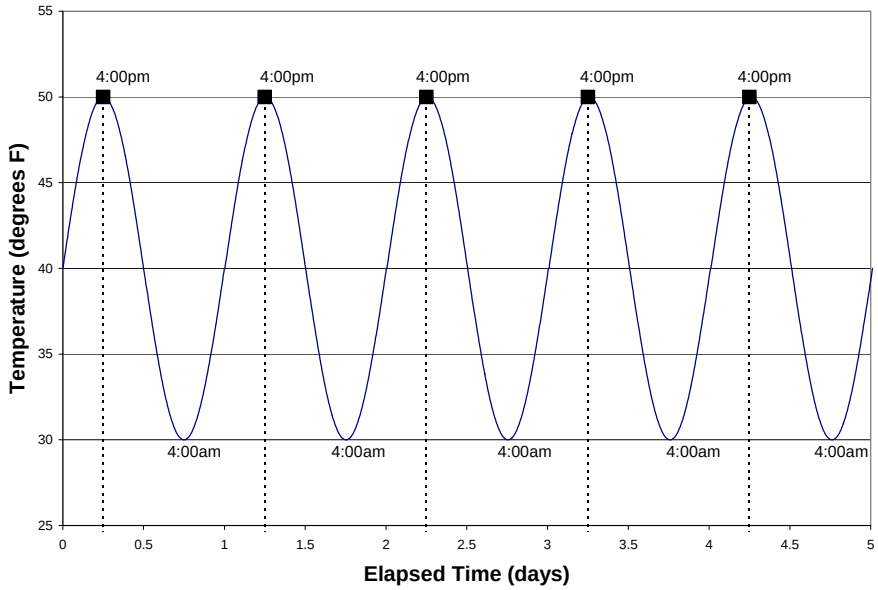

Figure 2.15 Plot of pond temperature variation sampled once per day

aliasing error resulted because the rate of sampling was too slow to produce a sufficient number of data points to properly define the curve.

The solution to this problem is to increase the rate at which the measurements are taken. Shannon's sampling theorem can be used to define the minimum sampling rate

necessary to prevent aliasing from occurring. The minimum sampling rate is called the Nyquist frequency and can be determined using Equation 2.41.

$$f_n \geq 2 f_i \tag{2.41}$$

where f_n = Nyquist frequency
f_i = highest input frequency

Equation 2.41 says that the minimum sampling rate must be greater than or equal to twice the highest frequency component of the input (Labview Measurements Manual, 2000).

To test this new sampling rate it will be applied to the original example of the temperature variation of the pond. The input signal is a single sine wave that has a frequency of one cycle per day, therefore a minimum of two samples must be taken per day according to Shannon's sampling theorem. Figure 2.16 shows the temperature variation of the pond sampled two times per day. Sampling at this rate has produced samples that when connected will yield a triangular wave. From this triangular wave the original wave can be recovered using a low-pass filter (discussed later). It should be apparent that as the rate of sampling is increased the more accurate the digital representation of the original input signal will be (Marven, 1996).

In order to apply the Nyquist criterion to establish a minimum sampling rate the maximum frequency component of the input signal must be known. This parameter is rarely known when dealing with signals in the real world. To overcome this problem a low-pass filter is used to limit the frequency range of the input signal. This low-pass filter is called an anti-alias filter. Figure 2.17a shows that an ideal anti-alias filter passes all of the frequency components of a signal that are less than a set frequency limit, while eliminating all of the frequency components of a signal that are higher than the set limit. Ideal anti-alias filters do not exist, however, and real anti-alias filters have the

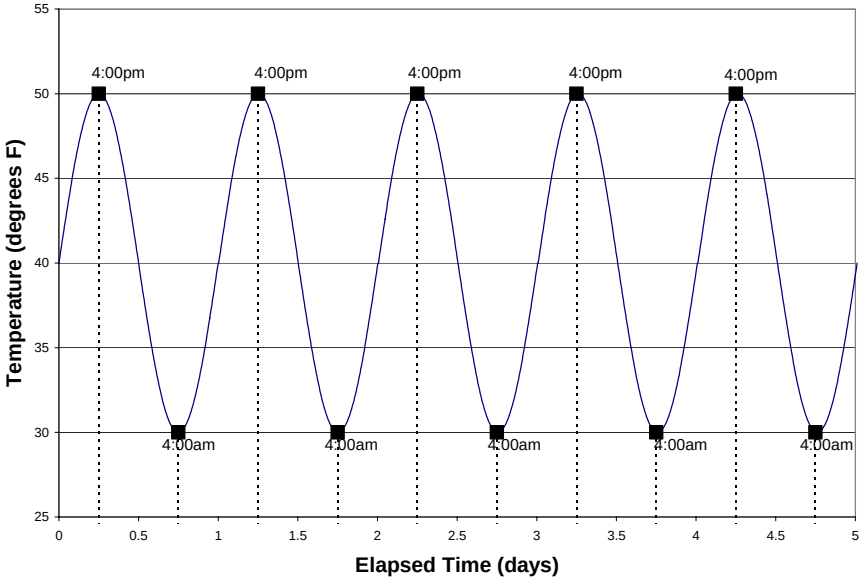

Figure 2.16 Plot of pond temperature variation sampled at the Nyquist frequency

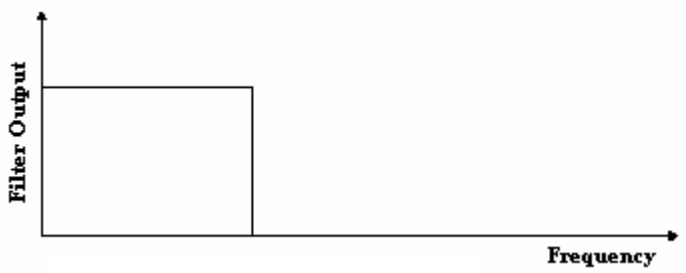

(a) Ideal anti-alias filter

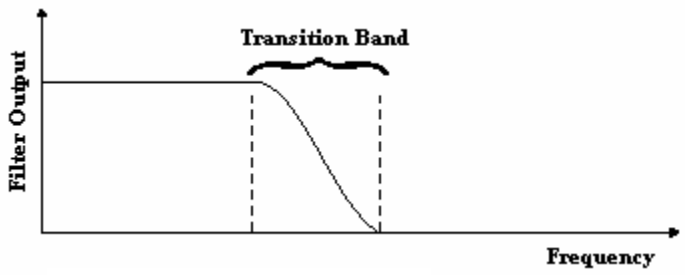

(b) Realistic anti-alias filter

Figure 2.17 Ideal and realistic anti-alias filters (From Agilent Technologies, 2000)

characteristics shown in Figure 2.17b. A real anti-alias filter has a transition zone in which frequency components will not be completely stopped from aliasing into the desired frequency. To account for this the actual sampling rate used in practice is raised to twice the highest frequency component of the transition band. This can lead to sampling rates that are from 2.5 to 4 times the maximum desired input frequency, depending on the size of the transition band of the anti-alias filter (Agilent Technologies, 2000).

2.2.2.2 Quantization

Sampling of an analog signal is physically performed using a sample and hold circuit. A sample and hold circuit operates by measuring the voltage level of the input signal and holding that sampled voltage level until the next sample is taken. The result of sampling in this manner is that a stepped signal is created to represent the original signal. These stepped sampled values are turned into binary numbers that are recognizable by a computer through the use of an analog to digital converter (ADC). Quantization is the name for the method the ADC uses to transform the stepped signal into numbers (Marven, 1996).

To show how an analog to digital converter digitally represents a signal using quantization an example will be presented. Figure 2.18a shows an input signal in the time domain. If the time signal is sampled at evenly spaced time intervals t_s its digital appearance would be a series of points, as shown in Figure 2.18b. Because a sample and hold circuit is used, however, the actual digital appearance is that of a stepped waveform, shown in Figure 2.19. The most basic quantization scheme is to classify each sample of the input signal into one of two groups, assigning a 1 if the amplitude (voltage) of the

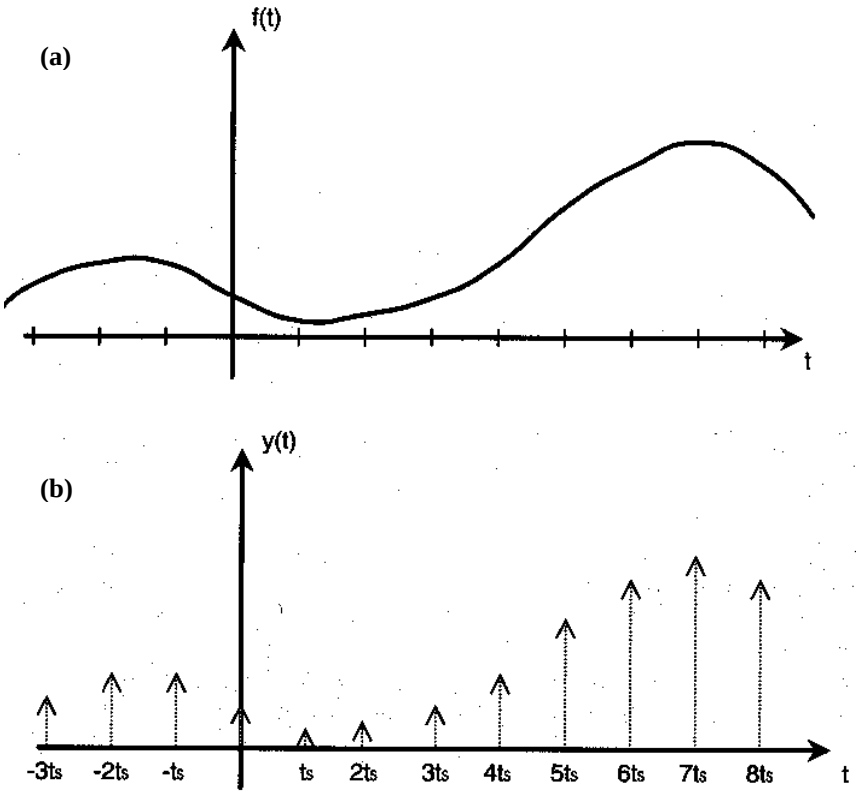

Figure 2.18 (a) Input signal in the time domain. (b) Sampled version of signal using constant time interval (From Marven, 1996)

input signal is above a certain level (designated as "a" in Figure 2.19), and a 0 if not. Using this scheme, the sample and hold circuit will read a voltage at sample time 1 (t_s), the sample will be classified as either a 0 or a 1 depending on its level, the circuit will hold the voltage level until it is time to take the next sample at time $2t_s$, the new sample will be classified as a 0 or 1, the voltage level will hold until the next sample, and the process is continued. This process provides the computer with a stream of binary input which it can understand. Figure 2.20 shows how the signal from Figure 2.18 would appear using one bit (0,1) quantization.

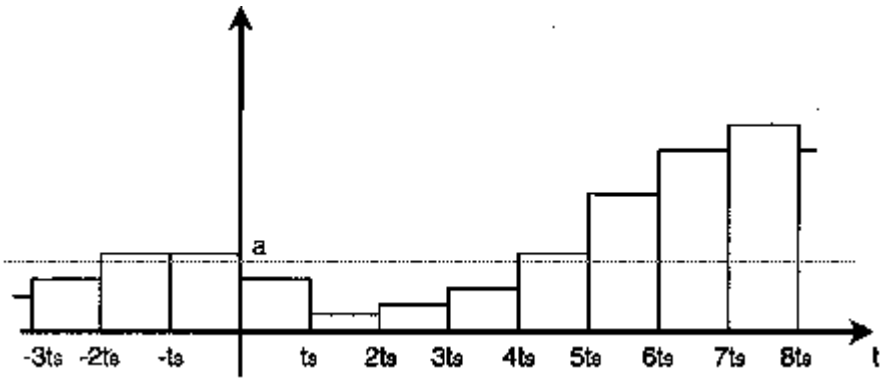

Figure 2.19 Sampled version of time signal using a sample and hold circuit (From Marven, 1996)

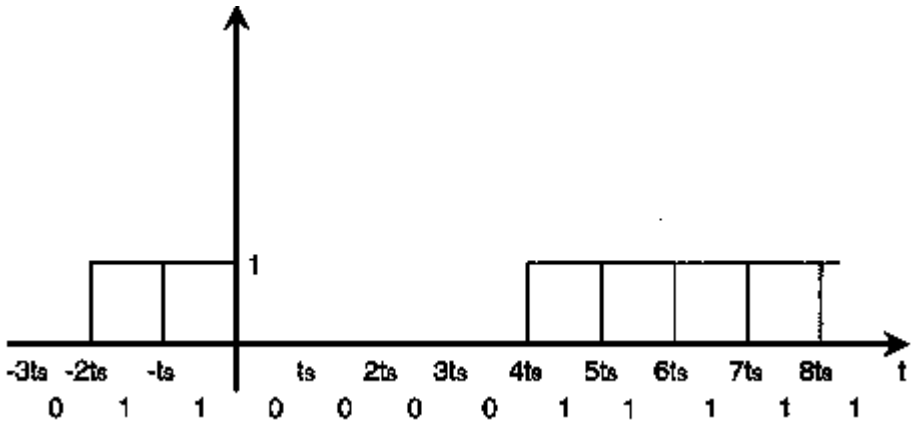

Figure 2.20 One bit quantization of input signal (From Marven, 1996)

The simple one bit quantization example did not really capture the input signal very well. To improve the accuracy of the digital representation more than two levels need to be used to describe the voltage of the input signal. Figure 2.21 shows how the input signal would appear if a two bit quantization scheme is used. When two bits are used four combinations of 0's and 1's exist which allows four levels to be used to define the input voltage (00, 01, 10, 11). The number of levels available to classify an input signal is dependent upon the number of bits and can be determined by the relationship

$$\#levels = 2^{\#bits} \tag{2.42}$$

Most signal processing systems will have an analog to digital converter that uses at least 10 to 12 bits, allowing for 1024 to 4096 levels available to classify the input voltage. Another way to think of this concept is that an input signal varying from 0 to 3.16V is broken down into 3.09mV levels using a 10 bit ADC and 0.77mV levels using a 12 bit ADC. The 3.09mV and 0.77mV levels can also be referred to as the least significant bit (LSB), and indicate how well an ADC can digitally represent an input signal (Marven, 1996).

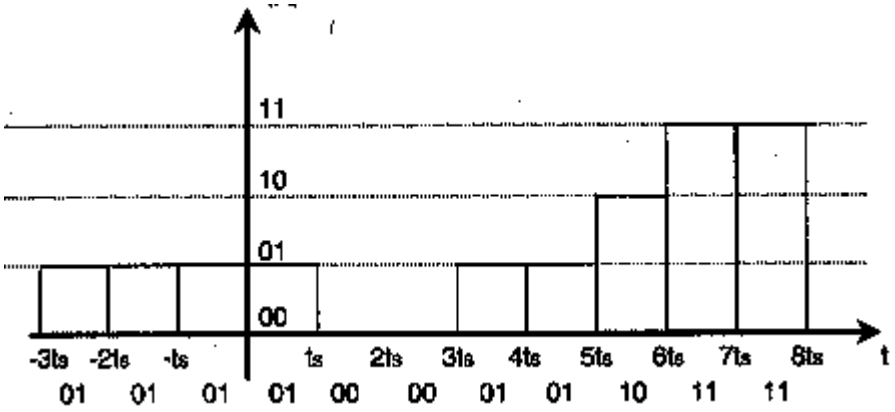

Figure 2.21 Two bit quantization of input signal (From Marven, 1996)

The difference between the quantized waveform and the original input signal is called quantization error. Figure 2.22 shows the quantization error that resulted from modeling the input signal from Figure 2.18 using two bit quantization. Quantization error produces an effect called quantization noise. As long as the ADC has a sufficient number of bits available to classify the input signal the effect of quantization noise is negligible when compared to other sources of noise typically encountered (Marven, 1996).

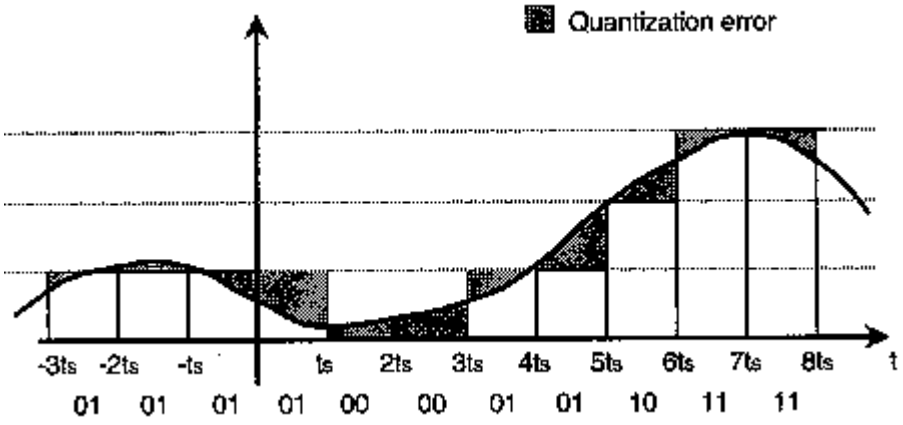

Figure 2.22 Comparison of original input signal to two bit quantized waveform (From Marven, 1996)

2.2.2.3 Windowing and Leakage

Although windowing and leakage are not actually a part of the analog to digital conversion process, they are included in this section because they are issues that arise due to the need for a discrete number of points to model an analog input. When the FFT is computed it operates on a time record composed of N equally spaced samples. To bypass the assumption that the integral used in the FFT must be carried out for an infinite amount of time (section 2.2.1.4) an assumption must be made that this time record exactly repeats itself as a function of time. If the FFT is performed on a non-periodic time record, a phenomenon known as leakage will occur that will cause distortions of the frequency domain predicted for the time record. Figure 2.23 shows a sine wave whose actual input is periodic, but whose time record is not. If the FFT performs its operations based on the assumed input shown in 2.23c, leakage error will occur.

The phenomenon of leakage is defined as a translation of energy from the actual frequencies present in the input signal to nearby frequencies (Foti, 2000). The translation of energy is how the FFT accounts for either non-periodic time records, or poor

frequency resolution. Leakage from poor frequency resolution results because; if frequencies present in the original signal are not present in the discrete frequency domain

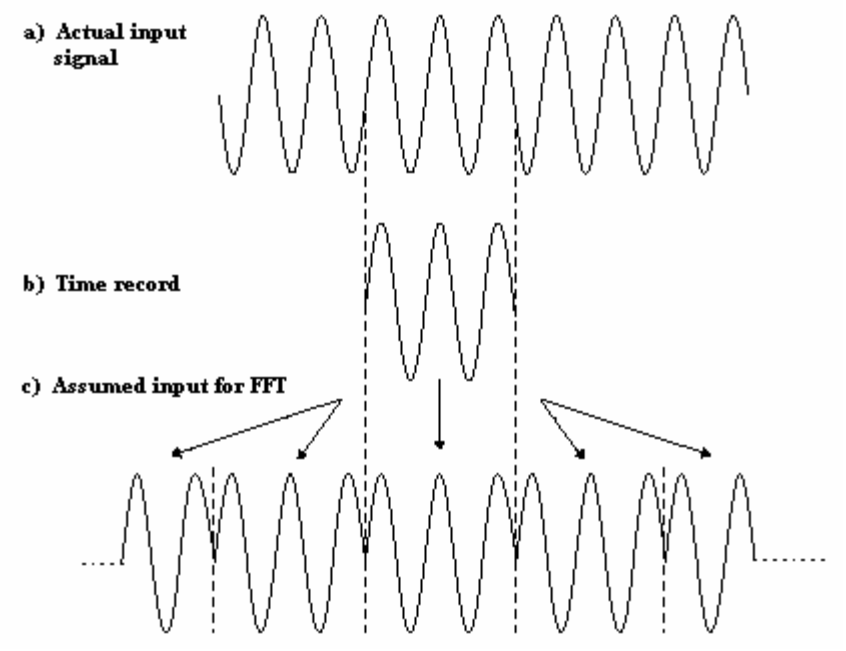

Figure 2.23 Effect of time record on a periodic signal (From Agilent Technologies, 2000)

generated, the associated energy is assigned to a nearby frequency. This problem can be avoided by having enough frequency lines to define the domain. Leakage due to non-periodic time records results because the FFT is forced to introduce false high frequency components to compensate for sharp breaks between the beginning and ending of linked time records (Agilent Technologies, 2000).

To solve the problem of non-periodic time records, a process called windowing is used. Windowing works by forcing a time record to become periodic through a weighting process. A variety of windowing functions exist depending upon the type of signal to be analyzed, and a complete discussion would become repetitive. The transient

signal is the signal type used for SASW testing, therefore the remainder of this section will focus on aspects of windowing that apply to transient signals.

If the time record used to record a transient signal is long enough to completely capture the signal the uniform windowing function is applied. A uniform window equally weights all of the data, and is basically the same as applying no window at all. The reason a signal of this type needs no window is that if it is assumed to repeat itself as a function of time the original signal is not distorted. Figure 2.24 shows a transient signal which dies out in the time record. This type of signal can be referred to as self-windowing.

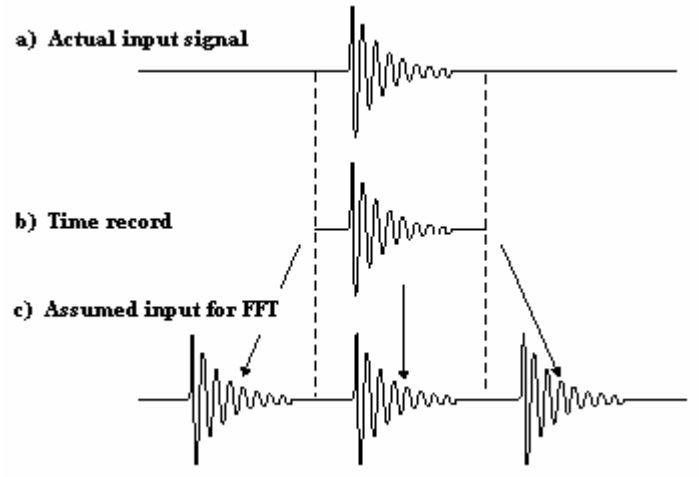

Figure 2.24 Effect of time record on a transient signal (From Agilent Technologies, 2000)

If, however, the transient does not decay to zero by the end of the time record, a windowing function becomes necessary. In this case a window called the response window is used to force the tail end of the signal to a zero value. Figure 2.25 shows this situation. By forcing the end of the transient to zero no leakage will occur in the obtained

frequency domain. This type of window may also be used to correct a signal if excessive noise causes truncation errors (Foti, 2000).

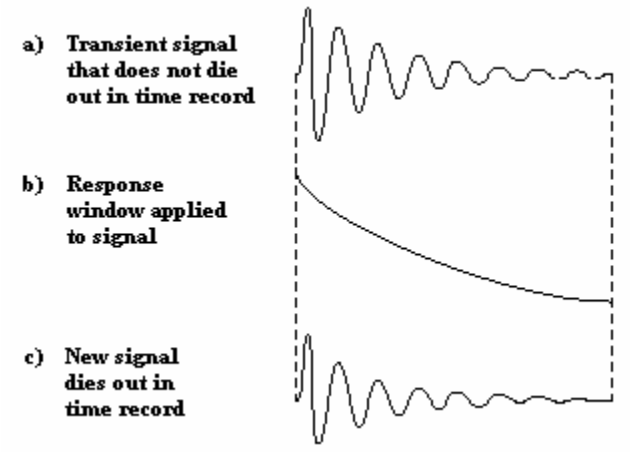

Figure 2.25 Response windowing function applied to a transient signal (From Agilent Technologies, 2000)

2.2.2.4 Resolution

It has been established that the FFT is a method of transforming a time record composed of N equally spaced samples into a frequency domain representation of the original signal. The amount of time taken between successive measurements, or sampling frequency, therefore determines the resolution of the digital version of the time domain of the signal. As was shown in the aliasing example, the shorter the sampling frequency, the better the representation (resolution) of the original signal in the time domain.

Resolution in the frequency domain is determined by the total length of the time record. The resolution in the frequency domain is closely related to the resolution in the time domain (Foti, 2000), and the relationship is defined by the equation

$$\Delta f = \frac{1}{N\Delta t} \tag{2.43}$$

Equation 2.43 indicates that there is a trade-off in resolutions for a fixed number of samples N. This is an important relationship because if good resolution is sought in one domain poor resolution in the other domain may result. In SASW testing good resolution in the frequency domain is important, and therefore good resolution of the time domain signal may not be realized. The poor definition of the time domain signal is not a significant problem, however, as long as the minimum sampling frequency needed to prevent aliasing is met (Nazarian, 1984).

2.2.3 Spectral Analysis

Up to this point this discussion has been concerned with a single signal that is recorded in the time domain, and then transformed into the frequency domain via Fourier analysis. Due to the random nature of physical signals (including those used in SASW analysis) it is often necessary to obtain average values that are more stable to provide meaningful interpretations of signals (Beauchamp, 1979). It is also common to investigate the similarities that exist between signals. Investigating two signals allows for 2 port network analysis. When obtaining average values to describe signals, or comparing signals to one another, it becomes necessary to employ statistical methods. Spectral analysis is the title given to a set of statistical methods used to analyze signals in the frequency domain.

The first topic covered in this section is network analysis. Network analysis is the general analysis method employed to perform spectral analysis of surface waves. The spectral analysis functions used during network analysis are then described in sections 2.2.3.2 through 2.2.3.6. These spectral analysis functions are the foundation for SASW testing and are used extensively throughout this research.

2.2.3.1 Network Analysis

Network analysis in its broadest definition is the process of determining how a system responds to a given input. 2 port network analysis evaluates the behavior of a system by monitoring the response that occurs at a second port due to an input at the first port. Another way of writing this is that response x will occur due to input y. If the condition of linearity is imposed network analysis becomes even more powerful, allowing the principle of superposition to be employed. Now not only will response x occur due to input y, and response q occur to input p; but if y and p are input simultaneously the response will be equal to x + q. Now the response of a linear network can be said to be the sum of the responses to each component of the input (Agilent Technologies, 2000).

This type of analysis is directly analogous to the method used to perform SASW testing. In SASW testing the network is the pavement system and a seismic disturbance resulting from a vertical impact is the input. The properties of the pavement system are evaluated by comparing the output signal measured from one transducer to the input signal measured from another transducer. The pavement system is considered to behave linearly which allows the principle of superposition to apply. Figure 2.26a shows the idealized network analysis system.

The actual system encountered in practice is shown in Figure 2.26b. This system takes into account the presence of background noise. To reduce the effect of background noise an averaging technique is often used. The reason that averaging is effective in

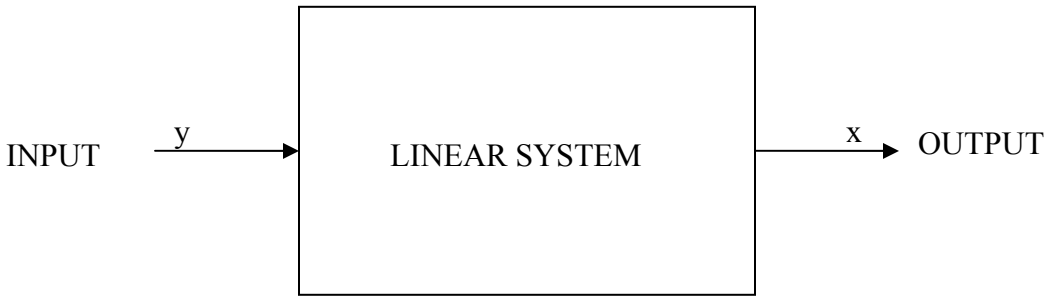

a) Idealized linear system

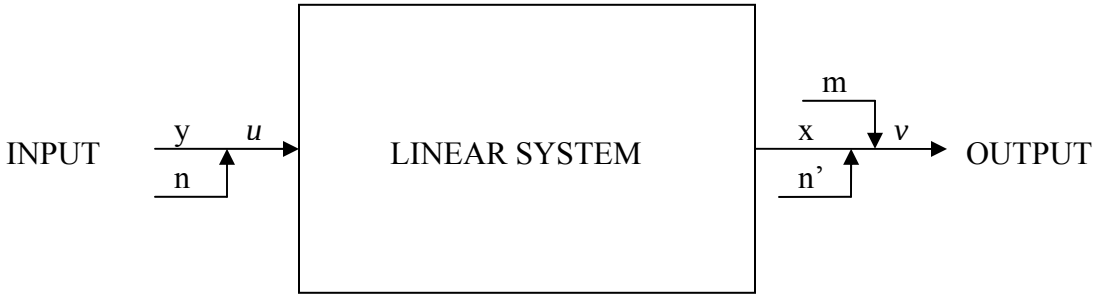

a) Actual linear system

y = Input from experiment
x = Output from experiment
n = Noise present at input
n' = Output caused by noise present at input
m = Noise present at output
u = y + n = Actual input
v = x + m + n = Actual output

Figure 2.26 Idealized linear system (a) and actual linear system (b)

eliminating the effects of background noise stems from the assumptions that background noise is random in nature and the input signal that is repeatable. The effects of an averaged repeatable input signal on a linear network will tend toward the true value of the input signal, while the effects of the random background noise averaged over time will tend towards zero. Eliminating the effects of background noise by averaging allows the actual system being tested to be approximated using the idealized system (Nazarian, 1984).

2.2.3.2 Linear Spectrum

The basic information required to perform spectral analysis is the linear spectrum of an input signal, an output signal, or both an input and an output signal. The linear spectrum is nothing more than the Fourier transform of a signal, and is called the linear spectrum because each frequency component is represented as a line in the frequency domain. The linear spectrum of a signal x(t) is typically denoted $S_x(f)$ and is defined as

$$S_x(f) = \int_{-\infty}^{\infty} x(t) e^{-j2\pi mt} \cdot dt \tag{2.44}$$

The linear spectrum contains both magnitude and absolute phase information for each of the frequency components of the frequency range (bandwidth) over which the measurement is taken (Heisey, 1982).

2.2.3.3 Auto Spectrum

The auto spectrum of a signal defines the power of a signal at each frequency over the measurement bandwidth. The auto spectrum is calculated by multiplying the linear spectrum by its complex conjugate. Multiplying the linear spectrum by its complex conjugate results in squaring the magnitude and negating the phase at each frequency.

Because of this, the auto spectrum is always real and all phase information is lost. $G_{xx}(f)$ is the symbol used to define the auto spectrum of signal x(t), and is represented by the equation

$$G_{xx}(f) = S_x(f) \cdot S^*_x(f) \tag{2.45}$$

where $S^*_x(f)$ = complex conjugate of $S_x(f)$

The auto spectrum measurement is performed on a single signal and can only be used when phase information is not required. However, an advantage of the auto spectrum measurement is that because no phase information is recorded no synchronizing trigger is necessary (Nazarian, 1984).

2.2.3.4 Cross Spectrum

A common goal in signal analysis is to investigate the amount of similarity that exists between two signals. To accomplish this task the cross spectrum measurement can be used. The cross spectrum is defined as the Fourier transform of the cross-correlation function performed between two signals x(t) and y(t). Mathematically, the cross spectrum G_{xy} is represented by the equation

$$G_{yx} = S_y(f) \cdot S^*_x(f) \tag{2.46}$$

Equation 2.46 states that the cross spectrum is found by multiplying the linear spectrum of output signal by the complex conjugate of the linear spectrum of the input signal. The cross spectrum is a complex function consisting of both magnitude and phase components. The magnitude of G_{yx} is the mutual power between the input and output signals and can be used to identify the predominant frequencies the two signals have in common. The phase of Gyx is a relative phase, or phase difference, between the two signals. Phase differences arise due to time delays, propagation delays, or varying wave

paths between points of measurement (Heisey, 1982). Because the phase is a relative phase, a synchronized trigger does not have to be used to perform measurements.

2.2.3.5 Frequency Response

The frequency response of a system is found by comparing the output signal from a system to the input signal applied to the system. The response of a linear system to a sine wave input can be shown to be a sine wave of the same frequency. The output sine wave will have a new amplitude that is proportional to the amplitude of the input sine wave, and the phase of the new sine wave will be shifted an amount that is dependent upon its frequency (Agilent Technologies, 2000). This concept is shown in Figure 2.27.

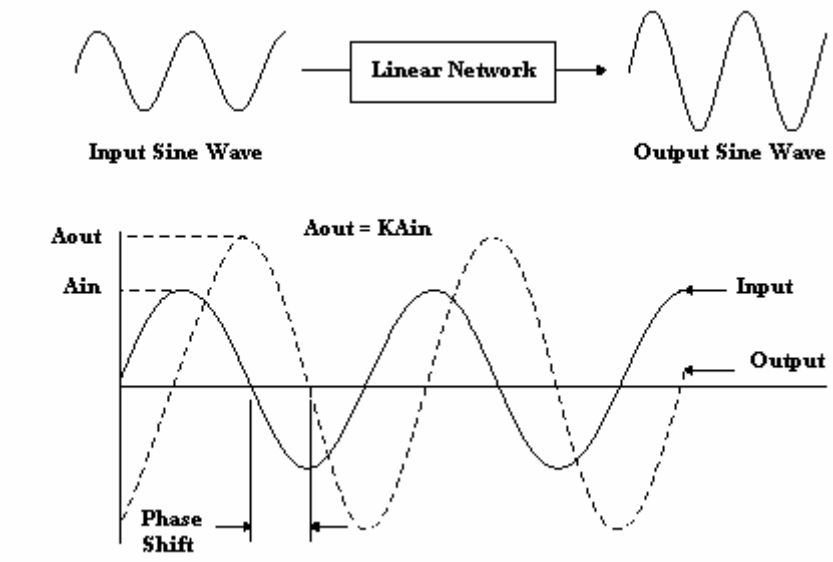

Figure 2.27 Response of a linear network to a single sine wave input signal (From Agilent Technologies, 2000)

To extend this concept, remember that any input signal x can be broken down into a series of sine waves. It has also been stated that the total response of a linear network is simply the sum of the responses of the linear network to the individual components of the input. These two facts lead to the conclusion that if the response of a network to each

sine wave component of the input is known the output can be predicted. To find the response of the network to any given sine wave, the frequency of the sine wave shown in Figure 2.27 is varied. As the frequency is varied the amplitude proportionality factor (gain) and amount of phase shift will change. The curves that represent the change of gain and phase shift as a function of the input frequency are called the frequency response function (Agilent Technologies, 2000). The frequency response is a property of a linear network that does not depend upon the stimulus. The frequency response can often be used to evaluate system properties such as impedance, dynamic stiffness, natural frequencies, and damping coefficients (Heisey, 1982).

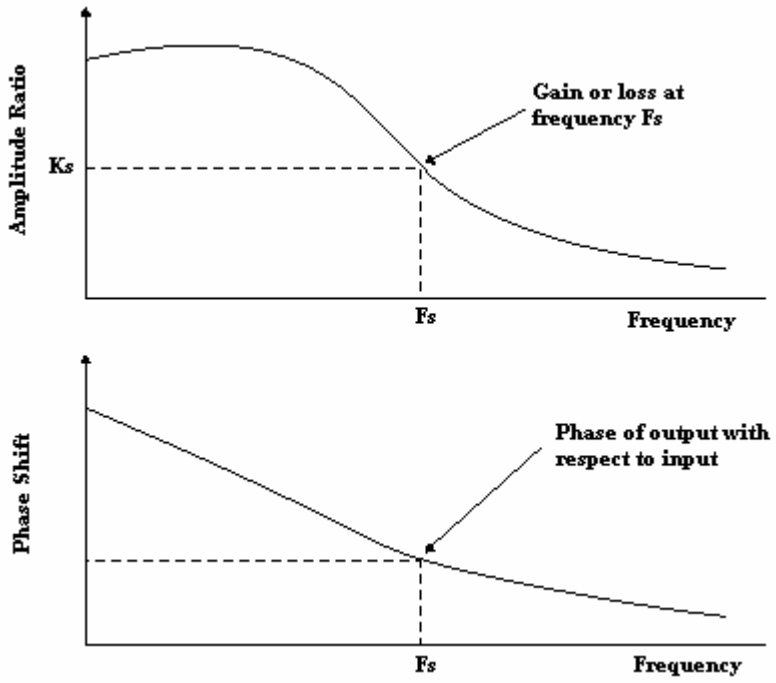

Figure 2.28 Frequency response components of a linear network (From Agilent Technologies, 2000)

Mathematically the frequency response function H(f) is defined as dividing the linear spectrum of the output by the linear spectrum of the input

$$H(f) = \frac{S_y(f)}{S_x(f)} \tag{2.47}$$

The frequency response function can also be shown to be the cross spectrum between signals x(t) and y(t) that has been normalized by the auto spectrum of the input G_{xx}. The frequency response function consists of both magnitude and phase components, as shown in Figure 2.28. The magnitude is the magnitude of the cross spectrum normalized by the magnitude of the auto spectrum. The phase component contains exactly the same phase information as the cross spectrum (Nazarian, 1984).

2.2.3.6 Coherence

The purpose of the coherence function is to provide a method to check the validity of the frequency response function (Labview Measurements Manual, 2000). Coherence measures the power present in the output signal that is caused by the power in the input signal. The term coherence is used because it is the output power that is coherent with the input power. The symbol γ^2 is used to represent coherence, and is defined in equation form as

$$\gamma^2 = \frac{G_{yx}(f) \cdot G^*_{yx}(f)}{G_{xx}(f) \cdot G_{yy}(f)} \tag{2.48}$$

γ^2 is the correlation coefficient between two signals x(t) and y(t) that shows how closely related they are. If the coherence is equal to one then all of the output power at that frequency is due to the input power. If, however, the coherence is equal to zero none of the output power at that frequency is associated with the input power. Values of coherence close to one indicate that high quality measurements are being taken. Low values of coherence are often obtained due to one of the following problems (Heisey, 1982):

1) Multiple input signals into the system that are not being measured
2) Presence of background noise
3) Low resolution in the frequency bandwidth
4) Waves in the zone of low coherence have not been properly excited

2.3 Literature Review Part III: Spectral Analysis of Surface Waves Approach

The purpose of this part of the literature review is to present how the spectral analysis of surface waves technique combines the seismic wave theory and the signal processing techniques, presented in parts I and II of the literature review, to allow for evaluation of the properties of layered pavement systems. SASW testing consists of three primary stages. The first stage of SASW testing is to measure the passage of seismic waves created by a transient impact on the surface of a pavement. This stage is described in detail in Chapter 3, and is only addressed peripherally in this part of the report. The next stage of SASW testing is to construct a Rayleigh wave velocity versus wavelength plot, called a dispersion curve, from the field measurements performed during stage one. This topic is the focus of section 2.3.1. The last stage taken in SASW testing is to create a dispersion curve that is a mathematical representation of the theoretical behavior of Rayleigh waves in a layered system. The shape of the theoretical dispersion curve is influenced by the thickness and elastic properties of each of the layers in the pavement system. These properties are varied until the theoretical dispersion curve matches the measured dispersion curve to estimate the properties of each layer. Section 2.3.2 addresses both how the theoretical dispersion curve is created, and what layer properties affect its shape. The approach used to estimate layer properties by matching the theoretical dispersion curve to the measured dispersion curve is discussed in section 2.3.3.

2.3.1 Experimental Dispersion Curve

In part II it was shown that the velocity of Rayleigh waves propagating in a semi-infinite elastic medium can be used to estimate the elastic properties of the medium

through which it travels. To apply this concept to the pavement systems of interest to this study, the discussion of Rayleigh wave propagation must be extended to include the effects of traveling through layered media. The first portion of this section addresses these effects, and how they change the relationships that exist between Rayleigh wave velocity and the elastic properties of the layered medium.

The second portion of this section describes two methods that can be used to measure Rayleigh waves traveling in a layered medium, allowing for the construction of an experimental dispersion curve. The first method is called the steady state vibration technique, and is conceptually simple but also very time consuming. The second method is the spectral analysis of surface waves technique, which is an improvement on the steady state technique that greatly reduces the required testing time by incorporating the aspects of signal analysis presented in part II of the literature review.

2.3.1.1 Rayleigh Waves in Layered Media

Equation 2.2 established that the velocity of any sinusoidal wave can be represented as the product of the wave's frequency and wavelength. In an ideal elastic half space material properties are constant as a function of depth. Therefore, the Rayleigh wave velocity predicted by Equation 2.2 must remain constant regardless of the frequency of the Rayleigh wave.

When the elastic properties of a system do not remain constant with depth a phenomenon known as dispersion occurs. Dispersion is the term used to describe the fact that Rayleigh wave velocity changes as a function of frequency in a vertically layered system (Foti, 2000). To understand why this phenomenon occurs, recall from section 2.1.3.2 that Rayleigh waves travel along the surface of a half space and that the particle

motion associated with the passage of the wave occurs at depths shallower than about one and a half wavelengths. Therefore, a Rayleigh wave that has a short wavelength (high frequency) will not travel through the same layers as a Rayleigh wave that has a long wavelength (low frequency) in a system that consists of horizontally stacked layers. Figure 2.29 illustrates this concept.

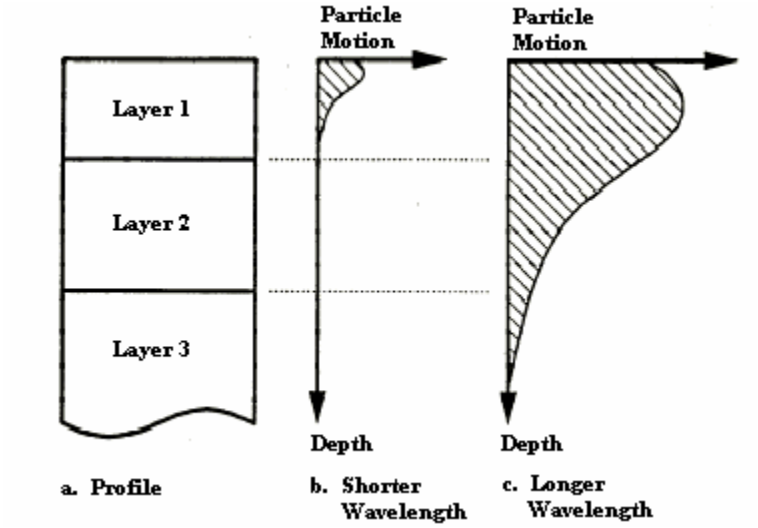

Figure 2.29 Effect of wavelength in a layered medium (from Foti, after Rix 1988)

A Rayleigh wave that has a short wavelength (high frequency) will only travel through the uppermost layer of a given profile. The velocity of these high frequency waves is solely a function of the material properties of the uppermost layer, therefore the relationships between Rayleigh wave velocity and elastic medium constants established in part I remain applicable to the top layer. As the wavelength of the Rayleigh wave is gradually increased, it penetrates increasingly deeper into the system. These lower frequency waves travel through more than one layer, each of which has its own material properties. The velocity of a Rayleigh wave which travels through more than one layer is

a function of some average value of the material properties of the layers through which it travels. In this situation the Rayleigh wave velocity no longer maintains a direct relationship to the elastic properties of any given layer. If, however, the assumption is made that the bottommost layer in the system extends to infinite depth (common assumption in SASW testing) the velocity of very low frequency Rayleigh waves will approach the velocity predicted by the elastic properties of the bottom layer alone. This occurs because the majority of the low frequency Rayleigh wave travels through the bottom layer, which heavily weights the averaged material properties towards those of the bottom layer (Foti, 2000).

A plot of the change in Rayleigh wave velocity as a function of wavelength (frequency) is called a dispersion curve. The shape of the dispersion curve is closely related to the stiffness profile of the system (Nazarian, 1984). Two major types of dispersion curves are typically obtained, depending on the type of site under investigation. Sites that have profiles in which stiffness increases with depth are said to be normally dispersive. Many sites consisting of multiple soil layers exhibit this type of profile. Sites that have profiles in which stiffer layers are located above softer layers are called inversely dispersive. The pavement sites investigated during this study have profiles that are inversely dispersive because paving materials are stiffer than base course materials which are stiffer than subgrade materials. Figure 2.30 shows the general shapes of dispersion curves obtained from sites with normally dispersive profiles (a) and from sites having inversely dispersive profiles (b).

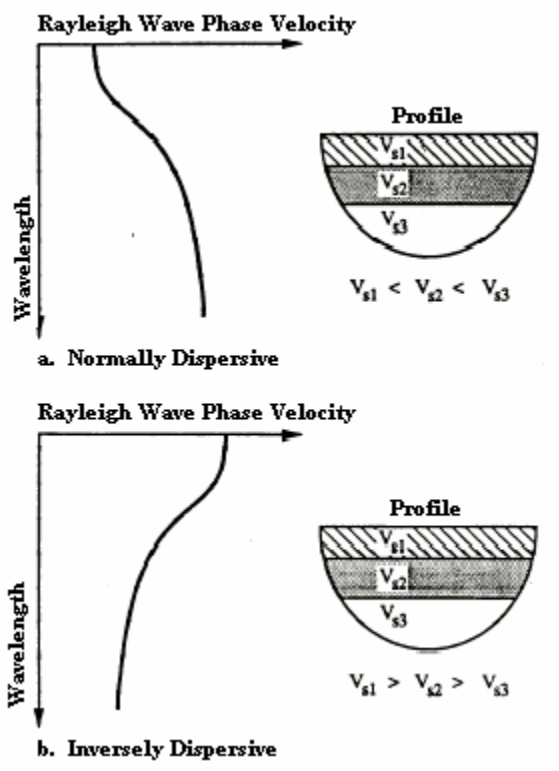

Figure 2.30 Typical shape of dispersion curves obtained from normally and inversely dispersive profiles (From Foti, after Rix 1988)

2.3.1.2 Determination of the Experimental Dispersion Curve

The simplest method used to experimentally determine the shape of the dispersion curve for a site is the steady state vibration technique. To perform this method at a pavement site, a sinusoidal wave generator is used to create a Rayleigh wave of known frequency. The wavelength of the Rayleigh wave is found by moving receivers that detect vertical motion along the pavement surface to find the distance between successive troughs or peaks of the generated wave (Richart et. al, 1970) . Once both the frequency and the wavelength are known, the velocity of the Rayleigh wave can be calculated using Equation 2.2. The combination of the velocity calculated and the wavelength measured gives one point on the dispersion curve. If this procedure is repeated using a large

number of input frequencies, a dispersion curve can be created. Figure 2.31 is a depiction of the steady state technique.

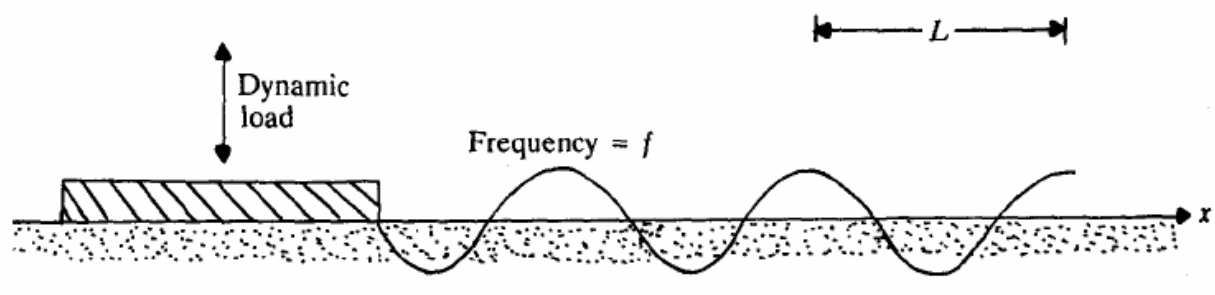

Figure 2.31 Concept of the steady state vibration technique to construct a dispersion curve (from Das, 1992)

Although the steady state method described above is a conceptually simple method that can be used to experimentally measure a dispersion curve, it is rarely utilized because it is very time consuming. A large number of frequencies have to be generated and measured to adequately define the dispersion curve at any given site (Richart et. a. 1970). To develop the steady state method into a more practical testing procedure, concepts of signal processing (presented in part II) are incorporated into the procedure. Combining signal processing with the steady state technique yields the spectral analysis of surface waves method.

Experimental determination of a dispersion curve using spectral analysis of surface wave testing is conceptually very similar to that of the steady state method. The primary difference is that a transient impact containing a large number of Rayleigh wave frequencies is used as the source instead of a single frequency sine wave from a sine wave generator. Fourier analysis allows the transient impact to be decomposed into a series of sine waves of various frequencies. The Rayleigh wave velocity and wavelength

of each of these sine waves can be calculated from the results of spectral analysis measurements. The amount of time needed to develop a dispersion curve is greatly reduced because of the ability to analyze a wide range of frequencies simultaneously as opposed to testing each frequency individually.

To perform SASW testing a vertical transient impact generates a wavefield that is dominated by Rayleigh waves. The waves are transformed into electrical signals as they pass by two receivers spaced a known distance x apart. The electrical signals are then transmitted to a digital signal analyzer which transforms them into digital representations. Fourier analysis is then used to break both the input signal (first receiver) and output signal (second receiver) into a series of sine waves of varying frequencies. The cross power or frequency response function is calculated which provides the relative phase between the input and output signals for each frequency (Heisey, 1982). The relative phase is analogous to the amount of phase shift experienced by a sine wave of frequency (f) as it travels from the near receiver to the far receiver. This phase shift (ϕ) can be used to calculate the amount of time (t) taken by the sine wave to travel between the two receivers using Equation 2.49

$$t(f) = \frac{\phi(f)}{360 \cdot f} \tag{2.49}$$

The distance (x) between the receivers is a known value, so the velocity of the wave can now be calculated using the simple relationship

$$V_R = x / t \tag{2.50}$$

The wavelength of a wave of frequency f is then calculated using Equation 2.2. Using equations 2.49, 2.50, and 2.2 for every frequency present in the transient impact yields the information necessary to create an experimental dispersion curve for the portion of

the site located between the two receivers. To fully test a site the receiver spacing is varied, allowing for differing sampling depths to be achieved. An example that demonstrates how this procedure is used to construct an experimental dispersion curve is located in Chapter 3.

2.3.2 Theoretical Dispersion Curve

2.3.2.1 General Model

The mathematical relationships between Rayleigh wave velocity and the elastic material properties of a medium presented in section 2.1.4.2 are based on the theory of elastic waves propagating through a single medium that is both homogenous and isotropic. To obtain the theoretical dispersion curve needed for SASW analysis, wave propagation theory has to be applied to a medium that satisfactorily models the pavement sites under investigation. To obtain a reasonable theoretical model of Rayleigh wave velocity for a site, wave propagation theory is applied to the ideal layered half space described in section 2.1.1.

Figure 2.32 shows this ideal layered half space model. This model makes the assumption that the medium is composed of a horizontal stack of homogenous, isotropic, linear elastic layers. Just as for the simplified single layer model used in part II, the Rayleigh wave velocity is solved for in terms of Lame's elastic parameters μ and λ (or some equivalent representation), and density. The difference is that there are now multiple elastic parameters and densities, as well as layer thicknesses to be considered because of the introduction of multiple layers. The addition of layers makes solving for Rayleigh wave velocity much more complex, necessitating the use of a numerical solution as opposed to an analytical solution. An additional assumption that must be

made to apply wave propagation theory to this model is that only in-plane waves are present. This leads to a plane strain condition which somewhat simplifies the solution of the wave equation (Foti, 2000).

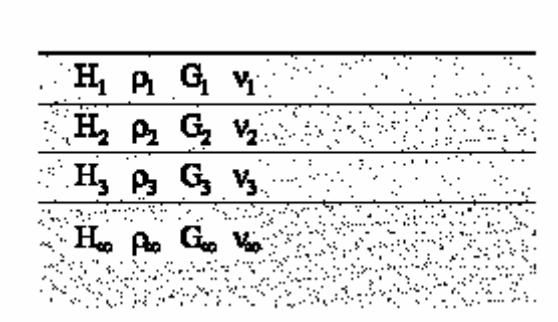

Figure 2.32 Horizontally layered model used to approximate site profiles. Note that the terms G and υ have been used instead of μ and λ (from Foti, 2000)

The general procedure (known as the propagator matrix method) used to mathematically model the profile shown in Figure 2.32 is to develop a matrix that describes Rayleigh wave behavior within a single layer, and to then establish boundary conditions between the layers that allow for a global matrix to be assembled. Different approaches can be taken to carry out this propagator-matrix procedure, the two most widely used approaches being the transfer matrix approach and the stiffness matrix approach. The differences between approaches lies in the principles used to develop the single layer matrix. The basics of the transfer matrix approach, also called the Haskell-Thompson approach, are presented below.

2.3.2.2 Haskell-Thompson Method

The first step taken in the Haskell-Thompson approach is to characterize Rayleigh wave behavior in a single layer. To accomplish this, equations that define both the

displacements and the stresses induced in the medium due to the passage of Rayleigh waves are necessary. Wave propagation theory predicts that the displacement at any point in a medium due to the passage of a Rayleigh wave can be expressed as

$$\rho \frac{\partial^2 u}{\partial t^2} = (\lambda + 2G)\frac{\partial^2 u}{\partial x^2} + (\lambda + G)\frac{\partial^2 w}{\partial x \partial z} + G\frac{\partial^2 u}{\partial z^2} \tag{2.51}$$

$$\rho \frac{\partial^2 w}{\partial t^2} = (\lambda + 2G)\frac{\partial^2 w}{\partial z^2} + (\lambda + G)\frac{\partial^2 u}{\partial x \partial z} + G\frac{\partial^2 w}{\partial x^2} \tag{2.52}$$

The variables u and w represent horizontal displacement and vertical displacement respectively (the plane strain assumption confines the problem to two dimensions), λ and G are elastic parameters, and x and z are the horizontal and vertical directions. The general solution of these two equations in terms of u and w takes the form

$$u = r_1(z;\omega,k)e^{i(kx-\omega t)} \tag{2.53}$$

$$w = ir_2(z;\omega,k)e^{i(kx-\omega t)} \tag{2.54}$$

where: r_i = coeffiecients
ω = angular frequency
k = wave number = $\frac{\omega}{V_{Phase}}$
V_{phase} = phase velocity

This allows the stresses induced on any horizontal plane (in x-z space) within the medium to be expressed as

$$\sigma = r_3(z;\omega,k)e^{i(kx-\omega t)} \tag{2.55}$$

$$\tau = ir_4(z;\omega,k)e^{i(kx-\omega t)} \tag{2.56}$$

These four equations describe the general behavior of a Rayleigh wave propagating within a single layer. The variables in the equations indicate that velocity (k

$= \omega/V_{phase}$) is now dependent on depth and frequency ($\omega = 2\pi f$). This was expected in light of the discussion presented in section 2.3.1.1.

Before extending this discussion to include multiple layers, it is convenient to represent the four equations that describe Rayleigh wave behavior in a single layer in vector form

$$S = [u, w, \sigma, \tau] \tag{2.57}$$

Now, if the boundary conditions that both the stresses and displacements at the bottom of one layer must be equal the stresses and displacements at the top of the next layer, the following equation can be developed

$$S_j^{Bottom} = S_{j+1}^{Top} \tag{2.58}$$

The transfer matrix method gets its name from a 4×4 matrix (T) that relates the stresses and displacements at the top of layer S to the stresses and displacements at any point within layer S (Nazarian et. al 1995). The original development of this matrix was performed by Haskell in 1953, and the specifics are beyond the scope of this study. The transfer matrix is a function of phase velocity, frequency, and the elastic parameters of the layers.

Utilizing this transfer matrix allows for continuity of stresses and displacements to be established throughout a layered system. This continuity allows for the stresses and displacements at any point in a layered system to be related to the stresses and displacements at the ground surface (Nazarian el. al. 1985). If the transfer matrix is used to relate the displacements and stresses at the ground surface to the displacements and stresses at the deepest interface of a system containing N layers, the equation takes the form

$$S_N^{Top} = T_{N-1}T_{N-2}\cdots T_1 S_1^{Top} \tag{2.59}$$

Section 2.1.3.1 established that all Rayleigh waves are composed of the complex interaction of P and S waves that occur at boundary surfaces. In a two-dimensional space this interaction can be decomposed into four components; upward traveling P-waves (P_{up}), downward traveling P-waves (P_{dn}) , upward traveling S-waves (S_{up}), and downward traveling S-waves (S_{dn}). Applying this concept, multiplying the transfer matrices from each layer, and expressing in matrix form gives the equation

$$\begin{bmatrix} P_{up} \\ S_{up} \\ P_{dn} \\ S_{dn} \end{bmatrix} = \begin{bmatrix} r_{11} & r_{12} & r_{13} & r_{14} \\ r_{21} & r_{22} & r_{23} & r_{24} \\ r_{31} & r_{32} & r_{33} & r_{34} \\ r_{41} & r_{42} & r_{43} & r_{44} \end{bmatrix} \begin{bmatrix} u_1 \\ w_1 \\ \sigma_1 \\ \tau_1 \end{bmatrix} \tag{2.60}$$

A phenomenon known as the radiation condition exists in layered elastic half spaces that states waves in the bottom layer (layer N) caused by an excitation at the surface of the half space can only travel downwards. Also, the boundary condition of null stress at the surface can be applied (Nazarian, 1995). Theses two conditions allow the matrix to be rewritten as

$$\begin{bmatrix} 0 \\ 0 \\ P_{dn} \\ S_{dn} \end{bmatrix} = \begin{bmatrix} r_{11} & r_{12} & r_{13} & r_{14} \\ r_{21} & r_{22} & r_{23} & r_{24} \\ r_{31} & r_{32} & r_{33} & r_{34} \\ r_{41} & r_{42} & r_{43} & r_{44} \end{bmatrix} \begin{bmatrix} u_1 \\ w_1 \\ 0 \\ 0 \end{bmatrix} \tag{2.61}$$

To solve this matrix it can be partitioned into submatrices and expressed as

$$\begin{bmatrix} 0 \\ X \end{bmatrix} = \begin{bmatrix} R_{11} & R_{12} \\ R_{21} & R_{22} \end{bmatrix} \begin{bmatrix} Y \\ 0 \end{bmatrix} \tag{2.62}$$

The only way to obtain a non-trivial answer is to set the determinant of R_{11} equal to zero

$$\det\begin{bmatrix} r_{11} & r_{12} \\ r_{21} & r_{22} \end{bmatrix} = 0 \tag{2.63}$$

Recalling that the transfer matrix was a function of phase velocity, frequency, and the elastic parameters of the layers, it can be seen that this equation depends on the same three parameters. If the elastic parameters of the layers are known, the theoretical dispersion curve can be computed by assuming values of frequency and computing the corresponding values for phase velocity.

It should be noted that due to the periodic nature of ω it may be possible to compute more than one phase velocity for any given frequency. These multiple values correspond to different modes of propagation. Physically, these different modes are the result of constructive interference (Foti, 2000). The software and analysis procedures used in this study analyze the fundamental mode only. The fundamental mode is regarded as the desired mode for SASW analysis (Nazarian et. al. 1995).

2.3.3 Estimation of Layer Properties

The process of estimating layer thicknesses and properties from an experimental dispersion curve is generally referred to as inversion. The earliest attempts to perform this process were carried out by assuming direct relationships existed between sampling depth and wavelength, and shear wave velocity and Rayleigh wave velocity (Richart et. al. 1970). These early attempts will be referred to as the "simplified inversion process" for the remainder of this study. An overview of this procedure is presented below.

The simplified inversion process related the wavelength calculated during the construction of the experimental dispersion curve to sampling depth by assuming that the effective sampling depth was equal to one-half to one-third of the wavelength. This assumption was based on the curves representing the theoretical attenuation a Rayleigh

waves as a function of depth (Figure 2.5). Referring to these curves, it can be seen that the majority of the Rayleigh wave propagates in the medium at depths of less than one wavelength. To find the average properties of the material through which the Rayleigh wave traveled, the average depth of the Rayliegh wave propagation was assumed to be appropriate. This rationale leads to the assumption of a one-half to one-third wavelength for effective sampling depth.

In section 2.1.4.2 the relationship between Rayleigh wave velocity and shear wave velocity for a given medium was established. This relationship stated that the Rayleigh wave and shear wave velocities were nearly identical, with the Rayleigh wave traveling just a bit more slowly than the shear wave. The simple inversion technique applied this relationship by assuming that the shear wave velocity could be estimated as 1.1 times the Rayleigh wave velocity obtained when constructing the experimental dispersion curve.

Two problems exist with the simplified inversion technique. The first problem is that the presence of a high velocity layer over lower velocity layers causes falsely high values to be obtained for the lower layers. This occurs because the wave velocities measured are apparent Rayleigh wave velocities, not actual Rayleigh wave velocities. The difference between apparent and actual Rayleigh wave velocities occurs because of the concept of averaging material properties, and thus the severity of the difference is influenced by both the thickness of the layers and the significance of stiffness contrasts between layers (Nazarian et. al. 1983). The second disadvantage to this method is that the effective sampling depth has to be assumed, and is not known for certain.

To overcome the shortcomings of the simplified inversion process, a method was developed to estimate layer properties from the experimental dispersion curve. The method estimates layer properties by comparing a theoretical dispersion curve constructed from an assumed profile to an experimental curve obtained from field measurements. If the theoretical curve closely matches the experimental curve, the assumed profile is assumed to be correct, and the layer properties are known. If the theoretical curve does not match the experimental curve, the assumed profile is changed and the new theoretical curve compared to the experimental curve. This process is repeated until the assumed profile produces a theoretical curve that matches the experimentally determined curve.

Section 2.3.2.2 presented the theory behind the calculation of the theoretical dispersion curve using the Haskell-Thompson matrix. It was shown that the shape of the dispersion curve is dependent upon the elastic parameters of the layers. In particular, the Poisson's ratio, mass density, and shear wave velocity (or shear modulus) define the shape, and must be known to calculate the theoretical dispersion curve. However, it has been shown by others that the effect of both Poisson's ratio and mass density are relatively negligible, and can be approximated using typical values without introducing a significant amount of error into the solution (Nazarian, 1984). Thus, shear wave velocity is the only variable that need be altered between iterations. It has been found that this method can typically predict shear wave velocities to within approximately 10% of the true value (Nazarian, 1984).

2.4 Literature Review Part IV: Case Histories

Three case histories are presented in this section to demonstrate how others have used spectral analysis of surface wave testing to determine modulus values and thicknesses for pavement sections. The case histories are presented in chronological order to show how the SASW method has become more sophisticated over time. The first example was performed by Heisey, Stokoe, and Meyer in 1982. The case study uses the simple inversion process described in section 2.3.3 to estimate the shear wave velocity profile from the measured dispersion curve. An early attempt at using the Haskell-Thompson approach is described in the second case study. The second case study was conducted in 1984 by Nazarian and Stokoe. The third case history was conducted in 1995 by Nazarian, Yuan, and Baker. The shear wave velocity profile for this case study was estimated using a program based on the Haskell-Thompson transfer matrix approach. The program fully automates the data reduction procedure, and is the same program utilized in the data reduction section of the current study. All three case histories compare the shear wave velocity profiles predicted by SASW tests to those obtained from either falling weight deflectometer (FWD) tests or cross-hole tests.

2.4.1 Site 1: I-35 in Austin, Texas (1982)

The first case study presents the findings from spectral analysis of surface wave testing conducted on a section of Interstate-35 in Austin Texas. The site profile consisted of 6.5 inches of asphalt concrete over 15 inches of crushed limestone base course compacted in three 5 inch layers. A 1 foot thick sandy subbase layer was located beneath the base course. The subgrade was described as a stiff, silty clay. A unit weight and

Poisson's ratio were assumed for each layer. Figure 2.33 shows the site profile as well as the assumed unit weights and Poisson's ratios.

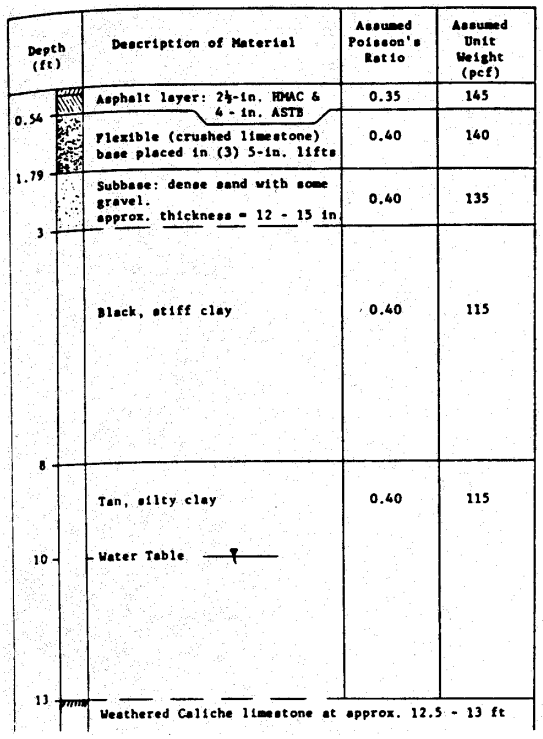

Figure 2.33 Site profile for I-35 in Austin Texas

Two different sources were used to create the surface waves measured during this experiment. The first source was a falling weight deflectometer. The FWD created a transient impact by dropping a 331 pound weight from various heights. This source was able to excite frequencies up to approximately 250 Hz, which only allowed for velocities to be obtained for depths greater than 15 inches. The second source used was a drop hammer consisting of a 6 pound steel cylindrical mass that could be dropped from any height up to 24 inches. The drop hammer was able to excite frequencies up to approximately 1600 Hz, which allowed for shallower depths to be sampled. A comparison of the phase component of the cross power spectrum for the two sources (at

an identical receiver spacing) is shown in Figure 2.34. Notice that the phase measured using the FWD as the source becomes erratic at frequencies greater than 250 Hz.

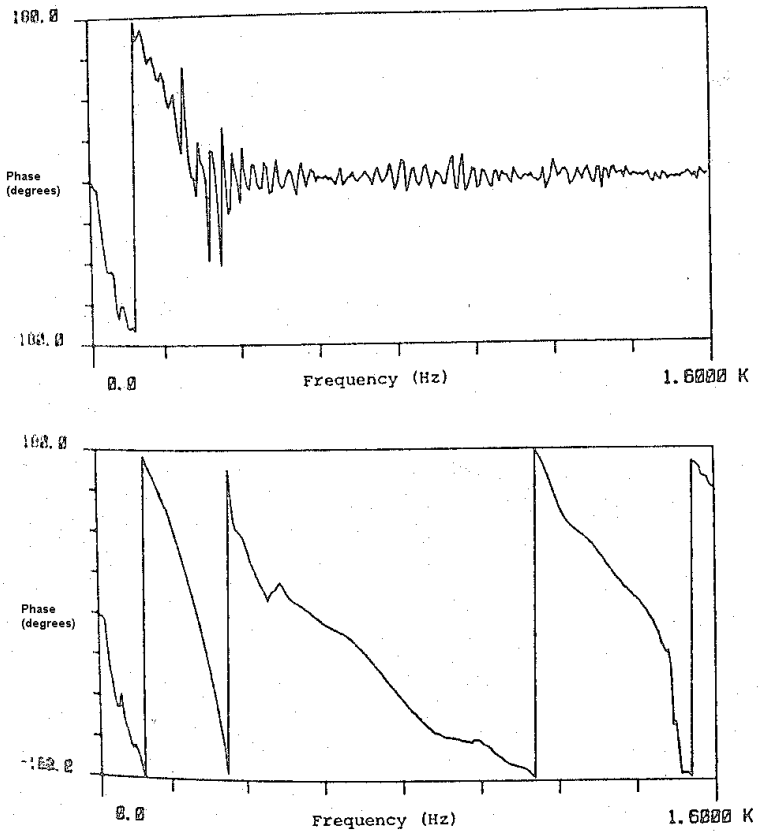

Figure 2.34 Comparison of phase component of cross power spectrum measured using FWD as the source (top) and drop hammer as the source (bottom)

Geophones were used to detect the passage of the surface waves. The geophones were mounted on steel blocks that were, in turn, epoxied to the asphalt surface. The geophones had a natural frequency of 14 Hz, and a linear response between 20 and 1600 Hz. During the test, vertical receivers were placed in a straight line running parallel to the roadway. Vertical receivers were located at distances of 1, 2, 5, and 10 feet from the source. The receiver spacing was used to name the measurements performed in the study, such that a measurement performed between a receiver located 2 feet from the source and a receiver located 5 feet from the source is denoted measurement V2-V5.

Horizontal geophones were placed at the same locations as the vertical geophones, however, data obtained from these geophones was not used to determine the shear wave velocity profile for the site.

The signals from the geophones were recorded and processed using a two channel Hewlett-Packard 5420A digital signal analyzer. This analyzer filtered the incoming signal, performed the required analog to digital conversion, made frequency domain measurements, and stored the digital signal using a magnetic cassette tape recording device. The analyzer also provided averaging and triggering capabilities. The pre-triggering option was used to ensure the incoming signal was completely captured. Each measurement was made using 5 averages. Figure 2.35 shows the configuration of the equipment used at the Austin site.

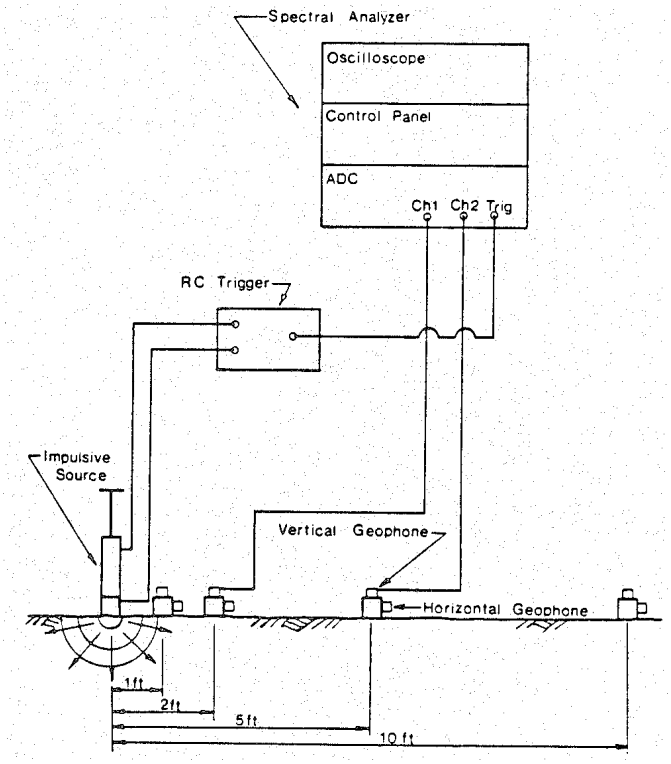

Figure 2.35 Equipment configuration at Austin site

The Rayleigh wave velocity profile for the site was constructed using three measurements where the FWD was used as the source, and one measurement where the drop hammer was used as the source. The measurements using the FWD were V1-V2 with a bandwidth of 200 Hz, V2-V5 with a bandwidth of 1600 Hz, and V2-V10 with a bandwidth of 100 Hz. The drop hammer measurement was V2-V5 with a bandwidth of 1600 Hz. The velocities obtained for each measurement are shown plotted versus depth in Figure 2.36. Depth was estimated by assuming an effective sampling depth of 1/3 of the wavelength, and the velocity is the Rayleigh wave velocity. This plot is not a true experimental dispersion curve because the wavelength has been converted to an estimated sampling depth.

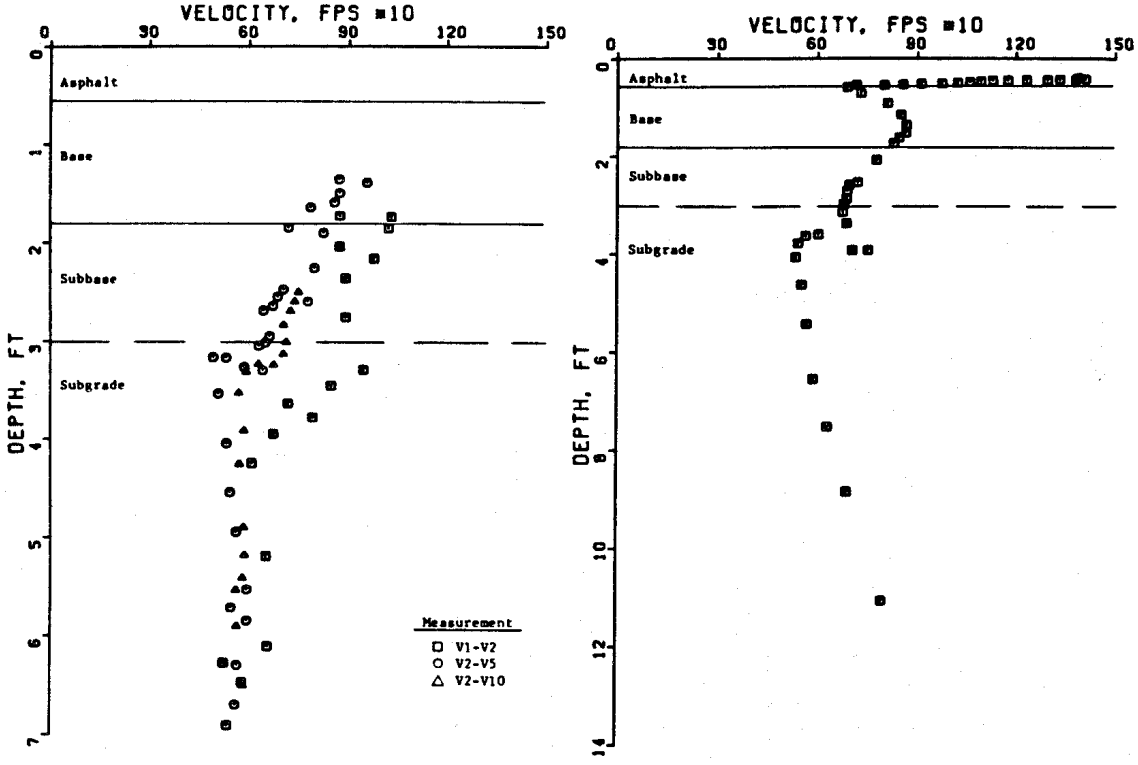

(a) FWD as source **(b) Drop hammer as source**

Figure 2.36 Rayleigh wave velocity profile

Two borings were made at the Austin site which allowed for cross-hole tests to be performed. The velocities obtained from the cross-hole tests are plotted alongside the velocities obtained from SASW testing (using both FWD and drop hammer measurements) in Figure 2.37. Table 2.2 lists the shear wave velocities obtained for each layer using SASW testing and cross-hole testing. These shear wave velocities were then used to calculated the Young's modulus for each layer. Young's modulus was also calculated using a deflection basin fitting procedure on data obtained from FWD testing. Table 2.3 shows the Young's modulus predicted by the deflection basin method and those predicted by the SASW method.

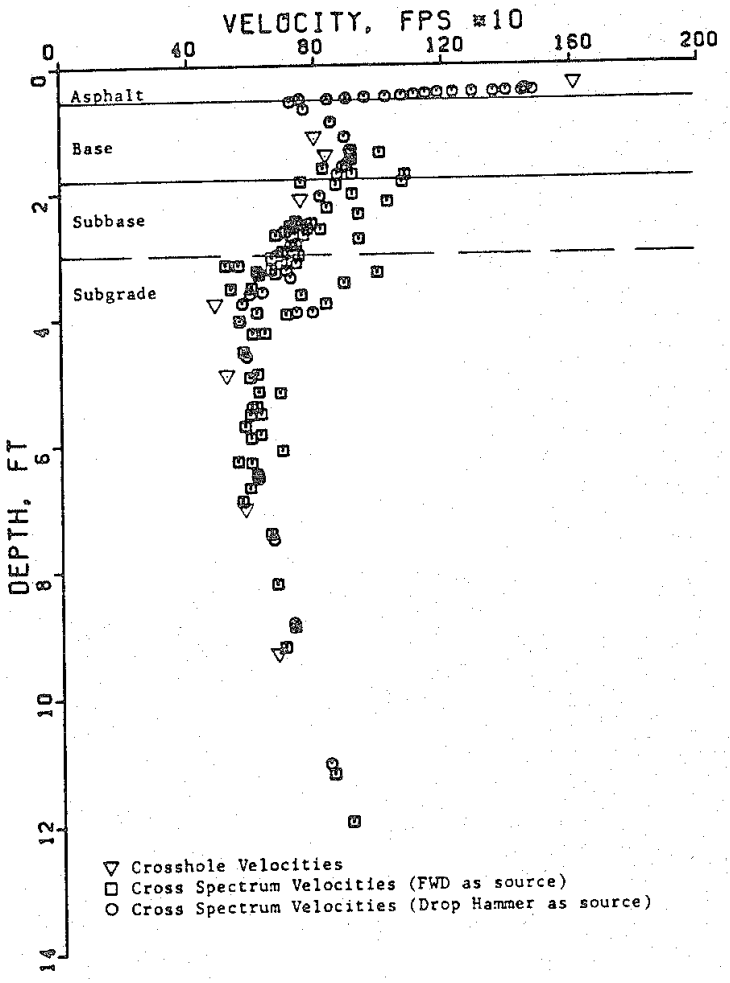

Figure 2.37 Comparison of velocities obtained from SASW testing and cross-hole testing

Table 2.2 Shear wave velocities obtained from SASW testing and cross-hole testing

Material	S-wave Velocity (ft/s)		Percentage of Difference
	Cross- Spectrum Measurements	Cross-hole Tests	
Asphalt	1500	1610	6.8
Base	925	823	12.4
Subbase	740	743	0.4
Subgrade	605	565	7.1

Table 2.3 Young's modulus predicted by SASW and FWD methods

Material	Shear Modulus (ksi)	Young's Modulus, E (ksi)	
		SASW	Deflection Basin
Asphalt	70	190	250
Base	26	72	108
Subbase	16	45	40
Subgrade	9	25	17

This case study demonstrated how the simple inversion process was used to estimate the shear wave velocities (and subsequently Young's moduli) for a four-layered flexible pavement section. Tables 2.2 and 2.3 show that the data obtained from the SASW procedure compares favorably with data from both cross-hole and FWD procedures. This agreement indicates that the method has some ability to predict pavement moduli, even though a rigorous inversion process is not used. Additionally, Figure 2.37 demonstrates that approximate layer thicknesses may in some cases be determined using this method.

2.4.2 Site 2: Tyndall Air Force Base (1984)

The second case study was performed on the concrete apron area of Tyndall Air Force base. Two different pavement sections were located on the site, and are designated as sections "A" and "B". Section A was the older of the two pavement sections and the profile consisted of 6 inches of unreinforced concrete over a sand subgrade. The overall slab dimension was 10 feet wide by 15.5 feet long. Section B contained 10 inches of

unreinforced concrete over 4 inches of cement treated base. The subgrade soil beneath section B was sand. The slab dimensions for this section were 14.5 feet wide by 25.5 feet long. Both of the sections appeared to be in good condition, and did not exhibit any severe signs of distress. The profiles for the two sections are shown in Figure 2.38.

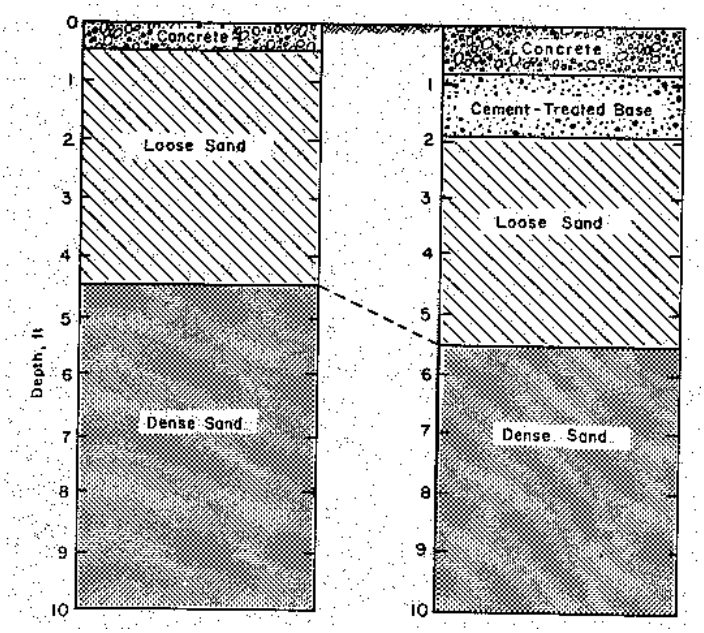

Figure 2.38 Material profiles for old pavement section A (left) and new pavement section B (right)

Three types of sources were used to generate surface waves over an appropriate frequency range. For the shorter receiver spacings (1 to 2 ft), a hammer and chisel were used to generate a signal which contained high frequency content. At slightly longer receiver spacings (4ft), a claw hammer was used. The surface waves required to evaluate the pavement section over the longest receiver spacings (8-32 ft) were produced by a 15 pound sledge hammer. Common receivers midpoint geometry was used during testing (discussed in Chapter 3), so the distance from the source to the nearest active geophone was always equal to the distance between the two geophones being used to perform the measurement.

Vertical geophones having a natural frequency of 4.5 Hz were used to sense the passage of the surface waves. Section A was tested using receivers spaced at 1, 2, 4, 14, and 24 ft. Section B was tested using receivers spaced at 1, 2, 4, 8, 16, and 32 ft. Different receiver spacings were used for each slab because of the difference in the lengths of the slabs.

A two channel spectral analyzer was used to capture the incoming time domain signals from the geophones. The bandwidth measured by the analyzer varied from 0-12,800 Hz for measurements made at 1 foot receiver spacings to 0-400 Hz for measurements made at the 32 foot receiver spacing. Fourier analysis was used to transform the recorded signals into the frequency domain so that spectral analysis could be performed. In particular, the cross power and coherence functions between the signals was determined so that an experimental dispersion curve could be calculated. The spectral analysis measurements were made on a signal averaged from five impacts. Figure 2.39 shows the equipment configuration used during testing.

Experimental dispersion curves for each of the two pavement sections were created by analyzing the phase information of the measured cross power spectrum. Each point of the dispersion curve was obtained by calculating a Rayleigh wave velocity and wavelength at each frequency, using the method presented in section 2.3.1.2. Points that did not have corresponding coherence measurements close to unity were discarded because of the likelihood of inaccuracy due to interference from background noise. Points whose wavelengths were either less than half or more than three times the distance between the receivers from which the measurement was made, were also discarded. Typical coherence and cross power spectrum measurements are shown in Figure 2.40.

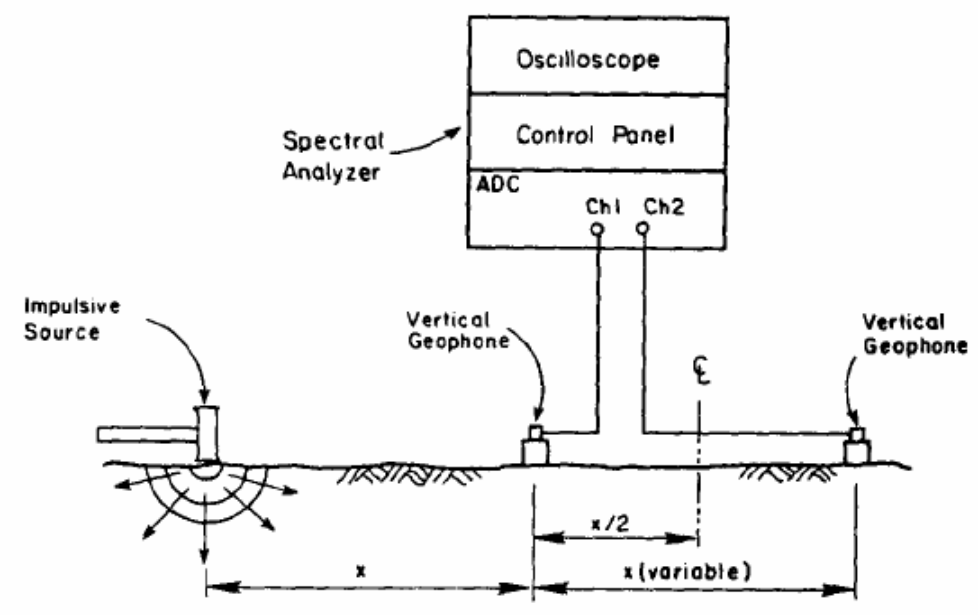

Figure 2.39 Equipment configuration used during SASW testing at Tyndall AFB

The set of calculations necessary to calculate one point on the dispersion curve is included in the figure as well. The complete experimental dispersion curve developed for pavement section A is shown in Figure 2.41.

Theoretical dispersion curves were produced for both of the pavement sections using the Haskell-Thompson transfer matrix approach. To calculate the theoretical curves, the known pavement section profiles were subdivided into a number of sublayers. Reasonable values for Poisson's ratio and mass density were assumed for each layer. Trial shear wave velocities were then picked for each layer, and the theoretical curves were calculated and compared to the experimental curves. If the two curves did not match well, the shear wave velocities of the layers were varied until the theoretical curve matched the measured curve. The final theoretical curve and the measured experimental

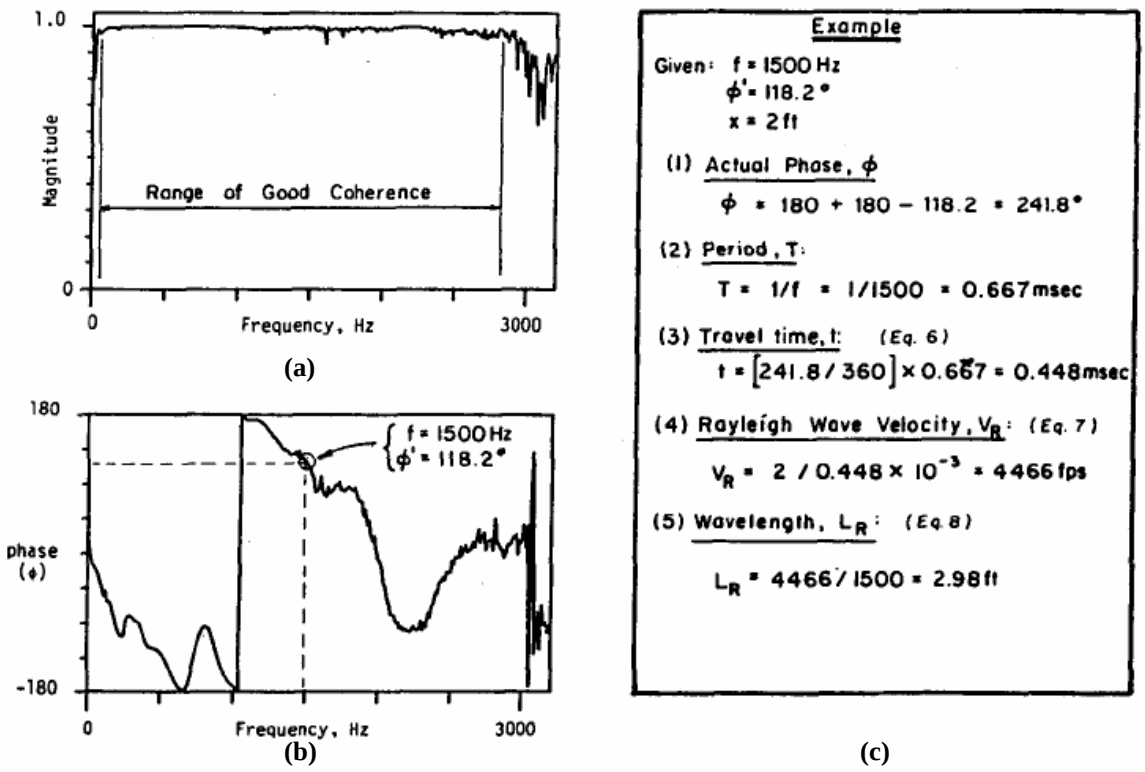

Figure 2.40 (a) Typical coherence measurement, (b) typical cross power spectrum measurement, (c) and set of calculations to compute one point on the dispersion curve

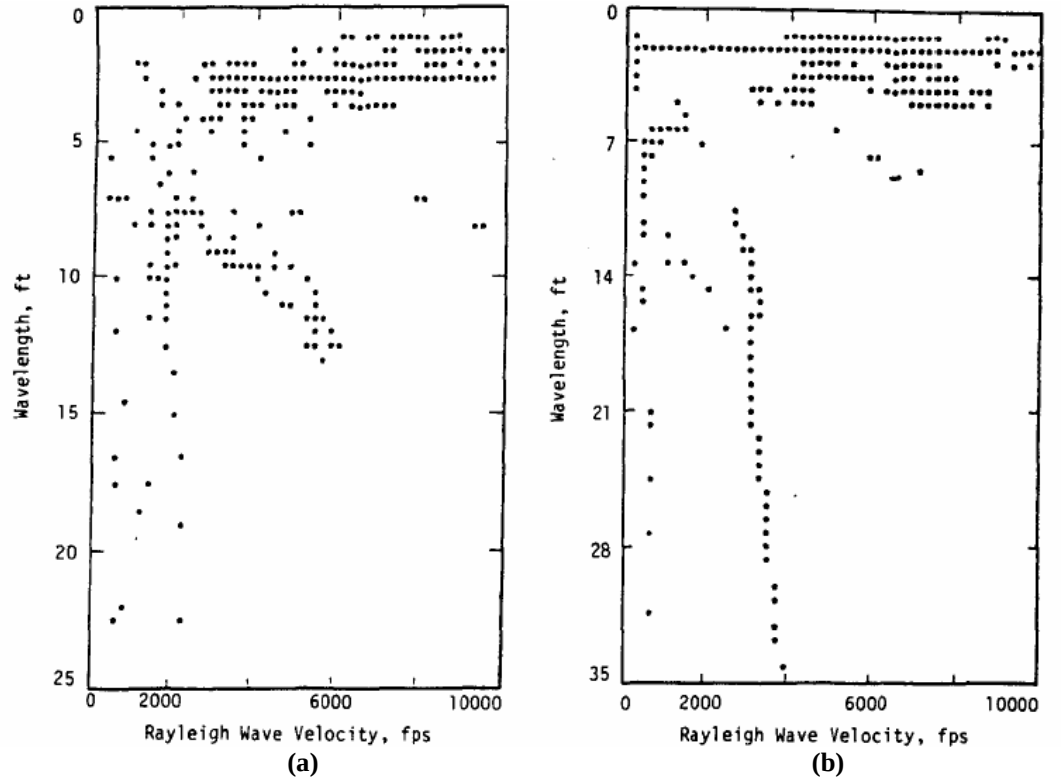

Figure 2.41 Two portions of the experimental dispersion curve for old pavement section A

curve for pavement section A are shown in Figure 2.42. It can be seen that the shape of the dispersion curve predicted by the theoretical curve closely fits the measured data points.

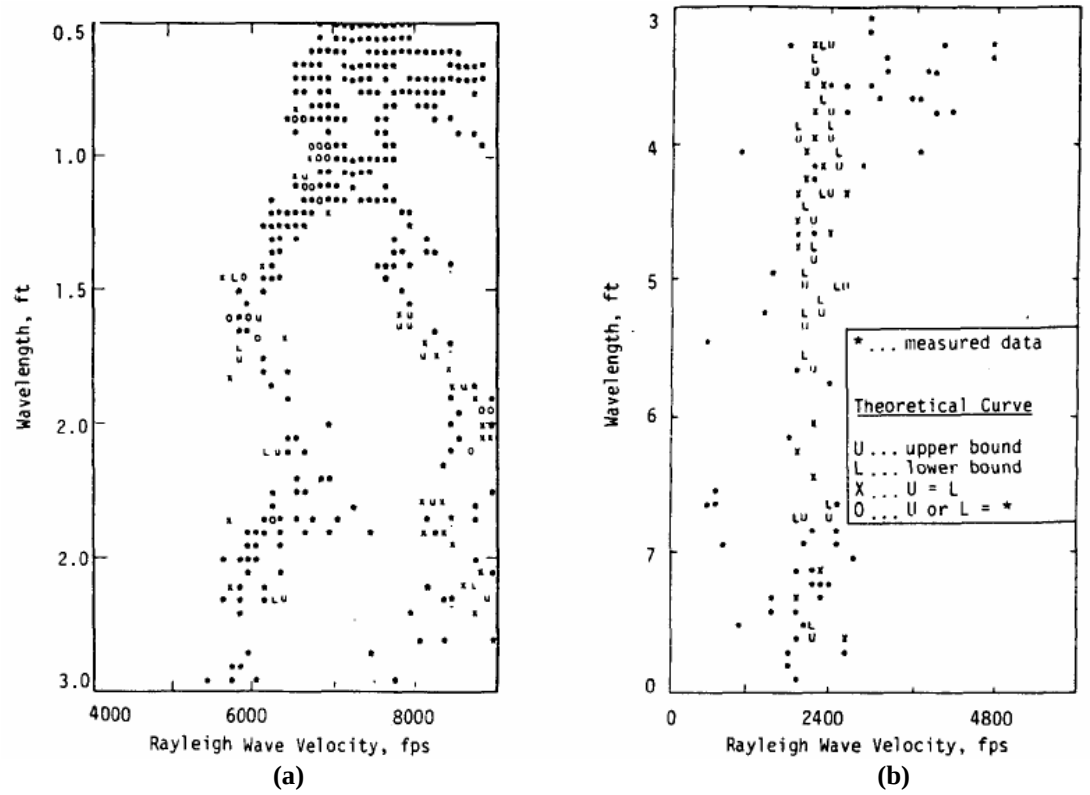

Figure 2.42 Experimental dispersion curve and final theoretical dispersion curve for old pavement section A

Cross hole testing was performed at the site to check the validity of the shear wave velocity profile obtained from the SASW procedure. The shear wave velocity profiles predicted by both the cross hole method and SASW testing are shown in Figures 2.43 and 2.44. The two profiles agree very well with one another, indicating that the SASW procedure accurately predicted the shear wave velocity of the layers. The average difference between the two profiles was found to be 10% for pavement section A, and 12% for pavement section B.

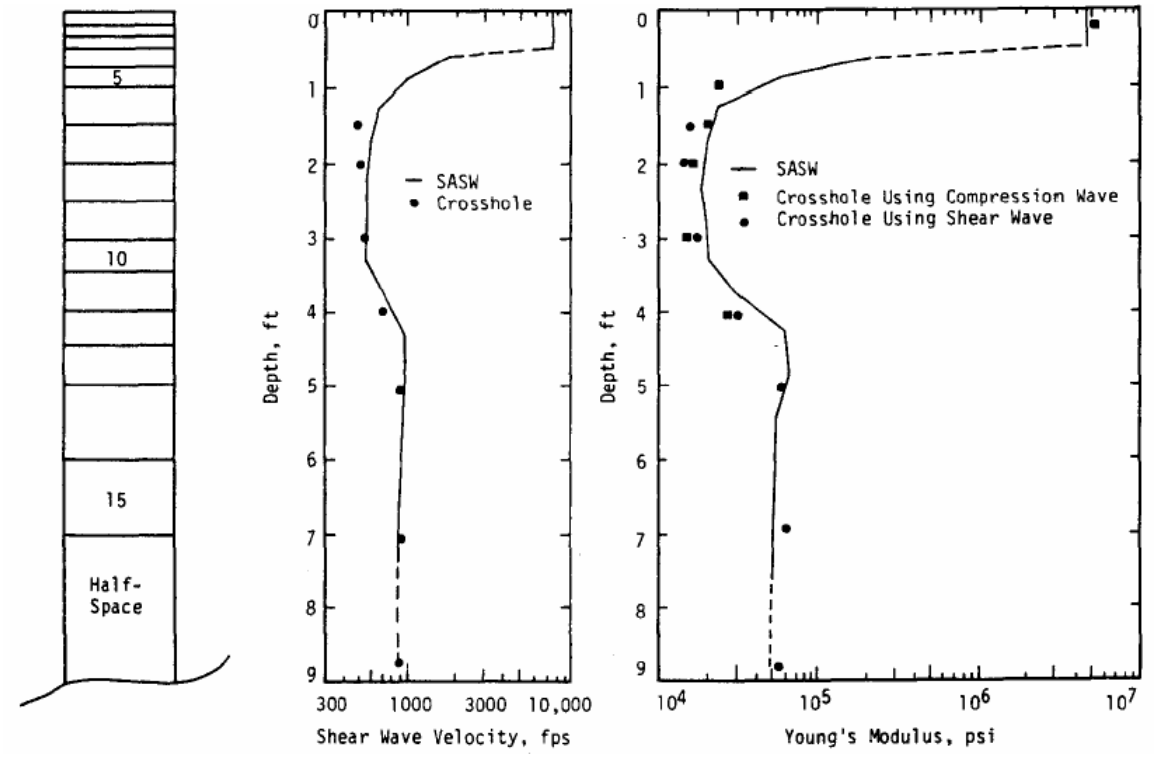

Figure 2.43 Shear wave velocity and Young's modulus profiles predicted using SASW and cross hole tests for pavement section A

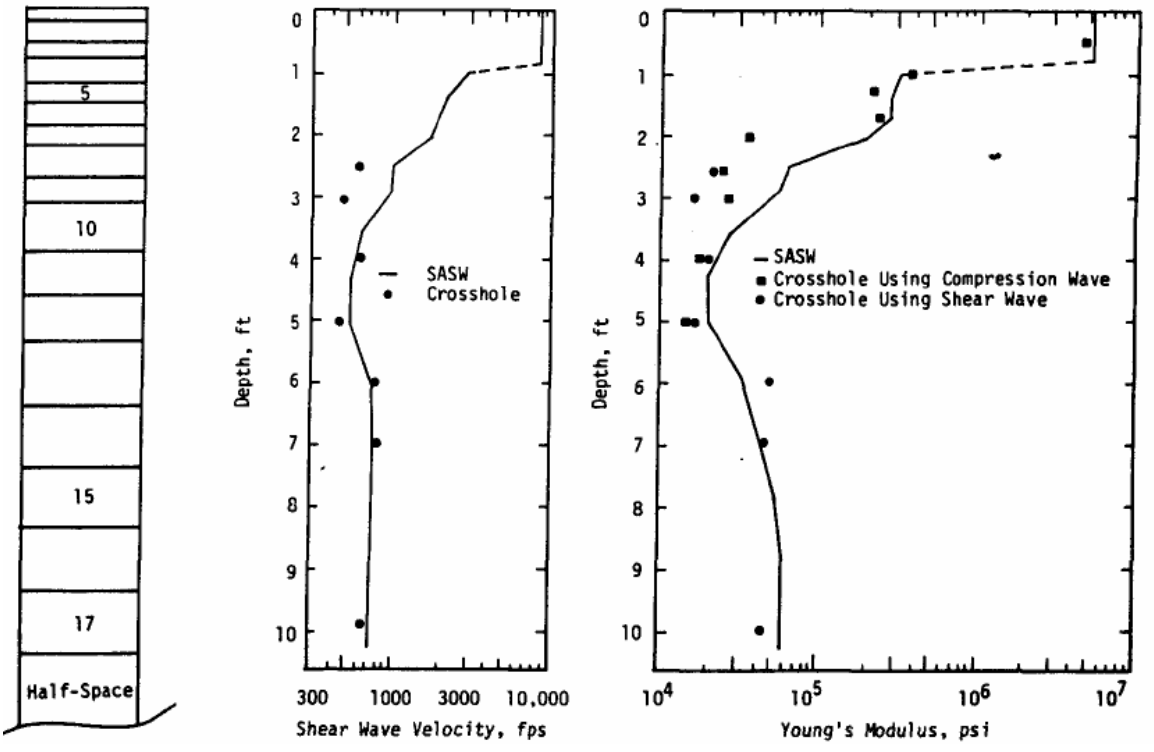

Figure 2.44 Shear wave velocity and Young's modulus profiles predicted using SASW and cross hole tests for pavement section B

This case study shows how the Haskell-Thompson transfer matrix approach was incorporated into SASW testing to allow for a more theoretically sound prediction of layer moduli. Using the transfer matrix approach allowed for elimination of most of the simplifying assumptions associated with the simplified inversion procedure. Shear wave velocity profiles, and consequently Young's moduli profiles, were predicted for two multi-layered pavement sections. The profiles that were predicted by SASW were shown to be reasonable through comparisons to profiles predicted from cross hole testing.

The testing procedure used in this case study had advantages over the procedure used in the SASW testing of I-35 presented in the first example. One of the primary advantages was that the data collection procedure was automated, allowing for a much greater number of data points to be used to determine the shear wave velocity profile. Additionally, higher frequencies were both generated and measured, which allowed for the measurement of moduli at shallower depths. The source-receiver geometry was changed to common midpoints receiver (CRMP) geometry, which has been found to reduce the scatter typically present in the data collected.

2.4.3 U.S. 69 near Lufkin Texas (1995)

The third, and final, case study took place on U.S. Highway 69 near Lufkin Texas. Construction drawings indicated that the profile consisted of 175 millimeters of asphalt, 250 millimeters of flexible ash base, and subgrade located below. Actual coring of the site, however, revealed that the asphalt layer was severely stripped with only approximately 63 mm to 75 mm of the core able to be recovered. The remainder of the asphalt layer was found to have lost its binding agent, resulting in a much softer layer.

The testing procedure used to measure the experimental dispersion curve is very similar to the procedure used in the second case study. The primary difference was that the frequency range used to determine the experimental curve was much higher than for the previous case studies. This was accomplished by both incorporating the use of accelerometers as the receiver type, and by utilizing smaller sources able to produce higher frequency waves. The spectral analysis and recording equipment used were also much more powerful, and able to handle more data than for the previous cases.

The experimental dispersion curve obtained for the Lufkin site is shown in Figure 2.45. The significant reduction in scatter over the previous case studies is, in large part, due to the acquisition program used to form the dispersion curve. The dispersion curve is no longer a truly raw experimental curve, but rather an idealized experimental curve formed during acquisition. The idealized curve is formed using a series of steps that first eliminates unwanted data such as points obtained at frequencies with low values of coherence, or points that are considered to be outliers. The program then uses a least-absolute-value-best-fit criterion to fit an idealized experimental dispersion curve to the remainder of the data points. Once this procedure is completed, a window averaging process is used to reduce the number of data points down to a few dozen, to make the inversion process manageable. The appearance of the experimental dispersion curve from Figure 2.45 after the window averaging process is completed is illustrated in Figure 2.46.

Once the idealized experimental dispersion curve was formed, a trial profile was assumed so that a theoretical dispersion curve based on the Haskell-Thompson matrix

could be calculated. The trial profile used was based on the thicknesses given in the construction drawings, and assumptions made for Poisson's ratio and unit weight.

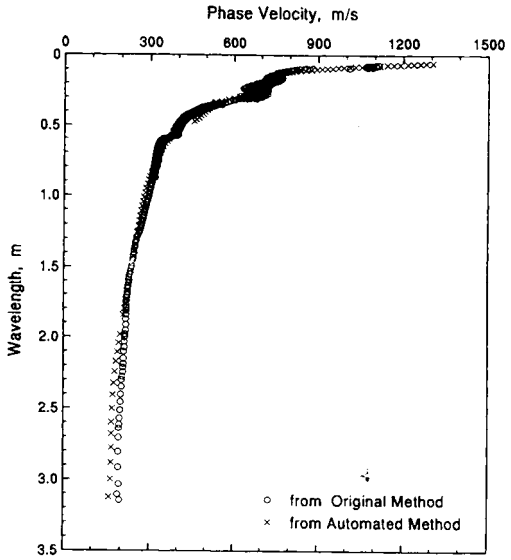

Figure 2.45 Experimental dispersion curve after unwanted data points have been removed

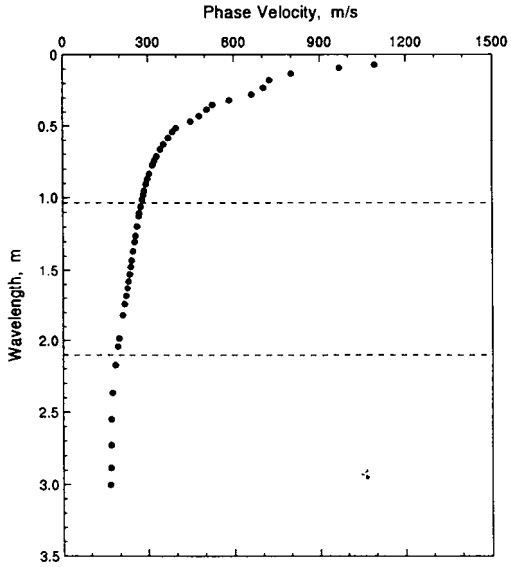

Figure 2.46 Idealized experimental dispersion curve after windowing averaging process

Iterations were made by varying the shear wave velocities and layer thickness until the theoretical dispersion curve and the idealized experimental curve matched one

another to within an acceptable amount of error. Figure 2.47 shows the initial trial profile and the final profile after the inversion process. The final theoretical dispersion curve and the idealized experimental curve are shown in Figure 2.48.

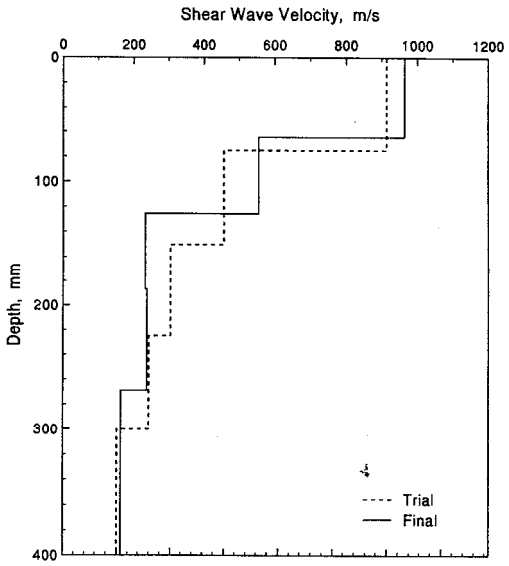

Figure 2.47 Trial and final shear wave velocity profiles

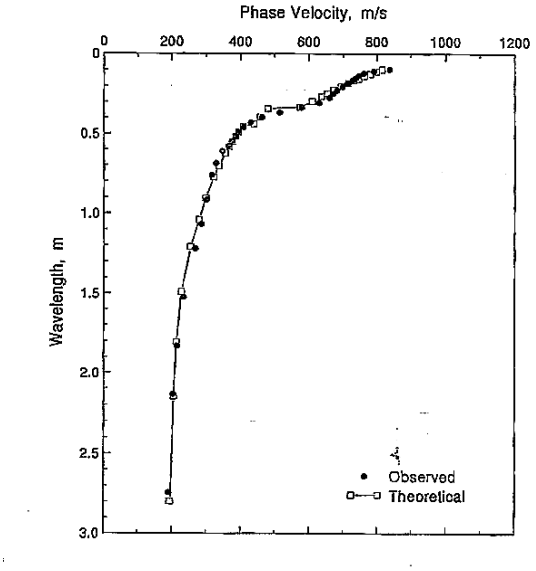

Figure 2.48 Idealized experimental dispersion curve and final theoretical dispersion curve

FWD tests were conducted at the site to provide a comparison to the SASW tests. The backcalculation of layer moduli from the raw FWD data was accomplished using program MODULUS 4.0 (Uzan et al, 1988). Three different pavement profiles were used to perform the backcalculation. The first profile used was the one specified in the construction drawings, the second profile used was obtained by analyzing the results of SASW testing, and the third profile used was the one observed during coring of the site. Table 2.4 summarizes the modulus values obtained from both SASW testing and FWD testing.

Table 2.4 Modulus values determined from SASW and FWD testing

Test Method	Young's Modulus (MPa)			
	Asphalt (intact layer)	Asphalt (stripped layer)	Base	Subgrade
SASW	4816	1603	287	147
FWD (construction drawings)	1351	N/A	42	147
FWD (SASW profile)	3500	2002	28	147
FWD (coring profile)	2261	1911	28	147

Table 2.4 shows some interesting trends. First, the subgrade modulus was predicted to be 147 MPa regardless of the method used. The modulus predicted for the base and asphalt layers, on the other hand, vary depending on the method. The asphalt modulus predicted by the SASW method was found to be substantially higher than any of the values predicted by the FWD data. The base course modulus predicted by the SASW method was much higher than that predicted by the FWD methods as well. The base course modulus predicted by the FWD methods was said to be unreasonably low for unknown reasons.

This final case study demonstrated how the data reduction phase of SASW testing can be fully automated to dramatically reduce the amount of time necessary to determine modulus and thickness profiles of pavement sections. The use of the computer program to form an idealized dispersion curve prior to performing the inversion process was the primary improvement over the procedure used in the second case study. Prior to the use of a program to form an appropriate dispersion curve, much of the data reduction process had to be completed by hand, making analysis of the data quite tedious and time consuming.

CHAPTER 3

RESEARCH METHODS

The purpose of this chapter is to discuss the procedures used to conduct the research presented in this study. This chapter is divided into three major topics. The first topic discussed is the equipment that was used to generate, analyze and record the seismic waves utilized in spectral analysis of surface waves testing, and is presented in section 3.1. The field testing procedures used during SASW testing are presented as the next major topic in section 3.2. The data reduction methods used to analyze the raw data collected in the field are discussed in section 3.3.

3.1 Equipment

The first task completed during this study was to obtain the equipment necessary to perform SASW testing. The equipment that composes a SASW testing setup consists of three major components; an impulsive source, receivers, and a data acquisition and analysis system (DAQ/DSA). Figure 3.1 shows the general configuration of the three components during field testing. Sections 3.1.1-3.1.3 describe the functions of each of the individual components, as well as the requirements that each of the components must satisfy in order to create a working SASW testing system.

3.1.1 Source

The source is the means of creating the seismic disturbance that is measured during SASW testing. The source is typically some form of hammer or weight that is used to impact the pavement, causing Rayleigh waves to propagate along the surface of

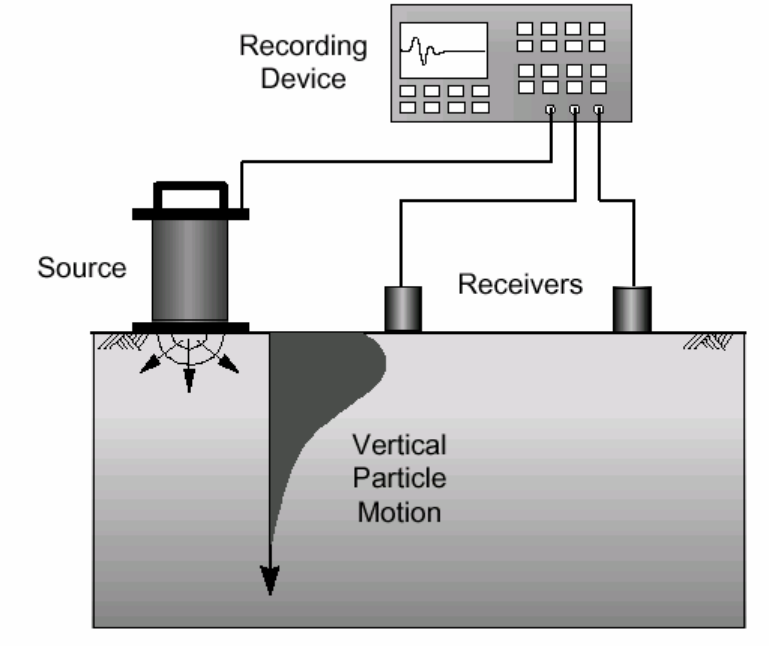

Figure 3.1 Configuration of the three major components used in SASW testing (From Zywicki, After Rix 1997)

the pavement. The source must be able to create Rayleigh waves that have an amplitude large enough to be recognized by the receivers that are used. When the distance between the source and the receivers is relatively small, the surface waves do not have to travel large distances. In this case a low energy impact that has a small amplitude can be used. As the distance between the source and the receivers increases, the amount of energy the source imparts to the pavement must be increased to prevent the Rayleigh wave amplitude from decaying to a point where it is no longer detectable when it reaches the receivers. In other words, the further the Rayleigh wave has to travel to reach the

receivers, the larger the impact must be to sustain an amplitude that the receivers can distinguish from background noise.

Because SASW analysis depends on the dispersive characteristics of Rayleigh waves, the source that is used must be able to generate a group of Rayleigh waves over a wide range of frequencies. The frequency range of interest changes as a function of the desired sampling depth. Higher frequencies correspond to short wavelengths which are used to sample shallow depths. When sampling shallow depths the receivers are placed close to one another and a source that produces low amplitude, high frequency waves is desirable. Theoretically, the shallowest sampling depth that can be achieved is limited only by the maximum frequency component generated by the source. A practical limit to the shallowest achievable sampling depth was suggested by Heisey, Stokoe and Meyer (Heisey, 1982). They suggested that wavelengths less than half of the distance between the receiver spacing produced unreliable data. Table 3.1 (see page 111) indicates the shallowest practical sampling depth as a function of receiver spacing assuming an effective sampling depth equal to ½ of the wavelength.

As the desired sampling depth increases the spacing between the receivers is also increased. The source used for larger receiver spacings should contain a lower frequency range which equates to longer wavelengths that, in turn, sample deeper layers. The source used for this scenario has to produce high amplitude/low frequency content waves to be effective. Theoretically, the deepest sampling depth that can be achieved is limited by the lowest frequency component generated by the source. Heisey, Stokoe and Meyer also proposed a practical limit to the deepest practical sampling depth. They suggested that the wavelengths greater than 3 times the distance between the receivers produced

unreliable data. Table 3.1 also indicates the practical sampling depth as a function of receiver spacing assuming an effective sampling depth equal to ½ of the wavelength.

In this study four sources were used to generate surface waves. A five ounce tack hammer was used when to sample shallow depths. This source allowed for high frequencies to be excited when the receivers were placed near one another. A twelve ounce claw hammer and three pound sledge hammer were used for sampling slightly deeper layers. These sources produce a lower range of frequencies than the tack hammer, and are able to produce the higher amplitudes that are necessary when the receivers are spaced increasingly farther apart. The largest source used in this study was an eight pound sledge hammer. The sledge hammer was only used when the receivers were spaced relatively far apart to allow for sampling of deep layers. The sledge hammer produces a low range of frequencies and high amplitudes that do not attenuate before reaching the receivers. Figure 3.2 shows the various types of sources that were used in this study.

Figure 3.2 Sources used during SASW testing. From left to right: tack hammer, claw hammer, 3 lb sledge hammer, 8 lb sledge hammer

3.1.2 Receivers

The function of the receivers in SASW testing is to measure the passage of the seismic disturbance created by the source. Two types of receivers were used in this study, accelerometers and geophones. Both of these receiver types are considered input transducers, which means that they measure some form of input energy and convert it into an electrical output. During SASW testing the receivers detect the particle motion associated with a seismic disturbance and convert it into an electrical signal that is output to a data acquisition system. The means by which each type of transducer converts the input particle motion into an electrical signal is discussed subsequently.

Accelerometers convert acceleration input into a proportional voltage output. Many types of accelerometers are available, each having its own principle of operation. One dimensional, piezoelectric shear accelerometers were used in this study. Piezoelectric shear accelerometers contain crystals that are attached to a center post that extends from the casing of the accelerometer. A small seismic mass is attached to the opposite side of each of the crystals. When the accelerometer is moved the masses imposes shear stresses on the crystals which generates electric charges that accumulate on the surfaces of the crystals. The amount of charge that builds up is directly proportional to the amount of acceleration (g) felt by the transducer. A small charge sensitive amplifier that is built into the accelerometer outputs a voltage that is proportional to the amount of charge on the surfaces of the crystals (PCB Piezotronics). Figure 3.3 shows how a typical piezoelectric shear accelerometer is constructed.

The major parameters associated with the performance of accelerometers are the measurement range, the sensitivity, and the resonant frequency. The measurement range

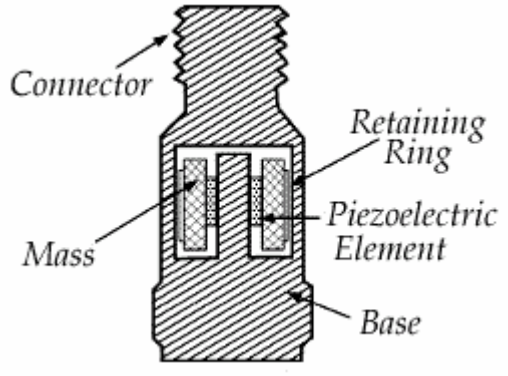

Figure 5.3 Piezoelectric shear accelerometer (From PCB Piezotronics, 2004)

of an accelerometer defines the maximum amount of acceleration in g's the sensor can accurately measure. The sensitivity is the gain of the built in amplifier, or the ratio of the output voltage to acceleration. The sensitivity can be thought of as a type of calibration factor, and has units of millivolts per g (mV/g). The frequency at which an accelerometer will ring at if it is struck sharply is called the resonant frequency. The resonant frequency is important in that measurements taken at or near the resonant frequency may be distorted due to the natural tendency for the sensor to ring at that frequency (PCB Piezotronics, 2004).

Two accelerometer models were used in this study, and are depicted in Figure 3.4. The accelerometers are high sensitivity sensors manufactured by PCB Piezotronics, model numbers 352C68 and 353B33. Model number 352C68 is the smaller, of the two accelerometers. The measurement range, sensitivity, and resonant frequency of this sensor are +/-50g, 100mV/g, and 35kHz respectively. Having a measurement range of +/-50g and a sensitivity of 100mV/g indicates that if the output signal voltage is greater than 5 volts the measurement range of the accelerometer has been exceeded. The larger

of the two sensors used is model number 353B33. This accelerometer has a measurement range of +/-50g, a sensitivity of 100mV/g, and a resonant frequency of 22kHz.

Figure 3.4 Accelerometers used for SASW tests. Model 352C68 shown at left, model 353B33 shown at right.

Geophones are transducers that produce an output voltage that is proportional to input velocity. A geophone consists of a coil wrapped mass that is suspended from a spring. A magnet that is fixed to the pavement surface surrounds the coil wrapped mass. When a seismic disturbance reaches the geophone the associated particle motion causes the magnet to move, but the suspended mass remains stationary. The motion of the coil wrapped mass within the magnetic field produces a voltage in the coil that is proportional to the velocity of the movement.

The parameters that affect the performance of a geophone are its natural frequency, transductivity, and damping ratio. The natural frequency of a geophone is the point at which it behaves as a high pass filter to ground velocity. This means that the natural frequency defines the lowest frequency the geophone can accurately measure. The transductivity of a geophone is analogous to the sensitivity of an accelerometer. The transductivity is the ratio of the velocity felt by the geophone to the voltage output. Thus,

like sensitivity, transductivity is a calibration factor that relates the output voltage to the input phenomenon (velocity in this case). The damping ratio of a geophone describes the attenuation of motion as a function of time.

The geophone used in this study is the L-28Vmanufactured by Sercel. The natural frequency of the L-28V is 4.5 Hz, indicating that the sensor can not measure frequencies below 4.5 cycles per second. The transductivity constant is 795mV/in/s and the damping ratio is 0.6. The V at the end of the model number indicates that this sensor measures velocity that occurs in the vertical direction. The geophone was housed in a PVC case to protect it from environmental conditions. The geophone and PVC housing are shown in Figure 3.5.

Figure 3.5 L-28V geophone shown inside a PVC housing. A soldered wire lead is connected to the top of the geophone

To accurately capture the seismic waves generated by the source the type of receiver used was varied as a function of receiver spacing. The high sensitivities, small size, and high resonant frequencies of the accelerometers better suit them to smaller receiver spacings. The smaller accelerometers (352C68) were used for receiver spacings of 6 inches or less. The larger accelerometers (353B33) were used when the receiver spacing was between 6 and 48 inches. The geophones were more suited to measuring seismic disturbances when the receiver spacing was greater than 48 inches.

3.1.3 Data Acquisition and Signal Analysis System

The output voltage signal from the receivers is captured and analyzed by the data acquisition and signal analysis system (DAQ/DSA). This type of system is available in many different forms. The data acquisition and signal analysis system used during this study consisted of a signal conditioner, a data acquisition board mounted in an external P.C. expansion chassis, and a laptop computer. The important aspects of each of these parts are discussed below.

It was stated in section 3.1.2 that the accelerometers used in this study contain charge amplifiers which output a voltage signal that is proportional to the amount of charge that builds up on the surfaces of piezoelectric crystals. The amplifier is necessary because piezoelectric accelerometers are susceptible to external noise. The amplifier reduces the effects of noise, cable length, and other spurious effects. The drawback to using these amplifiers, however, is that they require a constant current to operate. The device that supplies this constant current to the charge amplifiers so that they can improve the ouput signal quality is called a signal conditioner.

The signal conditioner used in this study is the BNC-2140 manufactured by National Instruments. In addition to providing constant current to the accelerometers, the BNC-2140 serves as the means by which the receivers are physically connected to the data acquisition system. The BNC-2140 allows for up to four receivers (input channels) to be connected via BNC jacks. Adjacent to each BNC jack are two switches. The switch labeled *ICP* (Integrated Circuit Piezoelectric Device) *Enabled* turns a 0.4mA constant current supply for the charge amplifiers on and off. For this study the *ICP Enabled* switch was always turned on when an accelerometer was connected, and turned off when a geophone was connected. The geophones used in this study do not require a current supply to operate, and if applied causes noise to be introduced to the geophone output signal. The second switch allows for either floating or grounded input. During this study the differential setting was used. The BNC-2140 signal conditioner is shown in Figure 3.6.

The second portion of the data acquisition and signal analysis system is the actual digital signal analyzer (DSA). The DSA samples and digitizes the conditioned voltage signal output from the signal conditioner, and then performs Fourier and spectral analysis on the digitized signal. The important aspects of sampling, digitization, Fourier analysis, and spectral analysis are described in Part II of the literature review. The specific attributes of the DSA chosen for use in this study are presented below.

The digital signal analyzer used in this study was the NI-4552 DSA board manufactured by National Instruments. This DSA is contained on a full sized PCI board that was mounted in an external chassis made by MAGMA (model number CB2DC). The external chassis links the DSA board to a laptop computer through the use of a

Figure 3.6 BNC-2140 signal conditioner

Figure 3.7 NI-4552 digital signal analyzer mounted in PCI expansion chassis

PCMCIA card. The external chassis supplies the power to run the NI-4552 DSA board. The DSA board and the external chassis are shown in Figure 3.7.

The NI-4552 was used to simultaneously sample two input channels at a rate of 5.0 to 204.8 kS/s (kilo samples per second). Referring to Equation 2.41, the maximum analyzable input frequency is calculated to be 102.4 kHz. The NI-4552 board has built in anti-alias filters that serve to limit the maximum frequency of the input signal. The transition band of the anti-alias filter reduces the alias free bandwidth to 0.464 times the sampling frequency. Thus, the NI-4552 board is capable of analyzing signals with frequencies ranging from DC to 95 kHz.

The analog to digital conversion process is performed by a 16 bit delta sigma ADC. Using a 16 bit ADC allows for a total of 65536 voltage levels available to quantize the input signal according to Equation 2.42. During this study the voltage range was set at -3.16V to 3.16V. Dividing the voltage range by the number of available voltage levels gives a value for the least significant bit (LSB) of approximately 0.096mV. This value suggests that very little quantization error is introduced into the signal during the analog to digital conversion process.

When performing analysis in the frequency domain the NI-4552 board was configured to use 800 frequency lines. Setting the number of frequency lines establishes two important facts. The first fact is that the resolution in the frequency domain (Δf) can now be defined by

$$\Delta f = \frac{Bandwidth}{800} \tag{3.1}$$

The bandwidths used during this study varied from a minimum range of 0 to 2kHz for large receiver spacings to a maximum range of 0 to 80kHz for small receiver spacings.

Thus, the resolution in the frequency domain ranged anywhere from 100Hz to 2.5Hz depending on the receiver spacing. The second important fact established by using 800 frequency lines is that the length of the time record can be determined. Using Equation 3.32 and the fact that the time record length is equal to $N\Delta t$, the time record lengths can be determined to have ranged from 10 milliseconds to 400 milliseconds.

The DSA board allows for both averaging and triggering capabilities. The importance of averaging was discussed in section 2.2.3.1. Analog triggering allows for one to tell the acquisition system when to start taking and analyzing the signals felt by the recievers. A trigger is defined as any event that starts the capture of data, and in this study was a user defined voltage threshold. The trigger was set by assigning a voltage level to a receiver that caused data acquisition to begin once it was exceeded. To avoid problems associated with windowing and leakage (section 2.2.2.3), a pretriggering option was used. When pretriggering is used, the DSA board continuously samples the input channels, but only records data when the trigger conditions are met. A user defined number of samples that occurred before the trigger conditions were met can then be added to the beginning of the sampled signal. In the case of a transient signal (as used in SASW testing) pretriggering helps assure the acquired signal is self windowing.

The final function of the DSA board is to perform spectral analysis on the signals acquired. The NI-4552 is able to simultaneously acquire two channels of time domain data, find the FFT (1024 point) of both channels, calculate the auto spectrum of each channel, calculate the cross spectrum between the two channels, and find the coherence between the two channels.

The last component of the DAQ/DSA system used in this study is a semi-rugged laptop computer. The laptop is used to control the NI-4552 board through the use drivers and application software. Labview 6.1 was the software used to develop the program that controlled the SASW testing. A description of the control program is located in Appendix B. The laptop also allowed for the acquired data to be stored electronically.

The laptop used in this study was the Talon model supplied by Rugged Notebooks. The laptop contains uses a 2.0 GHz Intel Pentium 4 processor and 512 MB of RAM. A type II PCMCIA card slot controlled by a 32 bit Texas Instrument cardbus controller allows the laptop to be linked to the external chassis. The laptop also contains a sunlight readable LCD monitor to facilitate its use for outdoor testing. The laptop is considered semi-rugged as it contains features that help prevent damage from outdoor environmental conditions and is resistant to damage from vibration and shock. The laptop and PCMCIA card that connects the laptop to the expansion chassis are shown in Figure 3.8.

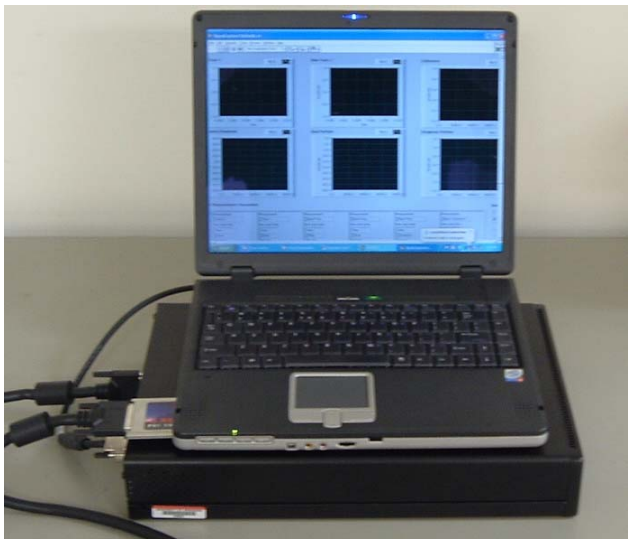

Figure 3.8 Laptop computer connected to the external chassis using a type II PCMCIA card

3.2 Field Testing Procedure

This section presents the field testing procedures used to conduct spectral analysis of surface wave testing at the twelve locations chosen for this project. A description of how the equipment was setup in the field is the first topic covered. The second portion of this section presents the step by step method that was used to conduct the testing. The last portion is devoted to a discussion of some of the limitations associated with the field testing performed for this study.

3.2.1 Equipment Setup

Prior to beginning the field testing phase of this project a wooden case was designed to house the DSA board mounted in the external chassis, the signal conditioner, and the laptop computer. Using this case served to both protect the equipment from environmental conditions and as a means of making the testing equipment portable. The case consists of two levels. The external chassis is secured in place on the bottom level of the case, and is cushioned with foam to prevent damage. A small opening in the case is present to allow for the chassis power cord. The case is vented to prevent heat from building up due to the operation of the equipment. The signal conditioner and laptop computer are located on the upper level of the case. A 68 pin analog cable connects the signal conditioner to the chassis below. A high speed cable connects to a PCI card inserted into the laptop at one end and the external chassis at the other. A picture of the equipment housed in the case is shown in Figure 3.9.

During field testing the wooden case was placed on or near the shoulder of the pavement system under study. The chassis and laptop were supplied with power using a 400 watt power inverter connected to a 12 volt battery with alligator clips. The

expansion chassis was allowed to run for a few minutes before turning the laptop on to allow for proper bus hierarchy to be established between the two devices. If the hierarchy is not properly established the DSA device will not be recognized by the computer.

Teflon cables containing a 10-32 connection on one end and a BNC connection on the other end linked the accelerometers to the signal conditioner. When geophones

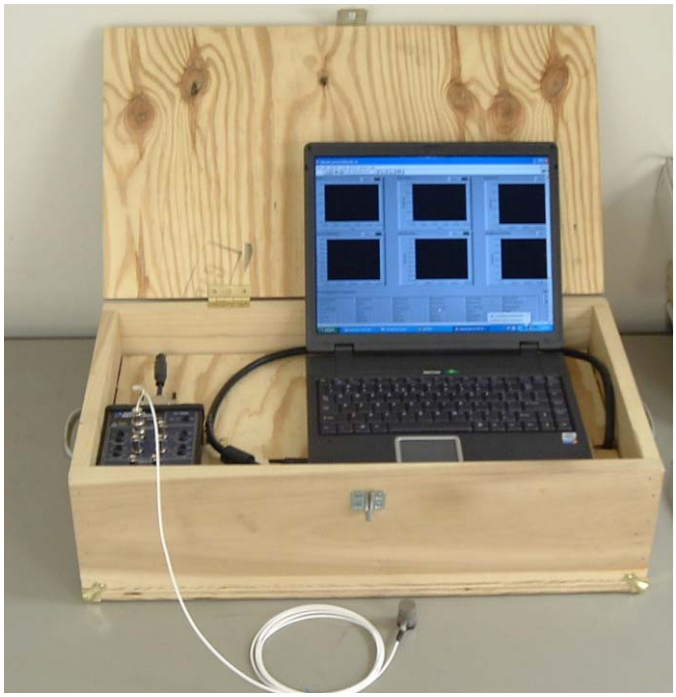

Figure 3.9 SASW testing equipment housed in wooden case. The external chassis is not visible as it is located below the laptop and signal conditioner

were used they were connected to the signal conditioner by a Teflon cable that was directly soldered to the geophone on one end and contained a BNC jack at the opposite end. All of the Teflon cables were 10 feet in length. For situations where the receivers needed to be placed at distances greater than 10 feet from the signal conditioner 50 foot RG58 cable leads containing male and female ends were available for use.

Initial receiver placement typically consisted of placing one of the smaller accelerometers at a zero mark and the other of the smaller accelerometers 3 inches from the first. The two larger accelerometers were placed at distances of 12 and 24 inches from the zero mark. A geophone was placed at a distance of 96 inches from the zero mark. The receivers were always placed such that they formed a straight line and that the spacing increased consecutively from one direction to the other (i.e. if the 3 inch receiver was located to the right of the zero mark all of the other receivers were located to the right of the zero mark). The receivers were mounted to the pavement surface using a sticky, gummy substance referred to as "ticky-tack." This substance is commonly used to hang posters and is made by 3GM. The smallest amount of ticky-tack required to both smooth out irregularities in the pavement surface and hold the receiver in place was used to minimize the potential for altering the dynamic characteristics of the receivers. Once the receivers had been placed, power was supplied to the signal conditioner. Figures 3.10-3.13 show the equipment assembled in the field.

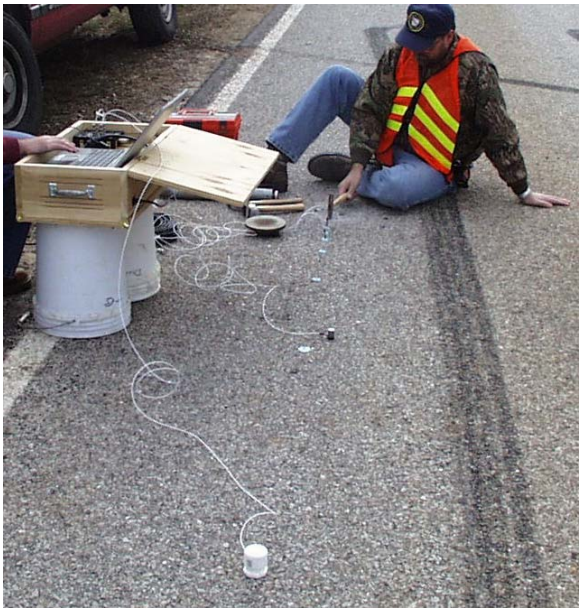

Figure 3.10 SASW test setup at Mountain Home

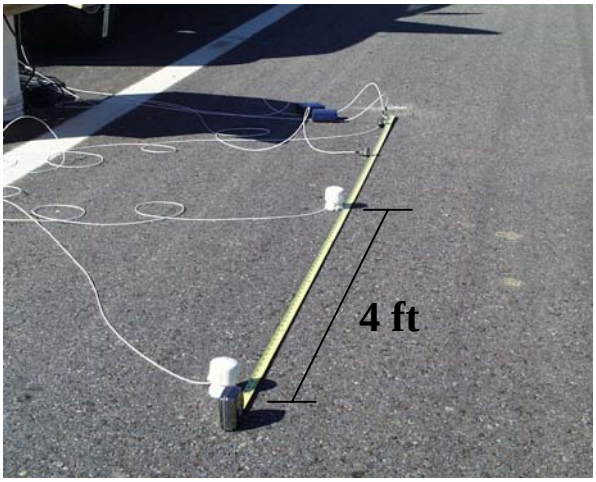

Figure 3.11 Receiver arrangement at Hamburg site

Figure 3.12 SASW equipment setup at Hot Springs site

Figure 3.13 SASW equipment setup at Beulah test site

3.2.2 Test Method

The first step that was taken when performing field testing was to setup the equipment as outlined in the previous section. Once all equipment was setup *Signalcapture1.vi* (virtual instrument), the program developed to control the digital signal analyzer during SASW testing, was initiated. The program defaults are set for SASW testing at a three inch receiver spacing (provided the near receiver is connected to channel 1 and the far receiver is connected to channel 2), the only information required by the program prior to testing is a file name to which the acquired data will be stored.

At the three inch receiver spacing a tack hammer was used to generate surface waves. The tack hammer was used to sharply strike the surface of the pavement, generating a group of waves containing high frequencies and low amplitudes. The hammer strike was performed along the same line formed by the receivers and at a distance ranging between three and eighteen inches from receiver placed at the zero mark. When the seismic waves generated by the impact passed by the first receiver (assigned as the trigger channel), data was acquired for a length of time dependent upon

the bandwidth setting (10 milliseconds for three inch spacing). This process was repeated four more times so that the averaging capability of the signal analyzer could be used to enhance the quality of the signal obtained. Five was the number chosen because it is the number recommended in the literature (Nazarian, 1984).

Signalcapture1.vi automatically stopped taking measurements once five measurements were obtained and averaged. At this point a quick field evaluation of the quality of the measurements was performed by viewing the display on the laptop screen. The time domain signal from both of the measured receivers and the coherence between the two receivers were the primary methods of quickly evaluating the usefulness of the obtained measurements. The time domain measurements were quickly "eyeballed" to ensure that the receivers were functioning properly, and that reasonable looking signals were obtained. The coherence function was evaluated to ensure that the signals from the two channels were in good agreement with one another over a significant portion of the sampled bandwidth. The signals were considered to be in good agreement with one another when the coherence value was above 0.8-0.9. If the acquired signals appeared to be erroneous the test file was discarded, and the entire process was repeated. Because a very small amount of time was needed to obtain additional measurements, five to twenty five tests were typically performed at any given receiver spacing.

The process described above for obtaining data from the 3 inch receiver spacing was repeated for receiver spacings of 6, 12, 24, 48, and 96 inches. The receiver line was always run parallel to the roadway. The only differences in subsequent measurements from the process described above are that:

1) Four receivers were connected to the acquisition system at any given time. However, the program only measures two channels (receivers) simultaneously. The program default was configured such that the receiver nearest to the source must be plugged into channel 1, and the far receiver of interest must be plugged into channel 2. In subsequent measurements the program was used to change which input channels were measured instead of physically moving the receivers after each measurement.
2) As mentioned in section 3.1.1, the type of source used is a function of receiver spacing. The type of source used for each receiver spacing is shown in Table 3.1.
3) The purpose of sampling at various receiver spacings is to sample at varying depths. The farther apart the receivers are spaced the deeper they are intended to sample. As such, the frequency range of interest changes as a function of receiver spacing. *Signalcapture1.vi* was used to change the measured frequency range to agree with the receiver spacing. The frequency bandwidths used for each receiver spacing during this study are shown in Table 3.1.

Table 3.1 Receivers, sources, and bandwidths used during field testing at each receiver Spacing; and practical shallowest and deepest depths sampled as each receiver spacing

Receiver Spacing (inches)	Zero Mark	3	6	12	24	48	96
Receiver Type	Small Accelerometer	Small Accelerometer	Small Accelerometer	Large Accelerometer	Large Accelerometer	Large Accelerometer and Geophone	Geophone
Source	N/A	Tack Hammer	Tack Hammer	Claw Hammer	Claw Hammer	Claw Hammer and 3lb Sledge Hammer	3lb and 8lb Sledge Hammer
Bandwidth KHz	N/A	0-80kHz	0-60kHz	0-20kHz	0-10kHz	0-5kHz	0-2kHz
Shallowest Depth Sampled (ft)	N/A	0.125	0..25	0.5	1	2	4
Deepest Depth Sampled (ft)	N/A	0.75	1.5	3	6	12	24

3.2.2.1 Field Procedures for FWD testing and Soil Sampling

Falling weight deflectometer (FWD) testing was performed by the Arkansas Highway and Transportation Department (AHTD) at each of the ten test sites. A drop load of 45 kN was used. FWD testing was scheduled to be completed at the same time as SASW testing in order to ensure identical environmental conditions were present. However, due to equipment difficulty FWD testing was only conducted at the same time as SASW testing at the Clarksville site. FWD testing was completed approximately one month after SASW testing at the remainder of the sites.

FWD data was analyzed using three software programs. The first program used was ROADHOG which is based on regression equations developed at the University of Arkansas. Elmod5 and Evercalc were also used to analyze the FWD data using deflection basin fitting methods. FWD data reduction is discussed further in Section 3.3.3.

Soil sampling at each of the sites consisted of a combination of split spoon sampling, Shelby tube sampling, and collection of auger cuttings. To allow for sampling beneath existing pavements, a 4 inch diameter asphalt core was cut at each site. The asphalt core was stored in an appropriate container and transferred back to the laboratory for determination of the individual asphalt and/or base layer thicknesses present in the recovered core. Soil samples were collected from beneath the pavement system through the use of a combination of split spoon and Shelby tube samplers. Sampling was terminated at depths ranging from about 5 to 7 ft below the existing pavement system. SPT, N-values were recorded in combination with split spoon sampling. Split spoon samples were stored in plastic baggies to prevent moisture loss during transportation.

Bulk soil samples were collected from the shoulder sections of the roadways to allow for soil index tests to be performed. Samples were obtained by collecting cuttings from holes augured in the shoulder areas. Bulk samples were stored in plastic buckets containing tight fitting lids to prevent substantial loss of moisture during sample transportation.

3.2.3 Limitations of SASW Field Testing

Certain limitations are present in the field testing that was conducted during this study. This section will address two major categories of limitations that exist; those due to the procedure used to collect SASW data, and those due to environmental conditions encountered in the field.

3.2.3.1 Procedural Limitations

One of the goals of this research work is to evaluate the possibility of utilizing a fully automated spectral analysis of surface waves testing system to determine the

resilient moduli of Arkansas pavement systems. To make automation of this testing procedure feasible certain equipment configurations had to be used which may have introduced some amount of error into the data collected. Specifically, the receivers were fixed in one place throughout the testing procedure. Additionally, the source was not allowed to vary more than twenty four inches away from the near receiver. The implications of these two facts are discussed below.

A common practice when performing SASW tests is to use either a common source/receiver geometry (CSR), or a common receivers midpoint geometry (CRMP). When using CSR geometry either receivers or the source is fixed in place while the other is allowed to move between tests performed at receiver spacings. The mobile component is moved such that the distance between the source and the near receiver is always equal to the distance between the two receivers. CRMP geometry establishes a centerline between the two receivers that remains in one location throughout the test. In this case both the receivers and the source are moved between tests performed at differing receiver spacings. Figures 3.14 and 3.15 show the locations of the source and receivers as a function of receiver spacing for both the CSR and CRMP geometries.

Another common practice when performing SASW testing is to repeat each test from the reverse direction. Performing a test in the reverse direction refers to the practice of applying the source from the opposite end of the line of receivers after a normal, forward test has been performed. Applying the source from the opposite side of the receivers causes the far receiver from the forward test to become the near receiver for the

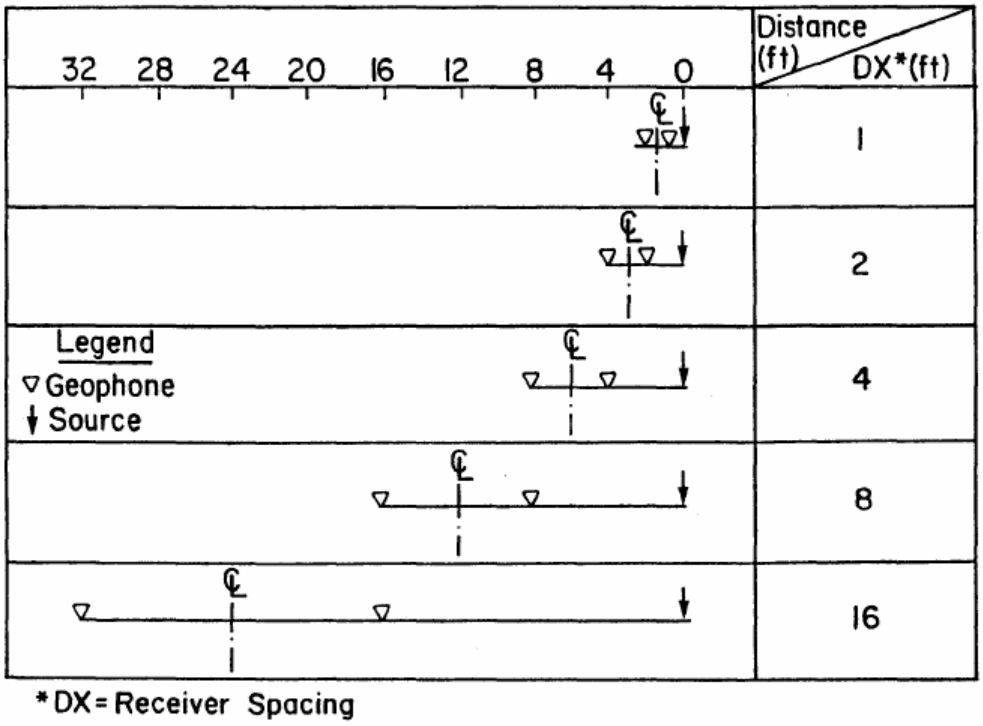

Figure 3.14 Location of source and receivers using CSR geometry (From Nazarian, 1984)

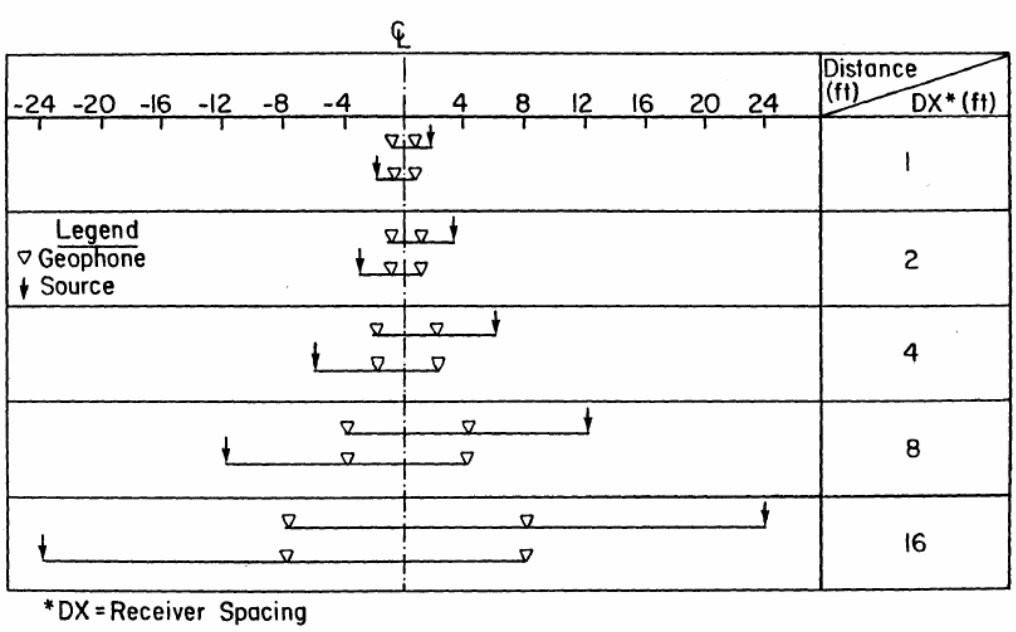

Figure 3.15 Location of source and receivers using CRMP geometry (From Nazarian 1894)

reversed test. Figure 3.15 illustrates the concept of reversing the test, showing two tests being performed at each receiver spacing where the source is moved to the opposite side of the receivers between tests.

It is apparent that the two practices presented above can not be achieved if the receiver and source (within 24 inches) locations are fixed. Not using these two practices may have the following ramifications:

1) The literature states that using the CRMP geometry reduces scatter in obtained data, especially at shorter receiver spacings. Not using CRMP geometry in this study may have caused more scatter in the data than necessary.
2) Performing both forward and reverse profiles and averaging the results minimizes any unwanted internal phase shifts between the receivers or between the receivers and the DSA (Nazarian, 1985).
3) Both using CRMP geometry and performing the forward and reverse profiling technique help to minimize the errors that occur when anisotropic or dipping layers are encountered. These techniques minimize these errors because the velocities obtained for each layer are averaged over the entire testing range (Nazarian, 1985). This type of error is typically small when dealing with pavement systems.
4) The energy associated with P and S waves may interfere with the desired R wave signal if the distance between the source and the near receiver is not great enough to allow the body waves to be adequately attenuated. This type of signal interference is termed “near field effect” (Zywicki, 1999).

5) The wave field may not fully develop before reaching the near receiver if the distance between the source and near receiver is too small.

3.2.3.2 Environmental Limitations

The sensitive nature of the equipment used to perform SASW testing has the disadvantage of being susceptible to problems associated with adverse weather conditions. Wet weather causes major problems when attempting to perform SASW testing. The sensor to cable connections and the cable to signal conditioner connections are not water proof which can cause ground loops to form, resulting in no signal acquisition. Also, direct impact of raindrops on the sensors during testing can lead to unwanted excitation of the sensors. Another difficulty associated with wet conditions is the matter of properly mounting the sensors to the pavement surface. Many types of adhesives do not work well on wet surfaces, which can lead to improper coupling between the sensors and the pavement surface.

Wet conditions were encountered at two sites during this study. Heavy rainfall was encountered when testing was conducted at the Van Buren site. The rain caused a ground loop to form at one of the receivers, which caused delay in the testing. The adhesive used in this study to mount receivers was found to be extremely sensitive to wet conditions. The adhesive would not properly bond to either the pavement surface or the receivers. These conditions caused the data obtained for the Van Buren site to be unusable. Wet conditions were also encountered at the Hot Springs site. The pavement surface was quite wet at this site due to recent precipitation. Testing could be performed only after portions of the pavement were manually dried to create areas where the adhesive could bond.

Another environmental condition that can cause an adverse effect is wind. Wind can cause cables that are not properly secured to sway, which causes unwanted motion to be transmitted to the sensors. If this additional motion occurs during testing it is interpreted as coming from surface waves emanating from the source. The detrimental effects due to wind can be minimized by laying the sensor cables as flat as possible on the ground surface (EM 1110-1-1802, 1985). Osceola was the only site at which windy conditions were encountered during this study. All of the cables were placed as low to the ground as possible, but because the cable connection for the small accelerometers are located at the top of the sensor some wind noise may have been introduced into the measurements.

Temperature should also be taken into consideration when performing SASW testing. Because the equipment used is electrical in nature, its performance is dependent upon temperature. The operating temperature recommended by the manufacturer for each piece of equipment is shown in Table 3.2 on the following page.

Table 3.2 Recommended operating temperature ranges for SASW equipment

	352C68 (Accel.)	353B33 (Accel.)	L-28V Geophone	NI-4552 DSA	CB2DC Chassis	BNC-2140 Signal Conditioner	Talon Laptop
High Temperature (˚F)	250	250	N/A	104	120	160	95
Low Temperature (˚F)	-65	-65	N/A	32	32	32	40

Temperatures encountered while field testing during this study were within the operating temperature ranges of the equipment at all of the sites except Osceola. The temperature at the Osceola site was approximately 35˚ F at the time testing was performed. This

temperature is slightly below the minimum recommended operating temperature of the Talon laptop. The effects due to testing slightly below the 40˚ F recommended minimum are thought to be minimal.

Another factor that can influence the quality of the data obtained is the condition of the surface of the pavement tested. Using the sources, receivers, and receiver mounting procedures described in this section; it was found that pavements with rough or uneven surfaces tended to give low quality data at short receiver spacings. The surface types that tended to be the most troublesome were chip sealed pavements, and pavements that exhibited severe surface fatigue. The sites at Clarksville and Mountain Home were chip sealed, while the site at Hope contained severely fatigued pavement.

Figure 3.16 Chip sealed pavement at Mountain Home site

Figure 3.17 Severely fatigued pavement at Hope site

Adjusting the procedure for striking the pavement surface and changing the method of mounting the receivers may be possible solutions to the problem of acquiring poor high frequency signals from chip sealed pavements. During this study the source

was used to directly strike the pavement. Due to the uneven nature of chip sealed pavement it was difficult to obtain a repeatable signal between source impacts. If a plate were to be attached to the pavement surface, and the source then applied to the plate, a more repeatable signal at high frequencies may have been obtained. The reasoning behind this is that the impact would be spread over a wider area, decreasing the amount of variability between impacts. The same concept may be applied to the mounting of the receivers. If the receivers were to be glued to a block or plate that was then adhered to the surface of the pavement, the acquired signal may be more accurate at high frequencies.

3.3 Data Reduction Methods

The processes used to analyze the raw data collected in the field are described in this section. Data analysis was carried out in two stages. The first stage was to manually construct experimental dispersion curves for each site tested. The simplified inversion method was used to create shear wave velocity profiles from the manually constructed experimental curves, allowing for layer thicknesses and moduli to be estimated. The second stage was to use a computer program provided by the University of Texas at El Paso (UTEP) to analyze the data. The program automatically constructed experimental dispersion curves from raw data files collected at each test site, and then used the Haskell-Thompson transfer matrix approach to create theoretical dispersion curves. The trial profiles necessary for calculation of the theoretical dispersion curves were the only manual input required to execute the UTEP program. The program used an iterative process to match the calculated theoretical dispersion curve to the experimental dispersion curve by varying both layer thicknesses and shear wave velocities. The final

shear wave velocity profile obtained was then used to estimate the resilient moduli and thickness of each layer.

To illustrate how these two data reduction procedures were carried out, a step-by-step example is presented. The example shows how data collected during testing of a site near Osceola, Arkansas were analyzed both manually, and then automatically using the UTEP software. The raw data files were collected using the equipment and procedures described in sections 3.1 and 3.2.

3.3.1 Simplified Inversion (Manual) Method

3.3.1.1 Data file structure

Before explaining how the manual construction of the experimental dispersion curve was carried out, one must understand how to interpret the information contained in the raw data files. Each raw data file collected by the data acquisition program contained six columns of data. Each of these columns contained data related to a single measurement type performed by the acquisition program. The six measurement types present in the files (from far left column to far right column in the data file) were the time domain signal from the first selected input channel, the time domain signal from the second selected input channel, the frequency response function between the two channels, the real component of the frequency response function, the imaginary component of the frequency response function, and the coherence between the two channels.

The rows in the data files defined discrete points in the time-frequency plane that, when plotted, represent the sampled form of the measurements. Because the data acquisition system was configured to sample at equal time intervals for time domain

measurements, and at equal frequency intervals for frequency domain measurements, the x (time) coordinates for every point were defined using just two rows of data to reduce the amount of space required to store the recorded file. The first two rows of data in the files contained this x (time) coordinate information. Each row below the first two contained the y (frequency) coordinate for a single sampled point. A total of 2048 points were used to represent each time domain measurement, and 800 points to represent each frequency domain measurement. Additionally, five impacts were recorded to take advantage of signal averaging. Thus, each raw data file contained 10,250 rows of data; 2 rows of x (time) coordinate data plus 2048 rows of y (frequency) coordinate data (0's are used for frequency domain measurements after 800 points) multiplied by 5 recorded impacts for averaging.

Table 3.3 represents a portion of a raw data file, showing the first ten rows of the raw data file obtained from the Osceola site using a receiver spacing of 24 inches. The actual raw data file does not contain the column and row labels shown in the table below.

Table 3.3 Portion of a raw data file showing measurements taken at a receiver spacing of 24 inches at the Osceola test site

	Time Trace 1	Time Trace 2	Frequency Response	Real Component	Imaginary Component	Coherence
X_0	0	0	0	0	0	0
Δx	0.0000195	0.0000195	25	25	25	25
Y_1	0.002	0.003	3.914	1.569	0	0.999
Y_2	0.002	0.003	-14.493	0.078	-0.172	0.712
Y_3	0.002	0.003	-12.069	0.071	-0.239	0.77
Y_4	0.002	0.003	-11.439	-0.042	-0.265	0.905
Y_5	0.002	0.003	-12.375	-0.102	-0.218	0.988
Y_6	0.002	0.003	-13.281	-0.126	-0.176	0.965
Y_7	0.002	0.003	-13.894	-0.161	-0.122	0.994
Y_8	0.002	0.003	-14.312	-0.176	-0.077	0.996
Y_9	0.002	0.003	-14.917	-0.176	-0.034	0.992
y_{10}	0.002	0.003	-15.596	-0.166	0.001	0.995

The file was saved such that the first row of each column is an initial value of the x axis, labeled x_0 in the figure above. For the two time measurements x_0 stands for the initial time at which measurements began, and for the remaining four measurements x_0 represents the initial frequency. The x_0 value was always zero for the measurements taken in this study because time measurements were always referenced from a trigger event designated as time 0, and frequency measurements were always made over a bandwidth extending from 0 to some finite value.

The second row of each column defines the resolution of each of the measurements, and is labeled Δx. For the time measurements Δx is synonymous with sampling rate, defining how often a sample was taken. In the example above, the time measurements were sampled every 0.0000195 seconds. Notice that the first two columns of data shown in Table 3.3 do not appear to be changing. This occurs because when the Labview program records the measurements, they are automatically rounded to the nearest thousandth. The change in the time between successive measurements is so small that the rounding masks the change between measurements in small data sets such as the one shown in Table 3.3.

A total of 2048 samples were used to define measurements in the time domain. Thus, given the total number of samples N, and the sampling rate Δx, it is apparent that the total length of the time record was 40 ms for this example. For the frequency measurements Δx represents the distance between the frequency lines that compose the measurement. The frequency resolution was always set to 800 lines, therefore the bandwidth over which the measurement in this example was taken can be determined to have been 20 kHz (800 * 25 Hz).

The x coordinate that corresponds to each of the y coordinates given in rows y_1 to y_{10} is not explicitly given in the raw data files, and must be calculated. The y coordinate given in y_1 corresponds to an x coordinate defined by $x_0 + 0\Delta x$, the value given in y_2 corresponds to $x_0 + 1\Delta x$, and the value given in y_n corresponds to the value of $x_0 + (n-1)\Delta x$. Knowing both the y values and the x values to which they correspond, allows for the measurements to be plotted. Figure 3.18 is the graphical form of the coherence function data contained in Table 3.3.

Coherence		
Sample	**x-coordinate**	**y-coordinate**
1	0	0.999
2	25	0.712
3	50	0.77
4	75	0.905
5	100	0.988
6	125	0.965
7	150	0.994
8	175	0.996
9	200	0.992
10	225	0.995

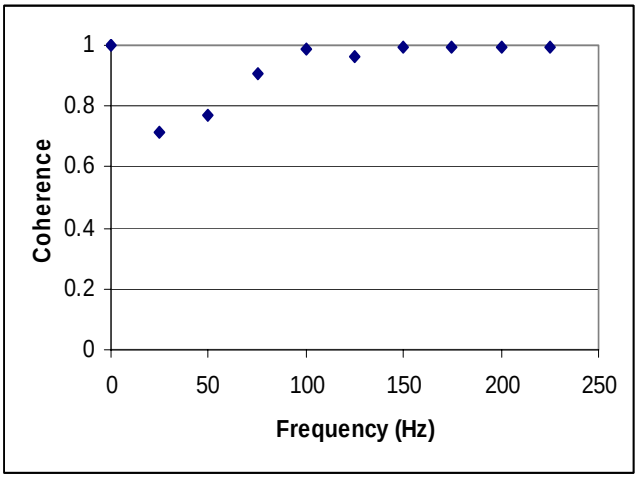

Figure 3.18 Coherence measurement from Table 3.3 plotted as a function of frequency

3.3.1.2 Construction of the Experimental Dispersion Curve

The data columns necessary to construct an experimental dispersion curve are the real component of the frequency response function, the imaginary component of the frequency response function, and the coherence function; all represented as a function of frequency. The first step taken to reduce the data in this study was to create a new data file that contained these four columns of information. Table 3.4 shows the ten samples

from Table 3.3 transformed into the format necessary for construction of the experimental dispersion curve. Notice that the frequency column was calculated using the relationship between Δx and y discussed in section 3.3.1.1. Also, note that the time information included in the raw data file is not needed for construction of the experimental dispersion curve, and is therefore omitted from the table.

During field testing multiple tests were performed at each receiver spacing, each test producing a single raw data file. At the Osceola site, 6 tests were performed for the 3 inch receiver spacing, 7 tests for the 6 inch receiver spacing, 5 tests for the 12 inch receiver spacing, 4 tests for the 24 inch receiver spacing, 6 tests for the 48 inch receiver spacing, and 5 tests for the 96 inch receiver spacing. Therefore, a total of 33 data files were available for analysis. To construct the experimental dispersion curve the file containing the highest quality data was chosen for each receiver spacing, reducing the total number of necessary files to 6. To choose the best data file all of the original raw data files were transformed into the format shown in Table 3.4. A graph of the coherence function was then created for each of the files. For a given receiver spacing, the best data file was selected by choosing the file for which the coherence value remained closest to one over an appropriate range of frequencies.

Table 3.4 Information from raw data file necessary to construct the experimental dispersion curve

Frequency	Real	Imaginary	Coherence
0	1.569	0	0.999
25	0.078	-0.172	0.712
50	0.071	-0.239	0.77
75	-0.042	-0.265	0.905
100	-0.102	-0.218	0.988
125	-0.126	-0.176	0.965
150	-0.161	-0.122	0.994
175	-0.176	-0.077	0.996
200	-0.176	-0.034	0.992
225	-0.166	0.001	0.995

The four tests performed at the 24 inch receiver spacing at the Osceola site are shown in Figure 3.19. The Osceola 24inch1 test file was selected to represent the 24 inch receiver spacing for construction of the experimental dispersion curve. This data file was chosen because the coherence remained close to one over a wider range of frequencies than the other available test files. Using files containing high values of coherence reduces the chance of analyzing data contaminated by background noise, and provides the maximum number of points to define the final dispersion curve.

Once the 6 best data files were selected, the next step was to calculate the phase shift (ϕ) that occurred between the two receivers for each frequency. The phase shift was

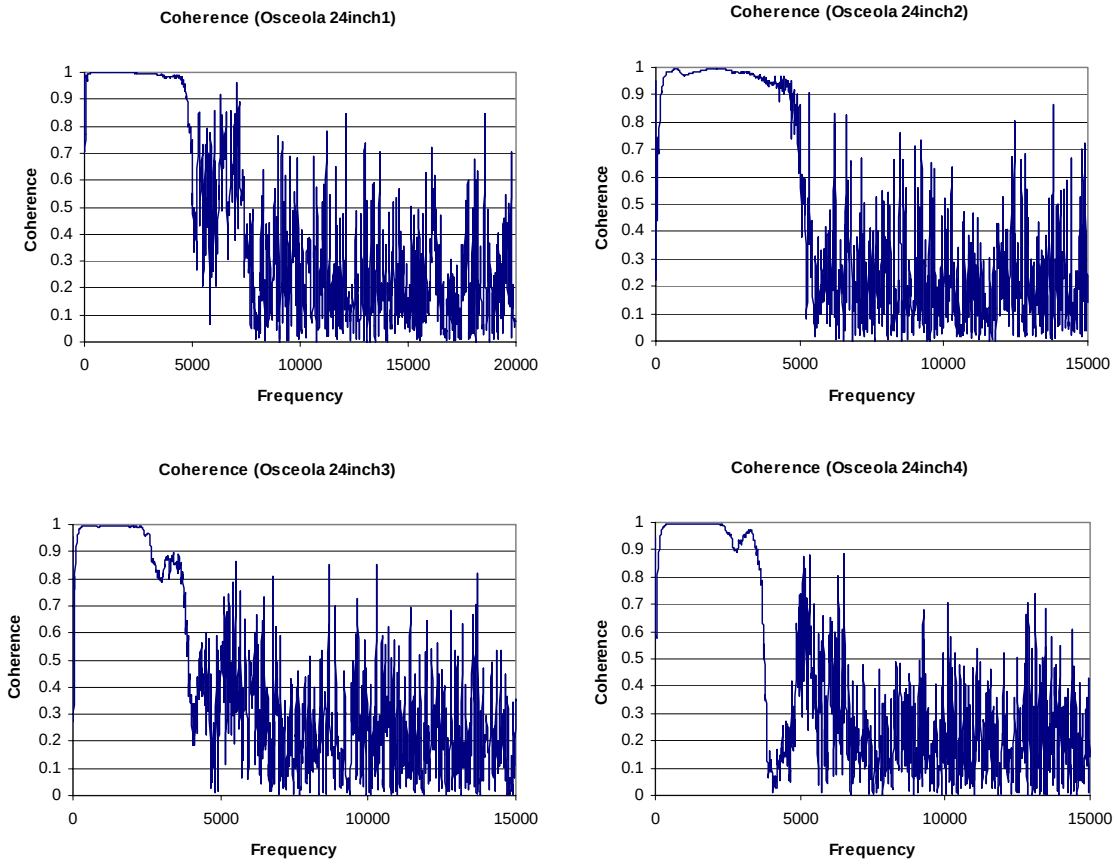

Figure 3.19 Coherence function plotted for four tests performed at 24 inch receiver spacing

calculated using the equation

$$\phi = \tan^{-1} \frac{\text{Re}}{\text{Im}} \tag{3.2}$$

Where Re is the real portion of the frequency response function and Im is the imaginary portion of the frequency response function. Table 3.5 shows the appearance of the example data up to this point.

The next step taken to reduce the data was to plot the phase shift calculated for each frequency. This plot is shown in Figure 3.5 for the example data. The coherence for each frequency is plotted in the figure as well.

Table 3.5 Data from 24 inch receiver spacing after removal of low coherence measurements and phase calculations

Frequency	Real	Imaginary	Coherence	Phase Shift (degrees)
0	1.57	0.00	1.00	0.00
25	0.08	-0.17	0.71	-65.61
50	0.07	-0.24	0.77	-73.45
75	-0.04	-0.27	0.91	80.99
100	-0.10	-0.22	0.99	64.93
125	-0.13	-0.18	0.97	54.40
150	-0.16	-0.12	0.99	37.15
175	-0.18	-0.08	1.00	23.63
200	-0.18	-0.03	0.99	10.93
225	-0.17	0.00	1.00	-0.35

The phase shift shown in Figure 3.20 is represented as oscillating in cycles. This is a common method of representing phase used in signal analysis. This type of phase representation is called a wrapped phase, and is not the actual phase shift that occurred between the receivers. To find the actual phase shift for a given frequency, the number of cycles occurring prior to the frequency of interest must be counted, and added to the measured value of the phase. The process of finding the actual phase for each frequency

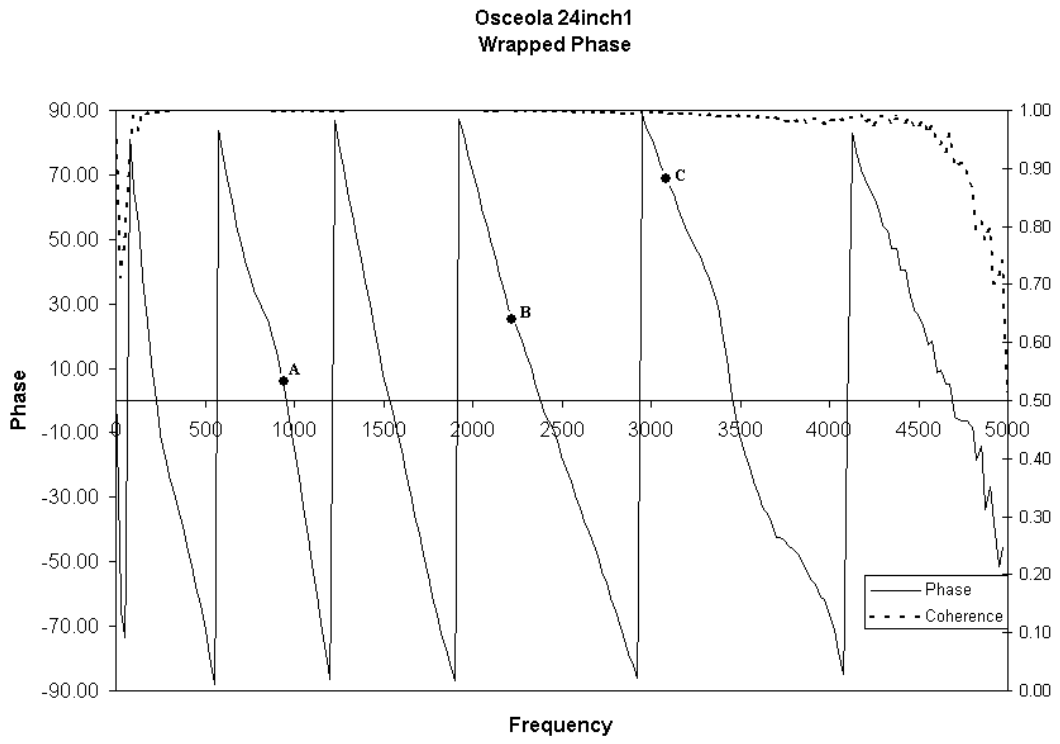

Figure 3.20 Wrapped phase shift between receivers for a distance of 24 inches from Osceola site

is called unwrapping the phase. To illustrate how unwrapping is performed, the calculations necessary to obtain the actual phase for the points labeled A-C in Figure 3.20 are shown on the following page. Figure 3.21 shows the unwrapped phase shift plotted as a function of frequency once the unwrapping procedure was performed on the example data file 24inch1 from the Osceola site. Points A-C from Figure 3.20 are shown in their new locations in the unwrapped phase plot.

Once the actual phase shift as a function of frequency is known, phase velocities and wavelengths for each frequency can be calculated using equations 2.2, 2.49, and 2.50. The combination of a single phase velocity and its corresponding wavelength

Point A

Measured Frequency	925 Hz
Wrapped Phase	8.9˚
Actual Phase	= 90+180+(90-8.9) = 351.1˚

Point B

Measured Frequency	2200 Hz
Wrapped Phase	28.8˚
Actual Phase	= 90+180+180+180+(90-28.8) = 691.2˚

Point C

Measured Frequency	3075 Hz
Wrapped Phase	70.3˚
Actual Phase	= 90+180+180+180+180+(90-70.3) = 829.7˚

(a)

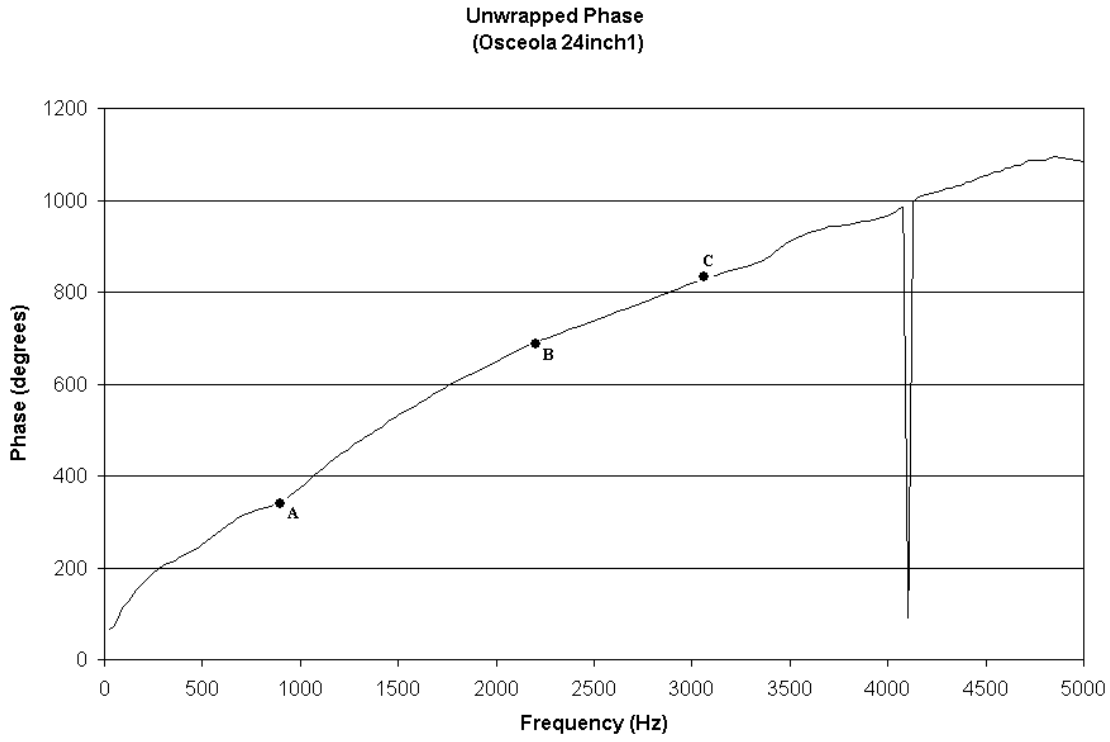

(b)

Figure 3.21 (a) Calculations necessary to unwrap the phase for points A-C. (b) Unwrapped phase shift between receivers for a distance of 24 inches from Osceola site

defines one point on the experimental dispersion curve. The calculations which transform points A-C from Figure 3.21 into points on the experimental dispersion curve are shown in Figure 3.22. Table 3.6 shows the first ten rows of the example data file after the same calculations were performed on the first ten rows of the example data file.

Point 1

Travel Time $t(f) = \frac{351.1}{(360 * 925)} =$ 1.05 msec

Phase Velocity $V_R = \frac{(24/12)}{1.05 * 10^{-3}} =$ 1897 ft/sec

Wavelength $\lambda =$ $1897 / 925 =$ 2.05 ft

Point 2

Travel Time $t(f) = \frac{691.2}{(360 * 2200)} =$ 0.880 msec

Phase Velocity $V_R = \frac{(24/12)}{0.880 * 10^{-3}} =$ 2292 ft/sec

Wavelength $\lambda =$ $2292 / 2200 =$ 1.04 ft

Point 3

Travel Time $t(f) = \frac{829.7}{(360 * 3075)} =$ 0.750 msec

Phase Velocity $V_R = \frac{(24/12)}{0.750 * 10^{-3}} =$ 2668 ft/sec

Wavelength $\lambda =$ $2668 / 3075 =$ 0.868 ft

Figure 3.22 Calcualations performed to transform Points A-C into points on the experimental dispersion curve

Table 3.6 Dispersion data for portion of Osceola 24inch1 data file

Frequency	Actual Phase (degrees)	Travel Time (sec)	Phase Velocity (ft/s)	Wavelength (ft)
0	0	N/A	N/A	N/A
25	65.6	0.0073	274.4	10.97
50	73.5	0.0041	490.1	9.80
75	99.0	0.0037	545.4	7.27
100	115.1	0.0032	625.7	6.26
125	125.6	0.0028	716.6	5.73
150	142.8	0.0026	756.1	5.04
175	156.4	0.0025	805.8	4.60
200	169.1	0.0023	851.7	4.26
225	180.3	0.0022	898.3	3.99

At this point, selection criteria were applied to select which of the points calculated were to be used as part of the final dispersion curve. The first criterion applied was that the coherence value associated with the point had to be greater than or equal to 0.8. The second criterion applied was that any point with a wavelength less than half of the distance between the receivers or more than three times the distance between the receivers was discarded. The second criterion was suggested by Heisey, Stokoe, and Meyer after conducting SASW tests at several sites (Heisey, 1982). Figure 3.23 shows the final dispersion curve calculated from the 24inch1 raw data file for the Osceola test site.

To construct a complete dispersion curve for the Osceola site the same process described above was carried out for receiver spacings of 3, 6, 12, 48, and 96 inches. The Complete final dispersion curve for the Osceola site is shown in Figure 3.24.

After the complete dispersion curve was formed by plotting the data obtained from each receiver spacing, the quality of the generated curve was evaluated by checking to see if the data obtained at the various receiver spacings agreed. The individual portions of the

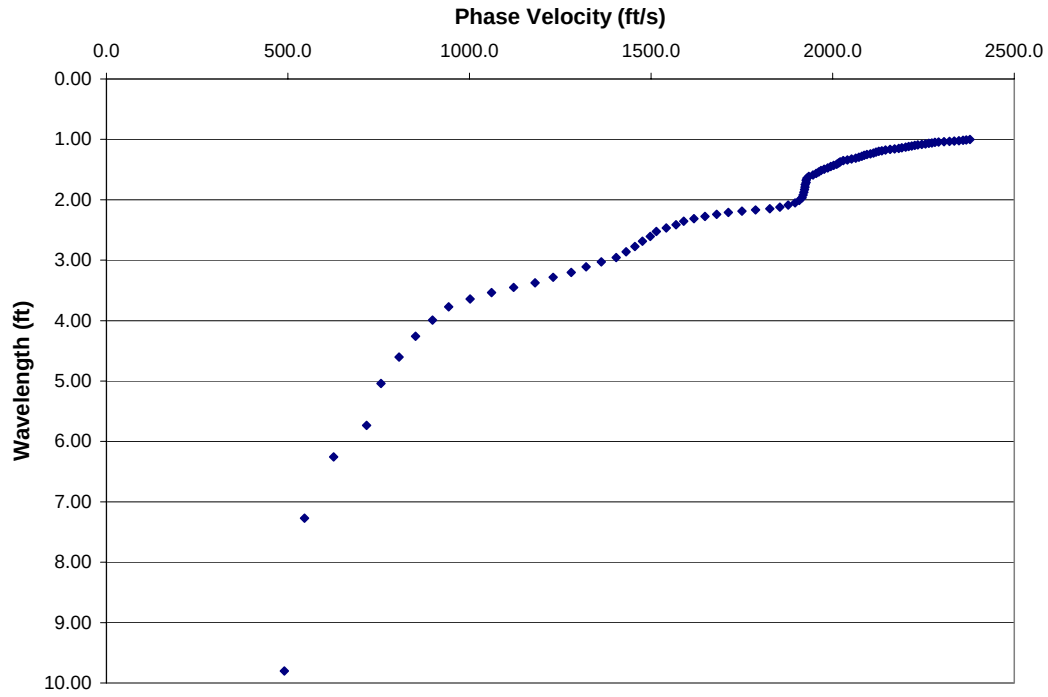

Figure 3.23 Dispersion curve for 24 inch receiver spacing at Osceola site

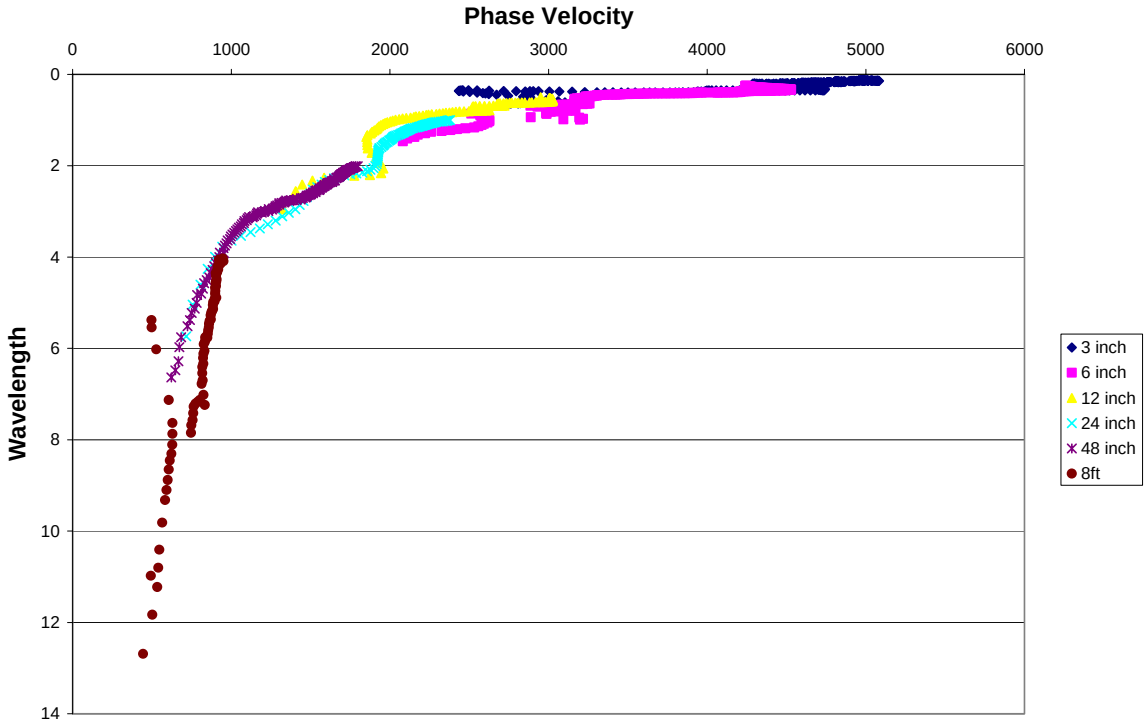

Figure 3.24 Dispersion curve using all receiver spacing data for Osceola site

dispersion curve formed for a single receiver spacing should overlap with the adjacent portions of the dispersion curve created using additional receiver spacings, forming one continuous curve. Looking at Figure 3.24, one can see that the data obtained for the Osceola test site exhibits very little scatter. Each individual portion of the dispersion curve overlaps very nicely with the adjacent portions of the dispersion curve formed by data obtained from additional receiver spacings. The shape of the curve is typical for an inversely dispersive profile, which was expected for the site. Additionally, the data obtained from the 8 ft receiver spacing forms two distinct branches, which is commonly seen as a result of different modes of propagation of Rayleigh waves through pavement systems.

3.3.1.3 Estimation of Layer Properties

To estimate the properties of the pavement system at the Osceola site using the simple inversion technique, the final experimental dispersion curve was transformed into a shear wave velocity profile using the recommendations given in section 2.3.3 of the literature review. Effective sampling depths of one half and one third of the wavelength were assumed, and the shear wave velocity was assumed to be equal to 1.1 times the Rayleigh wave velocity. Figure 3.25 shows the shear wave velocity profile obtained for the Osceola test site assuming an effective sampling depth of one half of the wavelength.

Once the shear wave velocity profile was established, the layer thicknesses that were recorded while drilling at the site were compared to the layers predicted by the velocity contrasts present in the shear wave velocity profile. The site profile obtained during the drilling operation is shown in Figure 3.25. To properly analyze the thin upper layers typically encountered with pavement structures, a close up view of the top 6 inches

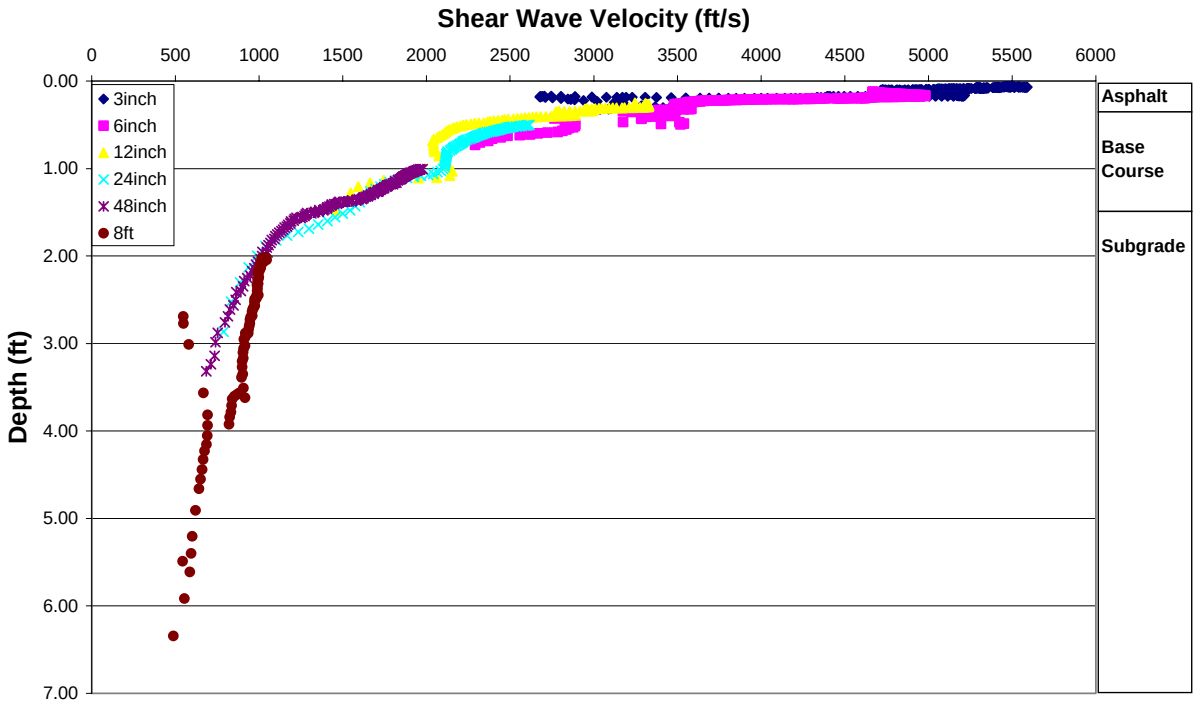

Figure 3.25 Shear wave velocity profile for Osceola site (Effective Depth = 1/2 Wavelength)

of the site profile is beneficial. A close up view of the top 6 inches for the Osceola site is shown in Figure 3.26. After obtaining layer thicknesses, modulus values were predicted by obtaining representative shear wave velocities for each layer, and then substituting into Equation 3.3.

$$M = 2\rho V_s^2(1+\nu) \qquad (3.3)$$

$$\text{where: } \rho = \frac{\gamma_t}{g}$$

The total unit weight (γ_t) and poisons ratio (ν) were assumed for each layer, allowing for a resilient modulus to be calculated for a given shear wave velocity.

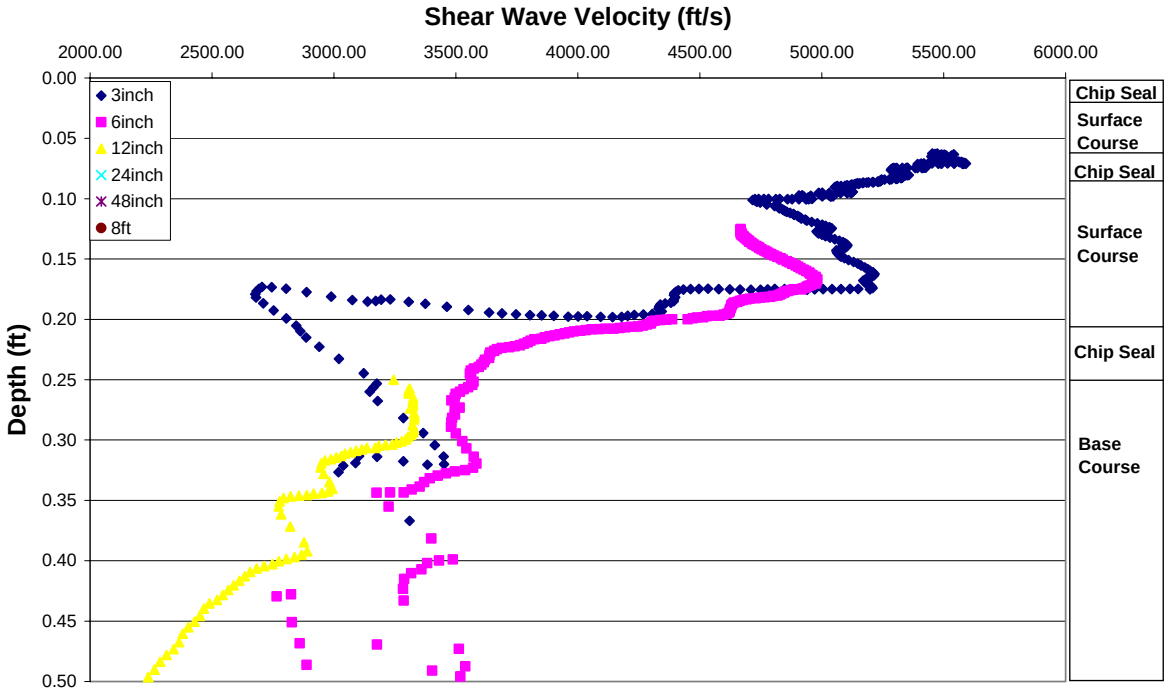

Figure 3.26 Top 6 inches of shear wave velocity profile for Osceola site

Table 3.7 presents the actual thicknesses of the layers present at the site as well as the layer thicknesses predicted using the simple inversion technique. The shear wave velocity for each layer as predicted by Figures 3.25 and 3.26, the assumed unit weight and Poisson's ratio for each layer, and the resilient modulus calculated from Equation 3.3 for each layer are all presented as well.

The values used for the Poisson's ratio and unit weight for each layer were chosen by assuming a value that fell within a range typically accepted for the type of material. Poisson's ratio for subgrade material typically varies from about 0.30 for sand to about 0.5 for saturated clay. A value of 0.40 was assumed for the Osceola site as the subgrade was clayey, but not saturated. Asphalt and base material typically have Poisson's ratios

between 0.30 and 0.40. An average value of 0.35 was taken for both of these materials. The unit weight of subgrade soils typically varies from about 100 to 120 lbs per cubic foot for clay, and from about 120 to 130 lbs per cubic foot for sand. An average value for clay of 110 lbs per cubic foot was assumed for the Osceola site. The unit weight of asphalt and base typically fall between 125 and 145 lbs per cubic foot. A unit weight of 140 lbs per cubic foot was chosen for both the asphalt and base for the Osceola site.

Table 3.7 Layer properties predicted for Osceola site using the simplified inversion technique

LAYER	ACTUAL THICKNESS (ft)	PREDICTED THICKNESS (ft)	SHEAR WAVE VELOCITY (ft/s)	UNIT WEIGHT (pcf)	POISSON RATIO	RESILIENT MODULUS (ksi)
Asphalt	0.25	0.20	5000	140	0.35	2038
Base	1.25	0.95	2000	140	0.35	326
Subgrade	N/A	N/A	480	110	0.40	15

In addition to predicting the total thickness of the asphalt layer fairly accurately, Figure 3.26 can also be used to gain useful information about individual layers of the asphalt. Unfortunately the upper two layers of asphalt, a 0.25 inch chip seal and 0.50 inch surface course layer, cannot be identified because they are too shallow to properly measure. The 1.5 inch surface course layer extending from depths of 0.083 ft to 0.208 ft (see Figure 3.26) can very easily be seen in the shear wave velocity profile. Figure 3.26 indicates that a lower velocity layer was present above the 1.5 inch surface course layer, and that a higher velocity layer was present above that. This was indeed the case at the site, as a thin chip seal layer was located on top of the 1.5 inch surface course layer, and a 0.5 inch surface course was present above the chip seal.

The thickness of the base layer was predicted using Figure 3.25. A large velocity contrast appears at a depth of approximately 1.15 ft (13.8 in), resulting in a

predicted base thickness of approximately 11.5 inches. The actual thickness of the base at the site was 15 inches. The discrepancy between the two values may be the result of contamination of the bottom 3 to 4 inches of base material with the fine grained clay subgrade present at the site.

The resilient modulus values reported in Table 3.7 are discussed in detail in the next section of this study, where they are compared to values obtained using FWD and laboratory triaxial testing.

3.3.2 UTEP Software

The second method used in this study to predict properties of pavement sections was to analyze raw data with a software program developed at the University of Texas at El Paso. Using this software provided two distinct advantages over the simplified inversion technique discussed previously. First, the program automatically constructs the experimental dispersion curve from the raw data file. Automatic construction of the dispersion curve greatly reduced the amount of time necessary to analyze the data. Secondly, the program uses the Haskell-Thompson matrix approach to produce a theoretical dispersion curve which matches the experimental dispersion curve. This approach is theoretically more sound, as it uses actual Rayleigh wave velocities to estimate resilient moduli instead of using apparent Rayleigh wave velocities, as is done when performing the simplified inversion technique.

The remainder of this section will discuss how the UTEP software manipulates the raw data files to predict layer thicknesses and resilient moduli of pavement layers. The data from the Osceola site will again be used for the example so that comparisons to the simplified inversion technique can be made. The discussion is designed to give an

outline of how the program operates. The reader is referred to Nazarian, Yuan, and Baker (1995) for specific information regarding the details of program operation.

3.3.2.1 Construction of Experimental Dispersion Curve

The program accepts up to five raw data files when constructing the experimental dispersion curve. The program was configured to accept raw data files collected from receiver spacings of 3, 6, 12, 24, and 48 inches. Each data file contained four columns of data representing frequency, the real portion of the frequency response function, the imaginary portion of the frequency response function, and the coherence. The raw data was organized identically to the data presented in Table 3.4. Multiple tests had been performed at each receiver spacing, which resulted in numerous raw data files being available for analysis. The coherence function was used to determine which raw data files were most appropriate to use, as was discussed in section 3.3.1.2.

Once the data files were selected the program calculated the phase shift that occurred between the receivers at each frequency, according to Equation 3.2. The phase shift and coherence values were then plotted as a function of frequency. The program then calculated a weighted least squares best-fit solution of the frequency response function to mathematically model the observed data (curve fitting technique). The model was created by dividing both the real and imaginary portions of the frequency response function into eight regions. The data contained within each region was modeled using a second degree polynomial. The coefficients for the polynomials were found by minimizing the error between the predicted and observed values. Data points containing a high value of coherence were weighted two times as much as data points containing low values of coherence when creating the mathematical model. The weighting was

carried out by introducing a weighting matrix into the calculation of the error between the observed and predicted data. The program used a threshold value of 0.9 to define which data points were weighted more heavily.

Figure 3.27 shows a screen shot of the observed phase shift and the phase shift predicted by the UTEP software using the curve fitting technique described above. The coherence function is plotted in the figure as well. From the figure it can be seen that the observed and predicted values match quite well, especially in the 500 to 2500 Hz frequency range. The program provided two settings, slowness and smoothness, to allow the user to manually adjust the predicted phase shift function if desired. The default values for slowness and smoothness were used for computation of the curve shown in Figure 3.27.

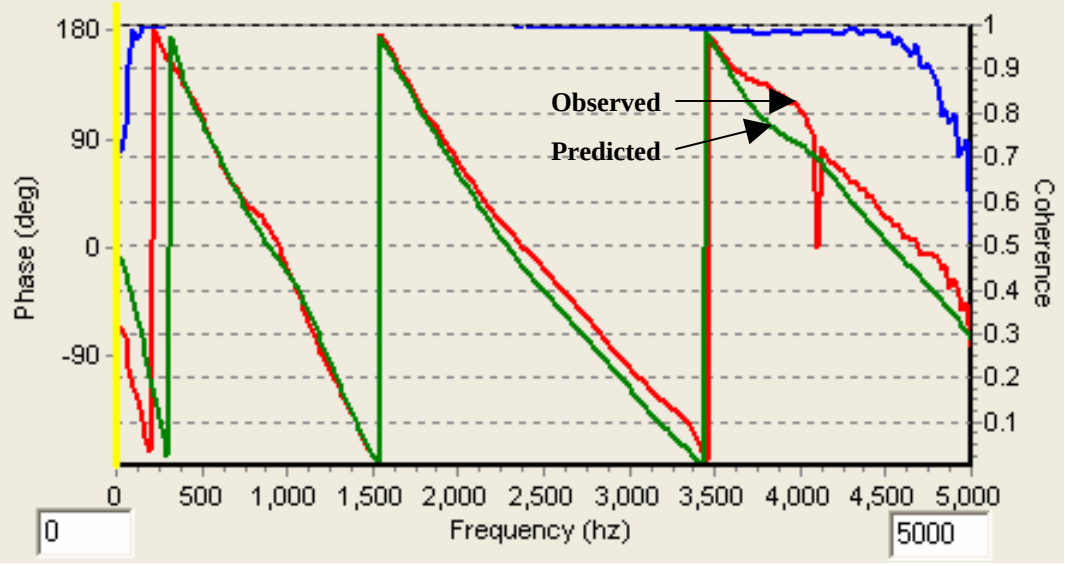

Figure 3.27 Observed and predicted phase shift values and coherence function from UTEP software

The agreement between Figure 3.27 and Figure 3.20, which was calculated as part of the simplified inversion process, should be noted. The only difference that exists between

Figure 3.27 and Figure 3.20 is that the UTEP software shows the phase wrapped over a 360 degree cycle instead of the 180 degree cycle used in the simplified inversion procedure. This difference in no way effects computations, and is only a difference in how the data is visually displayed. The similarity between the figures shows that up to this point the two pavement layer prediction methods are identical, with the exception that the UTEP program created a mathematical model of the phase shift using a curve fitting procedure. This mathematical model is useful in simplifying calculations later.

The program automatically defined a range of frequencies over which points for the dispersion curve were calculated, however a manual selection option was available to define the frequency range when so desired. The equations used to calculate each point on the dispersion curve over the specified range were identical to those used for the simplified inversion technique. The only difference between the two techniques was that the program obtained the value of phase shift using the mathematical model of the phase shift. The dispersion curve calculated for the 24 inch receiver spacing at the Osceola site is shown in Figure 3.28. The curve in Figure 3.28 is nearly identical to the curve in Figure 3.23 which was computed using the simplified inversion technique. This lends credibility to the use of a mathematically modeled phase shift when determining points on the dispersion curve.

The procedure used to create the portion of the dispersion curve from the 24 inch spacing raw data was also carried out on data from the other receiver spacings. To create the final dispersion curve, the program took all dispersion data points obtained using the procedure outlined above which contained coherence values greater than or equal to the threshold value of 0.9, and combined them into a separate file. The number of data

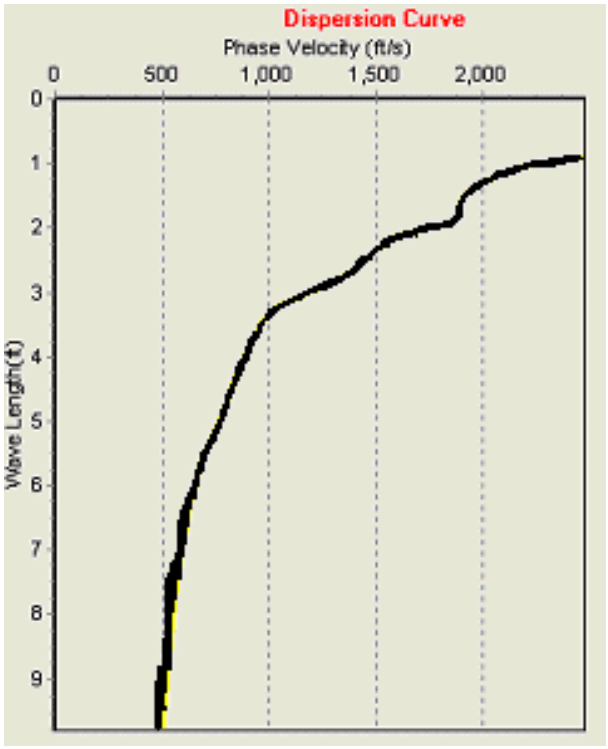

Figure 3.28 Dispersion curve from UTEP software for Osceola 24 inch receiver spacing

points contained in this file was on the order of thousands of data points, which would have made the time necessary to compute a final dispersion curve excessive. To prevent this problem, the program reduced the number of data points actually used to compute the dispersion curve using the following criteria:

1) Data points containing a coherence below the threshold value of 0.9 were discarded
2) Data points that were nearly identical were eliminated using an averaging process

The next step taken by the program was to perform a curve fitting technique on the remaining data points to obtain a final dispersion curve. The curve fitting technique used was based on a least-absolute-value best-fit method. The curve fitting technique was carried out by dividing the remaining data points into three equal sets, and fitting a

fourth degree polynomial to each of the sets. The polynomials obtained for each of the three sets were then combined to form the final dispersion curve. A window averaging process then further reduced the number of data points to facilitate the inversion process carried out next. Figure 3.29 shows the final dispersion curve calculated for the Osceola site. The final dispersion curves calculated using the outlined procedure contain between 20 and 50 points depending on the quality of the data. The dispersion curve for the Osceola site shown in Figure 3.29 is defined by 33 data points.

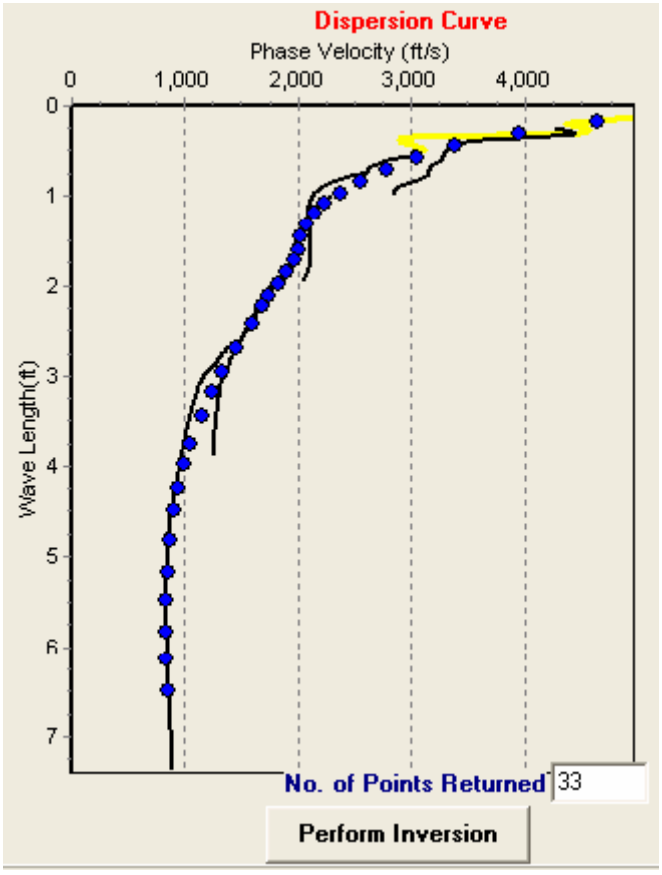

Figure 3.29 Final dispersion curve and idealized dispersion curve for Osceola site

3.3.2.2 Inversion Process and Estimation of Layer Properties

The first step taken to invert the final dispersion curve was to estimate a trial profile for the site. The trial profile contained estimated layer thicknesses, Poisson's ratios, unit weights, and shear wave velocities. The layer thicknesses were known from borings made at the site at the time SASW testing was performed. Poisson's ratio and unit weights for the layers were estimated by taking typical values for asphalt, base, and clay subgrade (clay subgrade was observed at the site). Initial values for shear wave velocities were supplied by the program. The trial profile used for the site is shown in Table 3.8.

Table 3.8 Trial profile used to perform inversion of dispersion data from Osceola site

	Thickness, in (known)	**Poisson's Ratio** (assumed from standard values)	**Unit Weight, pcf** (assumed from standard values)	**Shear Wave Velocity, ft/s** (provided by program)
ASPHALT	3	0.35	140	4004
BASE	15	0.35	140	1114
SUBGRADE	N/A	0.40	110	472

The program uses an iterative process based on general inverse theory to perform the inversion. To begin the process the program calculates a theoretical dispersion curve using the Haskell-Thompson matrix approach for the trial profile. The thicknesses and shear wave velocities of each layer are represented as a vector, and the goal of the program is to minimize the difference between the observed and theoretical data by performing successive iterations on the trial profile vector. The difference was considered to be acceptably small when the root mean squares error criterion reached a value of 0.9, or the maximum specified number of iterations (set to 50) had been reached. The resulting vector of layer thicknesses and shear wave velocities yielded the layer properties sought after for this study. The final profile obtained for the Osceola site after

the inversion process was performed is shown in Table 3.9. Figure 3.30 shows the experimental and final theoretical dispersion curves on the left, and the final modulus profile on the right.

Table 3.9 Layer properties predicted by inversion process using program defaults

Layer	Thickness (in)	Resilient Modulus (ksi)
Asphalt	1.6	2243
Base	4.8	420
Subgrade	N/A	12

The first point of interest is to examine the agreement between the observed and final theoretical (hereafter referred to as the theoretical curve). From Figure 3.30 it can be seen that the two dispersion curves match quite well, virtually overlapping one another. The second matter of interest is to compare the agreement between the modulus values predicted using the UTEP software and the simplified inversion technique

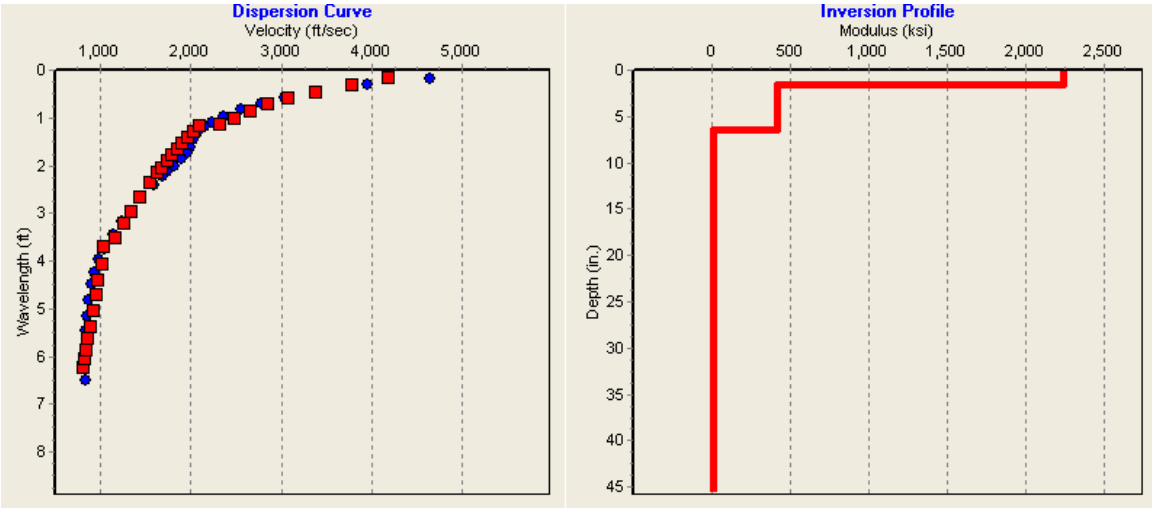

Figure 3.30 Experimental and final theoretical dispersion curves (left) and modulus profile (right) for Osceola site

previously discussed. Referring to Tables 3.7 and 3.9, it can be seen that the two techniques predicted modulus values reasonably close to one another. The third matter of interest is to compare how well the UTEP program predicted known layer thickness. Referring to Tables 3.8 and 3.9 reveals that the UTEP program did not predict layer thicknesses accurately using the given trial profile and default program settings.

At this point several parameters were varied to see if a theoretical curve could be obtained that both fit the experimental dispersion curve, and accurately predict layer thicknesses. Layer thickness was used as an estimate of the validity of the obtained theoretical curve because it was a known parameter. It was found that by changing the trial profile such that the initial guess for the Poissons ratio of the base was 0.38, a theoretical curve was calculated which both fit the experimental data and accurately estimated layer thicknesses. Figure 3.31 shows the experimental and theoretical curves as well as the modulus profile for this situation. Table 3.10 shows the layer thicknesses and resilient modulus values predicted by the simplified inversion technique, UTEP program using default settings/original trial profile, and UTEP program using default settings/modified trial profile.

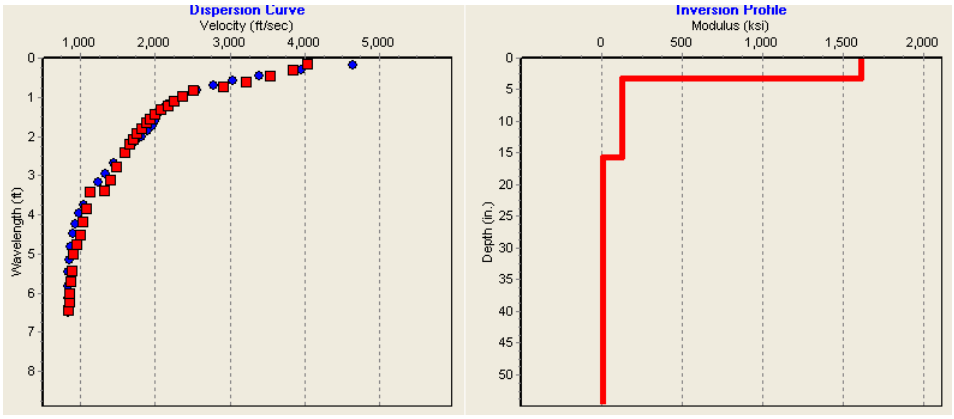

Figure 3.31 Experimental and theoretical dispersion curves and modulus profile for Osceola site using modified trial profile

Table 3.10 Layer properties predicted using modified trial profile for Osceola site

	Simplified Inversion		Program (default settings and initial profile)		Program (default settings and modified profile)	
Layer	**Thickness (in)**	**Modulus (ksi)**	**Thickness (in)**	**Modulus (ksi)**	**Thickness (in)**	**Modulus (ksi)**
Asphalt	2.4	2038	1.6	2243	3.2	1612
Base	11.4	326	4.8	420	12.4	130
Subgrade	N/A	15	N/A	12	N/A	9

The thicknesses predicted using the program with the modified trial profile are in much closer agreement with both actual measured thicknesses and the thicknesses predicted using the simplified inversion process. The predicted thickness of the base is still a bit lower than what was observed at the site, however this could have been the result of contamination of the lower portions of the base with fines (as was discussed earlier).

The resilient modulus values are substantially lower than those reported in Table 3.7 for the simplified inversion process. These values, and conclusions that can be drawn from them, are discussed in detail in the next section of this study, where they are compared to values obtained using FWD and laboratory triaxial testing.

Section 3.3.3 Falling Weight Deflectometer (FWD) Data Reduction

FWD data was reduced using three software programs, Roadhog, Elmod5, and Evercalc. Roadhog (Elliot, et. al.) is a straightforward program that estimates subgrade modulus based upon a series of regression equations. Elmod5 and Evercalc are more complex programs that allow for a variety of methods and options to be used to predict subgrade moduli based on the data collected during FWD testing. A brief description of how the data was reduced using each program is presented below.

Elmod5 allows for either deflection basin or radius of curvature analysis techniques to be used to predict the modulus of the pavement layers present at each site. The program can predict the modulus of each layer at a site, or the user may define a fixed value for one or more of the layers and allow the program to predict the modulus of the remaining layers. For this study, the data collected at each test site was analyzed using both the deflection basin and radius of curvature methods. Initially the program was allowed to predict the modulus of each of the pavement layers, and no modulus values were fixed by the user. A maximum of three layers were used to model each site; an asphalt layer, a base layer (if present) and a subgrade layer. After the initial analysis was completed, it was observed that at many locations the program predicted unreasonable values for the layers. As the subgrade modulus was the primary parameter of interest for this study, the next step taken was to fix the modulus values of the asphalt and base course layers, to allow the program to predict only the subgrade modulus. The base course modulus value was fixed at 45 ksi and the asphalt modulus was fixed both at 200 ksi and 2000 ksi. The results of the iterations are shown in Figure 3.32.

Evercalc was used to reduce the raw FWD data in much the same way as Elmod5. Initially Evercalc was used to calculate the modulus of each layer of the pavement system (maximum of 3 layers used) with no restrictions imposed. The next step taken was to impose restrictions upon the allowed modulus values for each layer. Instead of allowing the user to fix the modulus of a given layer as does Elmod5, Evercalc allows the user to specify a range of values into which the modulus of a layer may fall. The asphalt modulus range was set at 200 ksi to 2000 ksi, the base modulus range was set at 30 ksi to

60 ksi, and the subgrade modulus range was set at 1 ksi to 60 ksi. The results of the iterations are shown in Figure 3.32.

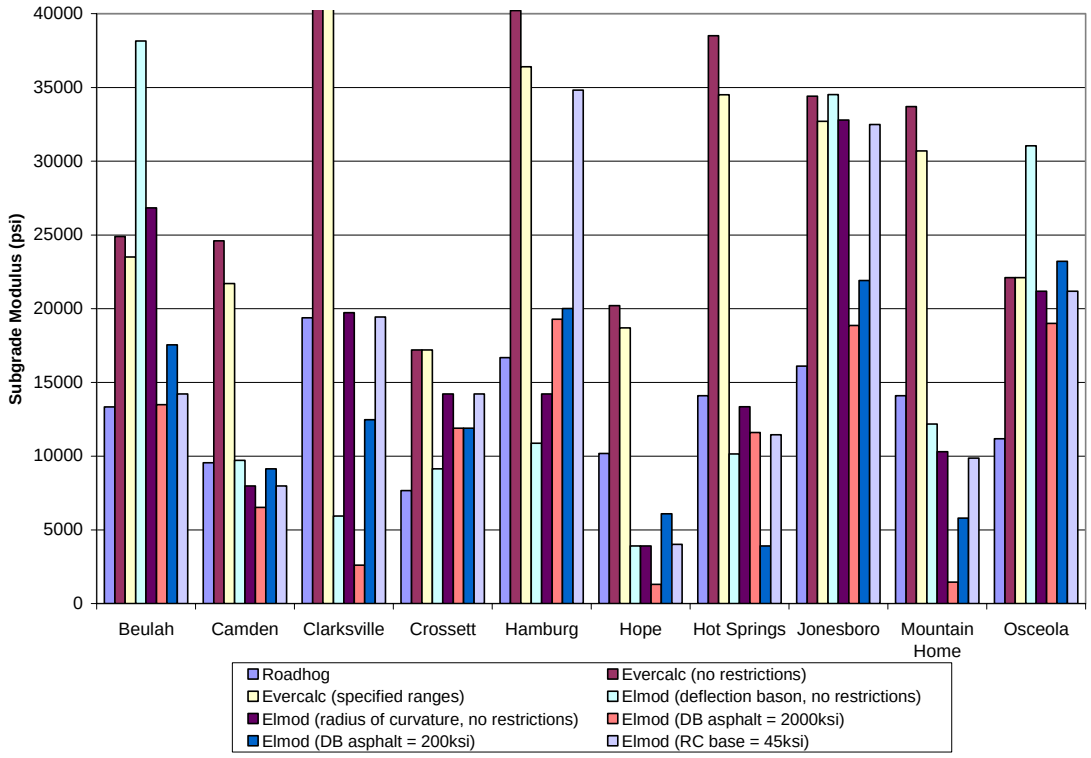

Figure 3.32 Subgrade modulus predicted by various FWD methods

Figure 3.32 shows that the various methods predicted a wide range of subgrade modulus values. To allow for SASW results to be compared to FWD, it was necessary to develop a single subgrade modulus value considered representative for each site. To do this several steps were taken. First, the radius of curvature methods were discarded. Next, the pavement condition at each site was taken into account by choosing the deflection basin fitting value that best represented each site. For example, the pavement condition at the Hope site was observed to be very poor, consequently the deflection basin value predicted using an asphalt modulus of 200 ksi was kept, while the deflection basin value predicted using an asphalt modulus of 2000 ksi was discarded. Finally, it was

observed that the modulus values predicted by Evercalc were very nearly twice the value as predicted by the other methods. Consequently, the values predicted by the Evercalc program were divided by two. The results for the FWD after these steps were taken are shown in Figure 3.33. From the results shown below, a single representative subgrade modulus value was able to be obtained for each site. The values used for each site are given in Chapter 4.

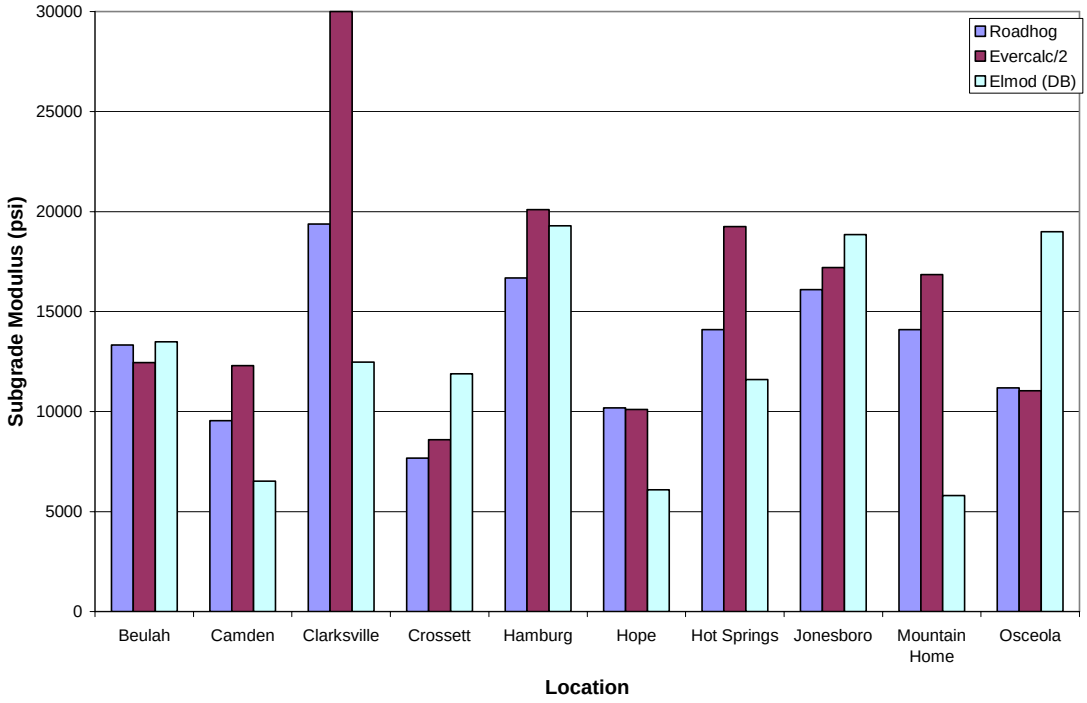

Figure 3.33 Subgrade modulus values predicted by applicable FWD methods

CHAPTER 4

PRESENTATION OF RESULTS

This chapter presents the results obtained from the testing of ten flexible pavement sites located throughout the state of Arkansas. The sites were chosen such that a wide variety of subgrade soils typically encountered in the state of Arkansas are represented. Figure 4.1 shows the general location of the sites tested. Appendix A contains information about each of the sites tested, including GPS coordinates.

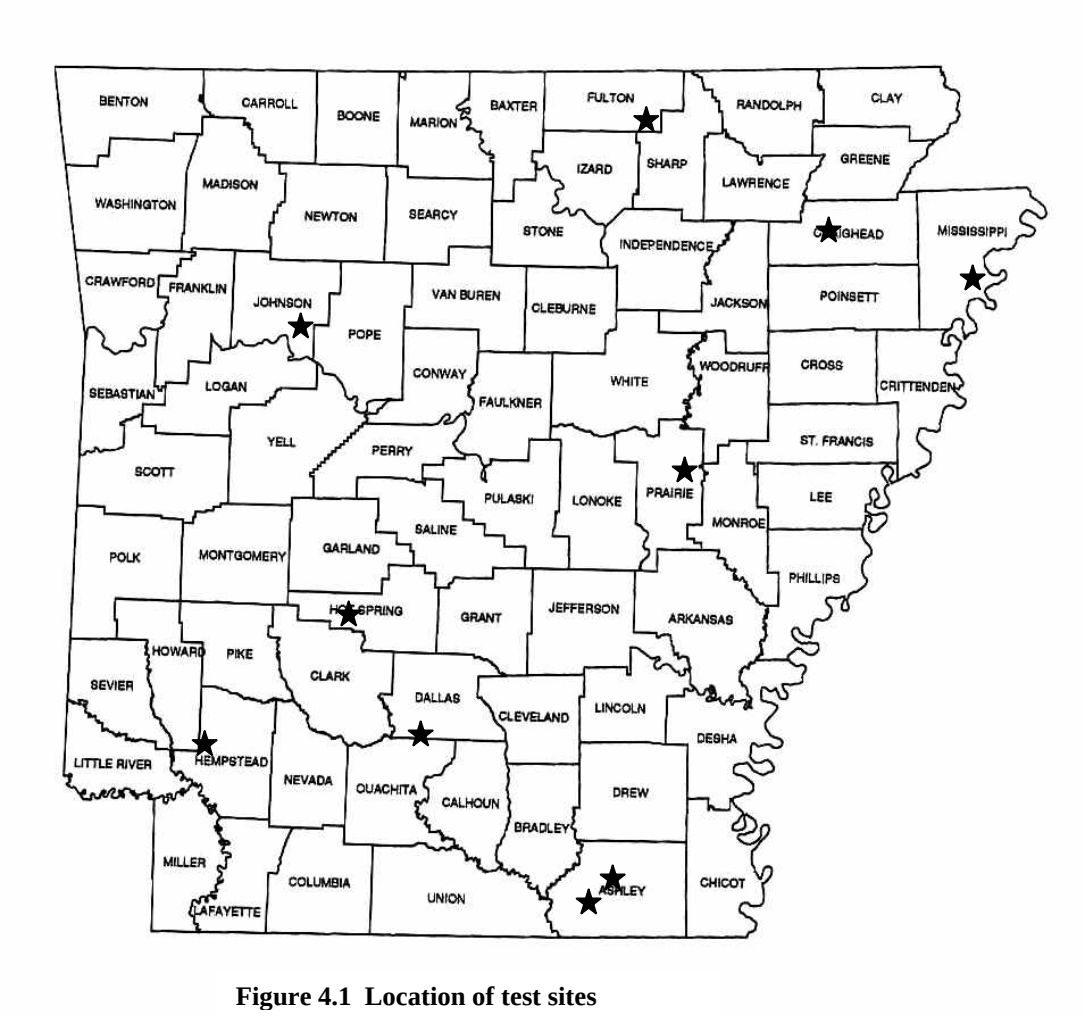

Figure 4.1 Location of test sites

A summary of the results from each of the testing methods used to evaluate the conditions of the pavement components and subgrade soils are contained in Tables 4.1 and 4.2. Table 4.1 contains the moduli of the pavement layers predicted from spectral analysis of surface wave testing. SASW testing was conducted using the procedures described in Chapter 3. The first four columns of data represent the modulus values predicted for the subgrade layer by both the simplified inversion (manual) method and by the software provided by the University of Texas at El Paso. The data reduction procedures for each of the methods are described in Chapter 3. The procedure for producing the data contained in the column labeled "UTEP Program Adjusted", however, was not described in Chapter 3, but is addressed in the ***UTEP Software*** portion of this chapter. Notice that there are several blanks present in the two columns of data which contain the results from the UTEP software. The reasons these blanks are present are discussed in section 4.2.

The last two columns of data contained in Table 4.1 represent the modulus of the asphalt and base course layers. The moduli reported for the asphalt and base course layers were predicted using the UTEP software by the layer constraint/modified profile method. This was the modulus selected for reporting because it is regarded as being the most reliable of the methods employed during this study, and reporting additional values would unnecessarily complicate the data. Note that no base course modulus is given for the Hamburg or Crossett test sites as no base course was present at these two locations.

Table 4.2 summarizes the test results obtained for the subgrade soils from laboratory resilient modulus testing, FWD, and the standard penetration test (SPT). The

Table 4.1 Resilient moduli of pavement layers predicted from spectral analysis of surface waves (SASW) method (English units)

	Subgrade Modulus				Asphalt and Base Course Modulus (UTEP Constrained)	
Location	M_r Simple Inversion (ksi)	M_r UTEP Program Defaults (ksi)	M_r UTEP Program Adjusted (ksi)	M_r UTEP Program Constraints (ksi)	Base Modulus (ksi)	Asphalt Modulus (ksi)
Beulah	26	36	-	25	119	2769
Camden	22	25	-	24	73	2074
Clarksville	44	-	36	35	81	1377
Crossett	9	32	13	15	-	3161
Hamburg	35	49	33	33	-	2571
Hope	7	-	6	4	94	3822
Hot Springs	7	-	10	9	20	1593
Jonesboro	15	25	-	25	48	2692
Mountain Home	28	26	-	33	123	1394
Osceola	15	11	-	9	130	1612

Table 4.2 Resilient modulus of subgrade soils from laboratory and FWD methods, and standard penetration test N-values (English units)

	Laboratory Triaxial Testing		FWD	Standard Penetration Test	
Location	Sample Depth (ft)	M_r (ksi)	M_r (ksi)	Sample Depth (ft)	N-Value
Buelah	4.0 - 4.5	6.5	13	6.5 - 8.0	8
Camden	-	N/A	10	1.5 - 3.0	18
Clarksville	-	N/A	20	0.5 - 2.0	43
Crossett	5.5 - 6.0	6.75	9	1.5 - 3.0	3
Hamburg	3.75 - 5.0	7.8	18	7.0 - 8.5	12
Hope	5.0 - 6.0	8.2	9	3.5 - 5.0	7
Hot Springs	2.0 - 4.5	N/A	14	0 - 1.5	10
Jonesboro	-	N/A	16	4.5 - 6.0	13
Mountain Home	3.7 - 4.2	6	15	4.5 - 6.0	18
Osceola	3.75 - 4.5	4.6	11	6.5 - 8.0	8

Table 4.3 Resilient moduli of pavement layers predicted from spectral analysis of surface waves (SASW) method (SI units)

	Subgrade Modulus				Asphalt and Base Course Modulus (UTEP Constrained)	
Location	M_r Simple Inversion (MPa)	M_r UTEP Program Defaults (MPa)	M_r UTEP Program Adjusted (MPa)	M_r UTEP Program Constraints (MPa)	Base Modulus (MPa)	Asphalt Modulus (MPa)
Beulah	179	248	-	172	821	19,090
Camden	152	172	-	166	503	14,300
Clarksville	303	-	248	241	559	9,490
Crossett	62	221	90	103	-	21,790
Hamburg	241	338	228	228	-	17,730
Hope	48	-	41	28	648	26,350
Hot Springs	48	-	69	62	138	10,980
Jonesboro	103	172	-	172	331	18,560
Mountain Home	193	179	-	228	848	9,610
Osceola	103	78	-	62	896	11,110

Table 4.4 Resilient modulus of subgrade soils from laboratory and FWD methods, and standard penetration test N-values (SI units)

	Laboratory Triaxial Testing		FWD	Standard Penetration Test	
Location	Sample Depth (m)	M_r (MPa)	M_r (MPa)	Sample Depth (m)	N-Value
Buelah	1.22 - 1.37	45	90	1.98 - 2.44	8
Camden	-	N/A	69	0.46 - 0.91	18
Clarksville	-	N/A	138	0.15 - 0.61	43
Crossett	1.68 - 1.83	47	62	0.46 - 0.91	3
Hamburg	1.14 - 1.52	54	124	2.13 - 2.59	12
Hope	1.52 - 1.83	57	62	1.07 - 1.52	7
Hot Springs	0.61 - 1.37	N/A	97	0 - 0.46	10
Jonesboro	-	N/A	110	1.37 - 1.83	13
Mountain Home	1.13 - 1.28	41	103	1.37 - 1.83	18
Osceola	1.14 - 1.37	32	76	1.98 - 2.44	8

depths at which undisturbed Shelby tube samples were obtained at each site for laboratory resilient modulus testing are also reported in Table 4.2. The depths at which SPT testing was conducted is reported as well. Results of these three test procedures are reported to allow for comparisons to SASW testing results, which gives an indication of whether or not the results obtained from SASW testing are reasonable. Tables 4.3 and 4.4 present the information from Tables 4.1 and 4.2 in terms of SI units.

Index properties of the subgrade soils encountered at each of the test sites are summarized in Table 4.5. These properties are included to give an indication of the type of engineering properties the subgrade soils are expected to exhibit. These properties may also give insight into the range of values that can be expected for resilient modulus. Soil classification by the Unified Soil Classification System (USCS) and AASHTO are also included in Table 4.5.

Resilient modulus is highly dependent upon the amount of moisture present in the subgrade soil. The moisture content at the time field testing was conducted and the moisture content at the time laboratory testing took place are included in Table 4.6. The optimum moisture content and maximum dry density of the subgrade soils as found by performing Standard Proctor tests, are also included in Table 4.6. The difference between the optimum moisture content and the moisture content measured during laboratory modulus testing is given in Table 4.6.

In section 3.2.2.1 it was mentioned that soil sampling was conducted through a combination of split spoon, Shelby tube, and bulk disturbed sampling techniques. Resilient modulus testing was conducted on the subgrade located directly beneath the

pavement sections. Subgrade index properties (excluding moisture contents) were found by testing the

Table 4.5 Index properties of subgrade soils present at test sites

Location	Specific Gravity	Liquid Limit	Plastic Limit	%Passing #200	USCS Classification	AASHTO CLASSIFICATION
Beulah	2.71	17	15	49	SM (Silty Sand)	A-4 (0)
Camden	2.69	NP	NP	38	SM (Silty Sand)	A-4 (0)
Clarksville	2.72	29	12	35	GC (Clayey Gravel w/Sand)	A-2-6 (1)
Crossett	2.73	23	14	80	CL (Lean Clay w/Sand)	A-4 (5)
Hamburg	2.73	27	17	87	CL (Lean Clay)	A-4 (7)
Hope	2.79	57	18	83	CH (Fat Clay w/Sand)	A-7-6 (33)
Hot Springs	2.70	23	15	55	CL (Sandy Lean Clay)	A-4 (2)
Jonesboro	2.72	34	15	81	CL (Lean Clay w/Sand)	A-6 (14)
Mountain Home	2.75	25	15	45	SC(Sandy Clay with Gravel)	A-4 (1)
Osceola	2.73	38	19	73	CL (Lean Clay w/Sand)	A-6 (12)

Table 4.6 Moisture content and Standard Proctor results for subgrade soils at test sites

Location	Moisture Content		Difference Between Lab Moisture and Optimum Moisture	Standard Proctor Test Results	
	In-situ	Mr Lab Testing		Optimum Moisture Content %	Maximum Dry Unit Weight (pcf)
Beulah	13.4	13.5	+3.7	9.8	127
Camden	10.6	Not Tested	N/A	9.5	120
Clarksville	15.2	Not Tested	N/A	13.6	119
Crossett	23.6	24.0	+12	12.5	121
Hamburg	19.4	18.9	+5.9	13	119
Hope	26.3	28.5	+11.5	17	107
Hot Springs	15.7	Not Tested	N/A	13.2	118
Jonesboro	34.4	Not Tested	N/A	16.1	113
Mountain Home	25.7	27.2	N/A	15.0	114.1
Osceola	30.5	30.6	+15.6	15.0	111

bulk disturbed soil samples collected from the shoulders of the roadways at each of the test sites. Moisture contents were found by testing recovered split spoon samples. Therefore, some error is inherently present when attempting to associate index properties to either in-situ moisture content data or to modulus results. This error can be seen in the fact that the in-situ moisture contents for Mountain Home, Jonesboro, and Crossett sites all appear to be above the liquid limit of the subgrade. This is likely not the case, and is a result of testing soils from differing locations.

The remainder of this chapter is devoted to discussion of the results contained in Tables 4.1 through 4.6. The discussion of the results will follow the same pattern as that used in the Data Reduction Methods portion of Chapter 3; the simplified inversion method results are discussed first, followed by the results obtained using various techniques involving the UTEP software package. Comparisons are made both between the SASW methods and between SASW and the testing methods listed in Table 4.2.

4.1 Simple Inversion (Manual) Results

The shear wave velocity profiles calculated for each test site are shown in Figures 4.2 through 4.21 beginning on the next page. The shear wave velocity profiles were created using the procedures outlined in Chapter 3. During the data reduction phase it was found that an effective sampling depth of one half of the wavelength yielded the most accurate results, Figures 4.2 through 4.21 were created using this assumption. Two views of each shear wave velocity profile are provided; a full-scale view, and a close-up view of the top 6 to 9 inches of the profile to allow the thinner upper layers of the pavement system to be identified. The thickness of each layer of the pavement system

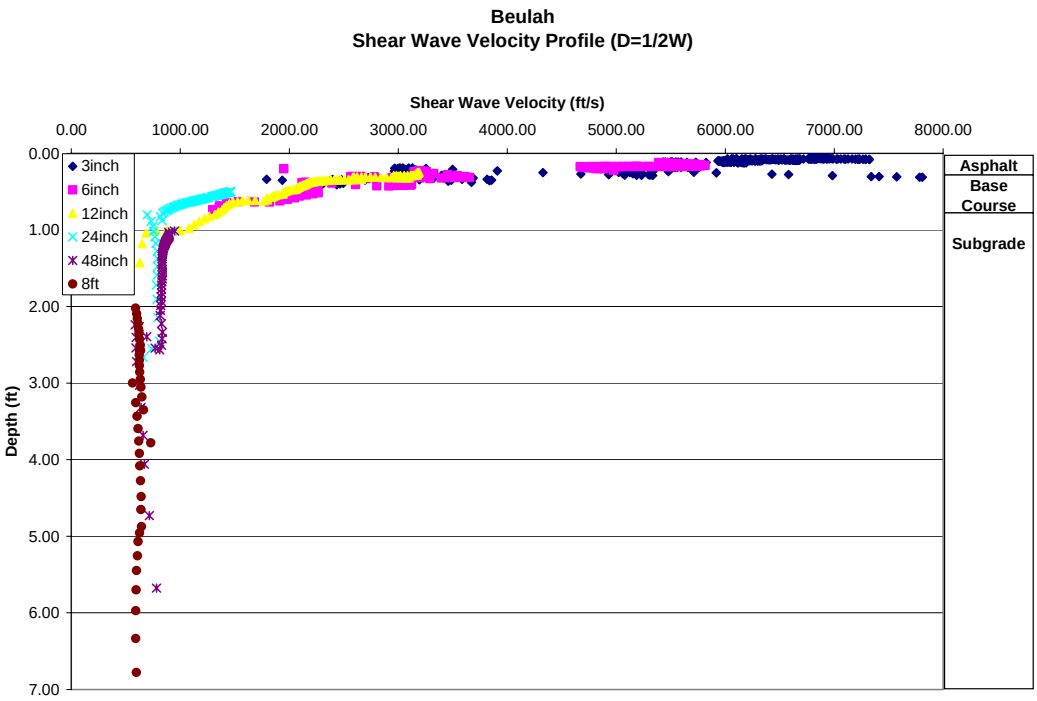

Figure 4.2 Full-scale view of Beulah shear wave velocity profile

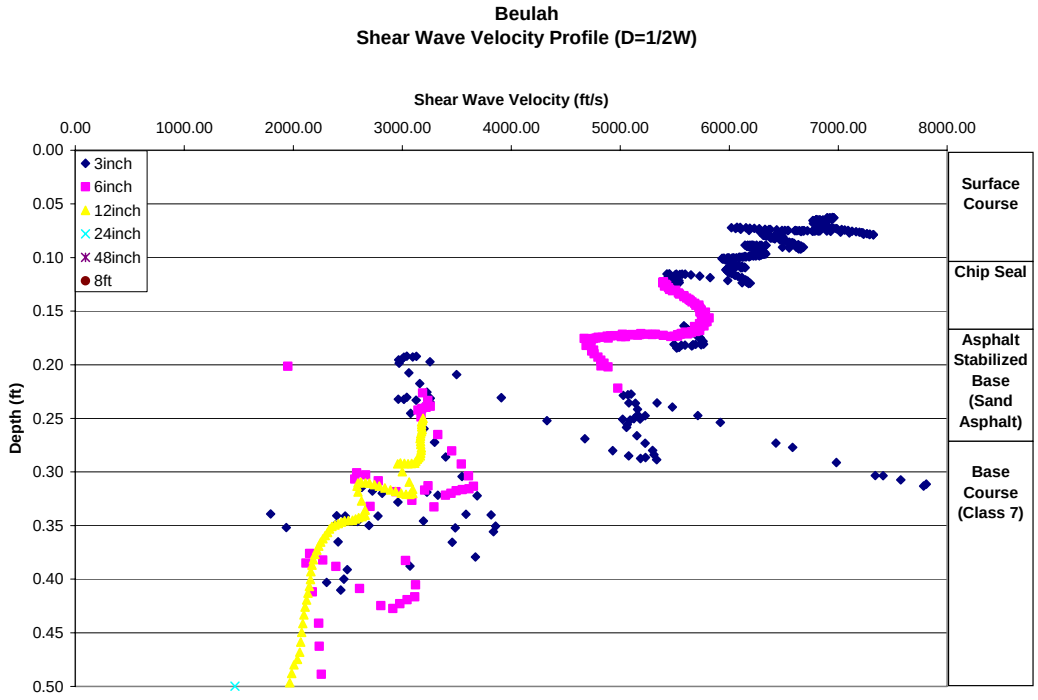

Figure 4.3 Close-up of top 6 inches of Beulah shear wave velocity profile

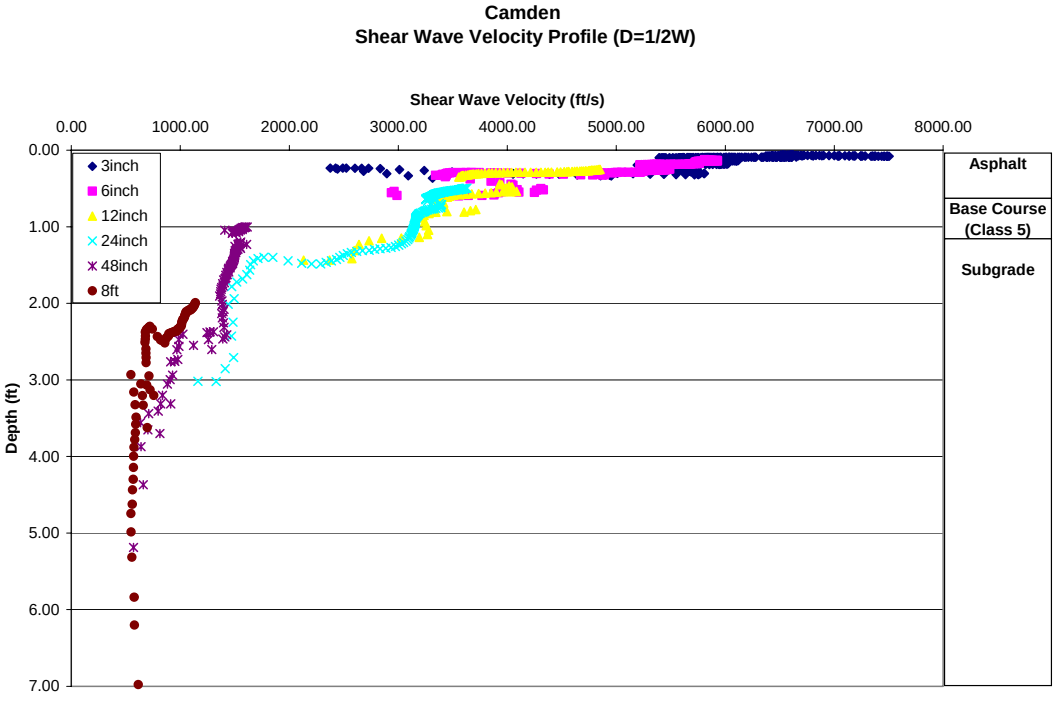

Figure 4.4 Full-scale view of Camden shear wave velocity profile

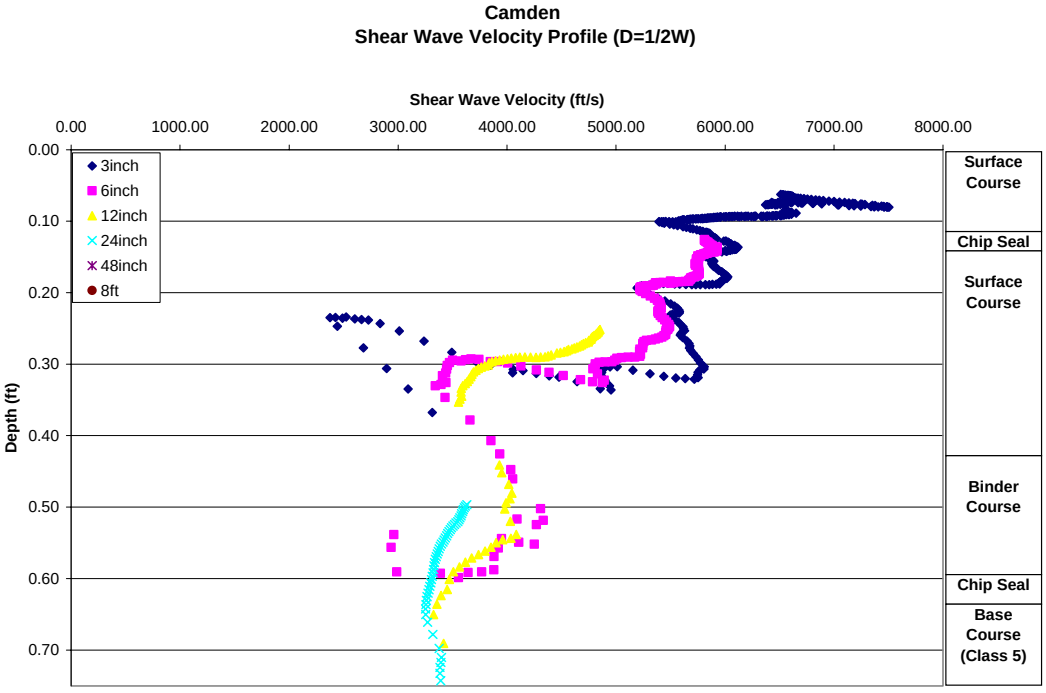

Figure 4.5 Close-up of top 9 inches of Camden shear wave velocity profile

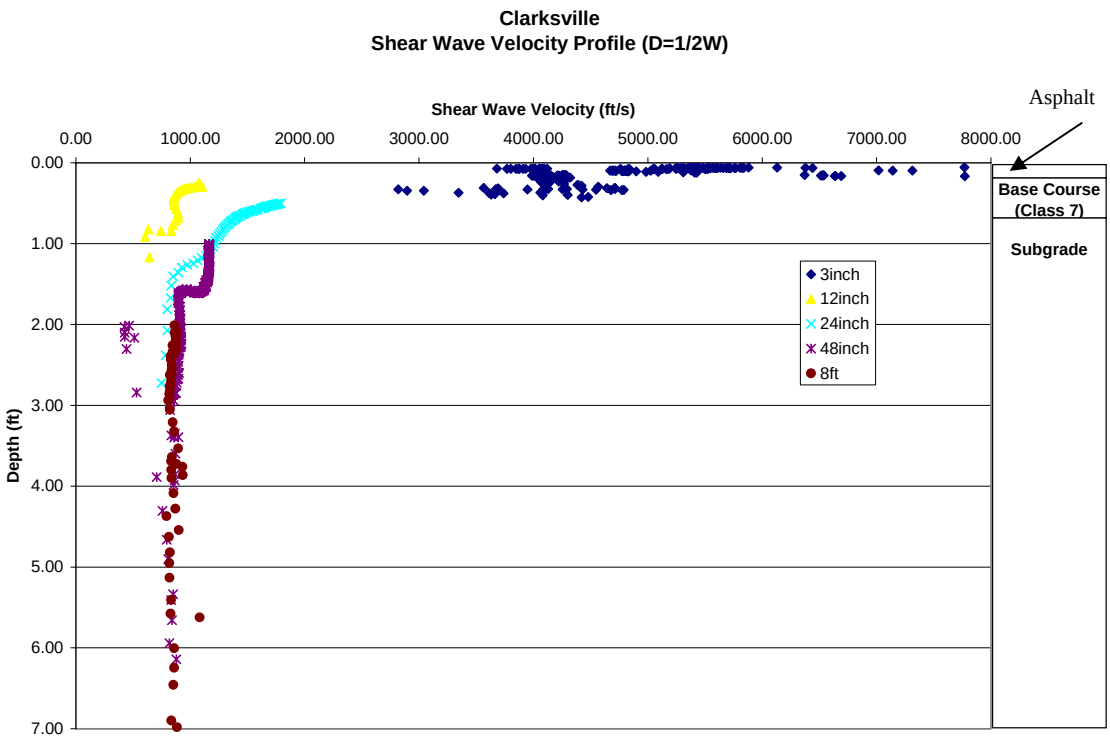

Figure 4.6 Full-scale view of Clarksville shear wave velocity profile

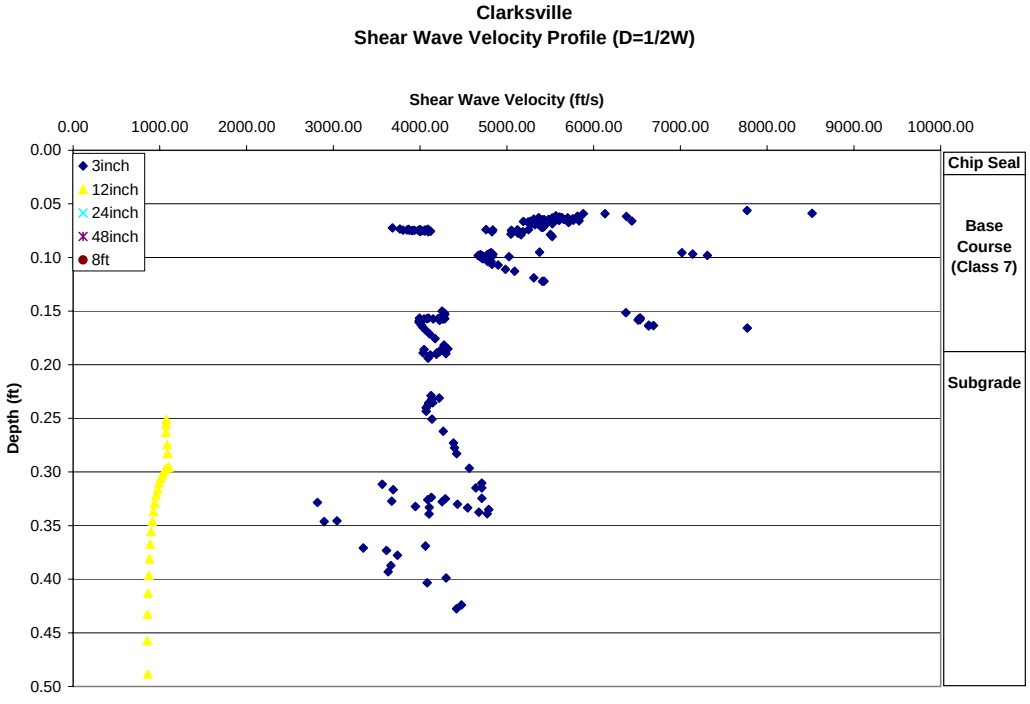

Figure 4.7 Close-up of top 6 inches of Clarksville shear wave velocity profile

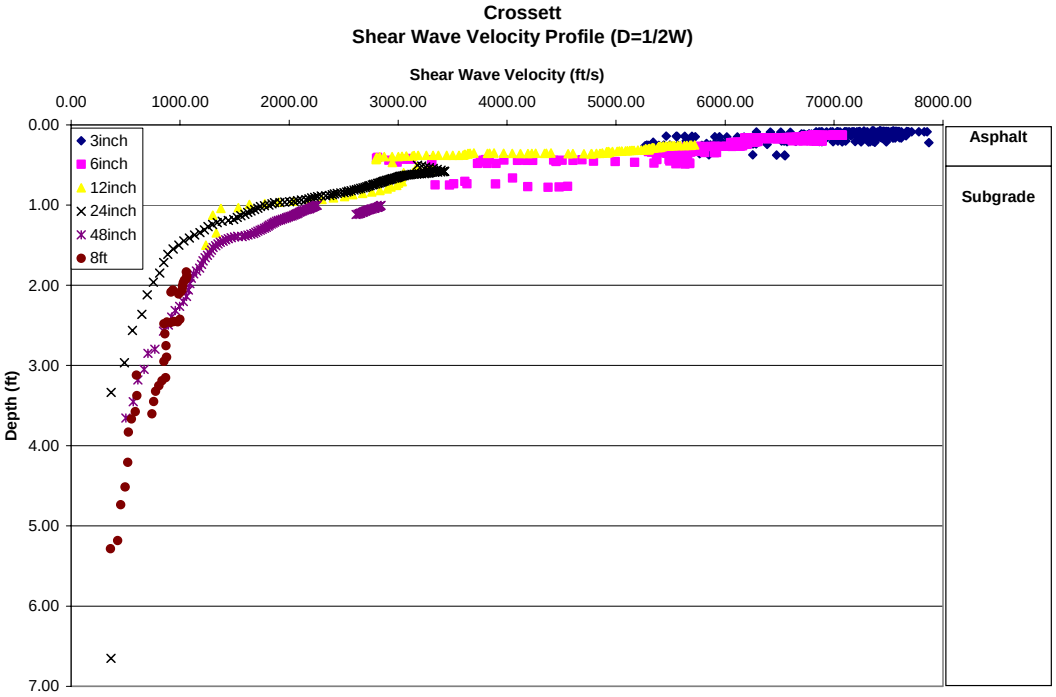

Figure 4.8 Full-scale view of Crossett shear wave velocity profile

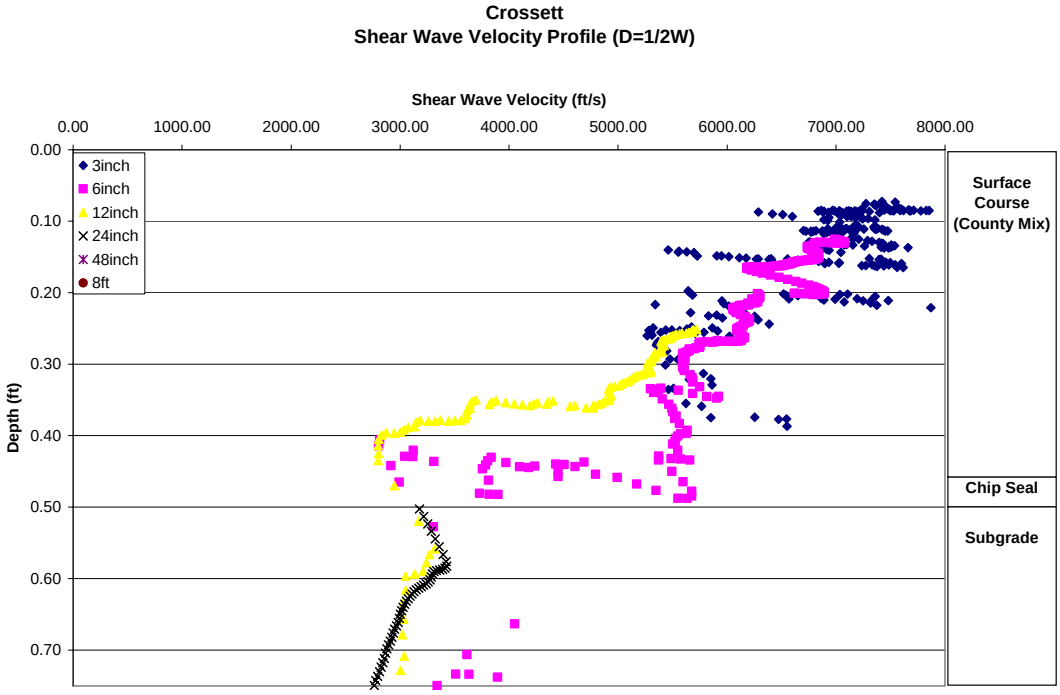

Figure 4.9 Close-up of top 9 inches of Crossett shear wave velocity profile

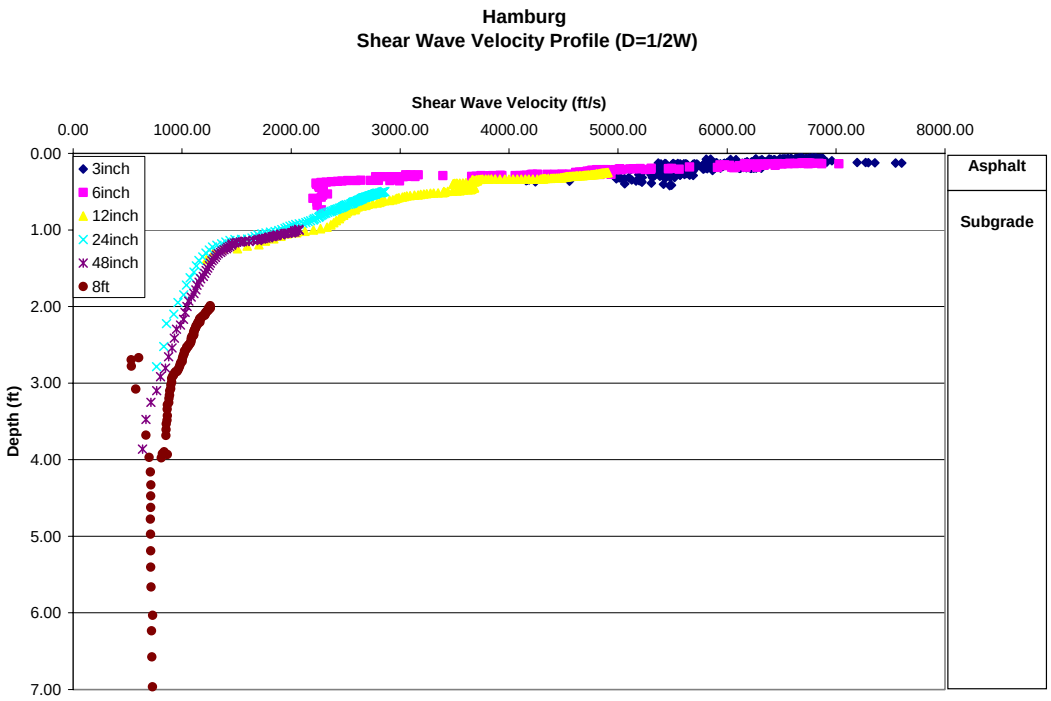

Figure 4.10 Full-scale view of Hamburg shear wave velocity profile

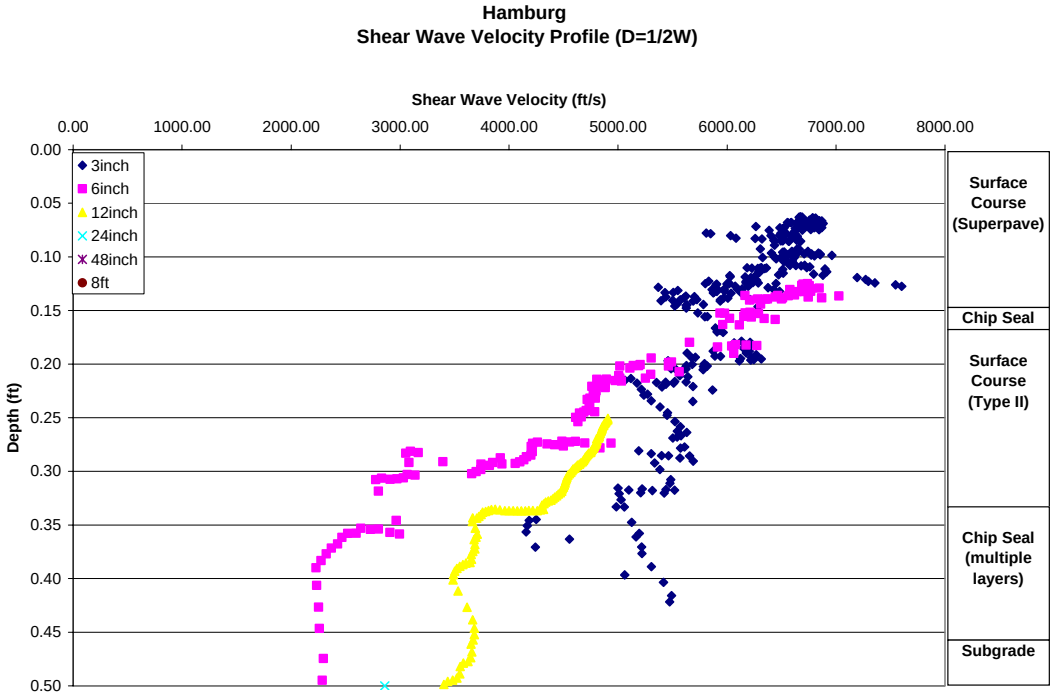

Figure 4.11 Close-up of top 6 inches of Hamburg shear wave velocity profile

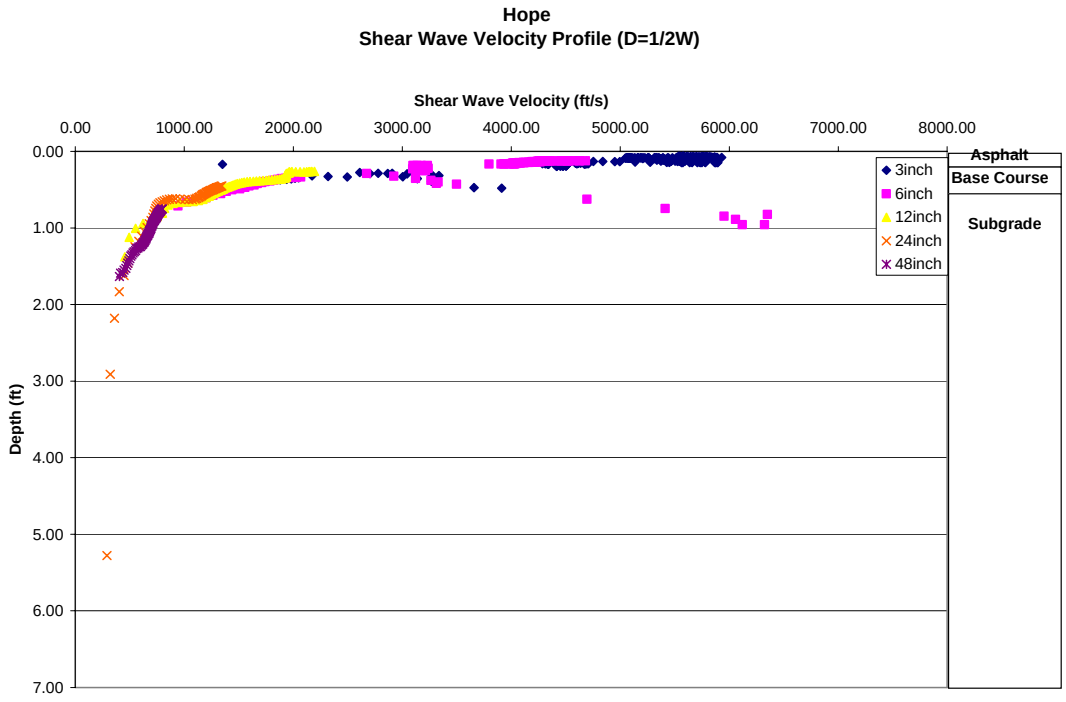

Figure 4.12 Full-scale view of Hope shear wave velocity profile

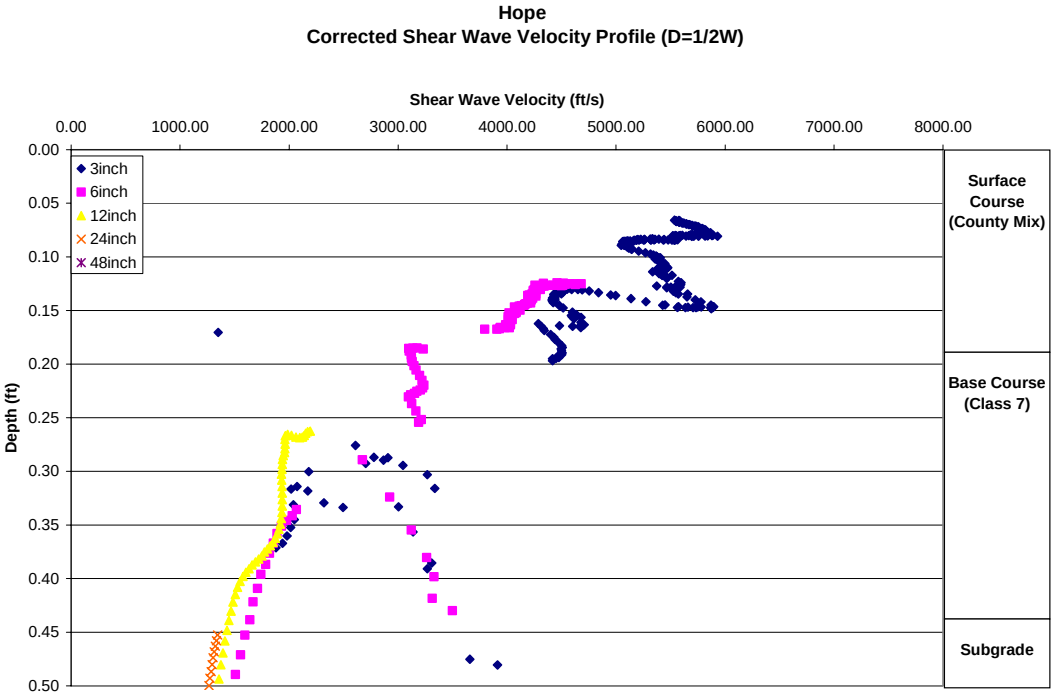

Figure 4.13 Close-up of top 6 inches of Hope shear wave velocity profile

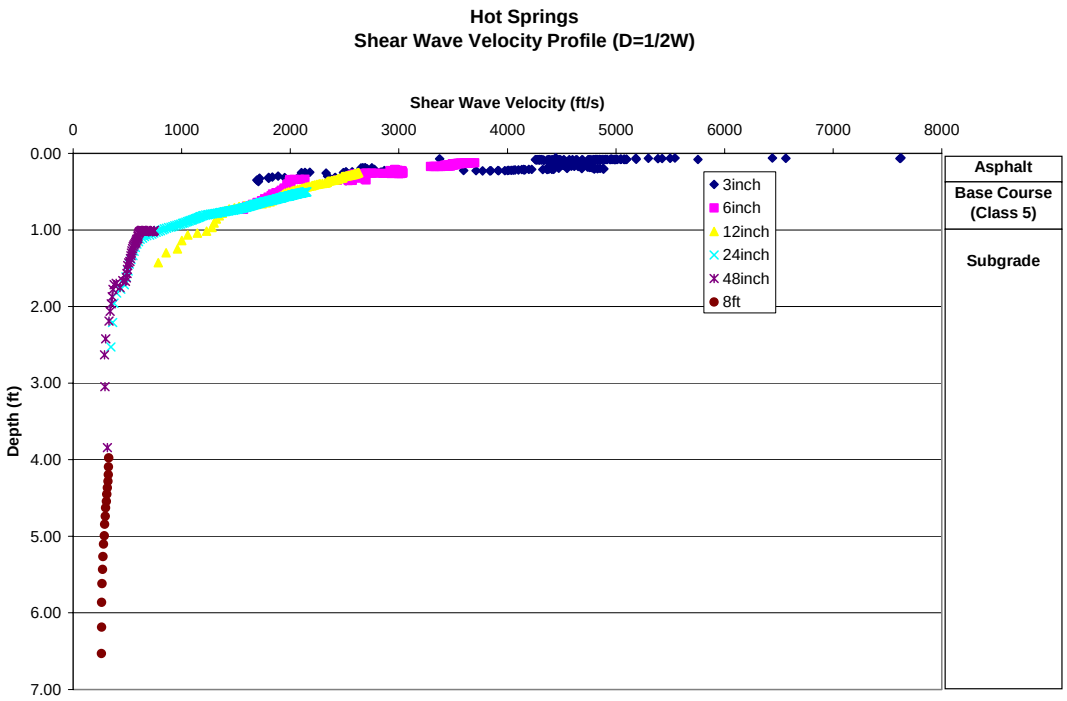

4.14 Full-scale view of Hot Springs shear wave velocity profile

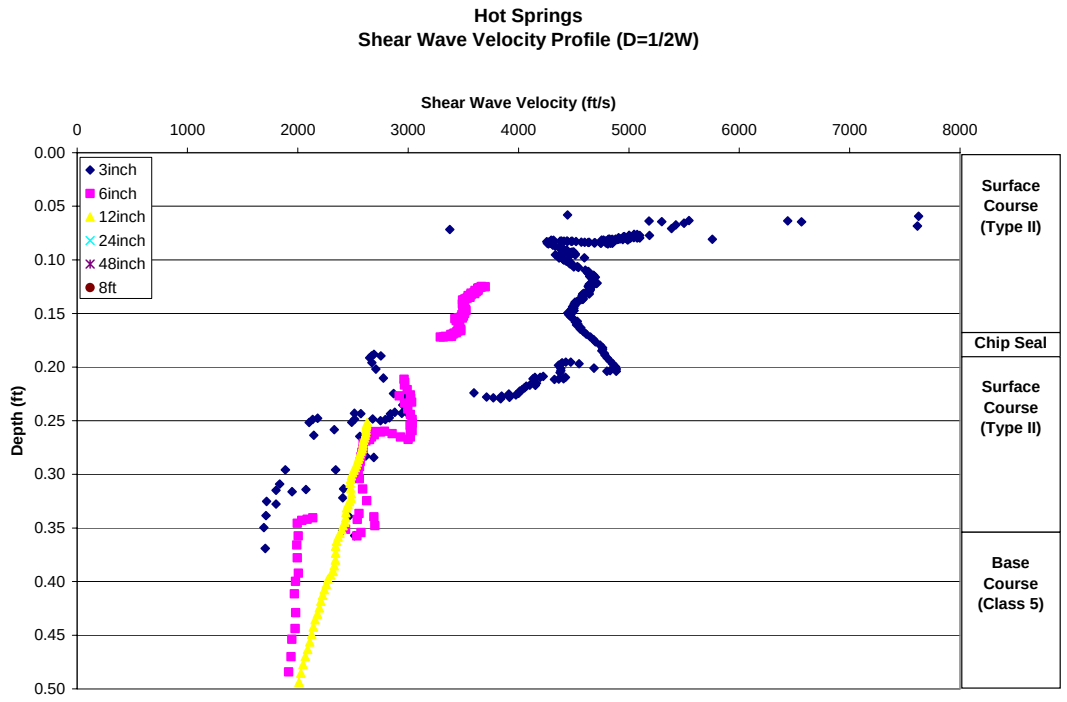

Figure 4.15 Close-up of top 6 inches of Hot Springs shear wave velocity profile

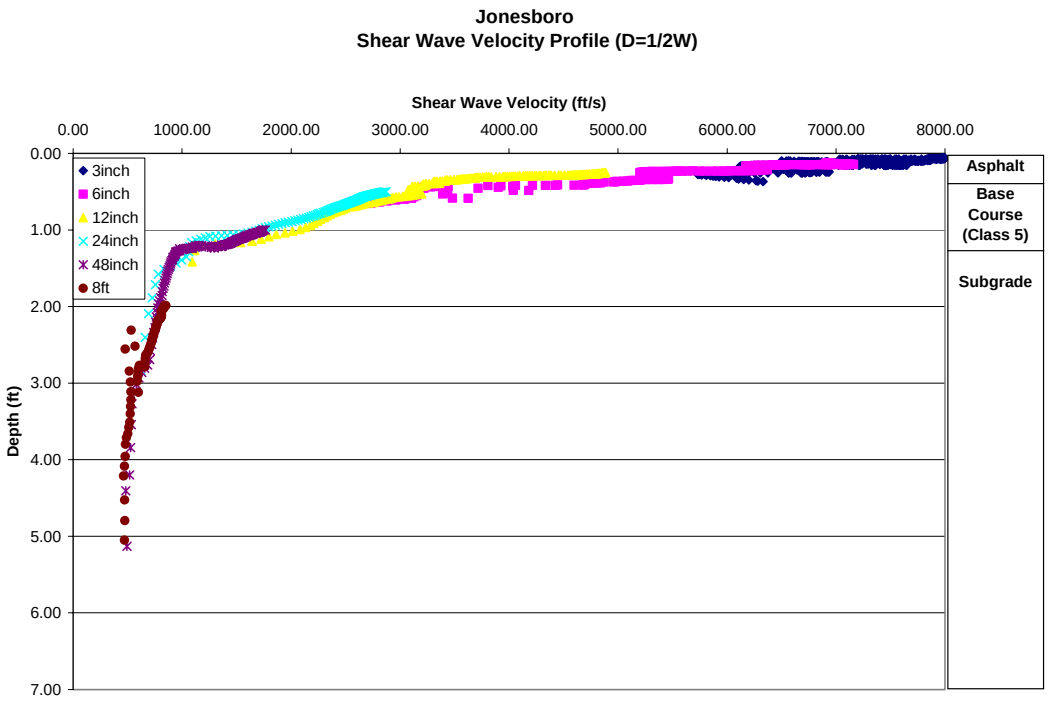

4.16 Full-scale view of Jonesboro shear wave velocity profile

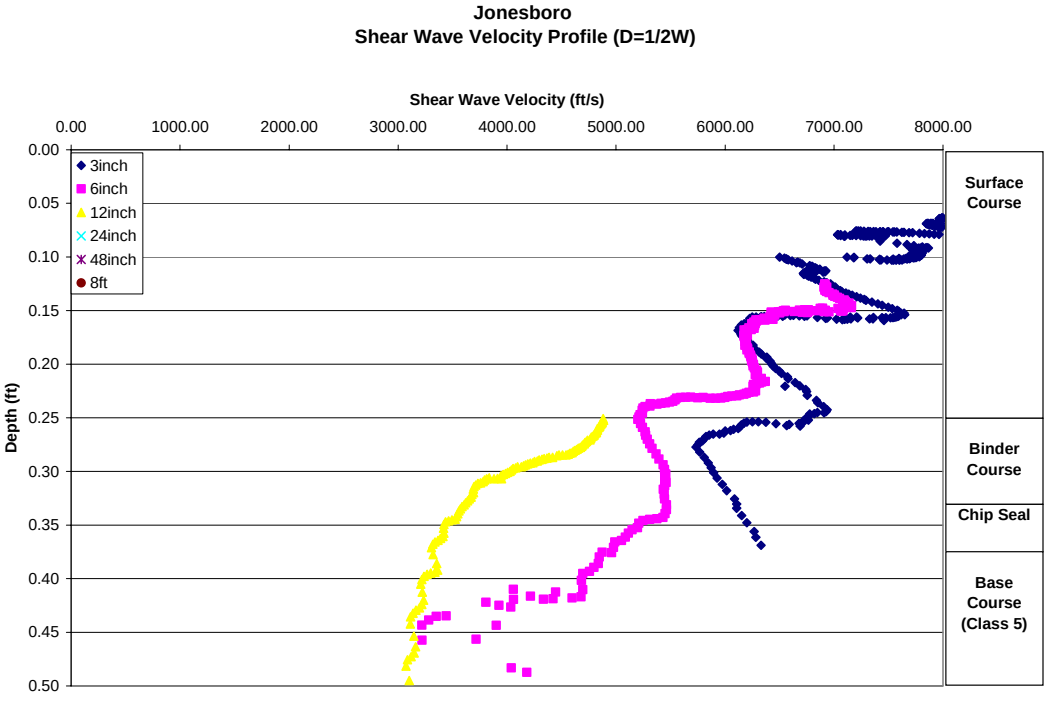

Figure 4.17 Close-up of top 6 inches of Jonesboro shear wave velocity profile

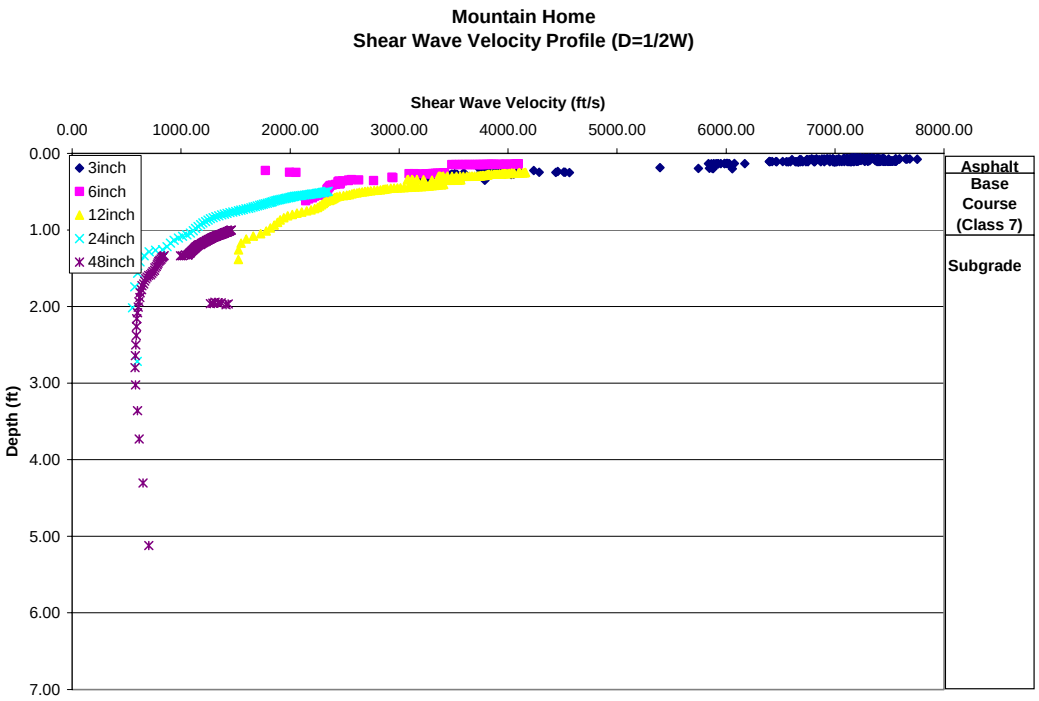

Figure 4.18 Full-scale view of Mountain Home shear wave velocity profile

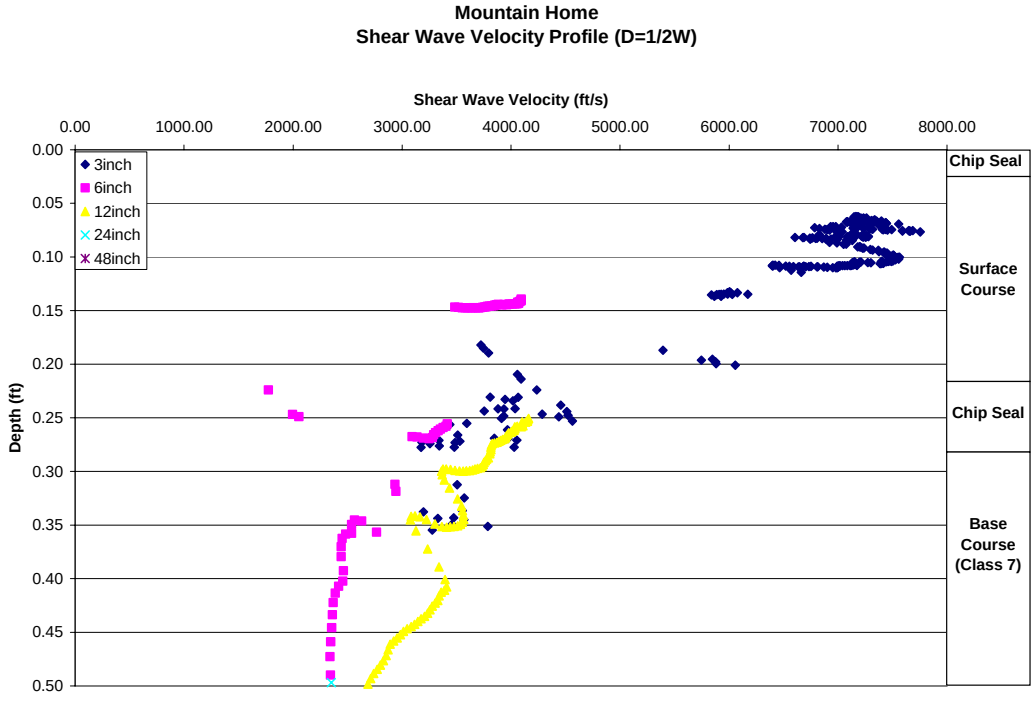

Figure 4.19 Close-up of top 6 inches of Mountain Home shear wave velocity profile

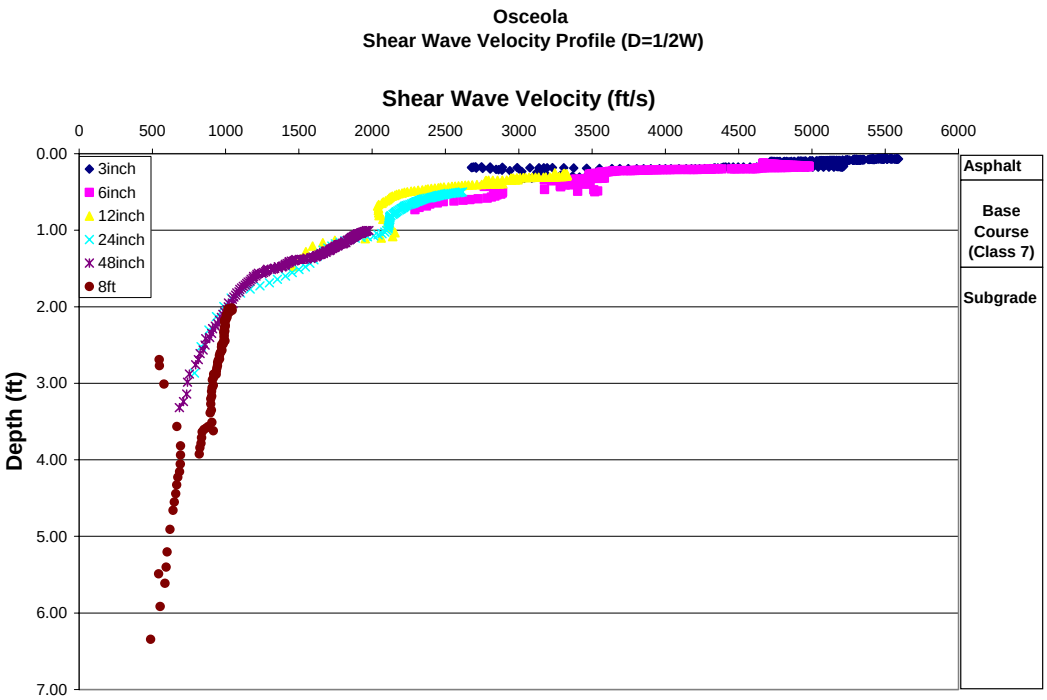

Figure 4.20 Full-scale view of Osceola shear wave velocity profile

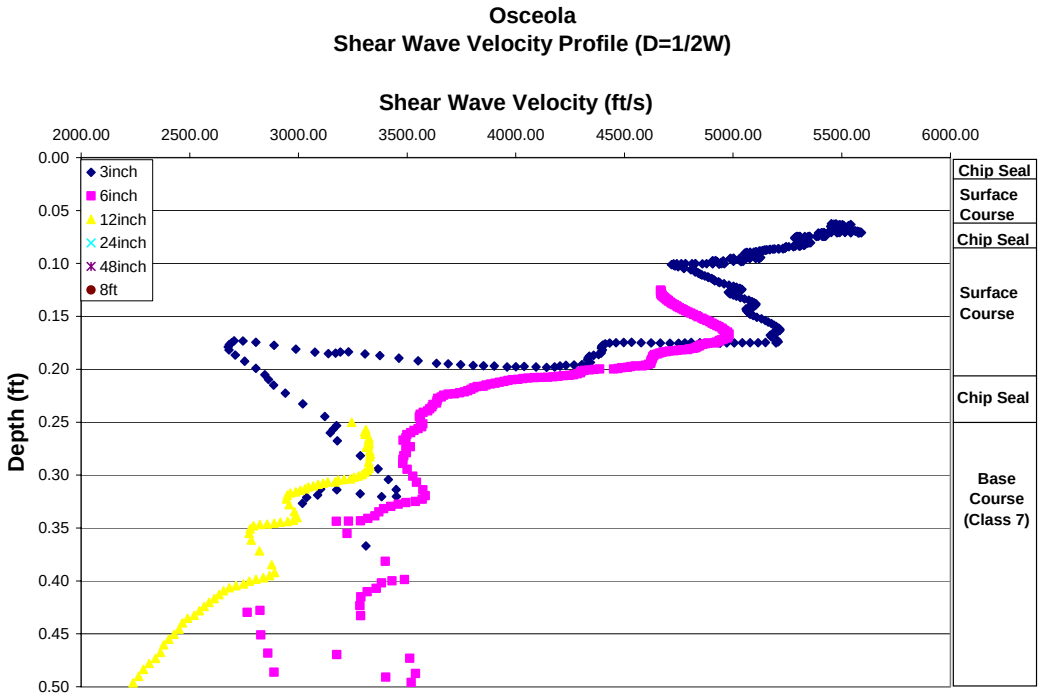

Figure 4.21 Close-up of top 6 inches of Osceola shear wave velocity profile

measured during field exploration is shown on the right side of each shear wave velocity profile.

Referring to Figures 4.2 through 4.21, it can be seen that the shear wave velocity profiles for the test sites are generally smooth, continuous curves and have the shape typicalfor an inversely dispersive profile. The shear wave velocity profiles were obtained by inverting dispersion data collected from receiver spacings of 3, 6, 12, 24, 48 and 96 inches. For all of the sites except Hope, Mountain Home and Clarksville; the data from every receiver spacing was used in construction of the dispersion curve. The Hope, Mountain Home and Clarksville sites each had data from one receiver spacing that did not match the data from the other receiver spacings. The data from the receiver spacing that did not agree with the others was discarded. The 8 ft receiver spacing was eliminated for the Hope and Mountain Home sites, and the 6 inch receiver spacing was eliminated for the Clarksville site. One possible reason for these sites having a poorer dataset than the others is the fact that these three sites contained a chip sealed surface which made SASW testing difficult. Effects of testing on a chip sealed surface, as well as possible methods for improving data quality in these areas is discussed in the next chapter of this report.

In most cases, the individual layers present at the sites (shown on the right side of the figures) can be seen as velocity contrasts present in the shear wave velocity profiles. The asphalt, base and subgrade layers are clearly visible for almost all of the sites, and in some cases individual layers within the asphalt structure can also be distinguished (Beulah – Figure 4.2, Jonesboro – Figure 4.17, and Osceola – Figure 4.21 sites are good

examples). Relatively thin asphalt layers (less than approximately 1 inch thick), however, do not show up well in the shear wave velocity profiles.

The shear wave velocity profiles shown previously were used to estimate the shear wave velocity of the subgrade layer at each of the test sites. Figure 4.22 shows the modulus of the subgrade for each site, calculated using the estimated shear wave velocities from the simple inversion technique. Figure 4.22 is a graphical representation of the values shown in the "M_r Simple Inversion" column shown in Table 4.1.

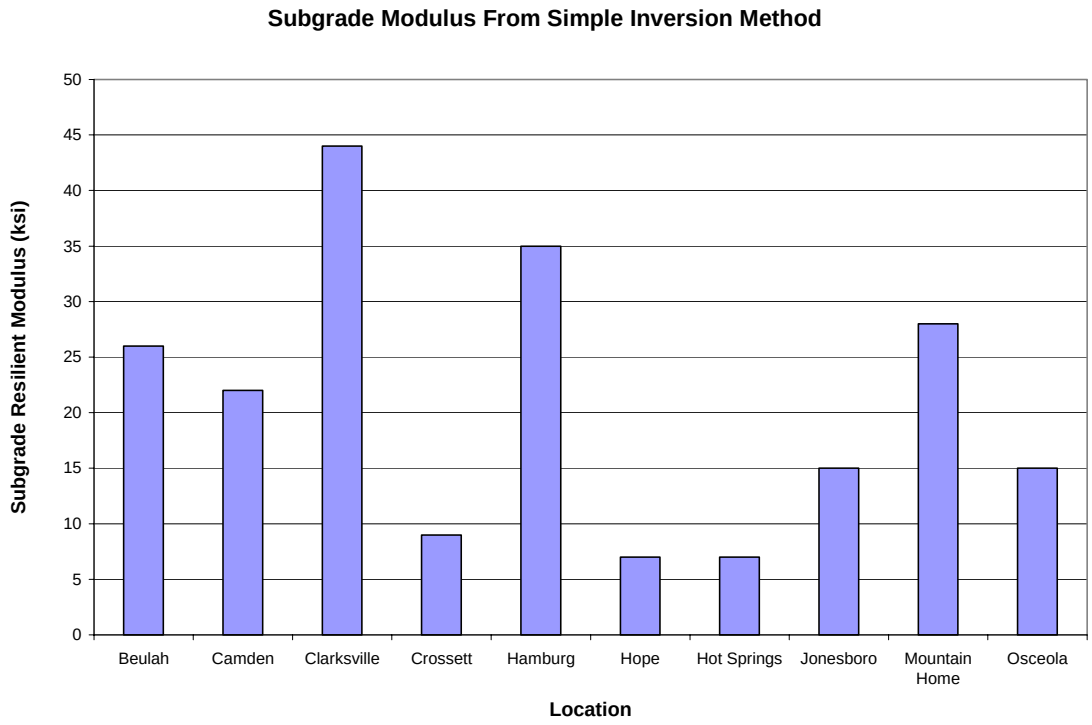

Figure 4.22 Subgrade modulus predicted using simplified inversion technique

Figure 4.22 indicates that the subgrade modulus values for the ten test sites ranged from a low of 7 ksi at the Hope and Hot Springs sites, to a high of 44 ksi at the Clarksville site. The range of modulus values predicted for the subgrade soils appears to

be reasonable for the level of strain associated with SASW testing. Resilient modulus values found at the strain levels associated with SASW testing are typically 2 to 3 (or more) times greater than the resilient modulus values found using laboratory testing procedures. Laboratory testing performed by Elliott and Thornton (1988) on a wide range of Arkansas subgrade soils show a range of approximately 1.5 ksi to 21 ksi. The range given by Elliott and Thornton was obtained using moisture contents that varied from approximately 70 to 120% of optimum and deviator stresses ranging from 2 to 16 psi.

The results shown in Figure 4.22 agree favorably with the soil property information contained in Table 4.5. The subgrade soils at the Clarksville and Mountain Home test sites both contained a significant portion of sand and gravel, and classify as clayey gravel with sand and clayey sand with gravel by the USCS classification system, respectively. The in-situ moisture content for these two sites was at or near the plastic limit. Standard penetration test N-values of 43 for the Clarksville site and 18 for the Mountain Home site indicate that the soils were in a very stiff state at the time of testing. Considering these factors, the value for the subgrade modulus was expected to be relatively high. This was indeed the case as the simplified SASW moduli for the subgrade soils at these two sites ranked number 1 and 3 among all sites tested, with a value of 44 ksi at the Clarksville site and a value of 28 ksi at the Mountain Home site.

The subgrade soils at the Beulah and Camden sites both classify as silty sand (SM). The in-situ moisture contents for the subgrade soils were relatively low. The simplified SASW moduli predicted for these soils were relatively high, but less than the

values predicted for the Clarksville and Mountain Home sites. This seems reasonable as the soils at the Beulah and Camden sites did not contain any gravel.

The subgrade soil present at the Hope test site is considered highly plastic with a liquid limit of 57 and a plasticity index of 39. Additionally, the in-situ moisture content was relatively high at 23.6%, and the particle size distribution reveals that nearly all of the particles are finer than the No. 200 sieve. The standard penetration test N-value of 7 obtained for the site indicates the soil was in a firm condition at the time of testing. Weighting all of these factors together, the modulus of the subgrade soil was expected to be relatively low. The simplified SASW modulus predicted for the Hope site was indeed predicted to be quite low by the manual SASW procedure, tying with Hot Springs as the site with the lowest predicted simplified SASW modulus.

The Crossett site subgrade soil is considered moderately plastic and classifies as lean clay with sand (CL), however, the in-situ moisture content was found to be at the liquid limit of the soil. Additionally, a very low SPT N-value of 3 was obtained for the soil. These two facts indicate that the soil was in a very soft and wet state at the time of testing, and reinforces visual observations made during field testing. Consequently, one would expect a relatively low modulus value for the material. The modulus for the Crossett site was indeed predicted to be low by the manual SASW method (9 ksi).

The subgrade present at the Hamburg test site also classifies as lean clay (CL), but at this site the in-situ moisture content is very nearly equal to the plastic limit of the soil. The SPT N-value of 12 indicates that the soil was in a stiff state at the time of testing. Consequently, a fairly high value for the resilient modulus was expected. The simplified inversion technique did indeed predict a high modulus. The predicted value of 35 ksi,

however, was higher than what was expected given the soil type, moisture state and SPT N-value.

The Osceola and Jonesboro test sites contained subgrade soils that are of medium plasticity and classify as lean clay (CL) with sand. SPT N-values for the Osceola and Jonesboro sites were found to be 8 and 13, respectively. The in-situ moisture content for the subgrade soil at the Osceola site was well beyond the plastic limit, and indicates that the soil was in a moist state. The in-situ moisture content for the Jonesboro test site was very near the liquid limit. The simplified SASW modulus value of 15 ksi predicted for these two sites appears to be reasonable given the available data.

The only simplified SASW subgrade modulus that does not appear to be reasonable is the very low value of 4 ksi predicted for the Hot Springs site. The soil classifies as sandy lean clay (CL), the in-situ moisture content is not exceptionally high, and the SPT N-value of 10 indicates that the soil was in a stiff state at the time of testing. The resilient modulus predicted by the manual SASW procedure appears to be too low.

4.2 UTEP Software Results

The UTEP software was used to analyze the raw data files collected from each site. The procedures described in section 3.3.2 of Chapter 3 were used to analyze the data. The column in Table 4.1 labeled "M_r UTEP Program Defaults" shows the results obtained using the program without making any adjustments to the default program settings. Notice that three of the sites (Clarksville, Hope, and Hot Springs) do not have an entry in this column. The reason no entry is present for these sites is that the experimental dispersion curve predicted by the program using the default settings for

these sites was not continuous, did not match the dispersion curve calculated using the simple inversion technique, and was considered to be in error. An example of a poor experimental dispersion curve is shown in Figure 4.23. The data presented in Figure 4.23 was obtained at the Hope test site.

Attempting to perform the inversion process on the dispersion curve shown in Figure 4.23 would not allow for meaningful results to be obtained. To correct erroneous dispersion curves, the UTEP program provides two settings, slowness and smoothness, that allow for the experimental dispersion curve to be modified. Figure 4.24 shows the dispersion curve for the Hope site after these two settings were used to correct the original erroneous dispersion curve.

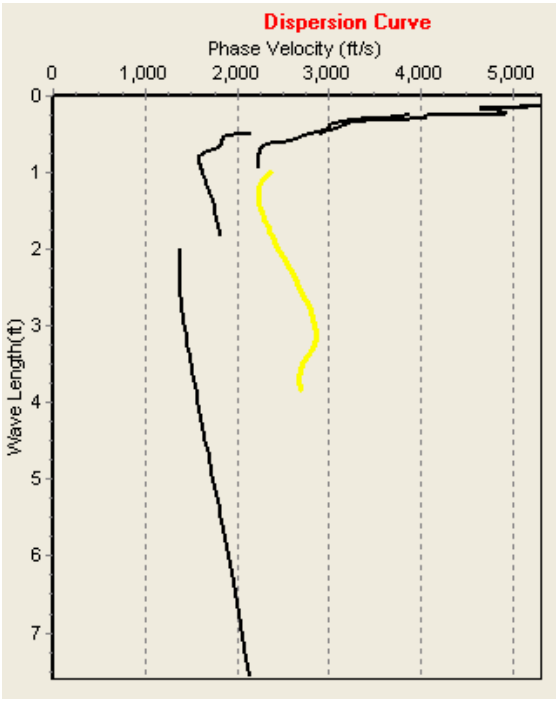

Figure 4.23 Example of poor experimental dispersion curve (from Hope site)

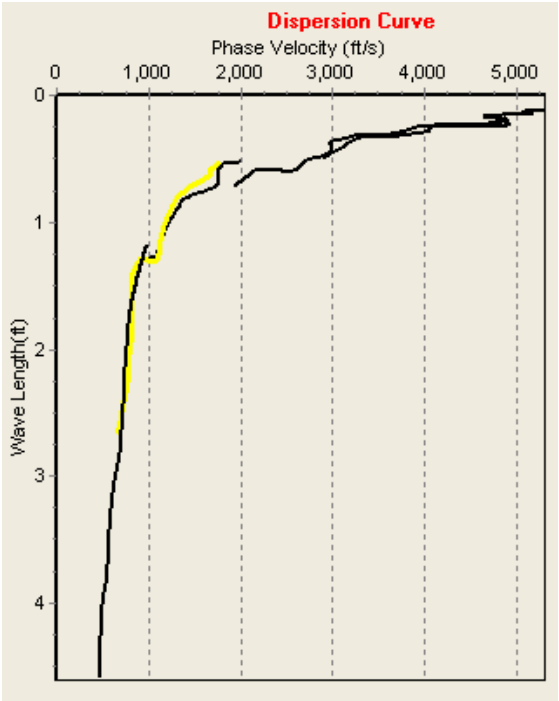

Figure 4.24 Adjusted experimental dispersion curve (from Hope site)

Two reasons are postulated as the cause of the low quality dispersion curves. The first reason is the low signal quality encountered at test sites having a chip sealed pavement surface. The second reason is that the FFT resolution, especially for wider receiver spacings, may have been inadequate to properly define the low frequency content of the acquired signals. This concept, and recommendations for eliminating this problem, are discussed further in the next chapter.

The subgrade modulus values for the test sites predicted using the default program settings where applicable, and the modulus values obtained using adjusted program settings for the sites which exhibited poorly aligned experimental dispersion curves, are shown in Figure 4.25.

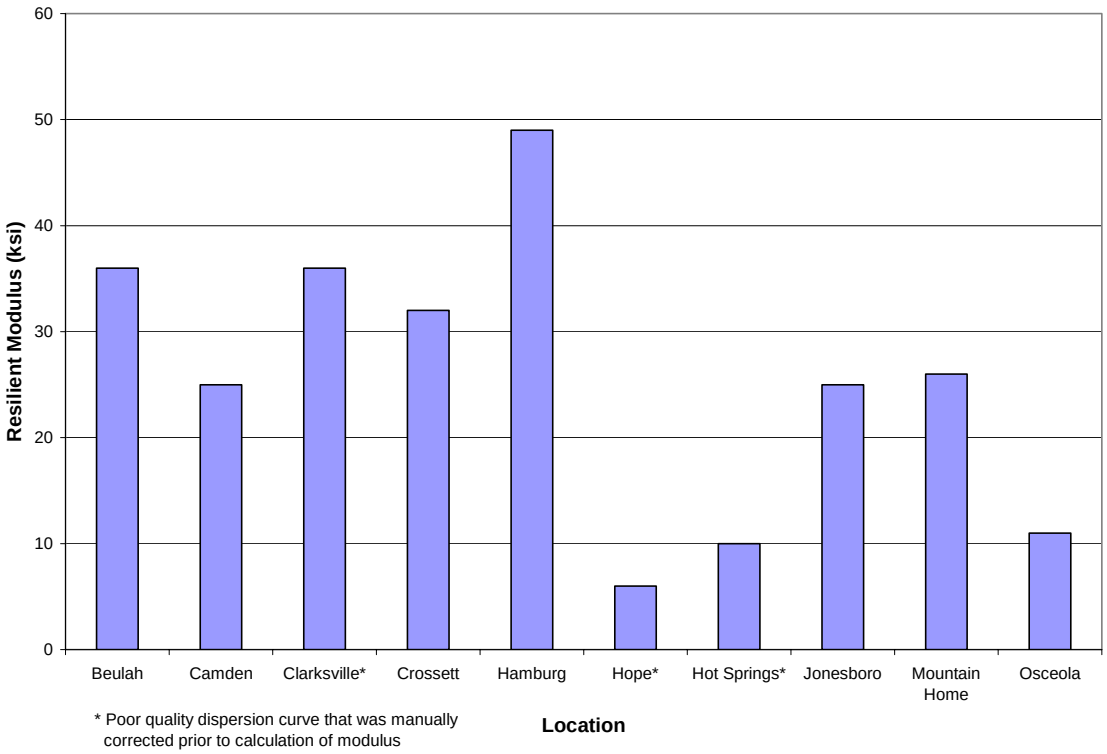

Figure 4.25 Subgrade modulus from UTEP program (default settings)

The program default settings produced theoretical dispersion curves that fit the experimental dispersion curves very well, however, it was found that using these settings did a poor job of predicting known layer thicknesses. Since layer thicknesses were a known quantity in this study, it was desirable to obtain a solution that predicted both layer thickness and a reasonable value for the modulus of each layer. To achieve this, the layer constraint option was used to force the layer thicknesses to remain within a percentage (typically 10 to 50 percent) of the known value. Forcing the layers thicknesses to remain within a constrained range caused somewhat of a mismatch to occur between the experimentally measured dispersion curves and the theoretical dispersion curves calculated by the program. To minimize the mismatch between the two curves, the trial material property profiles were adjusted until the best fit between the experimentally measured dispersion curve and theoretical dispersion curve predicted by the program was achieved. Figure 4.26 shows the subgrade modulus predicted by the UTEP program using constrained layer thicknesses and best-fit modified material profiles.

Results obtained by analyzing the data using the layer constraints and modified material profiles are considered to be the most accurate representation of the conditions present at the test sites during the time the study took place. This method allowed for a solution that included both reasonable values for layer thicknesses and resilient moduli. The modulus values predicted for the asphalt and base course (where applicable) layers using this method are also shown in Table 4.2.

The subgrade moduli predicted using this method appear to be reasonable with respect to the subgrade soil information contained in Table 4.3. The sites containing

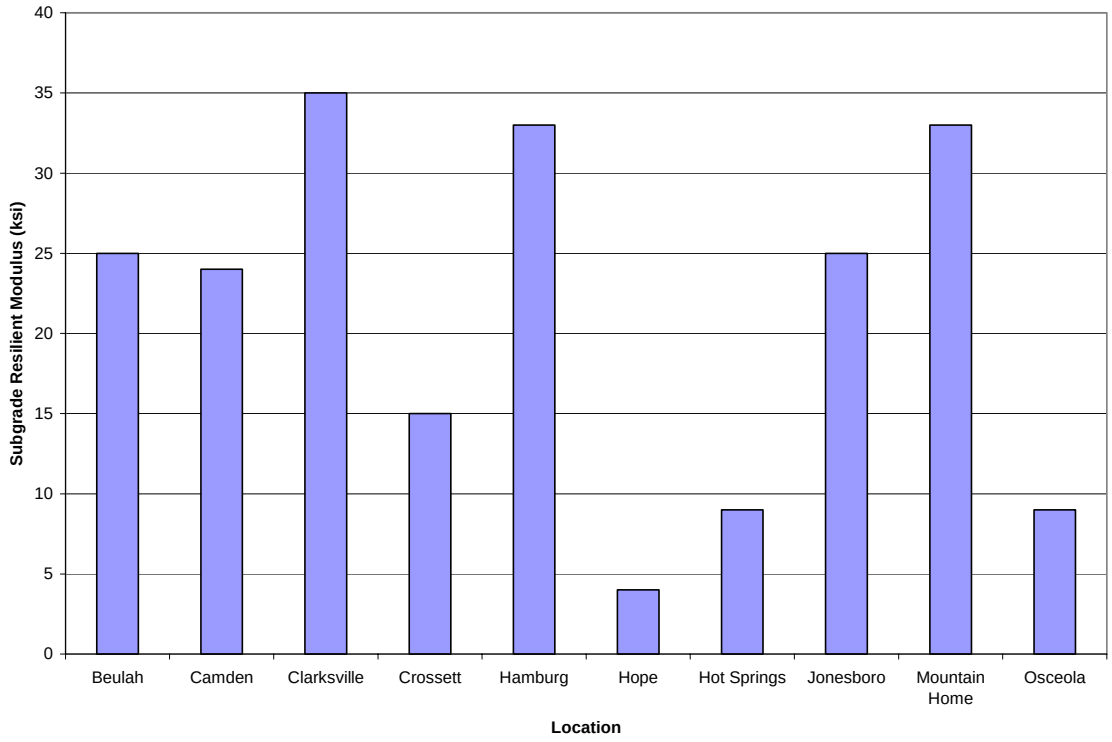

Figure 4.26 Subgrade modulus from UTEP program using layer constraints and modified material profiles

sandy and gravelly subgrade soils tend to have a higher predicted value of subgrade modulus (Clarksville, Mountain Home, Beulah, and Camden). Sites that contained subgrade soils which classified as CL and had moderate plasticity and in-situ moisture contents near the plastic limit also had relatively high predicted modulus values (Hamburg) Sites where the subgrade was either in a very saturated condition, or was highly plastic, had much lower predicted modulus (Hope, Crossett, and Osceola). Again, the only site that appears to be significantly out of the expected range is the Hot Springs site. The predicted modulus value is lower than what was expected when considering the soil type and state at the time of testing.

Analyzing the data using the UTEP software, in conjunction with constraining the layer thicknesses and modifying the trial material profiles, is considered to be the best

available method to analyze the data collected. This method is considered superior to the other methods used as it employs a theoretically sound and rigorous analysis procedure, and accounts for known layer thicknesses. However, there are two major drawbacks to this procedure. The first major drawback is the mismatch between the experimental and theoretical dispersion curves that occurs as a side effect of constraining the layer thicknesses. The greater the error between the two curves, the more questionable the results obtained. The amount of error present between the two curves for the sites tested during this study varied. The theoretical curve matched the experimental data very well for the Osceola (shown in Chapter 3), Clarksville, and Mountain Home test sites. The curves did not match as well for the remaining sites, with the largest amount of disagreement occurring at the Hamburg and Crossett sites. Experimental and theoretical dispersion curves for several sites are shown in Figures 4.27 through 4.30 to demonstrate how well the theoretical curve typically matched the experimental data.

It is postulated that the reason for the poor fit between the experimental and theoretical dispersion curves at the Hamburg and Crossett locations is due to the fact that no base course layer is present at either of these two sites. These sites were the only two tested that did not contain a base course layer. The sharp contrast in stiffness between the stiff

asphalt pavement layer and the much softer underlying subgrade may cause the program to have difficulty mathematically modeling the system.

The second major drawback to the constrained thickness/modified trial profile procedure is that varying the material properties of the layers caused much more variance in the obtained the results than was originally anticipated. Because a significant amount

of variance in the results was obtained by changing the material properties of the layers (even within reasonable ranges for the material properties) a substantial amount of judgment had to be exercised when choosing the most appropriate material profile. The amount of judgment needed to properly analyze the data necessitates analysis be performed by someone very familiar with SASW testing. As such, unskilled or untrained persons would not possess the requisite knowlege to obtain meaningful results using this procedure.

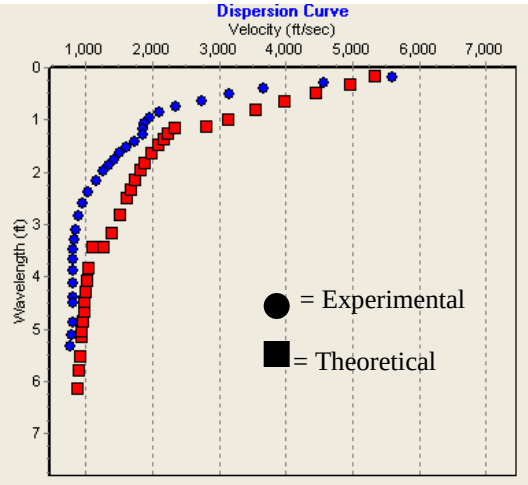

Figure 4.27 Experimental and theoretical dispersion curves from UTEP program for Beulah test site

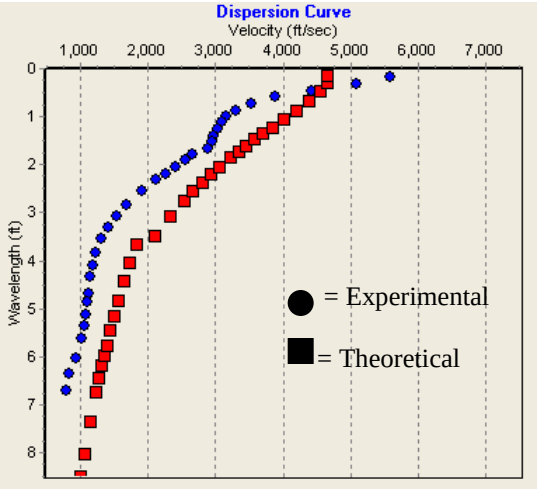

Figure 4.28 Experimental and theoretical dispersion curves from UTEP program for Camden test site

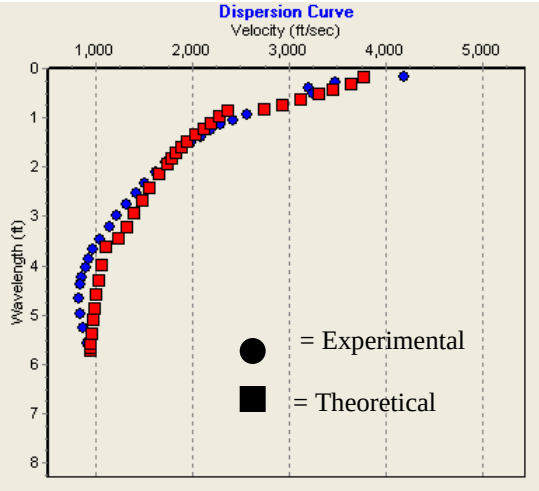

Figure 4.29 Experimental and theoretical dispersion curves from UTEP program for Mountain Home test site

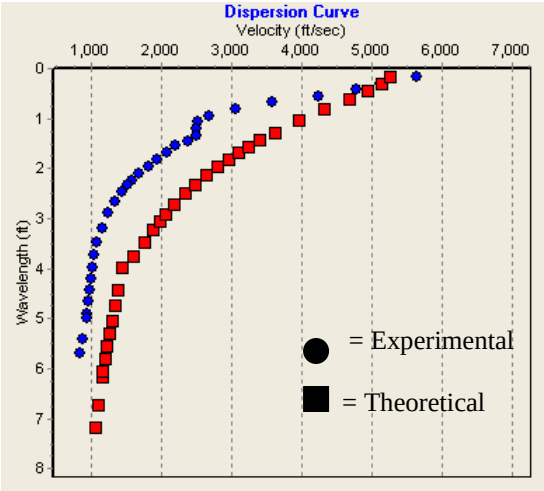

Figure 4.30 Experimental and theoretical dispersion curves from UTEP program for Hamburg test site

4.3 Comparison Between Methods

Figures 4.31 and 4.32 show the results of SASW testing using the simplified inversion technique plotted next to the results obtained using the UTEP software. As indicated by the figures, the subgrade moduli agree relatively well between the two methods for the majority of the sites. The two sites which exhibit the largest difference between methods are the Clarksville and Jonesboro sites, where a difference of about 10 ksi is seen.

Figure 4.33 shows the subgrade moduli predicted from both SASW procedures, as well as from FWD testing and SPT testing for each testing location. Looking at Figure 4.33 some general trends can be established. In general, the results from the FWD and SPT methods agree with the results from SASW testing. The Clarksville, Mountain Home, and Hamburg subgrade soils were consistently predicted to be stiffer and have higher modulus values by all methods. Likewise; the subgrade soils for the Osceola, Hope, and Crossett sites were consistently predicted to be softer and have a lower

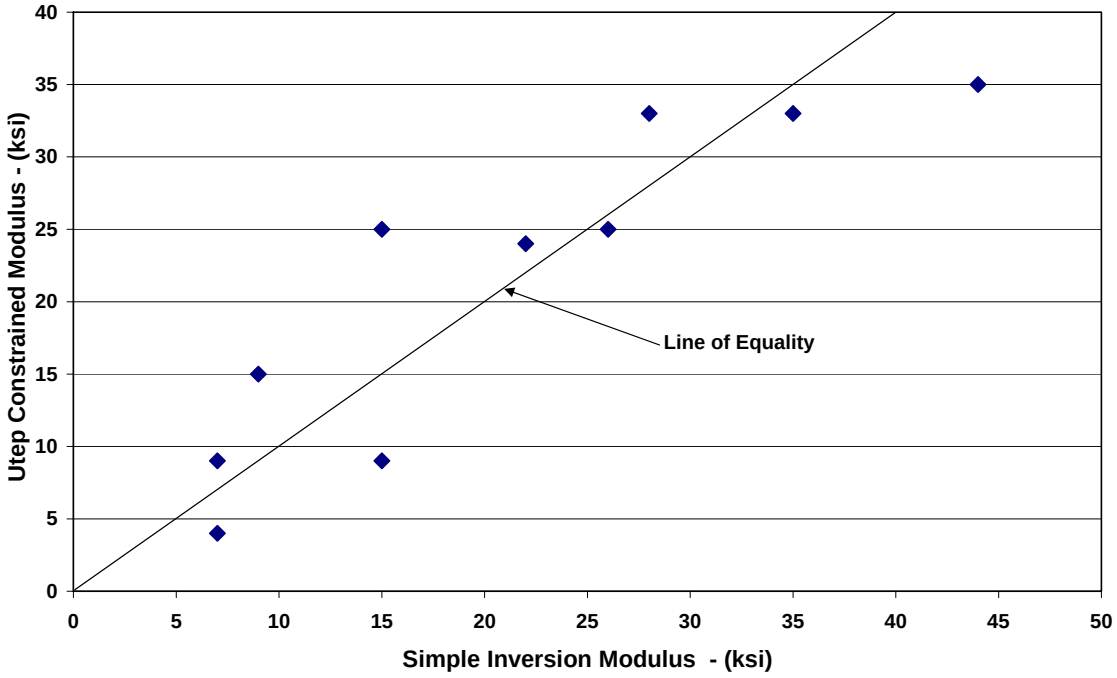

Figure 4.31 Comparison of subgrade moduli predicted using simplified inversion and UTEP program

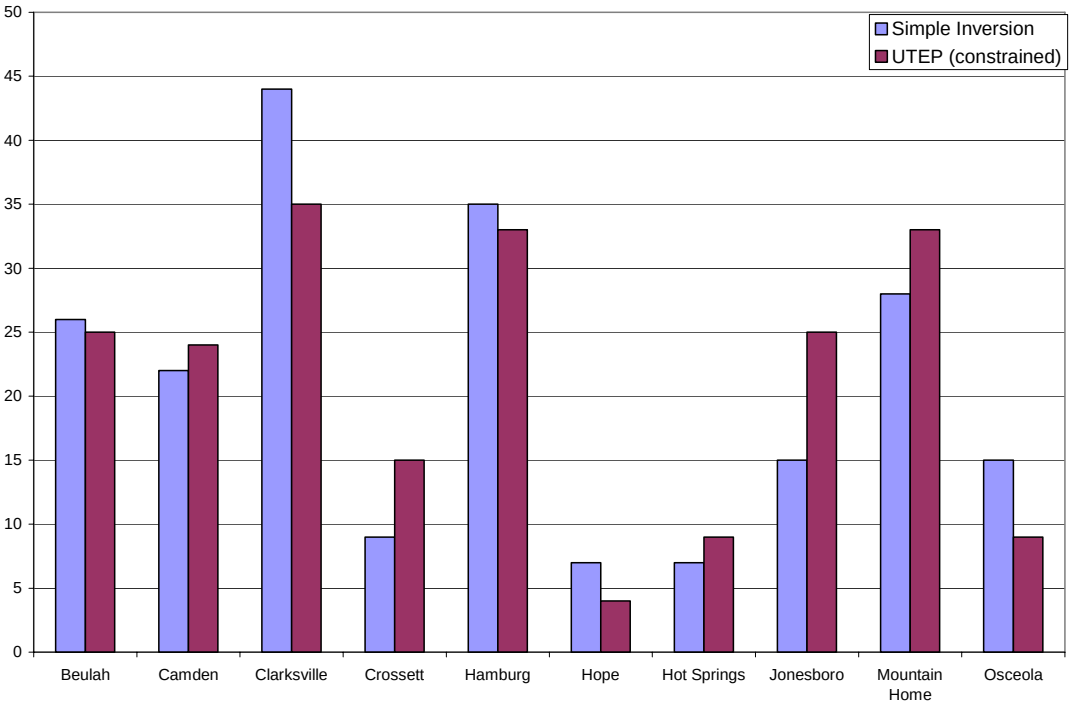

Figure 4.32 Comparison of subgrade moduli predicted using simplified inversion and UTEP program (by location)

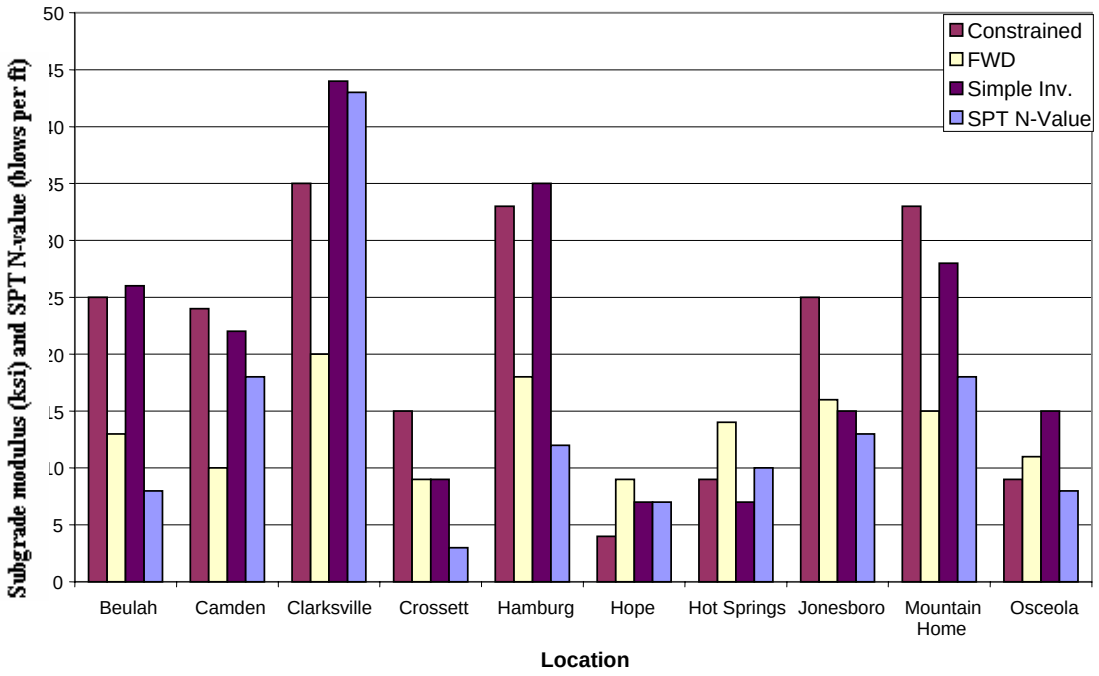

Figure 4.33 Subgrade modulus from SASW and FWD methods; and SPT N-values

modulus by all methods. The results obtained for the Beulah, Jonesboro, and Camden sites varied somewhat depending upon the test method used; however, as an overall trend, the resilient moduli of the subgrade soils at these sites appear to be located somewhere between the stiff group and soft group.

The Hot Springs site appears to be the only site in which there is significant disagreement between SASW results and the FWD and SPT test results. SASW testing predicts a low value for subgrade modulus, while both the FWD and SPT tests indicate the soils modulus to be somewhat higher. The reason for the disagreement between the testing methods is not known.

While general trends can be seen in Figure 4.33, no concrete relationship can be established for correlating SASW results to FWD or SPT test results. It appears that

SASW testing predicts subgrade modulus values that are approximately twice as high as those predicted by FWD for sites that contain higher quality subgrade material (Beulah, Camden, Clarksville, Hamburg, and Mountain Home). For sites which contain softer subgrade materials (Osceola, Hope, and Crossett) the SASW and FWD results are much closer to one another. SASW testing was expected to yield higher values of modulus than FWD due to the strain levels involved.

Figures 4.34 through 4.37 present a closer look at the moduli predicted by the two SASW methods versus the moduli predicted by FWD methods. Figures 4.34 and 4.35 compare the average FWD modulus value (explained in Chapter 3) to the simplified inversion modulus and the UTEP constrained modulus respectively. Figures 4.36 and 4.37 compare the FWD modulus as predicted by ROADHOG to the simplified inversion modlus and the UTEP constrained modulus respectively. Best fit trendlines and R^2 values are included in each of the figures.

Based on Figures 4.34 through 4.37 it appears that a loose correlation exists between seismic modulus and the modulus predicted by FWD methods. The R2 values indicated on the figures suggests that the level of reliability is about the same regardless of which method is used.

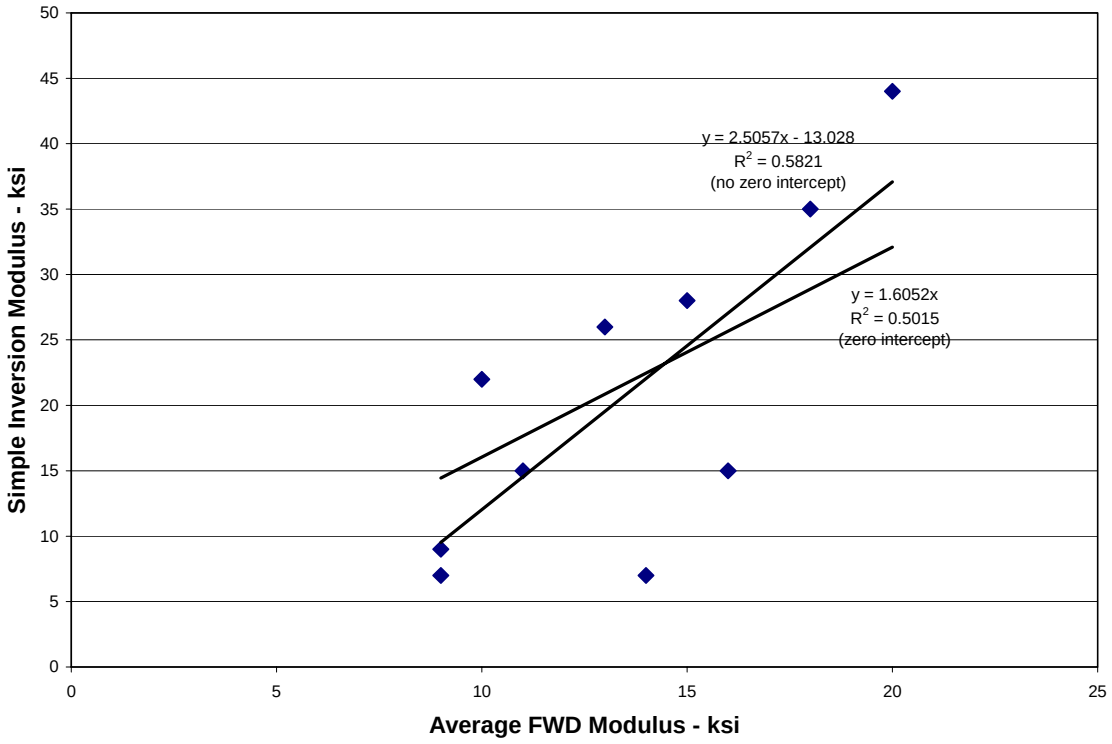

Figure 4.34 Simple inversion modulus versus average FWD modulus

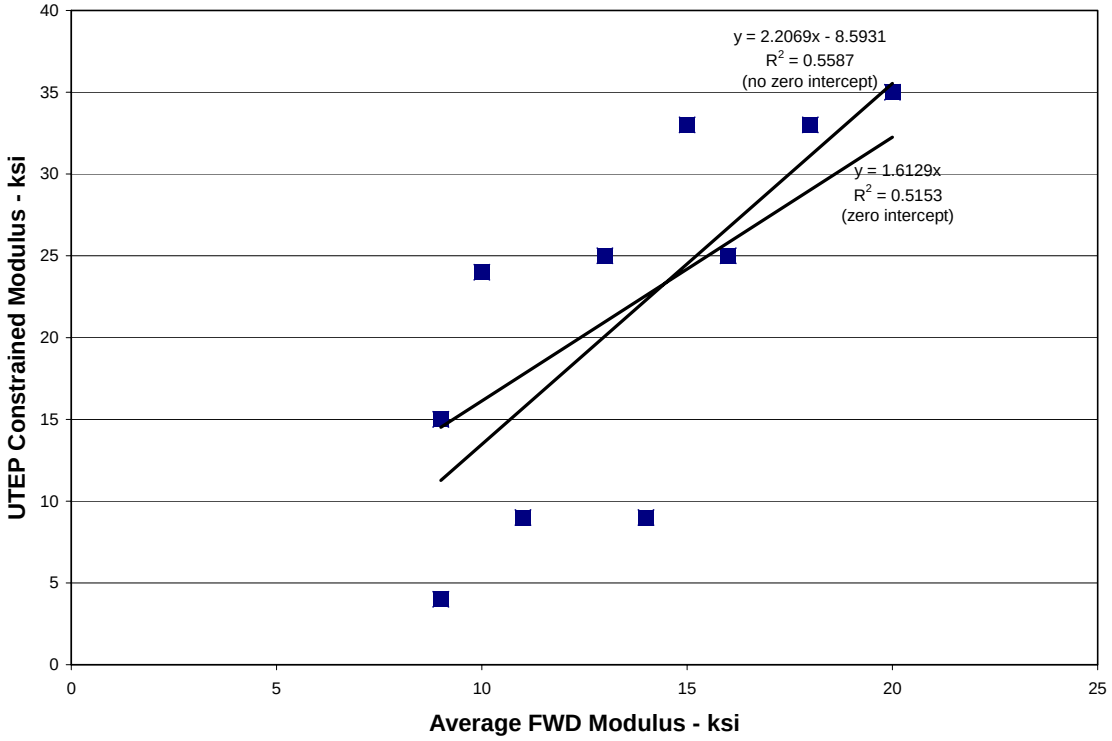

Figure 4.35 UTEP constrained modulus versus average FWD modulus

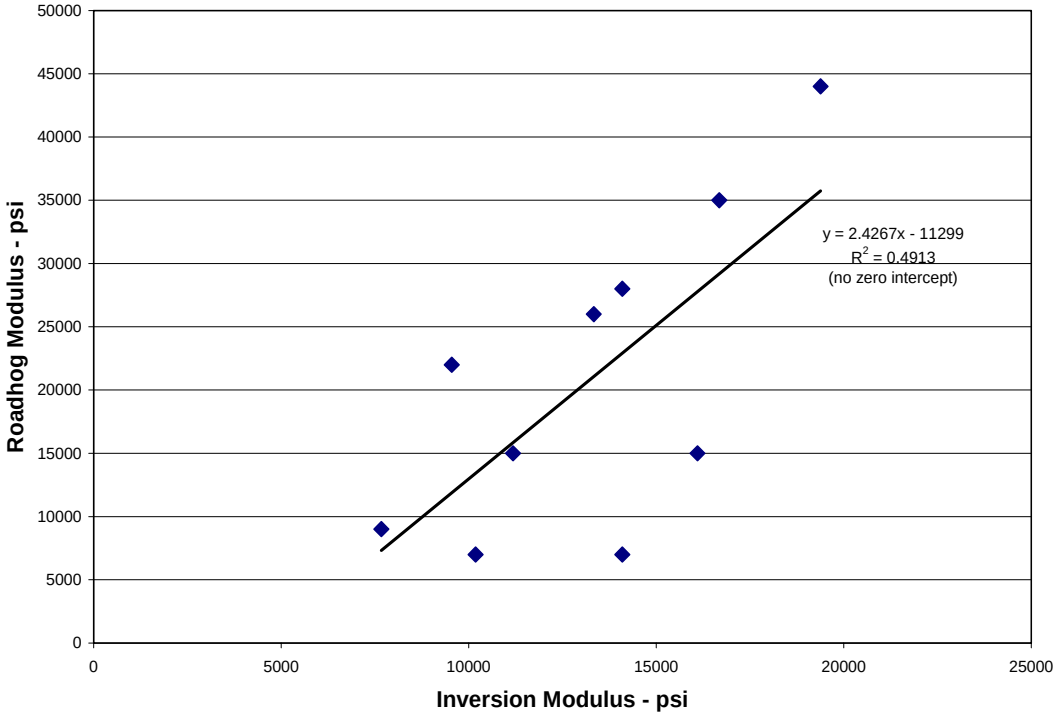

Figure 4.36 Roadhog FWD modulus versus simplified inversion modulus

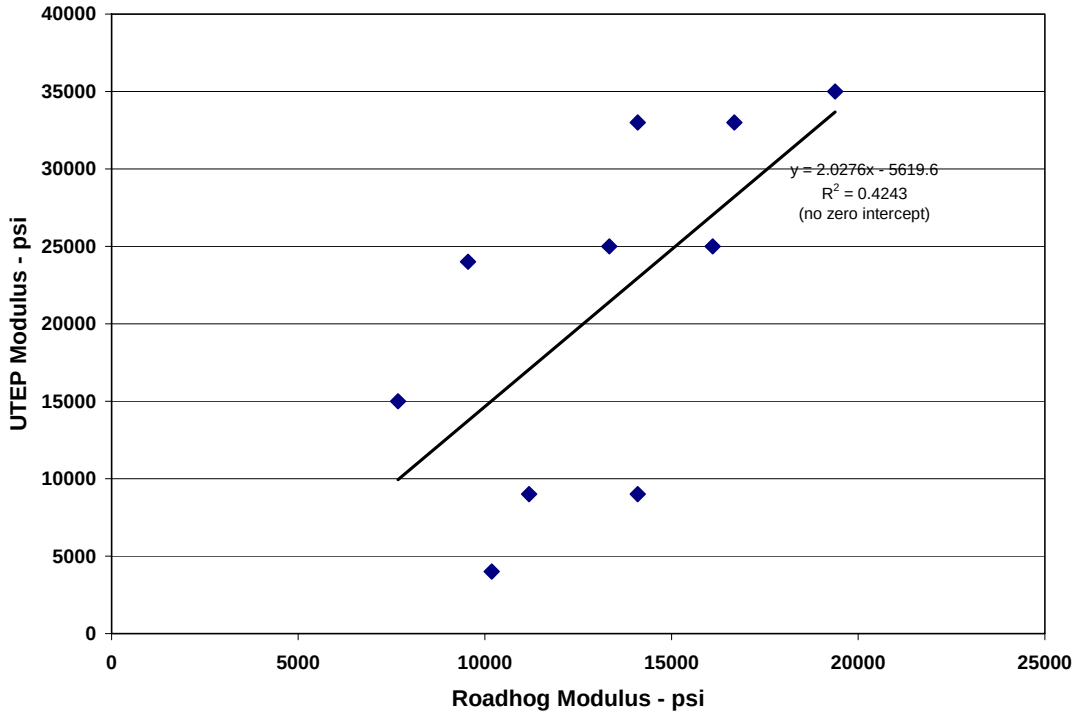

Figure 4.37 UTEP constrained modulus versus Roadhog modulus

Results from laboratory resilient modulus testing are shown in Figures 4.38 through 4.40. Laboratory testing was only conducted on subgrade soils from six of the ten sites. Intact samples suitable for testing could not be obtained from the remaining four test sites. The laboratory resilient modulus values shown in Figures 4.38 through 4.40 were obtained using a confining pressure (σ_c) of 3 psi for all of the sites tested except the Hope site where a confining pressure of 4 psi was used. Resilient modulus is stress dependent. The resilient modulus values shown in Figures 4.38 through 4.40 are for the breakpoint deviator stress (σ_{dbp})

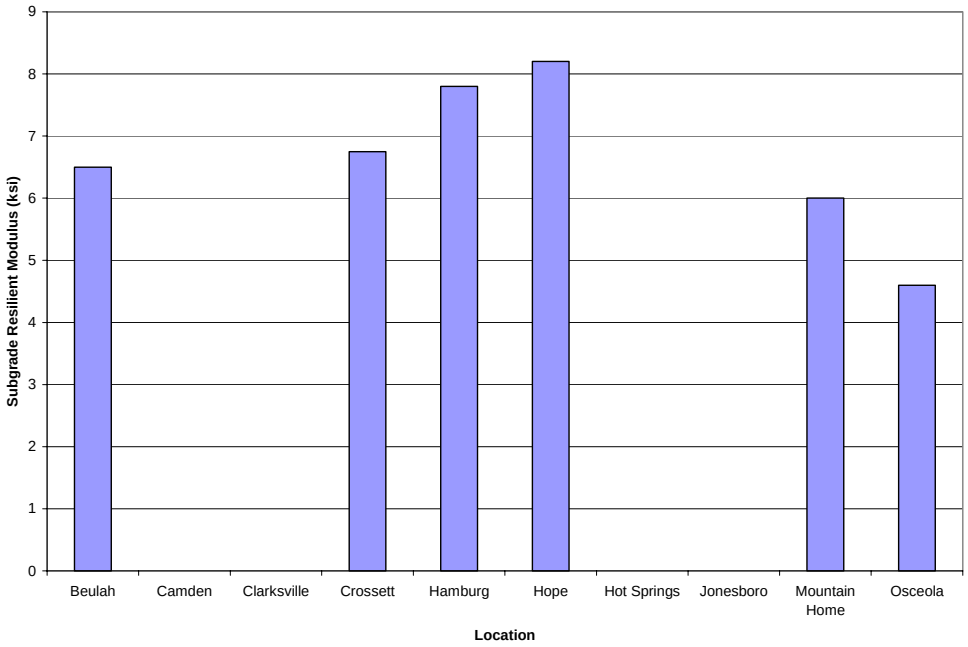

Figure 4.38 Subgrade M_r from laboratory testing (location)

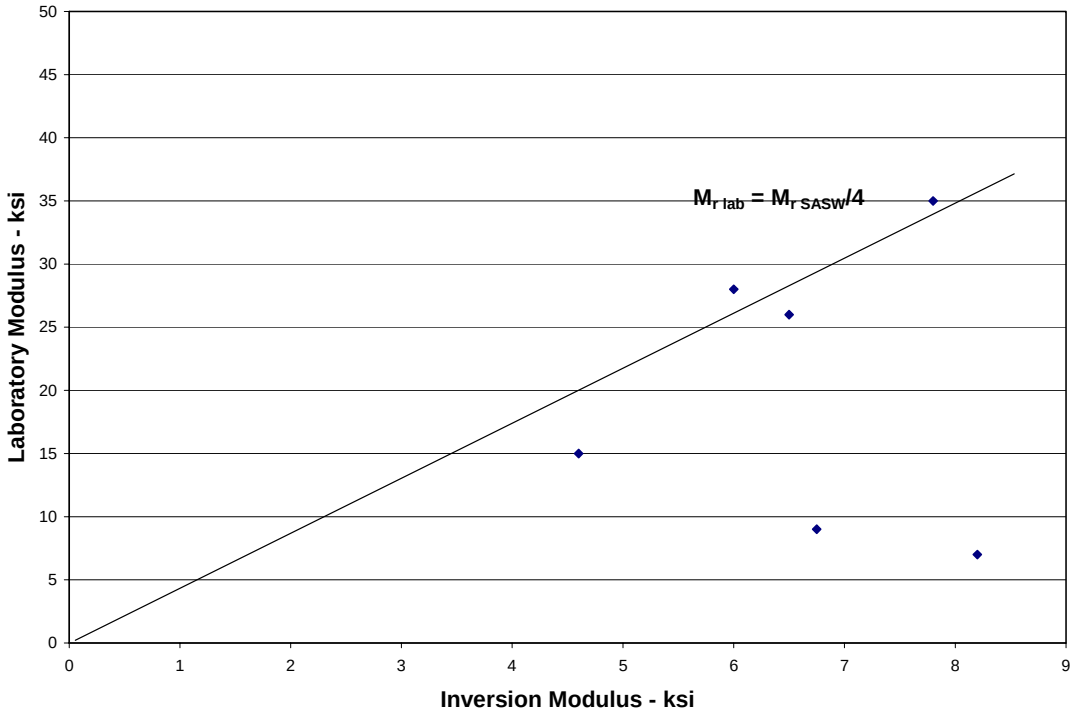

Figure 4.39 Laboratory modulus versus simple inversion modulus

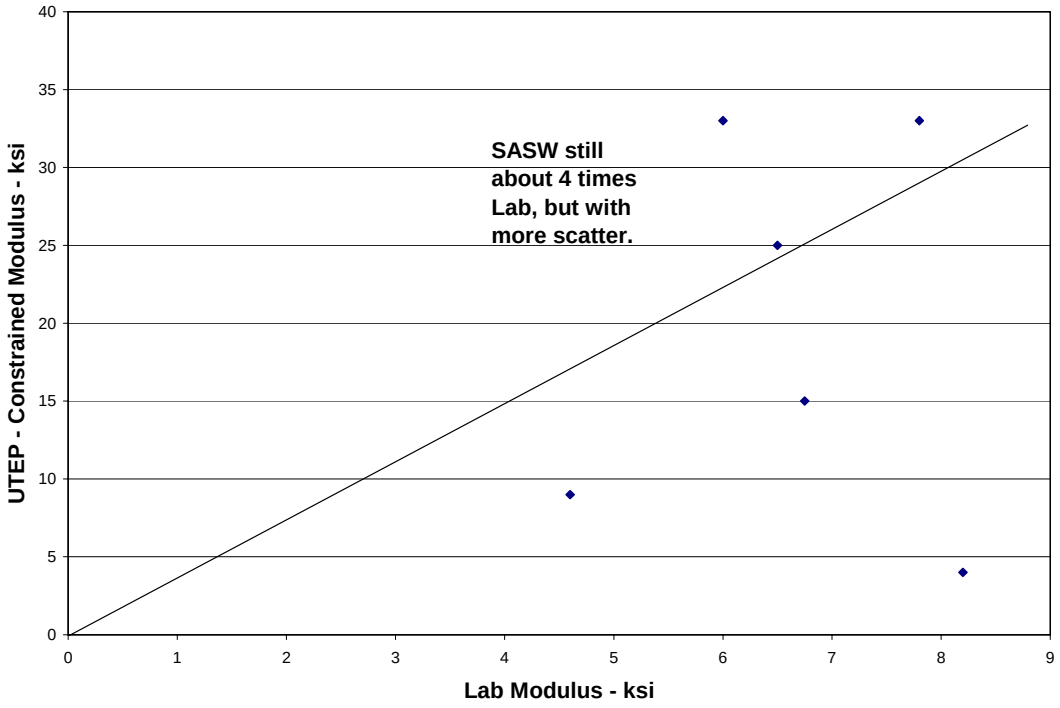

Figure 4.40 UTEP constrained modulus versus laboratory modulus

The laboratory resilient modulus testing results do not agree very well with the results obtained from any of the other methods used. The range of values obtained appears reasonable, and in general the values are four times less than those predicted by SASW and FWD testing. A possibility for the scatter present in the laboratory data may be related to the moisture content at which the fine grained specimens were tested (see Table 4.6). The moisture contents of the fine grained soils present at the Hope, Osceola and Crossett sites ranged from 11.5 to 15.6 percent above their respective optimum moisture contents. Thus, the soils were likely saturated or nearly saturated during laboratory testing. During laboratory resilient modulus testing the soil specimen is allowed to freely drain. However, given the rapid cyclical loading pattern used to perform laboratory resilient modulus testing and the fine grained nature of the soils at these three sites, it is unlikely that the pore water pressure in these saturated fine grained materials dissipated completely (or at all). Consequently, the laboratory resilient modulus results may be unreasonably high for the fine grained soils tested from the Crossett, Hope and Osceola sites as the test may have been partially measuring the compressibility of pore water.

4.4 Resilient Modulus of Base Course

The majority of aggregate base course material specified by the Arkansas Highway and Transportation Department (AHTD) in the construction of roadways falls into one of two categories: Class 7 and Class 5. Class 7 aggregate base course is composed of any mechanically crushed natural rock or stone of igneous, sedimentary, and/or metamorphic origin produced from a solid geological formation. Class 5 base

course material is typically composed of river or bank run gravel. Selection between the two materials is often dictated by geographic location and aggregate availability. Class 7 crushed stone particles are generally more angular and the AHTD gradation tolerances require a more coarse blend than that of Class 5 base. Class 7 aggregate base is regarded as a higher quality material, typically

providing higher shear strength and resilient modulus values. Section 303 of the AHTD Standard Specifications for Highway Construction (2003 edition) presents the gradation, Atterberg limits, and L.A. Abrasion requirements for both base course materials.

The type of base course material encountered at the sites during field testing was recorded to see if SASW testing would predict different values of modulus for different types of base materials. Five of the ten sites had a Class 7 base course layer, three had a Class 5 base course layer, and no base course was present at two of the sites. Table 4.4 shows the type and thickness of the base course material encountered at each site, as well as the modulus predicted for the base course by the software provided by the University of Texas at El Paso. The moduli reported were found using the same program settings and constraints as those described in the subgrade resilient modulus section. Figure 4.34 shows the information from Table 4.4 in graphical form.

Table 4.4 and Figure 4.41 show that the modulus predicted for Class 7 base is consistently higher than the modulus measured for Class 5 base. Predicted modulus values for Class 7 base course ranged from a low of 81 ksi at the Clarksville site to a high of 130 at the Osceola site, and averaged 109 ksi for the five sites containing Class 7 material. Modulus values predicted for Class 5 base course ranged from a low of 2 ksi

Table 4.7 Base Course Data from Test Sites

Location	Type	Thickness (in)	Resilient Modulus (ksi)
Beulah	Class 7	9	119
Camden	Class 5	6	73
Clarksville	Class 7	7	81
Crossett	None Present	-	-
Hamburg	None Present	-	-
Hope	Class 7	3	94
Hot Springs	Class 5	7.5	20
Jonesboro	Class 5	9	48
Mountain Home	Class 7	9	123
Osceola	Class 7	15	130

at the Hot Springs site to a high of 73 ksi at the Camden site, and averaged 47 ksi over the three sites containing Class 5 material.

Modulus values of Class 7 aggregate base from laboratory cyclic triaxial testing was available to make comparisons to the data obtained from SASW testing. The laboratory data suggests that the modulus values of Class 7 base produced from quarries within the state of Arkansas range from approximately 15 ksi to 60 ksi at a confining pressure of 5 psi (Welcher, 2004). The average value found for Class 7 base by SASW testing was 109 ksi, and ranged from 81 to 130. The much larger values of base modulus found by SASW testing was expected because of the very low level of strain associated with seismic testing as compared to the relatively high level of strain associated with laboratory testing. Values of base course modulus found using surface wave techniques are typically 2 to 3 (or even more) times greater than those found by laboratory testing.

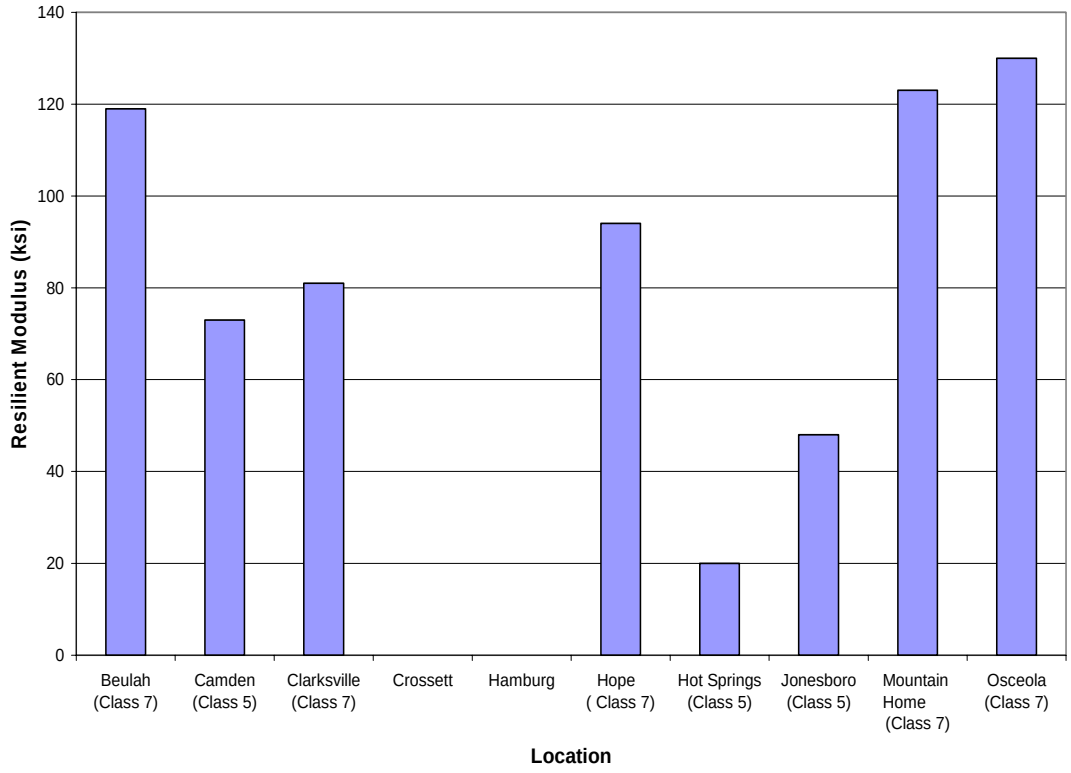

Figure 4.41 Moduli of base course materials predicted by UTEP software

4.5 Resilient Modulus of Asphalt Pavement

The general condition of the asphalt present at each test site was visually evaluated to see if SASW testing would consistently predict lower modulus values for pavements which appeared to be in poor condition. The pavement sections at the Hope, Clarksville, Osceola, and Mountain Home sites appeared to be in relatively poor condition. The pavement sections at the remainder of the sites appeared to be in good condition, with the pavement at the Hamburg and Camden sites appearing to be the highest quality pavements tested. Figure 4.42 shows the asphalt resilient moduli

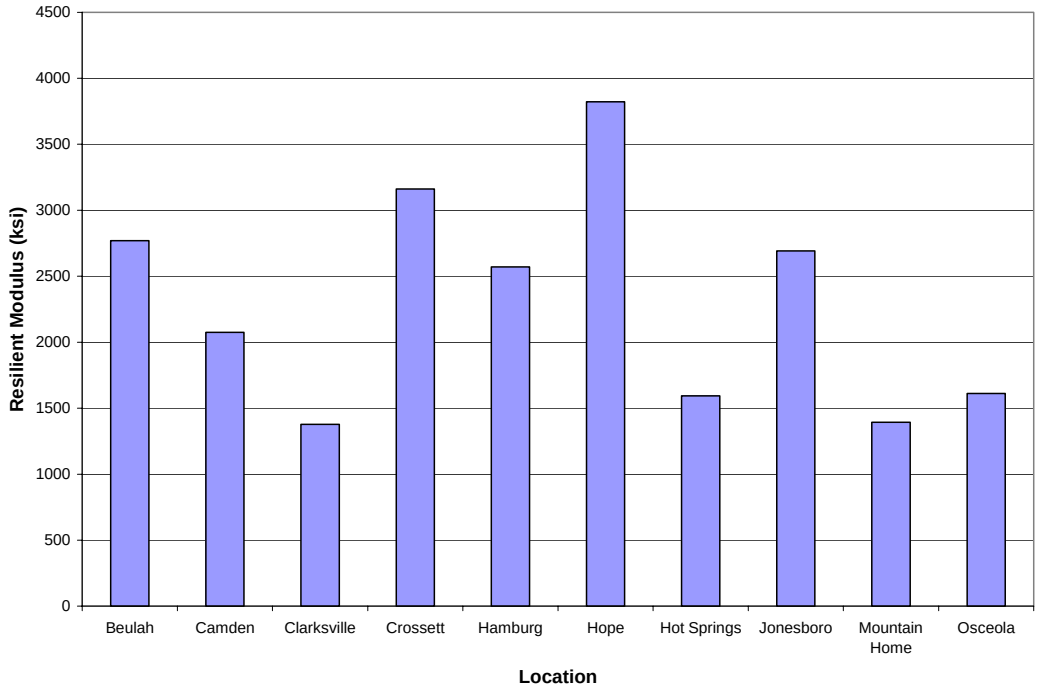

Figure 4.42 Asphalt pavement modulus predicted by SASW testing

predicted by the UTEP program using the layer constraint/modified profile procedure.

The results shown in Figure 4.42 indicate that the modulus of the asphalt sections tested vary from about 1400 ksi to 3800 ksi. The tests were conducted during the months of November and December, and the temperatures were typically between 35 to 50 degrees Fahrenheit. Available laboratory data for asphalt concrete indicates a range for resilient modulus of about 500 to 1000 ksi (Tran, 2000) for the temperatures indicated. The range is much higher for SASW testing, as expected.

The predicted moduli were lower for the Clarksville, Moutain Home, Osceola and Hot Springs sites. Three of these four coincide with the sites that were visually classified as having poor quality asphalt. The Hot Springs site did not appear to have distressed pavement, however. The pavement at the Hope test site was in observed to be severely

distressed with large ruts in the wheel paths and large areas of alligator cracking. The UTEP program predicted a high asphalt resilient modulus for this site, however this is considered to be an anomaly in the data caused by poor wave propagation through the distressed pavement. The dispersion curve obtained for this site exhibited very poor coherence and a poorly aligned dispersion curve which indicates poor data quality.

CHAPTER 5

CONCLUSIONS AND RECOMMENDATIONS

5.1 Conclusions

This study has provided a procedure for the use of the Spectral Analysis of Surface Waves (SASW) method for determining the thickness and resilient moduli of pavement systems. A system capable of rapidly collecting the in-situ data necessary to perform SASW analysis was developed, and subsequently used to collect data at ten flexible pavement sites throughout the state of Arkansas. The thickness and resilient modulus of each layer of the pavement sections were then estimated from the collected data using two methods of analysis; simple inversion, and using software provided by the University of Texas at El Paso. The thickness results obtained from SASW analysis were compared to known thicknesses measured from cores taken at each of the test sites. The resilient moduli predicted by SASW analysis were compared to the resilient moduli predicted by laboratory resilient modulus testing, the resilient moduli predicted by FWD analysis, and to Standard Penetration test N-values. Specific conclusions that can be drawn from this research are:

1. Spectral analysis of surface waves testing conducted as presented within this research is not yet ready to be used as the primary method to determine resilient modulus values for use in design, although the results presented herein indicate that SASW is a promising new method of rapidly determining in-situ moduli of pavement sections.

2. The SASW equipment and data acquisition program developed during this study were successfully used to collect in-situ data and to develop experimental dispersion curves for the test sites. The experimental dispersion curves appear to be reasonable with regards to the experimental dispersion curves found in the literature.
3. An effective sampling depth of ½ of the wavelength was found to produce the most accurate results when using the simple inversion technique. Thicknesses of the asphalt and base layers were typically predicted fairly accurately using this effective sampling depth. At some locations, individual asphalt layers could be distinguished as well.
4. SASW testing predicted values of resilient modulus for asphalt, base course, and subgrade soils that are within reasonable ranges for the levels of strain associated with SASW testing.
5. A loose correlation appears to exist between SASW methods and FWD methods (R^2 values typically near 0.5). The reliability of the correlation does not change much depending upon the method used.
6. However, SASW testing predicted a resilient modulus approximately twice that of FWD testing at sites that had stiff subgrade soils (as expected), but predicted resilient modulus values very nearly equal to or slightly less than those predicted by FWD at sites that had a softer subgrade material.
7. The resilient moduli of the subgrade soils predicted by SASW testing agreed well with the condition of the subgrade soil observed at the time of testing as

evaluated by considering Standard Penetration Test N-values, Atterberg limits, gradation, and in-situ moisture content information.

8. No concrete relationship could be established between the resilient modulus obtained by laboratory resilient modulus testing and SASW testing. However, it appears that the modulus predicted in the laboratory is approximately 4 times smaller than that predicted using seismic methods. Additionally, only a limited number of laboratory tests were performed, and saturated conditions may account for some of the scatter observed in the data.
9. The SASW analysis procedures used did not appear to work well for situations where a large stiffness contrast was present in the pavement profile (when no base course was present).
10. SASW testing consistently predicted a higher value of resilient modulus for Class 7 base course than for Class 5 base course.
11. The dispersion data collected at sites containing a chip seal surface layer was of poor quality.
12. The SASW analysis procedures used require a substantial amount of interpretation, and therefore requires a highly trained individual to perform the analysis.

5.2 Recommendations

This study represents the first steps taken by the Mack-Blackwell Transportation Center and the Arkansas Highway and Transportation Department towards the evaluation of the use of SASW testing to determine the resilient moduli of pavement sections in the

state of Arkansas. This study has demonstrated that this method has the potential of being a fast and efficient method of evaluating resilient properties of pavement sections in-situ. However, in order for SASW to be implemented, the method must be further refined. The loose correlation established as part of this study points to the need for more testing to fill in gaps in the obtained data and to identify and remove outlying data points. Much more testing will be needed to establish statistically significant relationships between resilient moduli predicted by SASW testing and FWD and laboratory resilient modulus testing. Specific recommendations on how the field testing and data analysis procedures should be improved are:

1. The resolution of the dispersion data should be improved by narrowing the bandwidth used when performing the Fourier Transform on the acquired signals. This is especially needed in the low frequency range. Increasing the resolution will both increase the quality of the results and make the data reduction procedure much faster and more accurate. The table below lists the bandwidths that were used during this study and the newly recommended bandwidths for each receiver spacing.

Table 5.1 Recommended bandwidths for each receiver spacing for future research

Receiver Spacing (in)	Bandwidth Used During Study (kHz)	Recommended Bandwidth (kHz)
3	0-80	0-60
6	0-60	0-30
12	0-20	0-10
24	0-10	0-5
48	0-5	0-2
96	0-2	0-0.5

2. Some of the data reduction steps may be incorporated into the LabView acquisition software program to speed up the analysis procedure. In particular,

investigating the possibility of unwrapping the phase information within LabView may dramatically speed up data analysis.

3. The equipment setup should be made even more mobile than the setup used during this study. This may include developing a system in which the receivers are pre-mounted onto a fixture that can be adhered to a pavement surface as a single unit. The dynamic effects of fixing the receivers to such a fixture should be evaluated.
4. A more rigorous drilling and sampling routine should be employed. Asphalt cores should be taken in tested areas, followed by drilling beneath the roadway to evaluate subsurface conditions. The subsurface soils beneath the pavement need to be sampled at regular intervals by either split spoon or Shelby tube samplers as deemed appropriate. These samples should then be tested to develop well defined boring logs complete with soil type and resilient modulus (as found by laboratory testing) indicated. Bulk soil samples taken from the shoulder of test sites should not be used in any form of laboratory testing.
5. Investigating the use of more than three layers to perform the inversion process should be undertaken.
6. To test pavement systems that contain a chip sealed surface a plate should be adhered to the pavement surface. The hammer used to create the vertical transient impact should strike the plate that is adhered to the pavement surface. This procedure may reduce some of the scatter obtained in the data on chip sealed surfaces by creating a smooth surface that allows for a repeatable signal to be generated.

7. Collaboration with others who are familiar with SASW testing is highly recommended to speed up the development an SASW system capable of meeting the needs of the AHTD.

References

Bath, M. (1979) "Introduction to Seismology", 2nd Ed. Natur och Kultur, Boston.

Beauchamp, K.G., Yuen, C.K. (1979) "Digital Methods for Signal Analysis", George Allen and Unwen, London.

Braile, L.W. (2000) "Seismic Waves and the Slinky: A guide for teachers." Informal Publication.

Burger, R.H. (1992) "Exploration Geophysics of the Shallow Subsurface", Prentice Hall, New Jersey.

Das, B.M. (1992) "Principles of Soil Dynamics", PWS-Kent Publishing Company, Boston.

Elliott, R.P., Thornton, S.I. (1988). "Resilient Properties of Arkansas Subgrades." Final Report TRC-94 to the Arkansas Highway and Transportation Department. Little Rock, Arkansas.

Foti S. (2000) "Multistation Methods for Geotechnical Characterization using Surface Waves", PhD Dissertation, Politecnico di Torino, Italy.

Graff, K.F. (1975) "Wave Motion in Elastic Solids", Dover, New York.

Heisey, J.S., Stokoe, K. H. II, Meyer, A.H. (1982) "Moduli of Pavement Systems from Spectral Analysis of Surface Waves", Transportation Research Record, vol 852, pp. 22-31.

Luna, R., Jadi, H. (2000) "Determination of Dynamic Soil Properties Using Geophysical Methods", Proceedings of the First International Conference on the Application of Geophysical and NDT Methodologies to Transportation Facilities and Infrastructure,St. Louis, pp. 1-15.

Marven, C., Ewers, G. (1996) "A Simple Approach to Digital Signal Processing", John Wiley and Sons, Inc., New York.

Mikhail, M.Y., Seeds, S.B., Alavi, S.H., Ott, W.C. (1999) "Evaluation of Laboratory and Backcalculated Resilient Moduli from the WesTrack Experiment," Transportation Research Record, vol 1687, pp. 55-65.

Nazarian, S., Stokoe, K.H. II, Hudson, W.R. (1983) "Use of Spectral Analysis Wave Method for Determination of Moduli and Thicknesses of Pavement Systems", Transportation Research Record, vol 930, pp. 38-45.

Nazarian, S. (1984) “In Situ Determination of Elastic Moduli of Soil Deposits and Pavement Systems by Specral Analysis of Surface Waves Method”, Ph.D. Diss., University of Texas at Austin.

Nazarian, S., Stokoe, K.H. II. (1984) “Nondestructive Testing of Pavements Using Surface Waves”, Transportation Research Record, vol 993, pp. 67-79.

Nazarian, S., Stokoe, K.H. II. (1986) “Use of Surface Waves in Pavement Evaluation”, Transportation Research Record, vol 1070, pp. 132-143.

Nazarian S., Yuan, D., Baker, M.R. (1995) “Rapid Determination of Pavement Moduli with Spectral-Analysis-of-Surface-Waves Method”, Research Project 0-1243, The Center for Geotechnical and Highway Materials Research, UTEP.

Richart, F.E. Jr., Wood, R.D., Hall, J.R. Jr. (1970) “Vibration of Soils and Foundations”, Prentice-Hall, New Jersey.

Tran, Nam. (2000) “” Masters Thesis, University of Arkansas.

Uzan, J., Scullion, T., Michalek, C.H., Parades, M., and Lytton, R.L. (1988). “A Microcomputer-Based Procedure for Backcalculating Layer Moduli from FWD Data,” Research Project 1123-1, Texas Transportation Institute, Texas A&M University, College Station.

Welcher, R.M. (2004) “Effect of Fines on the Shear Strength of Unbound Aggregate Base Course”, Masters Thesis, University of Arkansas.

Yuan, D., Nazarian, S. (1991) “Rapid Determination of Layer Properties of Pavements from Surface Wave Method”, Transportation Research Record, vol 1377, pp. 159-166.

Zywicki, D.J. (1999) “Advanced Signal Processing Methods Applied to Engineering Analysis of Seismic Surface Waves”, Ph.D. Diss., Georgia Institute of Technology.

“Labview 7 Express Measurements Manual.” National Instruments. Austin, Texas.

“BNC-2140 User Manual.” National Instruments. 3 Mar. 2004. <http://www.ni.com>.

“EM 1110-1-1802.” Engineering Manual dated August 1995. Army Corp of Engineers. 9 Feb. 2004 <http://www.usace.army.mil>.

“Introduction to Peizoelectric Accelerometers.” PCB Peizotronics. 10 Mar. 2004 <http://www.pcb.com>.

"The Fundamentals of Signal Analysis." Application Note 243. Agilent Technologies. 2 Feb. 2004 <http://we.home.agilent.com>.

APPENDIX A

Test Site Data Table and Vicinity Maps

Project Site Information Table

Site Name	Hot Springs	Osceola	Hamburg	Clarksville	Jonesboro	Beulah	Crossett	Camden	Mountain Home	Hope
County	Hot Springs	Mississippi	Ashley	Johnson	Craighead	Prarie	Ashley	Dallas	Fulton	Hempstead
Nearest Town	Bismark	Grider	Hamburg	Lamar	Jonesboro	Beulah	Crossett	Holly Springs	Kittle	Columbus
GPS Coordinates	N 34˚ 18.519' W 93˚ 11.260'	N 35˚ 38.895' W 89˚ 58.118'	N 33˚ 11.728' W 91˚ 44.577'	N 35˚ 28.733' W 93˚ 19.486'	N 35˚ 53.966' W 90˚ 38.831'	N 34˚ 52.355' W 91˚ 24.562'	N 33˚ 09.596' W 92˚ 01.707'	N 33˚ 52.250' W 92˚ 40.112'	N 36˚ 16.306' W 91˚ 37.718'	N 33˚ 47.025' W 93˚ 48.884'
Description	On Highway 84, 1.1 miles west of the intersection of Highway 7 and Highway 84	On Highway 198, 0.8 Miles north of the intersection of Highway 61 and Highway 198	On Highway 8, 4.1 miles east of the intersection of Highway 82 and Highway 8	On Highway 315, 2.4 miles north of the intersection of Highway 359 and Highway 315	On Highway 351, 2.9 miles north of the intersection of Highway 49 and Highway 351	On Highway 33, 1.6 miles North of the intersection of I-40 and Highway 33	On Ashley County Road 13, 1.4 miles north of County Road 13 and Highway 82	On Highway 9, 1.5 miles north of the intersection of Highway 273 and Highway 9	On Highway 289, 1.2 miles north of the intersection of Highway 62 and Highway 289	On County Road 35, 0.4 miles north of the intersection of Highway 73 and County Road 35
Meeting Location	Phillips 66 at the intersection of Highway 7 and Highway 84	Intersection of Highway 198 and Highway 61	Phillips 66 at the intersection of Highway 82 and Highway425 in Hamburg	Liberty gas station at the intersection of Highway 62 and Highway 359 in Lamar	Intersection of Highway 351 and Highway 49	On Site (1.6 miles North of the interstate)	Cc Mart Truck Stop at 2913 Highway 82 in West Crossett	Holly Springs Baptist Church parking lot on Highway 9 in Holly Springs	Intersection of Highway 289 (NORTH) and Highway 62	Phillips 66 at the intersection of Highway 278 and Holiday Lane in Hope.

Beulah site vicinity map

Camden site vicinity map

Clarksville site vicinity map

Crossett site vicinity map

Hamburg site vicinity map

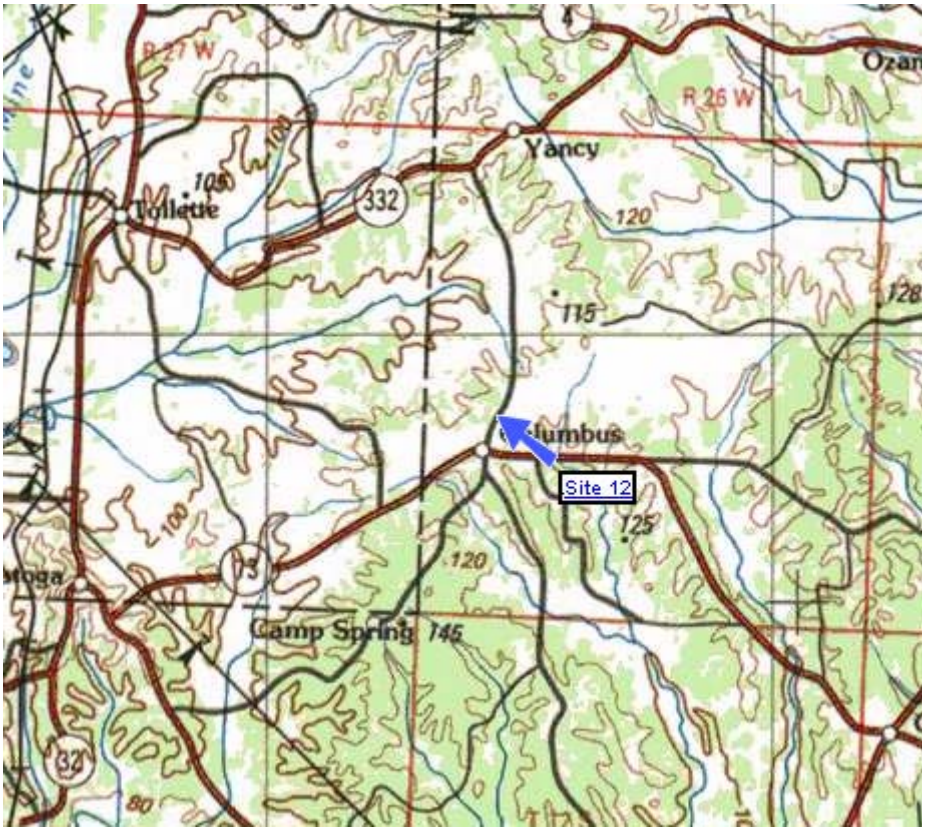

Hope site vicinity map

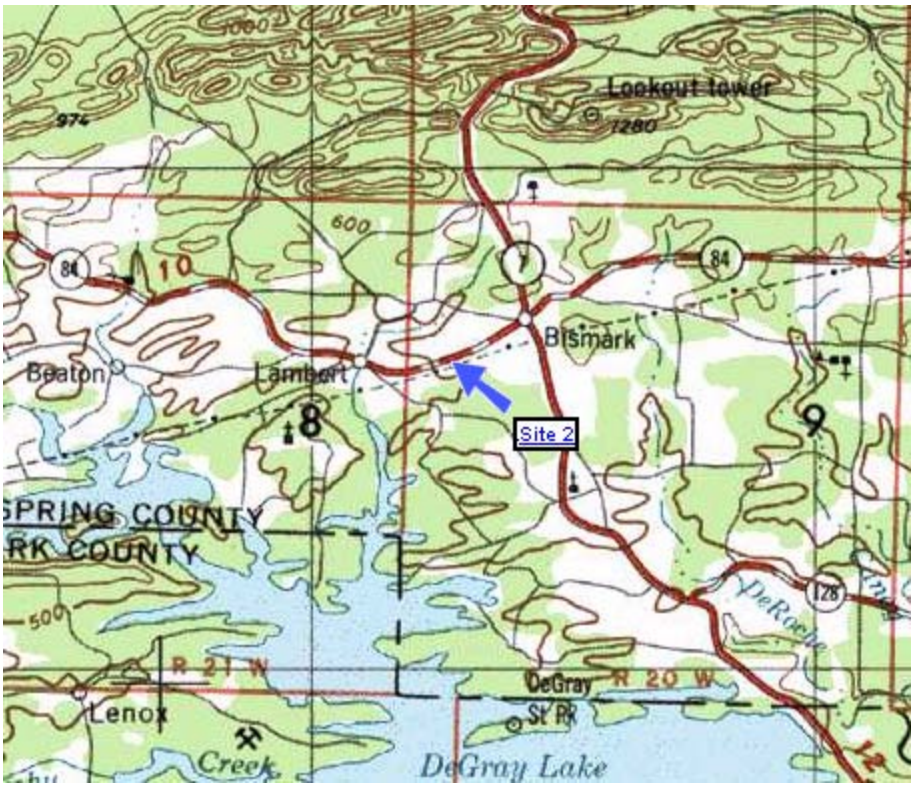

Hot Springs site vicinity map

Jonesboro Springs site vicinity map

Mountain Home site vicinity map

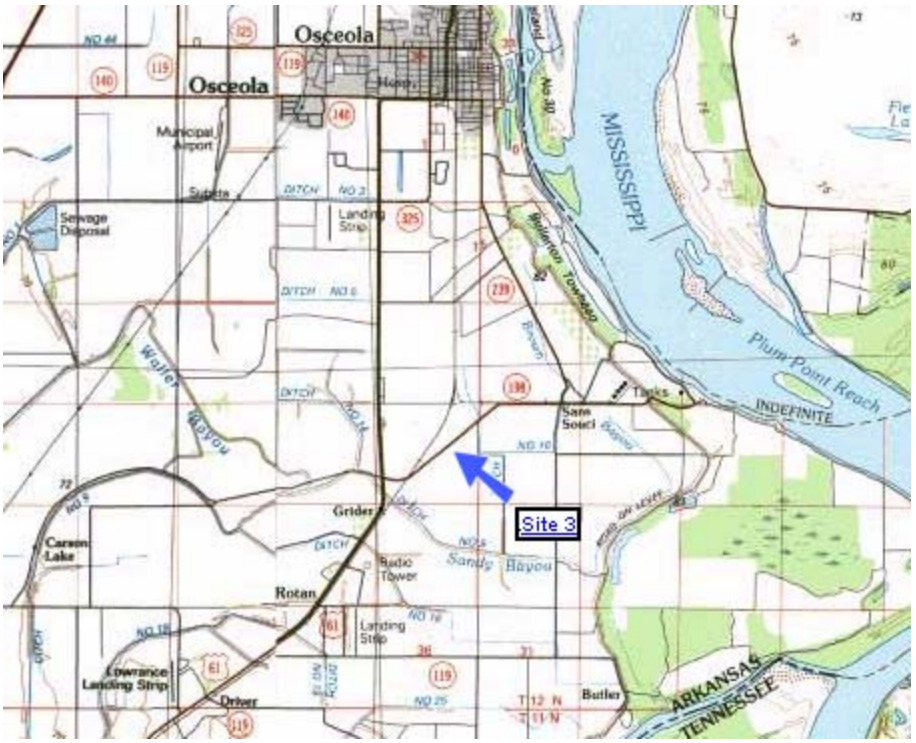

Osceola site vicinity map

SignalCapture1.VI
Description and Operation

SignalCapture1.vi is the name of the program that was developed to control the acquisition and analysis of surface waves for spectral analysis of surface waves (SASW) testing. SignalCapture1.vi was created using a graphical programming language called LabVIEW® marketed by National Instruments. VI stands for virtual instrument, and is LabVIEW's nomenclature for its programs. This section is provided to explain the purpose of the program, how the program functions, and how to operate the program to achieve the desired results. A copy of the virtual instrument is included on the CD attached.

Program Overview

The general function of this program is to acquire and partially analyze surface waves generated by impacting the surface of a pavement system. The program takes the raw waveforms measured by two receivers and transforms those waveforms into data that can be used by an inversion program to predict resilient modulii and layer thicknesses of the pavement structure. To begin the signal acquisition process SignalCapture1.vi configures the data acquisition board (NI-4552) to allow it to simultaneously acquire signals from two input channels. The two input channels are chosen from a list from channel 0 to channel 3. These channel numbers correspond to the channel numbers seen on the BNC-2140 signal conditioner. Up to four receivers can be connected to the signal conditioner at one time. However, the software program does not allow for signals to be collected from all four receivers at once, but does allow for a combination of any two receivers to be used. Also, the program can be used to change the combination of

receivers which are being read at any time during testing. This allows for all four receivers to be set up at the beginning of testing and not moved until completion of testing. Acquiring signals at various receiver spacings is accomplished by simply switching which channels are being sampled by the data acquisition board.

External analog triggering is used to coordinate the measurements with the signal excitation (hammer impact). The program allows the user to configure trigger settings so that certain requirements must be met before signal acquisition begins. The user designates the channel (receiver) that is used as the trigger. The user can then set the threshold voltage level at which signal acquisition will begin as well as whether the slope of the signal is rising or falling. A signal delay can also be used. For SASW testing a negative trigger delay is used, also called a pretrigger, which records the background noise present prior to the triggering event. Setting a negative trigger delay allows for detection of loss of signal that can result when the slope of the signal is very steep (Nazarian, 1984). Through the use of triggering, it becomes possible to measure the surface waves generated immediately after the hammer impacts the pavement. Setting the trigger level lets the user define how hard the pavement must be impacted before measurement will commence. If the pavement is not impacted hard enough the voltage generated by the receiver due to the surface waves will not exceed the minimum value set by the user and no measurement will be taken.

SignalCapture1.vi has averaging capabilities built in. To perform averaging, the program takes a set number of measurements from separate triggering events, and turns them into an average measurement. Averaging is important for two reasons. The first reason is that averaging increases the signal quality by reducing random background

noise. The impact of background noise is reduced because a random signal averaged over time tends towards zero (Nazarian). The second reason averaging is important is that it allows for the computation of the coherence function, which is a measure of signal quality between receivers. The program allows the user to set a variety of options that define the manner in which the averaging is carried out. The user can choose the averaging mode (RMS, vector, peak), the number of averages used, the way in which each measurement is weighted, and whether or not a measurement is rejected if its peak voltage is above a set value.

The expected input voltage range and input coupling are user inputs into the program as well. The input voltage range must be set in order to get accurate measurements from the NI 4552. If the maximum and minimum input voltages are not properly set then the gain and attenuation factors used by the DSA board will be incorrect, which may result in poor measurement quality. It may be necessary to adjust the input voltage range during testing depending on the type of source used to generate the surface waves.

SignalCapture1.vi allows the user adjust the frequency span over which measurements are taken, as well as how many lines are used to define the frequency domain. It is very important that the frequency span is set properly, as the frequency directly relates to the depth of sampling. The frequency range of interest will change as the spacing between the receivers changes. Higher frequencies are needed for smaller receiver spacings, and lower frequencies are needed for larger receiver spacings. The number of lines chosen is important in that it defines the resolution of the signal in the

frequency domain. Generally there will be no reason to change the number of lines used during testing.

Six separate measurements can be made at one time using SignalCapture1.vi. For the purposes of this project two major categories of measurements are used to conduct SASW analysis: time domain measurements and frequency domain measurements. The time domain measurements taken are the time signals recorded from two individual channels. The time domain signal for each of the receivers is displayed in its own plot labeled time trace 1 and time trace 2 respectively. The remaining four plots display frequency domain measurements. The frequency domain measurements taken are the frequency response between the two receivers and the coherence function. The frequency response is composed of two parts, a real portion called the magnitude and an imaginary portion called the phase angle (LabVIEW Measurement manual). To perform an SASW analysis the phase angle is required. To find the phase angle, the program displays the frequency response function. The frequency response function consists of both a real and imaginary portion, both of which must be known to determine the phase angle. The real portion of the frequency response function and the imaginary portion of the frequency response function are also displayed on individual plots. The coherence function is displayed on its own plot in the upper right hand corner of the display screen. A detailed discussion of each of the measurements is discussed in the literature review (Chapter 2).

The data obtained by SignalCapture1.vi during testing is saved to a data file that is named by the user at the beginning of the test. The data is written to file as a series of six columns of data. The first column of data represents time trace 1, the second is time

trace 2, the third represents the frequency response, the fourth represents the real portion of the frequency response, the fifth represents the imaginary portion of the frequency response, and the sixth represents the coherence. The top row of each column of data is the initial value (x0) of the measurement. The value of the top row should always be zero. The second row of data represents the distance between measurements, or dx. This value represents a change in time for time domain measurements and a change in frequency for frequency domain measurements. Starting with the third row, the values recorded represent a y measurement at an x value of x0 + [dx * (#of previous measurements + 1)]. Time domain measurements will always consist of 1024 points. Frequency domain measurements will consist of a number of points equal to the number of frequency lines selected. One measurement will be made and recorded, and then a second measurement will be appended to the end of the first measurement, then a third measurement appended to the end of the second measurement, etc… until the number of desired measurements for averaging has been reached and the program stops collecting data. Refer to the data reduction section of this document for a more in depth look at the format in which the data is saved, and how that data is prepared prior to the inversion process.

Using SignalCapture1.vi (front panel)

The LabVIEW software program is divided into two major components, the front panel and the block diagram. The block diagram is the area in which the code (in the form of graphical icons) is located. The front panel serves as the user interface between the user and the block diagram, and controls the execution of the code within the block diagram. The purpose of this section is to describe how to use the front panel of SignalCapture1.vi to configure the program to perform spectral analysis of surface wave

testing (SASW). Each of the settings available on the front panel will be addressed. A picture of the setting control as it appears on the front panel, along with its corresponding terminal in the code will be shown so that the user can determine where in the dataflow process the setting's information is introduced. The importance of each setting will be discussed, and suggested values will be given as well..

Entering Resource Name

Front Panel

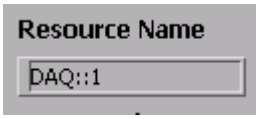

Block Diagram Terminal

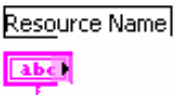

The resource name on the front panel is where the user defines the name of the instrument that is to be used to take measurements. The user must enter the name of the instrument to be used, or use the default name of DAQ::1. The resource name has to be entered as a string data type, as the terminal from the block diagram indicates. During the course of the project the name of the instrument used was DAQ::1.

Entering File Name

Front Panel

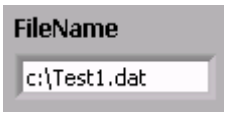

Block Diagram Terminal

Before measurements are taken a file name must be provided to tell the code where the acquired data will be stored. The user may either enter the name of an existing file or a new file name. If an existing file name is used the program will append all new information to the end of the existing file. The user should save the file either as a data file (.dat) or as a text file (.txt). The block diagram terminal shows that the file name is entered in as a string data type by the user. The string data type is then automatically turned into a path data type in the code.

Choosing Available Measurements

Front Panel

Block Diagram Terminal

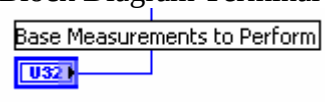

The type of measurements that the board will take needs to be specified in order for the program to properly configure the data acquisition board. The user must pick from a dropdown list that defines the types of measurement to be taken. To perform SASW testing the board must be able to take time domain, frequency domain, and cross spectrum measurements. The program uses a ring control to associate a numeric value to each possible selection in the dropdown list. The numeric value is then used in the code to configure the acquisition board.

Routing Base Analyzers

Front Panel

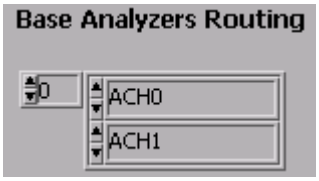

Block Diagram Terminal

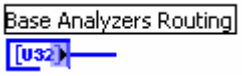

The section of the front panel shown above allows the user to route each channel to be analyzed to a baseband analyzer on the NI 4552 DSA board. Each analyzer can only handle measurements from one channel at a time. The single box on the left side of the control represents the number of the baseband analyzer to which a channel is being assigned (0-3). The box to the immediate right shows the channel that is currently assigned to the selected analyzer. The box below shows the channel that is associated with the next highest baseband analyzer. The analyzer routing selection shown above indicates that baseband analyzer 0 has channel 0 (ACH0) assigned to it, and that channel

1 (ACH1) is assigned to baseband analyzer 1. The user may assign any channel to any analyzer so long as each analyzer has only one channel assigned to it. Selecting the channel and selecting the baseband analyzer are accomplished by using the dropdown lists that are seen above.

Setting Input Coupling and Voltage Range

Front Panel

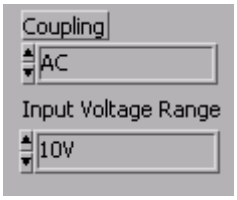

Block Diagram Terminals

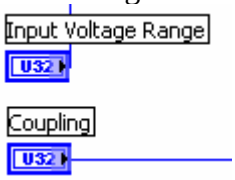

This section of the front panel allows the user to set the input coupling and voltage range. Two choices are available for the coupling, AC or DC. AC coupling is the default value and should be used to take SASW measurements. The input voltage range gives the board an expected range of signal voltages. The user may select from a list of expected voltage ranges by using the provided dropdown list. It is important to properly select the input voltage range. Choosing a value that is too high may result in a poor digital representation of the signal (Labview Manual). Choosing a value that is too low may cause the signal to become clipped which can introduce large errors. Testing revealed that a voltage range of +- 3.16 worked well for most situations.

Setting Averaging Parameters

Front Panel

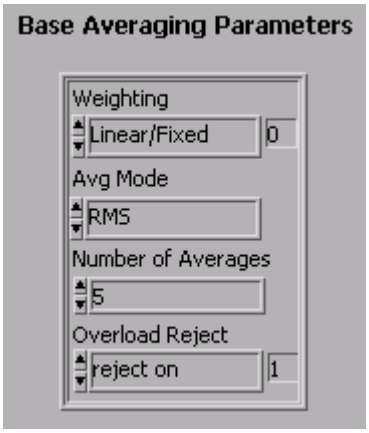

Block Diagram Terminals

Signal averaging is used to improve the accuracy of the signal by reducing the effects of background noise. This section of the front panel allows the user to choose how the averaging is accomplished from a dropdown list. The first parameter that is chosen is the weighting of the individual signals. The signals may either be linearly or exponentially weighted. Linear weighting gives equal importance to each signal that is acquired. Exponential weighting assigns more importance to newer signals than older signals. Linear weighting was used during SASW testing for this project.

The number of averages used may also be set by the program user. Theoretically the more averages taken the more accurate the results obtained. Practically, it was found that 5 averages where adequate to obtain an accurate representation of the signal (explained in the lit review). The user can increase or decrease the number of averages taken by using the up and down arrows on the right side of the controls, or can manually type in the number of averages to be taken. If the overload reject option is turned on any signal that exceeds the expected voltage range will not be averaged in with the other signals.

Overload reject is turned on and off by selecting an option from the dropdown list.

The averaging mode is also able to set by the program user. The averaging mode may be set to RMS, peak-to-peak, or vector. RMS averaging was used during the course of this project. To set the averaging mode the user may select an option from the provided dropdown list.

Setting the Trigger

Front Panel

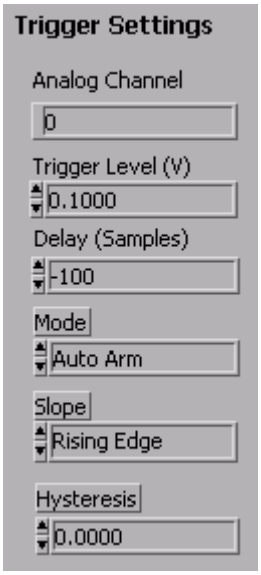

Block Diagram Terminals

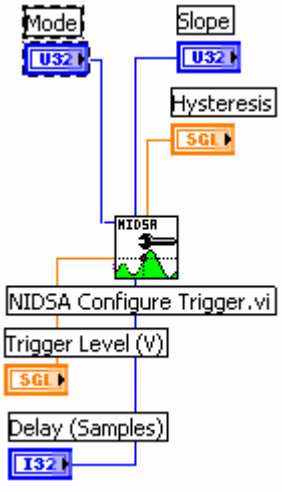

The portion of the front panel shown above is used to set the trigger used to control the start time of the data acquisition. The desired trigger channel is entered in the top control, and may be channel 0-3. The voltage signal required to trigger data acquisition is entered into the second box. The trigger level should be high enough to prevent accidental triggering, and low enough to allow for the trigger level to be achieved easily. A voltage level of 0.10 volts was found to work well for the testing associated with this project. The trigger level can be set by typing in a value in the trigger level control box, or by using the up and down arrows.

The trigger mode may also be set in this portion of the front panel. Three options are available for trigger mode; auto arm, manual arm, and free run. Free run mode allows the system to act as if no triggering is used. Auto arm tells the program to automatically rearm the trigger after each acquisition. The program user must manually rearm the trigger after each acquisition if the manual arm selection is made. Auto arm works well

with SASW testing. The trigger mode may be changed by making a choice from the dropdown menu.

A pretrigger delay is often desirable to ensure that the entire signal has been captured. The number of samples to record prior to triggering may be entered by the user in the Delay (samples) control box. One hundred samples was used as the pretrigger delay during SASW testing for this project. One hundred samples is roughly 10 percent of the total number of samples recorded, which is percentage recommended in the literature. The number of delay samples may be changed by using the up and down arrows or by simply typing in any whole number.

Values for the slope and hysteresis are also adjustable. The slope allows the user to define whether data acquisition will begin when the slope of the signal is rising or falling. This choice is made by simply choosing one of the two options from the provided menu. Hysteresis allows the user to more fully define the shape that the signal must have before a trigger is detected. A value of 0 was used for hysteresis throughout testing. If a value other than zero is desired for hysteresis the up and down arrows can be used, or a value can be simply typed into the control box.

Set Base Parameters

Front Panel

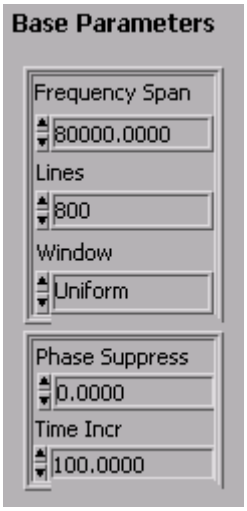

Block Diagram Terminals

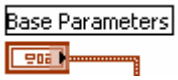

This section allows the user to configure the 4 baseband analyzers used to take the measurements. The frequency span over which measurements will be taken is set in the first control box. The maximum frequency that may sampled is 80,000 Hz when classical

lines are used and 95,000 Hz when extended lines are used. A maximum frequency span of 80,000 Hz was used for this project. The frequency span can be altered most easily by typing in the value (in Hz) in the provided box.

The number of lines of resolution used in the frequency domain may be set in the second control box. The greater the number of lines used the higher the resolution in the frequency domain. For this project, 800 lines was chosen. This number of lines was a convenient choice because a span of 80,000 Hz with 800 lines of resolution causes a measurement to be taken at every 100 Hz. This even division allows for easier computations. If a different number of resolution lines is desired, the value in the Lines control box may be changed by typing in a new integer value.

The window control box makes it possible to apply a weighting function to the acquired signal. The window that is most appropriate for measuring transient signals is the uniform window (Labview Manual). Using any window other than the uniform window can cause serious distortions in the signal and should not be used for SASW testing purposes.

The phase suppress can be used to set a threshold frequency below which the phase component will not be computed. For SASW testing phase information is required at all available frequencies, and therefore the phase suppress should be set to 0. The time increment tells the board how often to take another set of measurements. A time increment of 100 was used for testing during this project.

Setting Test Measurements

Front Panel

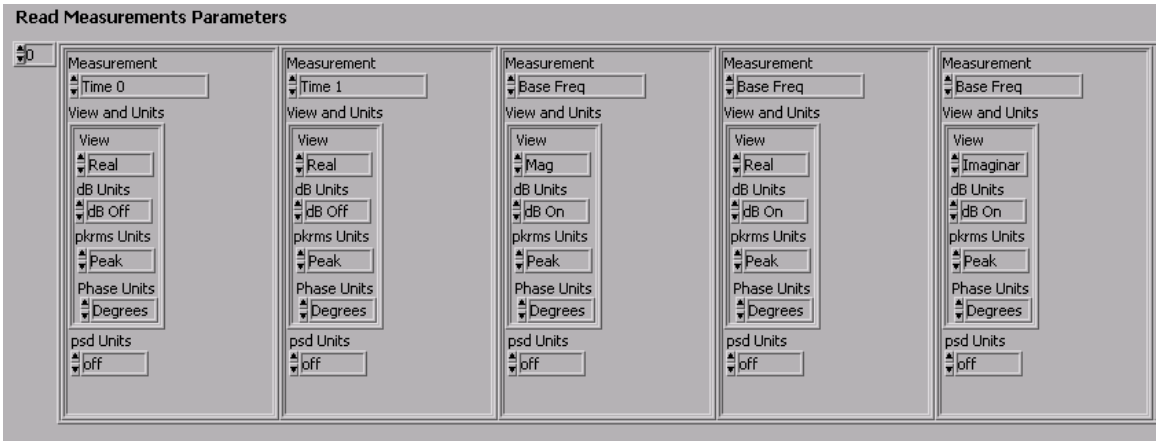

Block Diagram Terminal

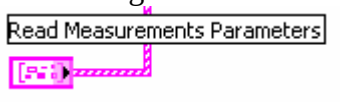

The read measurements parameters section of the front panel is where the user chooses which measurements will be taken and displayed. The list of possible choices is determined by the "base measurements to perform" setting discussed earlier. The program is setup so that a total of six selections may be made from the available list. View and units options for each measurement are made in this section as well. The view and units options can be set independently for each measurement chosen. The six measurements that were used for SASW testing, along with the appropriate view and units options for each, are discussed below.

Time Trace 0

The first measurement should be set to capture the time domain signal from channel 0. Capturing the signal in the time domain allows for a visual check of the signal. The peak value of the signal should be checked against the input voltage limit setting to make sure it does not exceed the specified limits. The signal can also be used to see whether the voltage range has been set too high. For example, a voltage range

setting of +- 10V for the time trace shown below would be inappropriate. A better voltage range would be +- 3.16V or +-1V.

The signal should also be inspected to make sure the entire pulse is captured. The signal should start out at zero, oscillate, and then return to zero by the completion of the time record. The time trace shown below shows a completely captured pulse. If the voltage range is not correct or/and the entire time signal is not captured, then adjustments will need to be made.

To correctly capture the time domain signal the view needs to set to real and the decibels turned off. Having an incorrect viewing option or having the decibels option turned on will severely distort the appearance of the signal. The units option should be set to peak for the magnitude and degrees for the phase. PSD units should be turned off.

Time Trace 1

The second measurement block should be set to capture the time domain signal from channel 1. The view and units options for time trace one are identical to the settings for time trace zero.

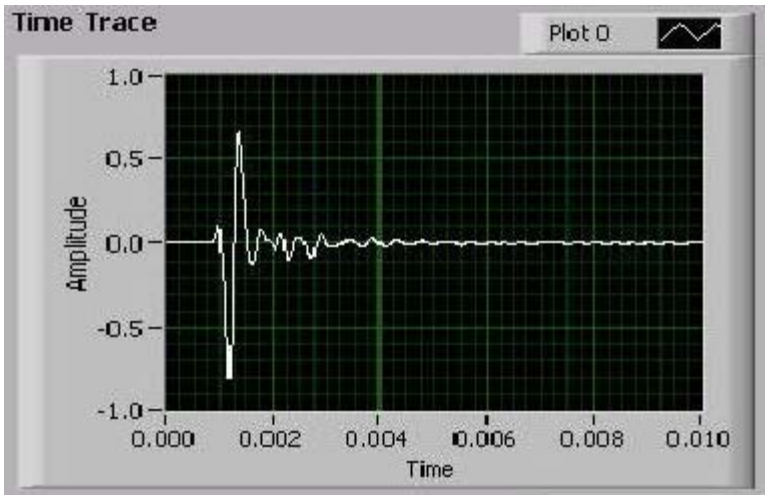

Base Frequency Response

The frequency response of the pavement system between two receivers at various spacing is the primary parameter of interest in SASW testing. The frequency response

function defines the change the input signal undergoes between channel 0 and channel 1. The change is measured in the frequency domain and consists of two portions, one real and one imaginary. The real portion of the frequency response measurement corresponds to change in magnitude and the imaginary portion of the measurement corresponds to change in phase. The inversion program used to create the final pavement profile requires both the real and imaginary components of the frequency response function to be entered as a function of frequency. Due to this, three of the measurement blocks on the front panel are devoted to measuring the frequency response. One block is used to measure and display the frequency response function as a whole, one block is used to measure and display the real component of the frequency response function, and one block is used to measure and display the imaginary component of the frequency response function.

The view and units settings for the three measurement blocks involving the frequency response function are very similar. Decibels should be turned on for all three measurements to easily distinguish lower magnitude signal components (HP Document). PKRMS units should be set to peak, phase units set to degrees, and PSD units turned off. The difference in the three measurements lies in the view setting. The view for the frequency response function as a whole should be mag, the view for the real component set to real, and the view for the imaginary component set to imaginary.

Coherence

The final measurement block on the front diagram is used to measure coherence. The coherence function is the ratio of the output power caused by the input signal to the total measured output (Nazarian, 1984). The primary function of the coherence function is to assess the quality of the measurements. A coherence value of one suggests that all

of the output signal was caused by the input signal and that no signal contamination was experienced (due to background noise or other possible input sources). The coherence measurement should be monitored during testing to ensure that high quality signals are obtained over the desired frequency range. Typically coherence values above 0.8 indicate that the signals are adequate for SASW testing (Nazarian, 1984).

The view and units settings used for the coherence measurement were: view set to mag, decibels turned off, PKRMS set to peak, phase units set to degrees, and PSD units turned off.

Starting and Stopping the Program

Front Panel

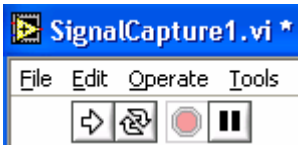

Block Diagram Terminal

N/A

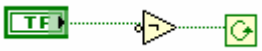

To begin the program the arrow icon shown above has to be single clicked. The appearance of the arrow will change to solid black when the program is operating. To stop the program one of two options may be used. The red stop sign shaped icon may be clicked or the stop button may be clicked. The arrow icon will appear as a white arrow once the program has been stopped.

Errors

Front Panel

Block Diagram Terminal

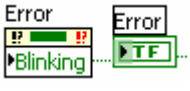

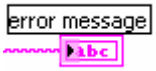

The front panel has two areas that alert the user to the occurrence of errors during the execution of the program. A red blinking error light will be seen if an error occurs along with a text message printed in the error out box. The error out box above shows the error message that is seen if the program does not detect an instrument or the instrument name is not valid.

Program Logic (block diagram)

This section is devoted to describing the programming logic that went into developing SignalCapture1.vi. As stated earlier, this program was created using LabVIEW®. The LabVIEW® programming language uses icons instead of text to create programs (LabVIEW manual). The portion of a fully developed LabVIEW® program that contains the source code looks somewhat like a flowchart, and is referred to as the block diagram. Dataflow programming is used to execute the code, which means that the flow of data through the icons that contain the source code controls the execution order of the program (LabVIEW manual). The program begins with the icon on the left hand side, and progresses to the right by following attached wires to successive icons.

SignalCapture1.vi's block diagram is shown in at the end of this appendix. Each component of the diagram is described in detail below to give the reader an understanding of how the program works, and to provide insight into how the program could be modified if necessary. The components of the diagram are discussed in order of execution. SignalCapture1.vi was created by modifying a program called AnalogTriggerExample.vi which was provided by National Instruments as part of the LabVIEW full development edition. The original program's block diagram is shown in Figure 2.

Initialize Instrument

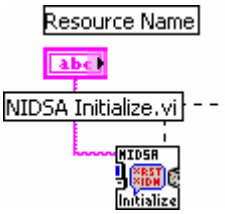

Input Nodes: Resource Name
Output Nodes: DSA Session
Error Out
Unused Nodes: ID Query (input)
Reset Device
Error In

The first step taken is to use NIDSA Initialize.vi to establish communication with the NI 4552 data acquisition board. The program chooses what instrument is used to perform the measurements by reading the resource name from the front panel via the Resource Name terminal. The name DAQ::1 was assigned to the NI 4552 data acquisition board for the dura tion of this project. If the name of the instrument were to be changed to anything other than DAQ::1 the name entered on the front panel would have to be changed accordingly in order for the name to be recognized by the vi. Once the program verifies that the named instrument is present it establishes communication with the board and assigns a DSA session number. The DSA session number is used to uniquely identify each set of measurements taken by the data acquisition board. If the program is not able to establish a connection with the named instrument an error message is sent out along with the DSA session number.

While Loop

The general function of a while loop is to perform whatever commands are contained within the loop until the conditional terminal (green arrow) reaches a certain value. The i is used to keep count of the number of iterations performed. The purpose of the while loop for this program is to force the NI 4552 board take continuous readings

until the program is stopped. If the while loop was not present the NI 4552 board would simply take one reading and then the program would terminate. This is obviously undesirable as each test must consist of hundreds of readings to accurately define the waveform that is captured by the receivers.

Conditional Terminal

This conditional terminal defines under what conditions the while loop will terminate. The Boolean T/F terminal is linked to a stop button on the front panel. This, in combination with the logical "not" operator tells the loop to continue as long as the stop button on the front panel has not been pressed. Thus, the while loop will continue to execute, and readings will continue to be made, until the stop button is depressed.

Iteration Counter

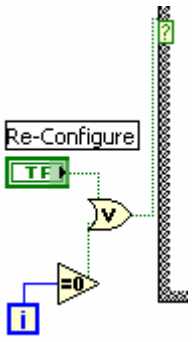

The iteration counter of the while loop in combination with the Re-Configure terminal, are used to control a case structure (explained below). The code snippet states that if the iteration counter (blue i) is equal to zero, or the Re-Configure button is pressed, then the True case of the case structure will occur. If, on the other hand, neither the Re-Configure button is depressed nor the iteration counter equal to zero, then the False case structure will occur.

Case Structure

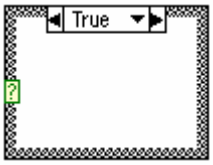

Case structures are used to allow for one of several sub-diagrams to be chosen for execution based on a set of conditions. The program decides which one of the possible sub-diagrams to execute based on the selector terminal located on the top border of the case structure. This program contains two possible cases, True and False. The true case structure is used to configure the NI 4552 board, and is executed if the iteration counter is equal to zero (beginning of test) or if the user depresses the Re-Configure button. The false case statement allows the program to skip reconfiguration for all successions of the while loop after the first iteration, unless the user depresses the Re-Configure button. If the True case structure is applicable the program flow causes data from NIDSA Initialize.vi into Configure Base Analyzer.vi. If False, the data flows from NIDSA Initialize.vi through the case structure and into NI-DSA Read Multi-View.vi.

Configure Base Analyzer

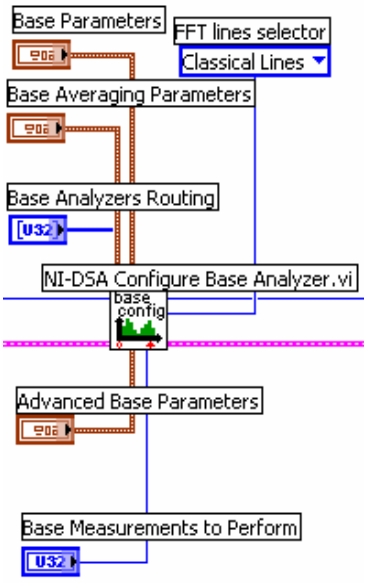

Input Nodes: DSA session in
Error in
Base parameters
Base averaging parameters
Base analyzers routing
Advance base parameters
Base measurements to perform
FFT lines selector

Output Nodes: DSA session out
Error out

Unused Nodes: Base select

If the True case structure is chosen the program will go through a series of steps to configure the NI 4552 board based on a set of options chosen on the front panel. The first step taken is to select which baseband analyzers will be used by the DSA board to take readings, and to configure those analyzers such that they are able to take the type of readings desired. The input terminals to NI-DSA Configure Base Analyzer are DSA session in and error in, both of which are wired to NIDSA Initialize.vi. If the board has been properly initialized then Configure Base Analyzer.vi will execute in full. If the board was not properly initialized, however, and an error message is passed to Configure Base Analyzer.vi, then Configure Base Analyzer.vi will not execute and will simply pass on the error message received.

The NI 4552 board contains four separate baseband analyzers (0-3). Each analyzer can handle one channel of input at one time. Configure Baseband Analyzer.vi allows the user to choose which channel is routed to each analyzer. The ability to route channels allows the user to change which channels are measured during testing. Changing the channel routing during testing facilitates testing receivers at different spacing without having to physically move receivers.

Configure Baseband Analyzer.vi tells the NI 4552 board what kind of measurements it will be expected to make. The options that can be selected are time waveforms; time waveforms and their Fourier transforms (FFT); time waveforms, their FFT, and their auto-power spectrums; or time waveforms, their FFT, their auto-power spectrums, and their cross-power spectrums. SASW testing requires that the signal from two receivers be compared, so the appropriate setting for this program will always

include the cross-power spectrum. Appropriately configuring this option is crucial as it defines what data the NI 4552 board will make available to the program.

Configure Base Analyzer.vi also allows the user to set the frequency span over which measurements will be taken, and the number of frequency lines which will be used in analysis. If the frequency line selector is set to classical the maximum span is 80 kHz, if the frequency line selector is set to extended, then the maximum span is extended to 95 kHz. The number of lines used dictates what the resolution will be in the frequency domain (FFT). Averaging parameters and windowing options are also set at this point in the program. The user can change any of these parameters using the front panel, except for the frequency line selector which must be changed within the block diagram.

If valid selections for all of the configuration options are made for all of the inputs, then the board is configured and the DSA session number is passed through the wire to the next sub vi (set input coupling sub vi). If invalid selections were made at some point then an error message will be passed along with the DSA session number to the next sub vi, and the board's baseband analyzers will not be configured.

Set Input Voltage Range

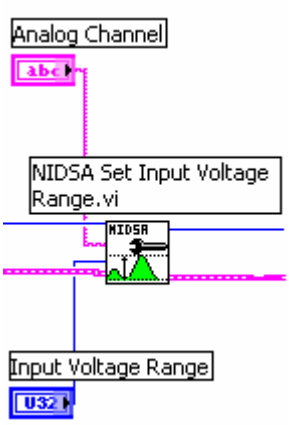

Input Nodes: DSA session in
Error in
Input select
Voltage range
Output Nodes: DSA session out
Error out
Unused Nodes: None

The next step taken to configure the data acquisition board is performed by NIDSA Set Input Voltage Range.vi. As the name implies, NIDSA Set Input Voltage Range.vi is used to tell the NI 4552 board what voltage to expect from the input channel. The program reads the voltage range from the Input Voltage Range terminal. The Analog Channel terminal defines which channel the input voltage range is associated with. Assuming there is no error into the vi, and the settings for the analog channel and voltage range have valid values, NIDSA Set Input Voltage Range.vi will configure the board to the selected settings, and pass along the DSA number to the next configuration procedure.

Set Input Coupling

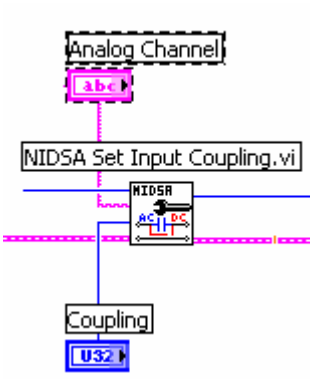

Input Nodes: DSA session in
Error in
Input select
Coupling

Output Nodes: DSA session out
Error out

Unused Nodes: None

The next configuration option carried out is fairly straightforward. NIDSA Set Input Coupling.vi sets the coupling of the selected input channel. The vi checks to see if an error in message is received. If there is an error the vi does not configure the board, and the error message is simply passed to the next vi (NIDSA Configure Trigger.vi). If no error in message is received, the board reads the values from both the coupling and analog channel terminals. The analog channel terminal connected to the trigger channel control on the front panel. Once the values are read by the vi, the board is configured accordingly, and the DSA session number is passed to NIDSA Configure Trigger.vi.

Configure Trigger

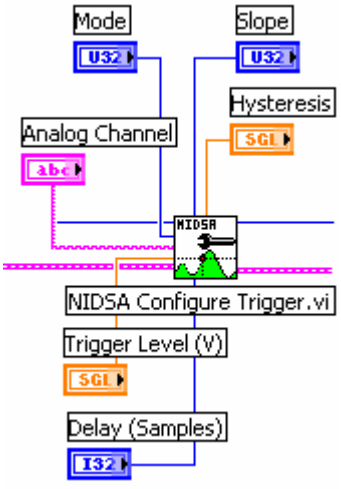

Input Nodes: DSA session in
Error in
Input select
Trigger mode
Trigger level
Delay
Slope
Hysteresis

Output Nodes: DSA session out
Error out

Unused Nodes: None

The final configuration procedure that is carried out is the configuration of a trigger. This vi allows a channel to be selected as a trigger, the trigger level (in volts) to be set, the trigger mode to be set, the delay (in # of samples) to be set, the slope of the signal to be set, and the hysteresis of the signal to be set. All of these parameters are set by the user when entering values in the appropriate controls located on the front panel.

NIDSA Configure Trigger.vi begins by making sure there is no incoming error message. If no error message is received the values entered into the terminals for each of the trigger parameters are retrieved. If valid values are found, the board is configured for triggered signal acquisition. If inappropriate values are found the board is not configured and an error message is generated. This is the last section of code located within the case structure. The remaining code executes as part of every iteration of the while loop.

Read Measurements

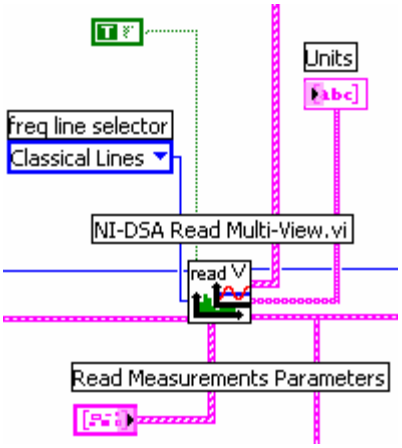

Input Nodes: DSA session in
Error in
Frequency line selector
Read measurement parameters
Get new measurement

Output Nodes: Units
Measurements
DSA session out
Error out

Unused Nodes: None

This section of the code is perhaps the most vital operation performed by the program. Read Multi-View.vi tells the program to read a list of user specified measurements that are to be taken by the NI 4552 board. This vi is located inside the while loop, which is important because it causes measurements to be taken each time the loop executes. The vi outputs an array containing all of the measurements that were made, along with an array which specifies what units are associated with each measurement.

The read multi-view vi begins its execution by first checking to see if there is an incoming error message from the preceding portion of the program. If there is no incoming error message the vi checks the T/F (true/false) operator to see if it is supposed to get a new measurement. For this program the T/F operator is always set to true, therefore the vi will look for an available measurement from the NI 4552 board during each iteration of the while loop. The vi then checks to see if it will read frequency domain measurements using classical or extended lines. The vi chooses which measurements to perform by checking the Read Measurements Parameters terminal, which is connected to an array control located on the front panel. The Read

Measurements Parameters terminal is where the program decides which measurements it will take, what units will be used to take the measurements, and the views that will be used to display the results.

Once these input parameters are known to the program the specified measurements are taken and placed into an output array labeled Measurements. The set of units associated with the measurements is placed into a separate array called Units. The units output array is linked directly to the front panel, and the results can be viewed by the user. The Measurements output array is passed on to a further section of code to be prepared for graphical display and saving. The DSA session number is also passed on to further sections of code.

Measurement Array

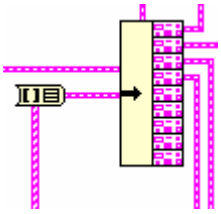

Input: Measurement cluster
Output: Measurement 1 cluster (Time trace 1)
Measurement 2 cluster (Time trace 2)
Measurement 3 cluster (Frequency response)
Measurement 4 cluster (Real portion of frequency response)
Measurement 5 cluster (Imaginary portion of frequency response)
Measurement 6 cluster (Coherence)

The measurement array that is generated by Read Multi-View.vi consists of a set of six measurements for each execution of the while loop. Typically the while loop will iterate 1024 times, resulting in an array containing 6 rows and 1024 columns. The 1024 data points for time domain readings are taken so that they are evenly spaced over the time interval used. Frequency domain measurements depend on the number of frequency lines selected. The measurement array for a frequency domain measurement consists of measured values for each column of data up to the number of frequency lines used. Each column after the number of frequency lines has been reached will contain a 0.

In order to view and save meaningful information from the output array it is necessary to separate the measurements from one another. This section of code uses an unbundle function to take the input cluster of six measurements and break it up into the six individual measurements.

Display

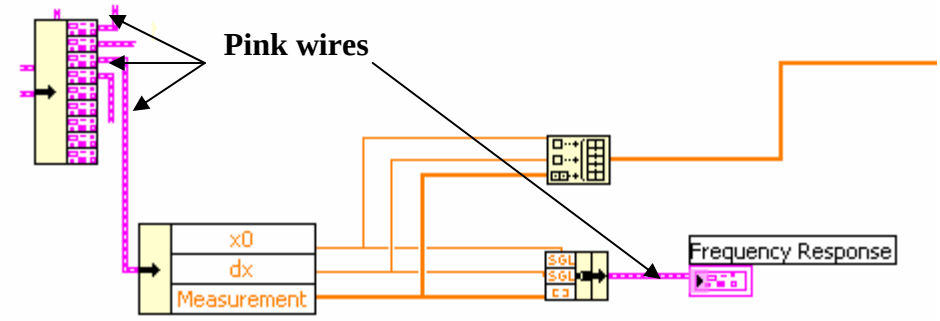

The section of code above illustrates one of the six measurements that has been unbundled from the output of the read mult-view vi. Keep in mind that five other sections of code exist that perform the same operations on each of the other unbundled measurements. The measurement shown above is the frequency response.

Once the measurement has been unbundled it is still in a cluster format. Each cluster (pink wire) consists of three pieces of information; the starting point of the measurement (x0), the interval between each successive measurement (dx), and the value of the measurement which can be thought of as y. The code takes the cluster and separates it into its individual components. After the measurement has been broken down into its components, it is reassembled, but in two different forms. The first form is to reform it into a cluster so that it can be graphed (the graph requires a cluster type input). The second form is a two dimensional array. The reason the data is reassembled as an

array is to organize the information for the next step of the program which is to save the data.

The cluster is passed to a graph terminal which connects to a corresponding graphical display on the front panel. A cluster is a wire containing more than one type of information. The user of the program can view the graph to see the measurement in graphical form. The 2-D array that is formed is passed on to the next section of code which is used to save the data to file.

Save

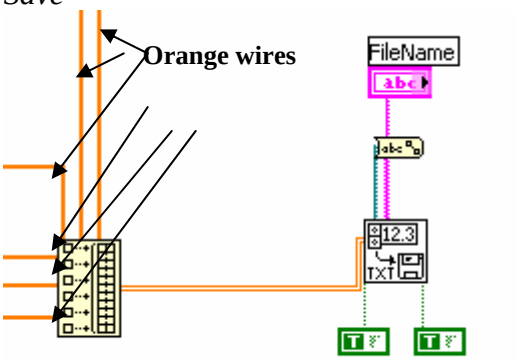

After each measurement has been transformed into an array the individual arrays are combined into one larger array. This can be seen at the left where the six orange wires are connected to the array icon. Once this array has been formed it is connected to the save to file operation. The two Boolean T/F operators tell the program to transpose the input array and to append the data to the bottom of the chosen file. The transpose command allows the data to be saved as six columns containing 1024 rows instead of 1024 columns containing six rows. The append command tells the program that all data should be placed at the end of the file instead of overwriting the data already present in the file. The program decides where information is to be saved by obtaining the name of the file from the FileName terminal which is connected to a control on the front panel.

Error Notification

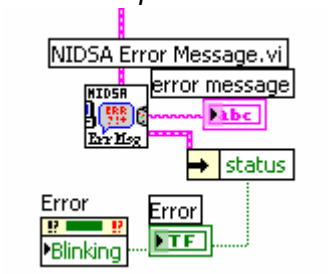

Input Nodes: Error message
Output Nodes: Error out
Error message
Unused Nodes: DSA session in
DSA session out
Error code

If an error has occurred anywhere up to this point in the program it is passed into this section of code. The error is carried into NIDSA Error Message.vi and transformed into a text message that is displayed on the front panel. The program also causes a red light to blink on the front panel when an error occurs. This section of code works by first testing to see if there is an incoming error. If no error is detected no error message is displayed. Also, as long as there is no error the status of the error out node remains false and no light blinks. If an incoming error is detected the vi sends an error message to the error message text box control on the front panel. Additionally, the status of the error out becomes true which causes the red light to start blinking.

Close

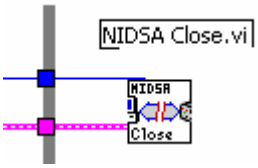

Input Nodes: DSA session in
Error in
Output Nodes: Error out
Unused Nodes: None

This section of the code simply closes the DSA session once the while loop stops executing.